Preclinical Evaluation of Rational Drug Combinations with BH3 mimetics in Colorectal and Small Cell Lung Cancer

A thesis submitted to The University of Manchester for the degree of Doctor of Philosophy (PhD) in the Faculty of Medical and Human Sciences

2015

Danielle Potter

School of Medicine

Table of contents

List of Figures

List of Tables

List of manuscript Figures and Tables

Chapter 3

Abstract

*Abstract of a thesis entitled "**Preclinical evaluation of rational drug combinations with BH3 mimetics in colorectal and small cell lung cancers,"** submitted by **Danielle Potter** for the degree of Doctor of Philosophy (PhD) to **The University of Manchester,** September 2015*

Colorectal (CRC) and small cell lung cancer (SCLC) are among the most common cancers and are leading causes of cancer related deaths worldwide. Prognosis is poor for both metastatic CRC (mCRC) and SCLC patients for reasons including eligibility for curative surgery, late diagnosis and limited treatment options. Five year survival rates of patients with mCRC or extensive stage SCLC are 5% and 2% respectively.

Standard of care (SOC) for mCRC is based on multiple chemotherapy regimens whilst more recently introduced targeted therapies such as Bevacizumab and Cetuximab have only improved survival of mCRC patients by 1.5-2.6 months. SOC for SCLC patients is platinum based chemotherapy +/- radiation whereby the majority are initially chemo-sensitive followed by an inevitable chemotherapy-resistant relapse within 3-18 months. In both mCRC and SCLC, disease progression is largely due to a high degree of tumour heterogeneity and innate/acquired resistance to therapy due to multiple mutations in non-redundant pathways. As such treatment for both mCRC and SCLC has made little progress in 30 years resulting in a clear unmet need to improve current/develop new therapies for these patients.

Several hallmarks of cancer including sustained proliferation and resistance to cell death implicate Phosphoinositide 3-kinase (PI3K) signaling, frequently deregulated in both CRC and SCLC whilst anti-apoptotic proteins including Bcl-2 family members are commonly upregulated in all cancers. The rational drug combination of a PI3K inhibitor (PI3Ki; PI-103 or GDC-0941) and a Bcl-2 family targeted BH3 mimetic (ABT-737 or Navitoclax) was investigated in preclinical CRC and SCLC models. ABT-737 and Navitoclax directly interacts with the anti-apoptotic proteins, BCL-2, BCL-xL and BCL-w antagonising their interactions with pro-apoptotic, BH3-only proteins and effector proteins to induce apoptosis. The findings of this thesis confirm that combining ABT-737 with PI-103 increases the potency of ABT-737 *in vitro* in CRC and SCLC and the GDC-0941/Navitoclax combination improved overall survival of mice bearing human SCLC tumours compared to either drug as a single agent and to SCLC SOC. For the first time the Tec kinase BMX was also implicated in the observed responses to this combination.

Novel therapies are usually tested in combination with SOC in mCRC and SCLC patients. The BH3 profiling technique can determine how 'primed' a tumour cell is for apoptosis and reports mitochondrial outer membrane permeabilization (MOMP) after treatment with BH3 peptides. BH3 profiling was optimised for SCLC CTC (circulating tumour cell) Derived eXplants (CDX) models and the approach was validated retrospectively on chemo-sensitive and chemo-refractory CDX. Finally, prospective BH3 profiling was able to predict responses to SOC chemotherapy in paired CDX models derived from chemotherapy-naïve patients and again at relapse with disease progression. The overall conclusions from this thesis are (i) use of PI3K inhibitors and BH3 mimetics in combination should be tested in the clinic, particularly in SCLC, (ii) BH3 profiling should be optimised as a CTC assay to predict chemotherapy responses in SCLC.

Declaration

No portion of this work referred to in this thesis has been submitted in support of an application for degree or qualification of this or any other university or other institution of learning.

Copyright Statement

The following four notes on copyright and the ownership of intellectual property rights must be included as written below:

i. The author of this thesis (including any appendices and/or schedules to this thesis) owns certain copyright or related rights in it (the “Copyright”) and she has given The University of Manchester certain rights to use such Copyright, including for administrative purposes.

ii. Copies of this thesis, either in full or in extracts and whether in hard or electronic copy, may be made **only** in accordance with the Copyright, Designs and Patents Act 1988 (as amended) and regulations issued under it or, where appropriate, in accordance with licensing agreements which the University has from time to time. This page must form part of any such copies made.

iii. The ownership of certain Copyright, patents, designs, trademarks and other intellectual property (the “Intellectual Property”) and any reproductions of copyright works in the thesis, for example graphs and tables (“Reproductions”), which may be described in this thesis, may not be owned by the author and may be owned by third parties. Such Intellectual Property and Reproductions cannot and must not be made available for use without the prior written permission of the owner(s) of the relevant Intellectual Property and/or Reproductions.

iv. Further information on the conditions under which disclosure, publication and commercialisation of this thesis, the Copyright and any Intellectual Property and/or Reproductions described in it may take place is available in the University IP Policy (see http://documents.manchester.ac.uk/DocuInfo.aspx?DocID=487), in any relevant Thesis restriction declarations deposited in the University Library, The University Library’s regulations (see http://www.manchester.ac.uk/library/aboutus/regulations) and in The University’s policy on Presentation of Theses

Acknowledgements

Firstly, I would like to thank my two supervisors, Professor Caroline Dive and Dr Christopher Morrow for selecting me for this PhD project and for guidance and support over the last four years. They both have helped build my confidence and courage as a young researcher. Chris has helped me learn and develop new laboratory techniques. I would also like to give thanks to the preclinical *in vivo* team (Cassandra Hodgkinson, Melanie Galvin and Stewart Brown) for their wisdom and guidance with planning *in vivo* studies, for teaching me *in vivo* techniques and for help monitoring my studies if and when I needed. Additionally I would like to thank the preclinical team (Kathryn Simpson, Kristopher Frese, Francesca Trapani, Stuart Williamson, Becky Bola and Alice Lallo) for providing a scientific environment to discuss ideas, plan experiments, guide, troubleshoot and help one another. Also I am very grateful to Aileen Jardine for help with organising meetings and various bookings during my PhD and to the lab manager Matthew Lancashire for putting up with all my demands.

The last few months of my PhD were very testing so I would like to say a special thank you to Kris and Kathryn for help with thesis writing. Also thanks to everyone that helped me proof read and edit my thesis (Aileen, Alice, Grace Hampson, Melanie, Scarlett Martindale, Stuart, my mum and sister-in law Anastasia). This was invaluable and I really appreciate the help.

I would also like to thank all my friends (Sianette, Gabrielle, Lottie, Verity, Nicole, Hayley, Kelly, Gemma, Kylie and Charlie) for being so patient with me and understanding why I had to work so much and for giving me constant support throughout my life especially as a PhD student. I would like to give an extra special thank you to my mum, dad, step dad, twin brother, big brother and sister for their support throughout my life, without them I wouldn't be the person I am today.

Finally I would like to thank Carlos for putting up with me over the last two years. For understanding why I couldn't give him the time and attention he deserved. He supported me when I was struggling. He allowed me to vent my frustrations and helped put things into perspective.

Author's contributions

This thesis has been submitted in alternative format because the work carried out amounts to three distinct chapters that have been published, submitted for publication in peer reviewed journals or written as manuscripts. The alternative format therefore offers the most appropriate structure in which to present the results of the research performed.

Chapter 3

Paper 1: *BMX Acts Downstream of PI3K to Promote Colorectal Cancer Cell Survival and Pathway Inhibition Sensitizes to the BH3 mimetic ABT-737*

Danielle S. Potter, Paul Kelly, Olive Denneny, Veronique Juvin, Len R. Stephens, Caroline Dive and Christopher J. Morrow

Published in Neoplasia 2014, DOI 10.1593/neo.131376

80% of the research in this manuscript was carried out by the first author (specifically Figures 1A, 1B, 2A, 2B, 2C, 3A, 3C, 3D, 4A, 4B, 4C, 4D, W1, W2, W4, W5, W6, W7 and W8; Tables 1, 2, W1, W3, W4, W5, W6 and W7 and writing of the manuscript). Paul Kelly and Olive Denneny helped Christopher Morrow with the remainder of the experiments. Veronique Juvin and Len R. Stephens provided a list of PH domain proteins they put together from a literature search. Christopher Morrow and Caroline Dive helped write and edit the manuscript.

Chapter 4

4. Paper 2: *Inhibition of PI3K/BMX Cell Survival Pathway Sensitizes to BH3 mimetics in SCLC*

Danielle S Potter, Melanie Galvin, Stewart Brown, Cassandra Hodgkinson, Fiona Blackhall, Christopher J Morrow and Caroline Dive

Submitted to Molecular Cancer Therapeutics 2015

100% of the research in this manuscript was carried out by the first author. Melanie Galvin provided guidance with immunohistochemistry. Stewart Brown

helped with monitoring *in vivo* experiments. Cassandra Hodgkinson provided guidance with *in vivo* experiment planning and set up. Fiona Blackhall is in charge of the patient recruitment and consent for CDX blood samples at The Christie. The manuscript was written by the first author and edited by Caroline Dive.

Chapter 5

5. Paper 3: *Mitochondrial Priming for Chemotherapy-induced Apoptosis in Chemosensitive, Chemorefractory and Relapsed, Progressive Small Cell Lung Cancer*

Danielle Potter, Jeremy Ryan, Christopher Morrow, Melanie Galvin, Cassandra Hodgkinson, Becky Bola, Lynsey Priest, Fiona Blackhall, Tony Letai and Caroline Dive

Will be submitted to Cancer Discovery 2015

80% of the research in this manuscript was carried out by the first author (the preclinical *in vivo* team carried out all of the *in vivo* cisplatin/etoposide efficacy studies on the CDX models; in vivo team, Christopher Morrow, Melanie Galvin and Cassandra Hodgkinson). The manuscript was written by the first author and edited by Caroline Dive. This paper was carried out in collaboration with Anthony Letai's group at the Dana-Farber Cancer Institute (Boston, MA, USA). Jeremy Ryan (from the Letai group) helped develop the BH3 profiling assay and taught this technique to the first author. Fiona Blackhall is in charge of the patient recruitment and consent for CDX blood samples at The Christie.

Abbreviations

= Equal to

– Minus

+ Plus

± Plus and minus

/ Divide

x Times

< Less than

> Greater than

≤ Less than or equal to

≥ Greater than or equal to

°C Degree Celsius

18S - 18S ribosomal RNA

A - Adenine

7-AAD - 7-Amino-Actinomycin

ABC - ATP-binding cassette

ACK1 - Activated CDC42 kinase 1

AGC - cAMP-dependent protein kinase, cGMP-dependent protein kinase and protein kinase C

ALL - Acute lymphocytic leukaemia

ANOVA - Analysis of variance

APAF1 - Apoptotic protease activating factor-1

APC - Adenomatous polyposis coli

ATCC - American Type Culture Collection

ATM - Ataxia-telangiectasia mutated

ATP - Adenosine triphosphate

ATR - Ataxia- and Rad3-related

BAD - BCL2-associated agonist of cell death

BAK - BCL2-antagonist/killer

BAX - BCL2-associated X protein

BBDL (BAX/BAK deficient lymphoma

BCA - Bicinchoninic acid

BCL-2 - B-cell lymphoma 2

BCL-xL - B-cell lymphoma-extra Large

BH - BCL-2 homology

BID - BH3 interacting domain death agonist

BIK - BCL2-interacting killer

BIM - BCL2-interacting mediator of cell death

BMF - BCL2-modifying factor

BMX - Bone marrow tyrosine kinase gene in chromosome X

BOK - BCL2-Related Ovarian Killer

BSA - Bovine serum albumin

BTK - Bruton's tyrosine kinase

C - Cytosine

C2 - Protein-kinase-C homology-2 domain

CA - California

Caspases - Cysteine-aspartic proteases

CD45 - Cluster of differentiation 45

CD56 - Cluster of differentiation 56

CDKI - Cyclin dependent kinase inhibitors

CRUK - Cancer Research United Kingdom

cDNA - Copy deoxyribonucleic acid

CDX - Circulating tumour cell derived xenograft

CIN - Chromosomal instability

CLL - Chronic lymphocytic leukaemia

CML - Chronic myeloid leukaemia

CO_2 - Carbon dioxide

CRC - Colorectal cancer

CT - Computed tomography

CTC - Circulating tumour cell

DAPI - 4',6-diamidino-2-phenylindole

ddH_2O – Double distilled water

Deptor - Disheveled, Egl-10, pleckstrin domain containing mTOR interacting protein

DFCI - Dana-Farber Cancer Institute

DMEM – Dubecco's modified eagles medium

DMSO – Dimethylsulfoxide

DNA - Deoxyribonucleic acid

DNA-PKcs - DNA-dependent protein kinase catalytic subunit

dNTP - Nucleotide triphosphates containing deoxyribose

EDTA – Ethylenediaminetetraacetic acid

EGF - Epidermal growth factor

EGFR - Epidermal growth factor receptor

EGTA - Ethylene glycol tetraacetic acid

EpCAM - Epithelial cell adhesion molecule

ER - Endoplasmic reticulum

ERK1/2 - Extracellular signal-regulated protein kinase 1 and 2

ES - Extensive stage

ETK - Epithelial and endothelial tyrosine kinase

FAK - Focal adhesion kinase

FBS – Fetal bovine serum

FDA - US Food and Drug Administration

FERM - Four-point-one, ezrin, radixin, moesin

FGFR1 - Fibroblast Growth Factor Receptor 1

FMO - Fluorescence minus one

FOLFIRI - Folinic acid plus 5-FU plus irinotecan

FOLFOX - Folinic acid plus 5-fluorouracil (5-FU) plus oxaliplatin

FOXO1 - Forkhead box protein O1

FOXO3 - Forkhead box protein O3

G - Guanine

GAB - GRB2 associated protein

GAP - GTPase activating protein

GAPDH - Glyceraldehyde 3-phosphate dehydrogenase

G-CSF - Granulocyte-colony stimulating factor

GEF - Guanine nucleotide exchange factor

GEMMs - Genetically engineered mouse models

GPCR - G-protein coupled receptor

GRB2 - Growth factor receptor bound protein 2

GSK-3β - Glycogen synthase kinase-3beta

GTP - Guanosine-5'-triphosphate

HBSS - Hanks' balanced salt solution

HCl - Hydrogen chloride (when is solution hydrochloric acid)

HEPES - 4-(2-hydroxyethyl)-1-piperazineethanesulfonic acid

HRK - Harakiri

HRP - Horseradish peroxidase

IAP - Inhibitor of apoptosis protein

IL - Illinois

ITK - Inducible T-cell kinase

JHU - John Hopkins University

KCl - Potassium chloride

kDa - Kilodalton

kg - Kilogram

KOH - Potassium hydroxide

L - Litre

LS - Limited stage

MA - Massachusetts

MAD - Median absolute deviation

MAPK - Mitogen-activated protein kinase

MCL-1 -Myeloid Cell Leukemia 1

mCRC - Metastatic colorectal cancer

MDM2 - Mouse double minute 2 homolog

MDR - Multidrug resistance

MDR1 - Multidrug resistance 1

MEFs - Mouse embryo fibroblasts

MES - 2-[N-morpholino]ethanesulfonic acid

mg - Milligram

MI - Michigan

mL - Millilitre

mM - Millimolar

mmol - Millimole

mm - Millimetre

M - Molar

M-MLV RT - Moloney Murine Leukemia Virus Reverse Transcriptase

MOMP - Mitochondrial outer membrane permeabilization

MOPS - 3-(*N*-morpholino)propanesulfonic acid

MRP1 - Multidrug resistance protein 1

MRP2 - Multidrug resistance protein 2

MSI - Microsatellite instability

mSIN1 - Mammalian stress-activated protein kinase interacting protein

MSKCC - Memorial Sloan-Kettering Cancer Centre

mTOR - Mammalian target of rapamycin

mTORC1 - Mammalian target of rapamycin complex-1

mTORC2 - Mammalian target of rapamycin complex-2

NCI - National Cancer Institute

ng - Nanogram

NJ - New Jersey

nM – Nanomolar

nmol - Nanomole

NRTK - Non-receptor tyrosine kinase

NSCLC - Non-small cell lung cancer

NSG - Non obese diabetic severe combined immunodeficient gamma

NT - Non-targeting

Oligo-dT - Short sequence of deoxy-thymine nucleotides

OMM - Outer mitochondrial membrane

OS - Overall survival

PBS - Phosphate buffered saline

PDGF - Platelet-derived growth factor

PDGFR - Platelet-derived growth factor receptor

PDPK1 - Phosphoinositide dependent protein kinase-1

PDX - Patient derived xenografts

PH - Pleckstrin homology

PI3K - Phosphoinositide 3-kinase

PKA - cAMP-dependent protein kinase

PKC - Protein kinase C

PKG - cGMP-dependent protein kinase

pmol - Pico moles

PRAS40 - Proline-rich AKT substrate of 40 kDa

PRR5 - Proline-rich protein 5

PtdIns - Phosphatidylinositol

PtdIns4P - PtdIns-4-phosphate

PtdIns(4,5)P2 - PtdIns-4,5-bisphosphate

PtdIns(3,4,5)P3 -PtdIns-3,4,5-triphosphate

PTEN - Phosphatase and tensin homologue deleted from chromosome 10

PUMA - p53 up-regulated modulator of apoptosis

qPCR - Quantitative or real time Polymerase Chain Reaction

RB1 - Retinoblastoma 1

RBD - RAS-binding domain

RECIST - Response evaluation criteria in solid tumors

RHEB - RAS homolog enriched in brain

Rictor - Rapamycin insensitive companion of TOR

RLK - Resting lymphocyte kinase

RNA - Ribonucleic acid

RNAi - RNA interference

rpm - Revolutions per minute

RPMI - Roswell Park Memorial Institute

RT - Room temperature

RTK - Receptor tyrosine kinase

S6 - Ribosomal protein S6

S6K - Ribosomal protein S6 kinase

SCID - Severe combined immunodeficient

SCLC - Small cell lung cancer

SDS - Sodium dodecyl sulphate

SEM - Standard error of the mean

SGK3 - Serum/glucocorticoid regulated kinase 3

SH2 - SRC Homology 2

SH3 - SRC Homology 3

siRNA - Small interfering RNA

SMAC - Second mitochondria derived activator of caspases

SMART - Simple modular architecture research tool

SOC - Standard of care

SOS - Son of sevenless

SRB - Sulforhodamine B

STAT - Signal transducer and activator of transcription

T - Thymine

TCA - Trichloroacetic acid

TFRC - Transferrin Receptor

TH - Tec homology

TNM - Staging system referring to tumour, lymph nodes and metastasis

TRAIL - Tumour necrosis factor-related apoptosis-inducing ligand

TRIS - Tris(hydroxymethyl)aminomethane

TRRAP - Transformation/transcription domain-associated protein

TSC1 - Tuberous sclerosis complex-1

TSC2 - Tuberous sclerosis complex-2

UK - United Kingdom

USA - United States of America

V – Volts

VA - Virginia

VEGF - Vascular endothelial growth factor

VEGFR2 - Vascular endothelial growth factor receptor 2

Vol - Volume

VPS34 - Vacuolar protein sorting-associated protein

WI – Wisconsin

Wt - Weight

XIAP - X-linked inhibitor of apoptosis protein

XELOX - Capecitabine plus oxaliplatin

µg - Microgram

µL - Microlitre

µm – Micrometre (micron)

µM - Micromolar

Dedication

To my nephew Aneurin Potter and niece Olivia Potter, I love you.

Chapter 1

Introduction

1. Introduction

1.1 Cancer

Cancer is a heterogeneous genetic disease caused by somatic or inherited mutations, leading to cellular transformation, uncontrolled proliferation, enhanced survival and ultimately tumour formation with capacity for invasion and dissemination to distant sites. Tumorigenesis requires cells to acquire a series of characteristics, coined the 'hallmarks of cancer' by Hanahan and Weinberg (Figure 1; (1, 2)). Cancer is a global problem with 14.1 million new cases and 8.2 million deaths a year. Lung, liver, stomach and colorectal cancers account for nearly a half of all cancer deaths. Lung cancer has a particularly poor prognosis, responsible for a fifth (the most) of all cancer deaths each year (3). As such there is an urgent need to improve or develop new therapeutic agents, determine mechanisms of acquired and innate drug resistance and identify with predictive biomarkers genetic subsets of patients who will respond to particular therapies. Due to the unmet clinical need, the focus of this thesis is on colorectal cancer (CRC) and small cell lung cancer (SCLC); which accounts for ~15% of lung cancer cases (4).

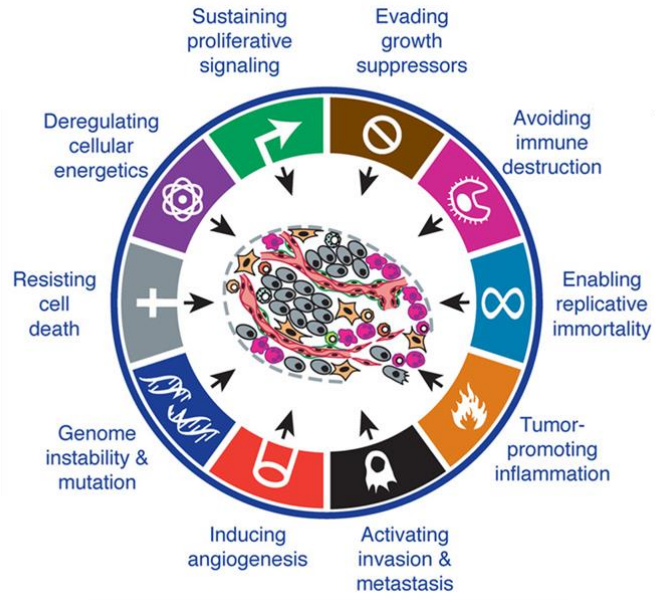

Figure 1: Hallmarks of cancer. Figure adapted from Hanahan and Weinberg (1, 2). Cancer is caused by acquired characteristics that drive tumorigenesis coined the hallmarks of cancer. The hallmarks of cancer are evolving as our understanding of cancer biology increases and to date ten hallmarks have been proposed.

1.1.1 Colorectal cancer

1.1.1.1 Colorectal cancer, staging and survival rates

During 2012, 1.4 million people were diagnosed with CRC (bowel cancer) worldwide (5). CRC is localised to the colon or rectum which constitutes the majority of the large intestine (Figure 2). CRC can be hereditary (8-15% of cases) or sporadic (85% of cases) (6) and 95 % of CRC are adenocarcinomas with the remainder being mucinous carcinomas and adenosquamous carcinomas (7). The major CRC risk factors are consumption of alcohol, red meat and processed meat as well as high whole body and abdominal fat (8). The Continuous Update Project analyses global research on diet, nutrition, exercise and weight and how this affects cancer risk and survival and estimated that 47 % of CRC could be prevented by eating and drinking healthily, exercising regularly and maintaining a healthy weight (9).

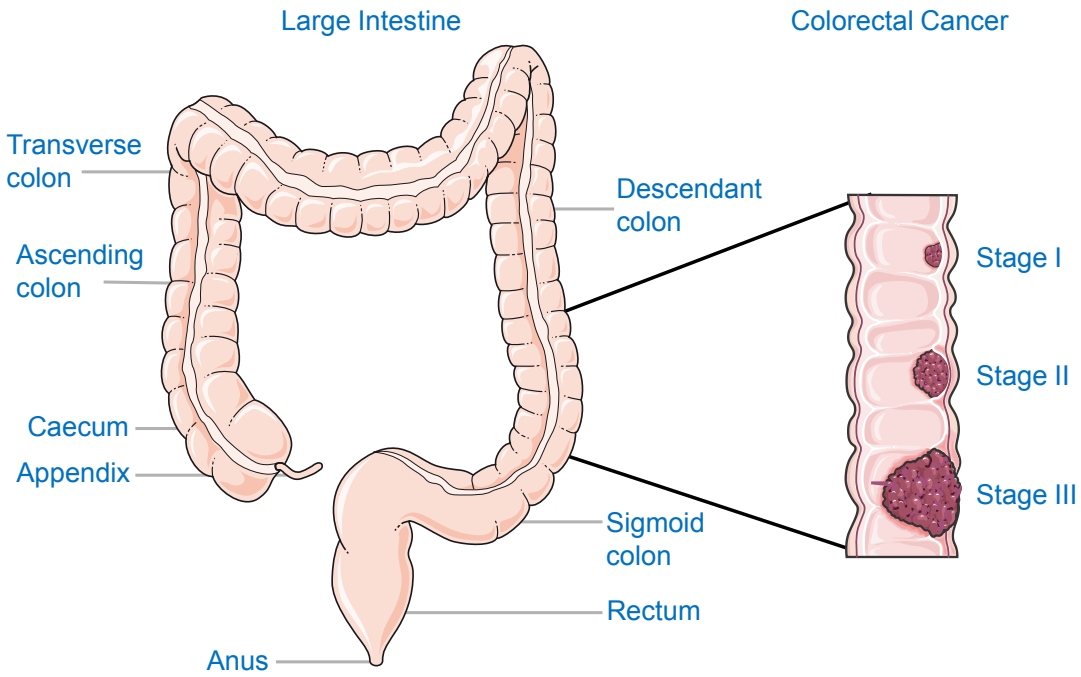

Figure 2: Schematic of the large intestine and colorectal cancer. Colorectal cancer (CRC) is located in the colon or rectum area. The colon is made up of the ascending, transverse, descending and the sigmoid colon. This diagram shows the increase staging of CRC as the tumour mass increases and spreads through the colon wall. Illustration made using Servier Medical Art.

Diagnosis of CRC is determined following colonoscopy (examines the whole colon) or sigmoidoscopy (examines the sigmoid colon) which uses an endoscope to transmit images of the colon to a camera (10). Biopsy of the tumour allows tumour staging which will determine the course of therapy (6). The common staging system used for CRC is the TNM staging system where these three factors each receives a score between 1-4 and these factors combined result in an individual stage (I-IV, with IV having the poorest prognosis) (Table 1; (6, 11)). The stage specific five year survival rate for CRC (Table 2) reveals that increased stage inversely correlates with survival. Early, low stage CRC is more curable primarily due to increased success of surgical intervention (6). Once distant metastases are present (stage IV) prognosis worsens significantly as complete tumour resection is not possible and the five year survival is ~5% (6, 12).

T = Primary Tumour	**N = Regional lymph nodes**	**M = Distant metastasis**
TX = primary tumour cannot be assessed	NX = regional lymph nodes cannot be assessed	MX = distance metastasis cannot be assessed
T0 = no evidence of primary tumour	N0 = no regional lymph node metastasis	M0 = no distance metastasis
Tis = carcinoma in situ	N1a = metastasis in one regional	M1a = distance metastasis to one site
T1 = tumour invades submucosa	N1b = metastasis in two to three regional lymph nodes	M1b = distant metastasis to more than one site
T2 = tumour invades muscularis propria	N2a = metastasis in four or six regional lymph nodes	
T3 = tumour invades into subserosa/non-peritonealised pericolic/ perirectal tissue	N2b = metastasis in seven or more regional lymph nodes	
T4a = tumour penetrates the surface of the visceral peritoneum		
T4b = tumour directly invades other organs or structure		

Table 1: Colorectal cancer staging, based on TNM classification. T describes the primary tumour and disease localisation. N describes the presence and number of regional lymph nodes affected and M describes whether metastases are present and at how many sites (6, 11).

Stage	Five year survival rate (%)
Stage I (T1, T2, N0)	97.1
Stage IIA (T3, N0)	87.5
Stage IIB (T4, N0)	71.5
Stage IIIA (T1, T2, N1)	87.7
Stage IIIB (T1, T2, N2)	75.0
Stage IIIB (T3, N1)	68.7
Stage IIIC (T3, N2)	47.3
Stage IIIC (T4, N1)	50.5
Stage IIIC (T4, N2)	27.1
Stage IV (M1a, M1b)	5

Table 2: Stage-specific five year survival rate for colorectal cancer (CRC). Stage-specific survival rate percentage for CRC, stage number is shown and in brackets the specific TNM staging (6, 12).

1.1.1.2 Colorectal cancer treatment

First line treatment for patients staged I-III is surgery. The aim is total tumour resection with adequate margins (6). High risk stage II (T4) patients and stage III (T3/4, N1/2) patients usually receive adjuvant chemotherapy in addition to surgical resection which consist of either FOLFOX (folinic acid plus 5-fluorouracil (5-FU) plus oxaliplatin) or capecitabine as a monotherapy (Figure 3). The mechanism of action for these drugs is to inhibit DNA synthesis and repair. Thus leading to accumulation of irreparably damaged DNA and eventual cell death (13-15). 5-FU is an analogue of uracil and interferes with dTMP synthesis. 5-FU is converted into a fraudulent nucleotide that can interact with thymidylate synthase (which generates dTMP) but cannot be converted into dTMP therefore inhibiting the enzyme and blocking DNA synthesis and repair. Folinic acid is used to enhance the efficacy of 5-FU by stabilising the 5-FU metabolite/thymidine synthase complex (16). Oxaliplatin forms intra-strand or inter-strand cross-links with DNA, which leads to defects in DNA replication and DNA damage; Capecitabine is a prodrug that is metabolised into 5-FU (13-15).

Surgical resection is not an option for patients with metastatic CRC (mCRC; stage IV) therefore treatment revolves around a chemotherapy regime (6). Chemotherapy typically involves FOLFOX as first line treatment followed by single agent irinotecan (a topoisomerase I inhibitor which prevents DNA from unwinding leading to inhibition of DNA replication and transcription) or FOLFOX as a first line treatment then FOLFIRI (folinic acid plus 5-FU plus irinotecan) as second line of treatment (Figure 3). Another option for these patients is XELOX (capecitabine plus oxaliplatin) as first line treatment then FOLFIRI as second line treatment (17). Radiotherapy can be used in locally advanced rectal cancer (stage II/III) primarily in the neoadjuvant setting in order to shrink the tumour before surgery, or in combination with chemotherapy (18). Radiotherapy is not the standard of care (SOC) for colon cancer because of potential serious toxicity to the small intestines and difficulties in specifically targeting the colon due to its mobility.

Targeted therapies are drugs designed to inhibit specific signalling pathways that drive tumorigenesis. The addition of such drugs to SOC (Figure 3) has led to a subtle improvement in mCRC patient overall survival (OS) (6). Treatment with monoclonal antibodies Bevacizumab (Avastin) and Cetuximab (Erbitux) which inhibit angiogenic and proliferative signalling via growth factor receptors VEGFR2 (vascular endothelial growth factor receptor 2) and EGFR (epidermal growth factor receptor) respectively were approved for use in 2004 by the FDA (US Food and Drug Administration) (14, 19). Bevacizumab binds to the VEGFR2 ligand VEGF-A, preventing activation of the pro-angiogenic receptor, reducing blood vessel formation in the tumour and starving the tumour of oxygen and nutrients (20, 21). Patients with mCRC OS was increased by 5 months and 2.2 months with the addition of bevacizumab to first line and second line therapy respectively (22). Cetuximab binds EGFR preventing binding and activation by EGF (epidermal growth factor) ligand which can be essential for CRC proliferation and survival (20). Cetuximab in combination with SOC increased OS by 2.6 months in mCRC patients (23). Single agent cetuximab is used as second line therapy for mCRC patients who were intolerant to chemotherapy and increased OS by 1.5 months (24). However, EGFR signal transduction pathway depends on activation of downstream effectors RAS/MAPK (mitogen-activated protein kinase) and PI3K (phosphoinositide 3-kinase) signalling pathways and clinical studies have already

demonstrated that cetuximab treatment is not effective in patients harbouring a *KRAS* mutation, whilst preclinical studies suggest the same may be true for patients with *BRAF* and *PIK3CA* mutations (20). Recently several other targeted therapies which inhibit the EGFR or VEGFR pathway have been approved by the FDA for treatment in CRC (Chapter 1.4.1, Table 4).

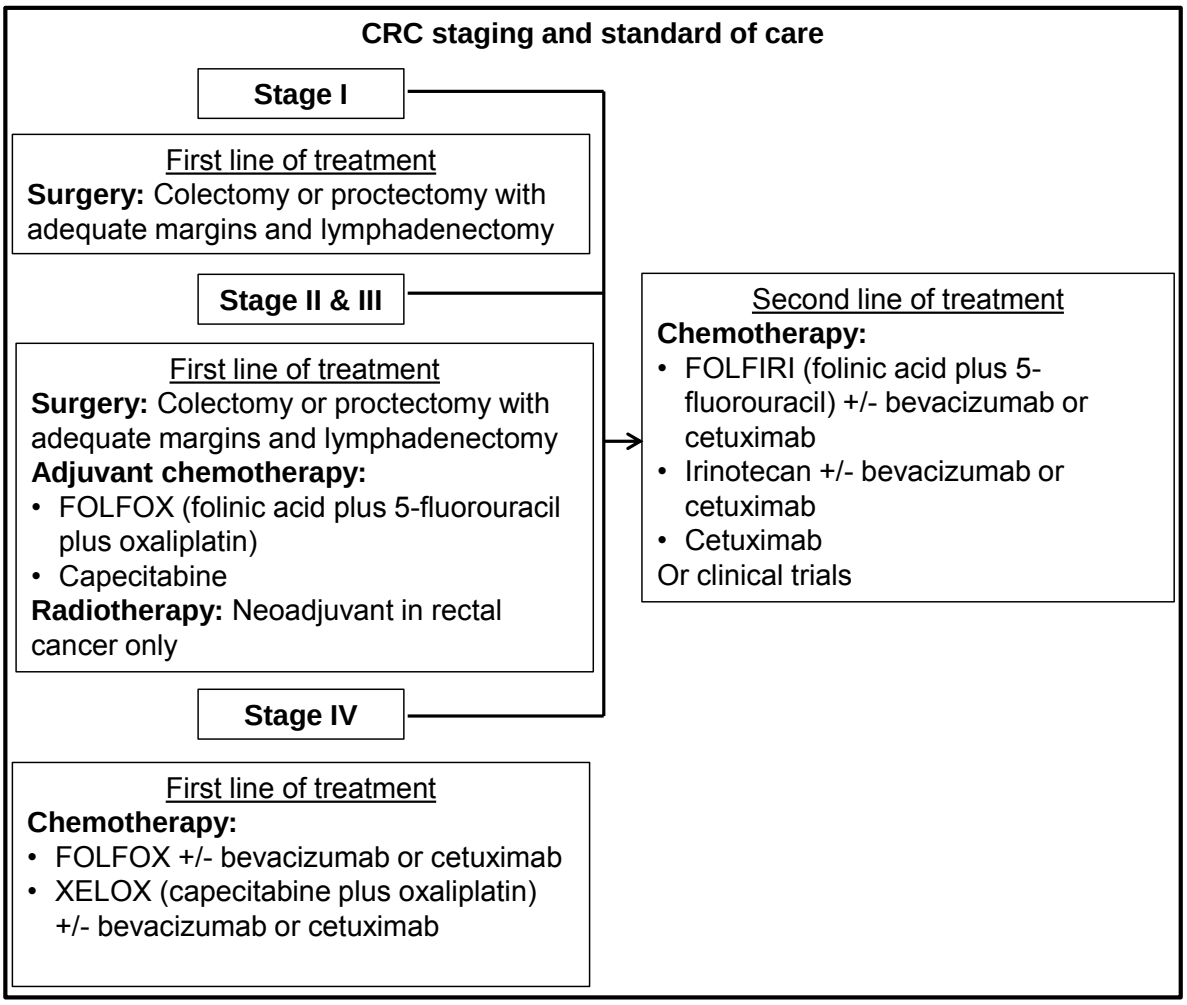

Figure 3: Colorectal stage specific first and second line therapy. Colorectal cancer treatment can involve surgery, chemotherapy, targeted therapy and radiotherapy depending on the stage and area of the cancer involved (6, 17, 20).

1.1.1.3 Multistep tumorigenesis and heterogeneity of colorectal cancer

CRC starts as a benign adenomatous polyp. CRC tumorigenesis has been described as an adenoma-carcinoma sequence of molecular events leading to cancer progression (25). Tumorigenesis is a complex multistep process with a number molecular events driving tumour formation that usually proceeds over a

period of years to decades. On average the transition from adenoma to carcinoma takes 8-12 years (6, 26, 27). Fearon and Vogelstein (26) proposed a linear tumorigenic model for CRC in 1990 (Figure 4) in which an initial inactivation of a tumour suppressor gene occurs followed by at least four more genetic mutations in oncogenes and/or tumour suppressors (26). Since its inception this basic model has been extended with knowledge gained about acquisition of specific mutations leading to tumour progression such as the hallmarks of cancer (Figure 1; (1, 2) which drive tumorigenesis. The initial mutation is rare but once it occurs, genomic instability can jeopardises the integrity of the genome increasing the likelihood of future mutations. A common initial mutation found in CRC is inactivation/loss of *APC* (adenomatous polyposis coli). Loss of *APC* been reported in 80 % of CRC cell lines (28). APC forms a destruction complex with other proteins such as GSK-3β (glycogen synthase kinase 3-beta) and Axin that negatively regulate β-catenin. β-catenin is a transcription factor/cell-cell adhesion molecule that drives the proliferative Wnt signalling pathway (29). Following the initial mutation, it is not the order of mutations that drive tumorigenesis but the accumulation of mutations which convey the various hallmarks of cancer (1, 2, 26) (Figure 4).

Common early mutations in CRC that drive tumorigenesis from a small to intermediate adenoma (25) include mutually exclusive activating mutations of the oncogenes *KRAS* (34% carcinomas and none in hyperplastic polyps) or *BRAF* (5.1% adenocarcinoma and 33% hyperplastic polyps), which activate the MAPK signalling pathway (Figure 4; (30)). Other mutations that drive tumorigenesis in CRC are activating mutations in PIK3CA causing activation of the PI3K pathway (PIK3CA mutations, pertinent to this thesis, will be discussed in more detail later), loss of the tumour suppressor p53 and inactivation of the TGFβ (transforming growth factor-β) signalling pathway (31, 32).

CRC is a highly heterogeneous disease due to this large variety and combination of molecular aberrations which occur during tumorigenesis as a result of genomic instability. CRC can differ in clinical presentation, molecular characterisation and prognosis. Even patients with clinically similar tumours can have a dramatically different response to therapy and OS, highlighting the problem of such a heterogeneous disease. CRC heterogeneity is further increased by the

involvement of factors such as tumour microenvironment, immune response or the intestinal microbiome (33, 34). CRC can be subtyped depending on molecular characteristics and this influences prognosis (Figure 5; (34)).

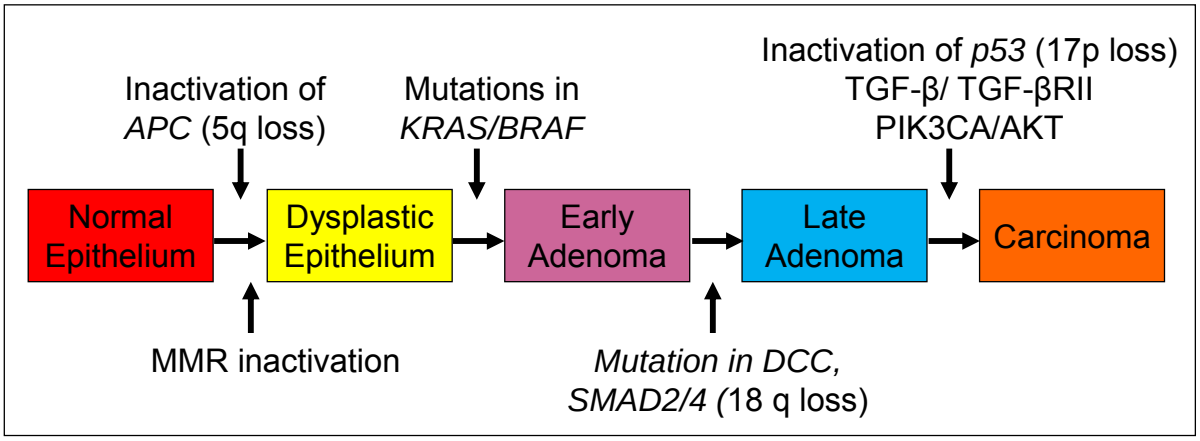

Figure 4: The Genetic Model for Tumorigenesis in Colorectal Cancer (CRC). Proposed by Fearon and Vogelstein (26), CRC tumour progression proceeds by the multistep accumulation of mutations in tumour suppressor genes and oncogenes. Normal colon/rectal epithelium acquire either an inherited or sporadic mutation likely to be in tumour suppressor genes such as *APC* (Adenomatous polyposis coli) gene or the genes coding the proteins involved in the mis-match repair (MMR) pathway. This can result in genomic instability which compromises the integrity of the genome resulting in further mutations over time. Mutation in oncogenes such as *KRAS/BRAF* causes progression to a larger more dysplastic adenoma tumour through clonal expansion. Further loss of chromosomal segments can be found, this is common in 5q, 17q and 18q regions of the genome and cause tumour progression to carcinoma. The accumulation rather than order of these mutations seem to be of importance in CRC tumorigenesis (26).

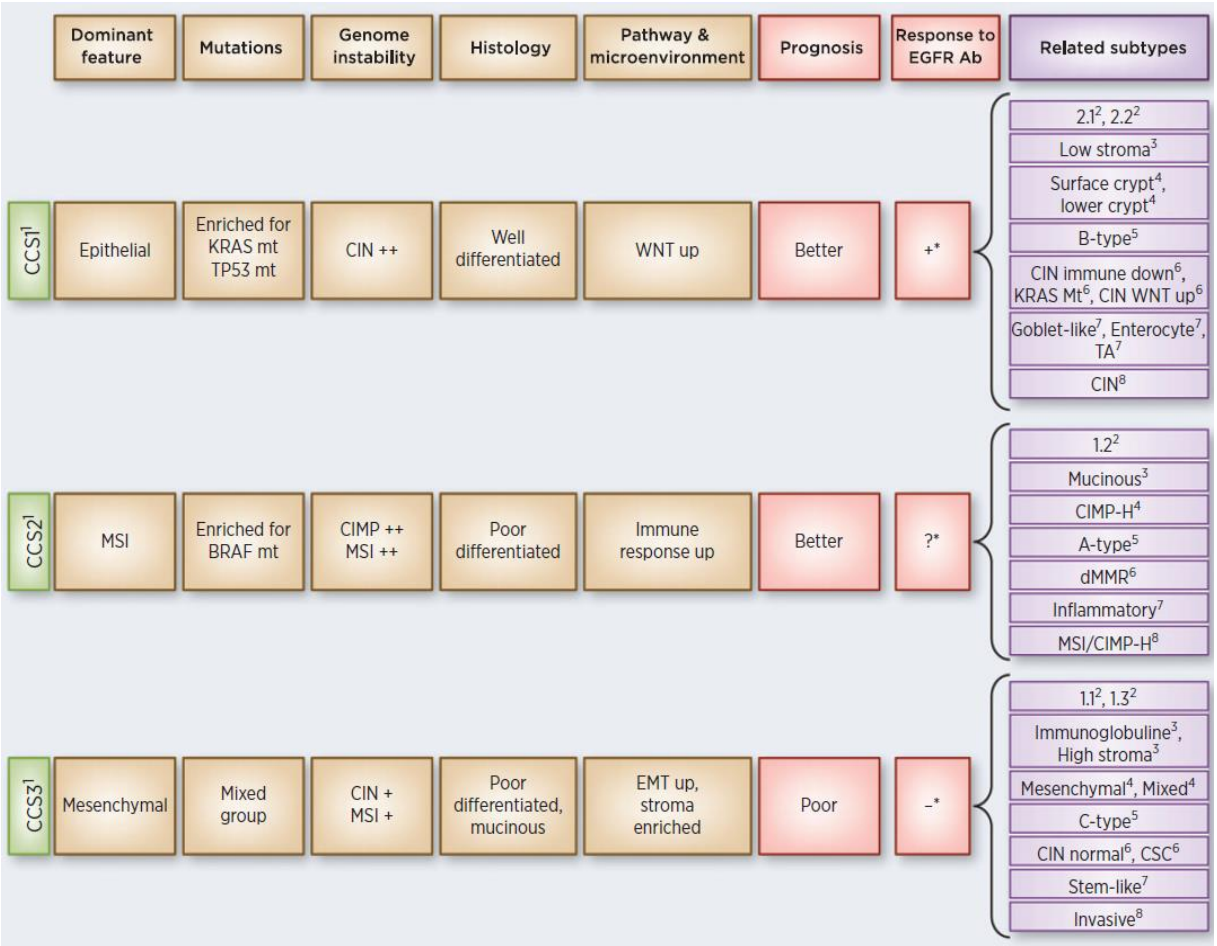

Figure 5: Molecular classification of colorectal cancer (CRC). Figure taken from Linnekamp *et al*. Molecular characteristics (shown in orange) can be sub-divided into groups containing dominant features (epithelial, microsatellite instability (MSI) or mesenchymal), mutations (*KRAS*, *BRAF* or mixed), genomic instability (chromosomal instability (CIN), MSI or mixed) and histology (well differentiated, poor differentiated or poor differentiated mucinous). CCS1 are more sensitive to EGFR targeted therapies such as cetuximab. CCS1 and CCS2 have a better prognosis compared to CCS3 CRC subtype (34).

1.1.2 Small Cell Lung Cancer (SCLC)

The CRUK Lung Cancer Centre of Excellence was established in 2014 at Manchester and UCL (University College London). This created a collaborative, integrated environment where lung cancer research can prosper. Professor Dive is the Manchester centre lead and over the previous years there has been an increased focus of Professor Dive's group on SCLC. Once I discovered that BMX (bone marrow tyrosine kinase gene in chromosome X) acted downstream of PI3K (Phosphoinositide 3-kinase) to promote CRC cell survival (Chapter 3) I wanted to investigate whether this mechanism was used in other cancer types. This lead to the discovery that BMX was expressed at relatively high levels in SCLC cell lines compared to other cancer types and that BMX acted downstream of PI3K to promote survival in SCLC cells (Chapter 4). This was an exciting find because of the focus of our group on SCLC and lead to my transition from CRC to SCLC.

1.1.2.1 Small Cell Lung Cancer, Staging and Survival

The two major histological types of lung cancer are non-small cell lung cancer (NSCLC) and SCLC. Lung cancer accounts for ~13% of newly diagnosed cases of cancer worldwide (35) with NSCLC accounting for ~85% of cases and SCLC accounting for the remainder (4). SCLC is characterised by small cells (generally less than the diameter of three small resting lymphocytes), scant cytoplasm, absent or faint nucleoli and high mitotic rate. SCLC is of neuroendocrine origin (36) and expressing neuroendocrine markers such as chromogranin, synaptophysin and CD56 in 90% of cases (37). Patients with SCLC are commonly elderly and either heavy or former smokers (38). Tobacco smoking is a major risk factor in SCLC that increases with intensity and duration but in a few rare cases SCLC patient have never smoked (39). Other risk factors include occupational or environmental exposures to uranium, radon, beryllium and silica for example (40).

SCLC is classified as either limited stage (LS, confined to one hemithorax; TNM stage I-III; Figure 6) or extensive stage (ES, more widespread; TNM stage IV; Figure 6). SCLC is a highly aggressive disease with ~70% of patients diagnosed with ES disease (41). Due to this advanced stage at diagnosis most patients have compromised lymph nodes and distant metastasis (42) and only 5% of patients

are eligible for surgery (43). Without any treatment the median OS of SCLC patients is 2-4 months (44). First line treatment is platinum based chemotherapy such as cisplatin or carboplatin combined with etoposide and in some cases sequential or concomitant lung radiotherapy (Figure 7; (45)). Cisplatin and carboplatin forms intra-strand or inter-strand crosslinks with DNA which inhibits DNA synthesis and repair thus leading to accumulation of irreparably damaged DNA and eventual cell death (46). The enzyme topoisomerase II is needed to unwind DNA during replication and etoposide is a topoisomerase II inhibitor which prevents DNA from unwinding leading DNA breaks (47). LS SCLC patients have a median OS of 15-20 months and ES SCLC patients have a median OS survival of 8-13 months following first and second line treatment (48). Brain metastases are common and as SOC chemotherapy is unable to cross the blood brain barriers all patients with brain metastases are offered prophylactic cranial irradiation (37). The five year survival rate for patients with LS SCLC are 31%, 19% and 8% for stage I, II and III respectively and for ES (IV) is 2% (49).

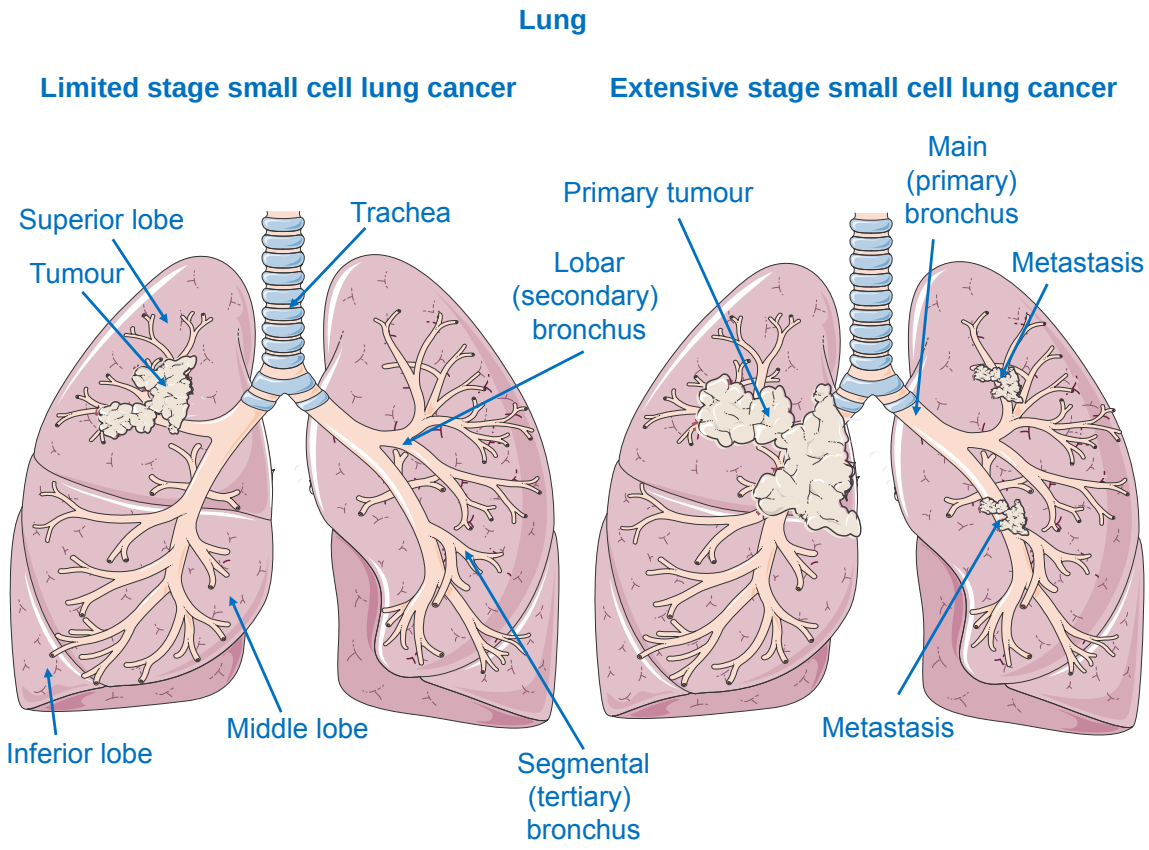

Figure 6: Limited and Extensive stage Small cell lung cancer (SCLC) schematic. Limited stage SCLC confined to one hemithorax (left) and extensive stage SCLC (right) that has metastasised and is more widespread. The lungs lobes and primary, secondary and tertiary bronchus are labelled. Illustration made using Servier Medical Art.

1.1.2.2 Chemotherapy resistance in small cell lung cancer

SCLC tumours can be classified as either chemo-sensitive (complete or partial response to therapy lasting greater than 90 days), chemo-resistant (partial response to therapy lasting less than 90 days after therapy) or refractory (progressive disease throughout therapy; (37)). Response to chemotherapy is determined according to RECIST (Response Evaluation Criteria In Solid Tumors) criteria. A complete response is determined when all lesions have disappeared, partial response is determined when at least 30% decrease in lesion is observed and progressive disease 20% increase in lesions is observed (50). SCLC is unique amongst solid tumours in that it is often exquisitely sensitive to first-line chemotherapy but this is followed by rapid relapse, potentially due to selection of pre-existing chemo-resistant cells (51). Patients whose tumours were chemo-sensitive to first-line therapy receive the same treatment as second line therapy. However, patients with resistant or refractory tumours will receive a different chemotherapy regimen in second line, which in the UK is topotecan (Figure 7; (37)).

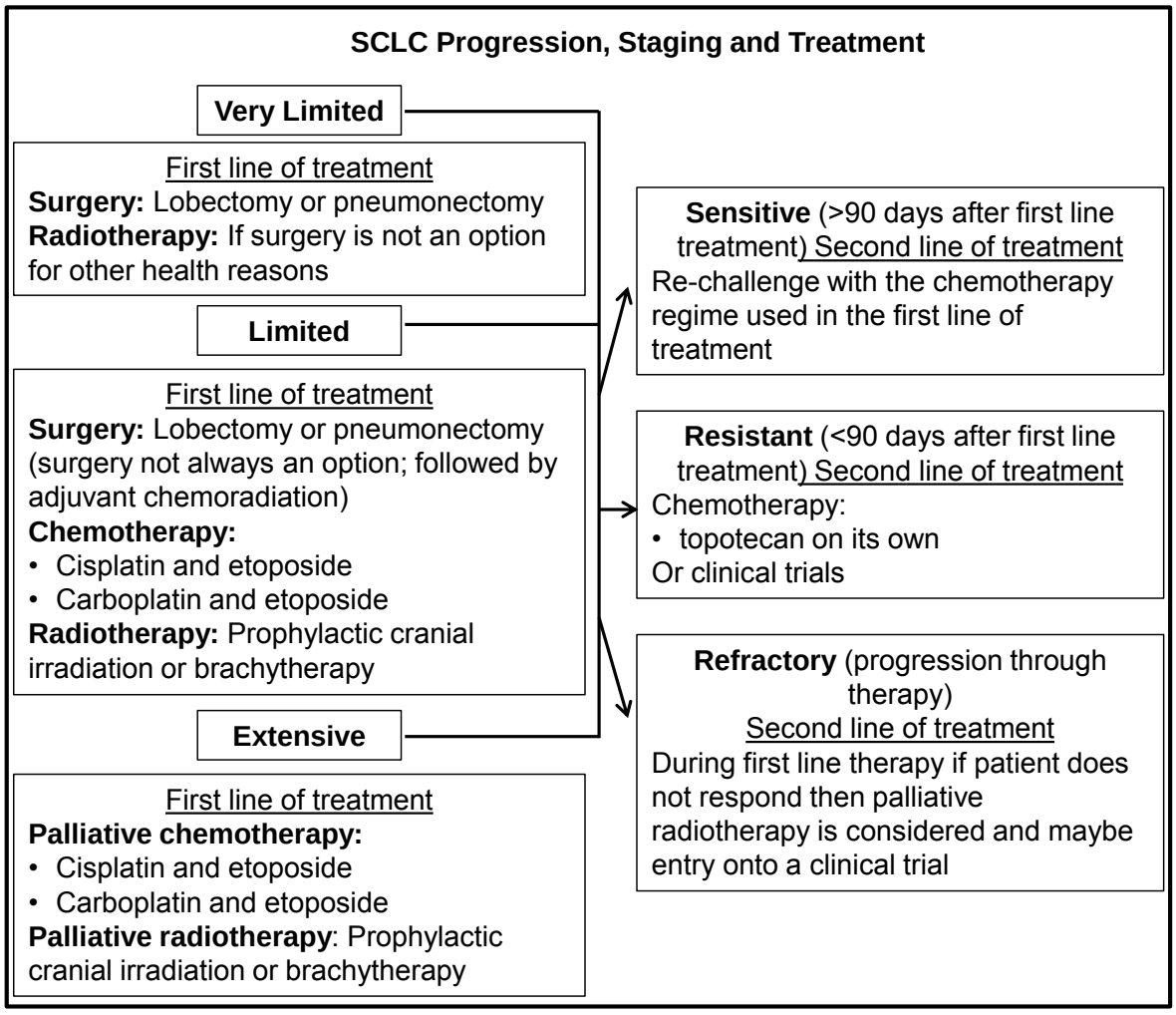

Figure 7: Small cell lung cancer progression and therapy. As small cell lung cancer (SCLC) progresses the staging increases and treatment can change. This figure summarises the current first line treatment for patients with SCLC depending on staging and the second line treatment depending on whether the tumour is sensitive, resistant or refractory to chemotherapy (37)

Chemotherapy resistance could be due to a number of factors such as blood flow and drug delivery to the tumour (effects amount of active drug reaching the tumour), extracellular matrix components (protect/prevent drug from reaching the tumour efficiently (52)), DNA repair (such as defects in mis-match repair pathway causing increased tolerance of DNA damaging agents (53)) and reduced apoptotic response (which is investigated in detail in this thesis) (52, 54). The intrinsic apoptotic pathway is regulated by the Bcl-2 family of proteins which are made up of anti-apoptotic members and pro-apoptotic members. Apoptosis is dependent on activation of caspases (cysteine-aspartic proteases). The caspase family are proteases that cleave proteins within the cell resulting in apoptosis (55). Apoptosis

and the Bcl-2 family will be discussed in detail in Chapter 1.4. Cisplatin treatment activates the apoptotic pathway in response to the increase in DNA damage caused by cisplatin intra- and inter-crosslinks. Many cisplatin resistance cancer cell lines exhibit downregulation of the pro-apoptotic Bcl-2 family members such as pro-apoptotic BAX and upregulation of the anti-apoptotic Bcl-2 family members such as BCL-2 (54) leading to a higher ratio of anti-apoptotic proteins present which buffer pro-apoptotic signals in response to cisplatin treatment therefore reducing cisplatin efficacy. IAPs (inhibitor of apoptosis proteins) inhibit pro-apoptotic proteins released from the mitochondria in response to pro-apoptotic signals (56). Overexpression of the IAPs such as XIAP (X-linked inhibitor of apoptosis protein) that inhibit caspases (56) has also been associated with cisplatin resistance and inhibition of XIAP increases cisplatin sensitivity in cancer cells (57, 58). Drugs directly targeting components of the apoptotic pathway will be discussed in Chapter 1.4.

Multidrug resistance (MDR) can hinder chemotherapy response whereby tumour cells that have been exposed to one cytotoxic agent can acquire resistance to multiple unrelated drugs (59). This usually occurs via upregulation of cell membrane transporters such as of MDR1 (multidrug resistance 1 also known as P-glycoprotein) which is from the family of ABC (ATP-binding cassette) transporters which pumps cytotoxic drugs out of the cancer cell therefore lowering the intracellular drug concentration. This can also occur intrinsically in some cancers with no prior exposure to cytotoxic agents. MRP1 (multidrug resistance protein 1) and MRP2 are the drug pumps responsible for efflux of etoposide and cisplatin, respectively (59). Biricodar (Vertex Pharmaceuticals) is a MDR1 inhibitor that was used in the clinical setting in SCLC. The rationale was that inhibition of MDR1 would reduce chemotherapy efflux out the cell and therefore increase the efficacy of the chemotherapy agent. Unfortunately this produced disappointing phase II clinical trial results highlighting the complexity of chemotherapy resistance (60).

SCLC patients have a high response rate of 70-90% to first line therapy (61, 62) but only 20% will respond to second line chemotherapy rechallenge, if they are able to tolerate further treatment (62). In 95% of SCLC cases, patients who

respond to first- and second-line therapy will eventually succumb to their disease. A greater understanding of the mechanisms of resistance is needed in order to discover new ways to target this disease and increase progression free survival (PFS) and OS (63). Moreover between 10-20% of LS and 15-30% of ES patients are considered resistant or refractory to first line chemotherapy (48, 61). Chemotherapy is likely to create a selection pressure which drives clonal expansion of resistant cells (64) and tumours may use a number of resistance mechanisms to escape cytostasis or cytotoxicity, highlighting that resistance is multifactorial (65).

1.1.2.3 Small cell lung cancer heterogeneity

Four recent comprehensive studies have described the genetic characterisation of SCLC tumour samples and cell lines (66-69). This revealed the high mutation rate (5.5-7.4 protein-changing mutations per million base pairs) (66, 67) and high degree of genetic diversity in SCLC compared to other cancer types (70). The high mutation rate is consistent with DNA damage caused by tobacco smoke carcinogens which induce a high frequency of G to T transversions and G to A and A to G transitions (71). The high degree of heterogeneity in SCLC was confirmed when ~8000 protein coding mutations were identified (30 % of total mutations identified) and only 22 were co-expressed in multiple SCLC tumours (67). Consequently identifying novel anti-cancer strategies for the treatment of SCLC patients remains extremely challenging.

The major genetic aberrations in SCLC involve the tumour suppressors *TP53* (mutated in 75-90% of cases; (72)) and *RB1* (Retinoblastoma 1; lost in 60-90% of cases; (4, 73)). Furthermore, amplification of *MYC* family genes was found to be mutually exclusive in 18-31% of SCLC samples (72) and amplification or overexpression of SOX2 was identified in 27 % of SCLC tumours (67), both are transcription factors. The transmembrane receptor *NOTCH* family genes are mutated in 25 % of SCLC (68). One genomic study showed PI3K pathway components were mutually exclusively altered in 36 % of SCLC patients. PI3K is a lipid kinase that regulates proliferative and survival pathway and will be discussed in detail in section 1.2 (69). Furthermore, 2-5 % of SCLC tumour samples have

inactivating mutations in *PTEN* (phosphatase and tensin homologue deleted from chromosome 10), the phosphatase that negatively regulates the PI3K pathway (74-76). Alterations in the PI3K signalling pathway were mutually exclusive with amplification of MYC family members (69) suggesting that PI3K pathway mutations are drivers in some SCLC and making it an attractive drug target (69).

Intra-tumour heterogeneity can occur on a genetic, phenotypic and functional level leading to the creation of diverse subclones (Figure 8). Adding to this complexity is the effect of the tumour microenvironment which can influence tumour behaviour by specific effects on certain tumour subpopulations (77). An example of this could be physical separation of a subclone by blood vessels creating differing environments within the tumour (Figure 8, subclone 2). Genetically similar subclones can function differently (Figure 8, *TP53* mutation found in subclone 1 (chemo-resistant) and subclone 3 (chemo-sensitive)). Genetically diverse subclones may function similarly (Figure 8, subclone 1 (*RB, PIK3CA, SOX2* mutations) and subclone 2 (*TP53, MYC, NOTCH* mutations) are both chemo-resistant (78)). Inter-cellular genetic heterogeneity may also be observed when a subclone shows diversity. This could be due to genomic instability, and could result in the emergence of a new tumour subclone (Figure 8, subclone 2 shows intercellular genetic diversity; (78)).

While 80-90% of LS and 70-80% of ES patients initially respond to therapy, virtually all will eventually relapse (48, 62). Inter-tumour heterogeneity of SCLC (Figure 8) makes the one size fits all treatment option highly unlikely to be successful (as shown by the eventual relapse to SOC in SCLC). The rapid rate of relapse and subsequent insensitivity to chemotherapy in the majority of SCLC cases highlights that chemotherapy resistance, where heterogeneity is likely to be a key factor, is a major problem in the treatment of SCLC (79). Personalised medicine for such a heterogeneous cancer is a major challenge, especially due to the lack of predictive biomarkers in SCLC and until recently a lack of druggable drivers of the disease.

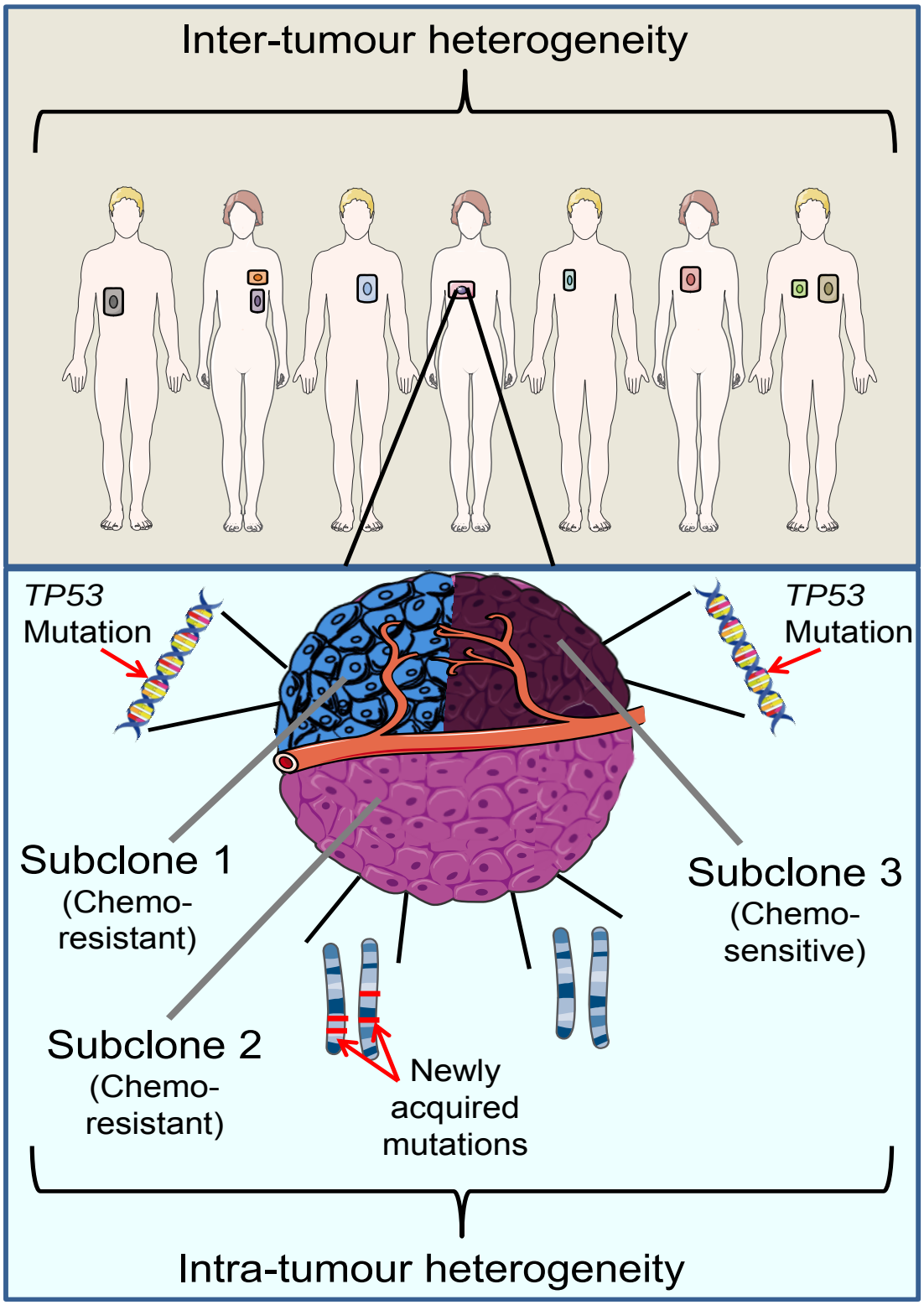

Figure 8: Inter-tumour and intra-tumour heterogeneity in small cell lung cancer. Small cell lung cancer displays inter-tumour heterogeneity between patients; intra-tumour heterogeneity between tumour subclones and inter-cellular genetic heterogeneity within the same subclone (subclone 2 newly acquired mutations in a cell). Illustration made using Servier Medical Art.

1.1.2.4 Preclinical models of small cell lung cancer

Only 5 % of SCLC tumours are surgically resected, (80) and although a diagnostic biopsy specimen is obtained from all patients, these specimens contain very few tumour cells. Specimens can be taken from the primary tumour, lymph nodes or any metastatic site by bronchoscopic biopsy or fine-needle aspiration (37) and often results in limited or no tumour tissue available after diagnosis is made for subsequent research purposes. Tumour samples are also often necrotic hampering molecular analyses. This lack of quantity and/or quality of tumour sample availability has limited our understanding of SCLC biology. Researchers are therefore reliant on preclinical models of SCLC such as cell lines and animal models to help further our understanding of disease progression and resistance to therapies. Although there are many advantages to using such resources, studies must be conducted with an awareness of the limitations of each SCLC preclinical models (81-86).

Historically, SCLC cell lines have been the 'workhorse' tools to enhance our understanding of SCLC and provide a cheap, accessible model to learn about the nature of SCLC such as molecular abnormalities and mutational profiles of the disease (66, 67). SCLC cell lines available represent all the genetic features discovered so far in patients but the disadvantage is they lack the degree of heterogeneity, do not readily mimic disease progression and do not model the tumour microenvironment. SCLC cell lines can be implanted into an immunocompromised mouse to produce xenograft (also referred to as secondary xenograft) models to study SCLC and treatment *in vivo*, as can Patient Derived Xenografts (PDX). However, cell lines, xenografts and PDX derived from the same patient sample had significant differences in gene expression (86) which suggests a possible reason for lack of efficacy in clinic for various novel agents tested in SCLC cell lines and xenografts with promising results. For example, the BH3 mimetics ABT-737 and Navitoclax (see Chapters 1.3.7 for more details) proved efficacious in cell lines (87) and cell line xenografts (88) but efficacy was not observed in the clinic (89) suggesting that important changes in gene expression cannot be rescued once lost due to cell culture conditions which may determine the efficacy of therapies.

Genetically Engineered Mouse Models (GEMMs) of SCLC have proven invaluable for studying SCLC development and progression because they provide a tumour microenvironment that can more closely recapitulate human SCLC than cell lines and cell line xenografts. Because *TP53* mutation and *RB1* loss are found in the majority of SCLC, a GEMM was developed containing a double conditional knock-out of *TP53* and *RB1* in mouse pulmonary epithelial cells (84). The inactivation of both genes led to the development of SCLC that resembled human SCLC within approximately 12 months and these tumours were highly aggressive and metastatic (81). Triple knock-outs additionally harbouring a conditional *p130* or *PTEN* knock-out allele in the *TP53/RB1* null background were subsequently developed which significantly reduced the latency phase for SCLC development (90). Furthermore the triple knock-out of *TP53*, *RB1* and *PTEN* deletion in neuroendocrine cells increased metastasis suggesting PTEN is a driver mutation in SCLC (82, 91). SCLC GEMMs have proved useful in studying novel therapies such as the CDK 7 inhibitor, THZ1 (92) but GEMMs are costly and time consuming to produce and thus makes routine drug screening unfeasible. Additionally, the high degree of heterogeneity in human SCLC is not fully recapitulated in GEMMs of SCLC and the absence of tobacco mutagens, known to be key factors in the development of SCLC means that GEMMs do not represent the true nature of SCLC genetic instability and complexity and therefore other preclinical models should be considered (93, 94).

As mentioned previously, PDX models offer an opportunity to study SCLC and have been found to retain important biological properties of the primary tumour such as gene amplification (95), gene expression (96) and cancer ‘stem’ cell or more accurately, tumour initiating biology (97, 98). SCLC PDX models have been successful in studying novel drug combinations (84) but unfortunately in addition to the lack of primary SCLC source material and the time consuming and labour intensive nature of this approach, evidence suggests that PDX models acquire new genomic changes, a faster growth rate and nuclear pleomorphism causing them to differ significantly from their primary tumour (99, 100). However SCLC PDXs may be the most appropriate preclinical tool to study SCLC disease progression and therapies as they capture the heterogeneity of the tumour (84-

86). PDX models are not suitable as true avatars because of the fast disease progression of SCLC and thus they cannot be used in co-clinical trials (84-86).

SCLC CDX (CTC (circulating tumour cell) derived xenograft) models have been recently developed in the Dive Laboratory (83) and offer an attractive alternative to PDX without the restrictions of challenging patient biopsies. CDX are developed using CTCs enriched from the blood of a SCLC patient. Enriched CTCs from a single patient are implanted subcutaneously into an immunocompromised mouse and in approximately 50% of cases the mice go on to develop tumours which can be readily passaged *in vivo*. CDX closely mimic the donor patient pathology and response to chemotherapy and highlights the high degree tumorigenicity of CTCs in SCLC (83): as few as 10 disaggregated CDX cells can rederive the tumour (Dive Laboratory submitted data). One of the main advantages of CDX compared to PDX is the ability to generate models serially at any stage of disease progression where resection or routine biopsy is not performed, without major deviation from standard clinical practice because only minimally invasive blood samples, routinely obtained are required.

1.2 Phosphoinositide 3-kinase (PI3K) Signalling Pathway

The focus on this thesis is the impact of targeting the PI3K pathway in CRC and SCLC in combination with Bcl-2 family targeted drugs.

1.2.1 Classification of Phosphoinositide 3-kinases

The Phosphoinositide 3-kinases are a conserved family of lipid kinases that catalyse the phosphorylation of the D-3 hydroxyl position on the inositol ring of phosphatidylinositol (PtdIns) species such as PtdIns, PtdIns-4-phosphate (PtdIns4P) and PtdIns-4,5-bisphosphate (PtdIns(4,5)P2), acting as a signal transducer to pathways involved in cellular metabolism, cytoplasmic rearrangement, proliferation, polarity and survival (32, 101). The PI3K family is made up of eight isoforms split into three classes (class I, II and III; Figure 9) depending on their structure and substrate specificity (102, 103). Class I PI3K preferentially utilise PtdIns(4,5)P2 as a substrate, producing PtdIns-3,4,5-triphosphate (PtdIns(3,4,5)P3). This class is further divided into class IA and IB depending on how they are activated. Class IA PI3K are activated by RTKs (receptor tyrosine kinase) or by certain oncogene products such as the monomeric G-protein, RAS. This class of PI3K are the focus of this thesis. Class IB are activated by GPCRs (G-protein coupled receptors), through interaction with trimeric G-proteins via the Gβγ subunit (31, 32).

Class II PI3K preferentially binds to the substrates PtdIns and PtdIns4P and consists of three isoforms that can be activated by RTKs, cytokine receptors and integrins. Class III PI3K consists of VPS34 (vacuolar protein sorting-associated protein) which is an essential regulator of vesicle transport that signals via mTOR (mammalian target of rapamycin). VPS34 uses PtdIns as a substrate producing PtdIns3P which is localised to the early and late endosome (103).

The PIKKs (phosphoinositide kinase related kinases) are a group of kinases closely related to PI3K family and consist of protein kinases that have evolved from a common ancestor to lipid PI3K. This includes proteins such as ATM (ataxia-telangiectasia mutated), ATR (ataxia- and Rad3-related), DNA-PKcs (DNA-

dependent protein kinase catalytic subunit), mTOR and TRRAP (transformation/transcription domain-associated protein; (104)).

1.2.2 Class IA PI3K structure

PI3K class IA are the most thoroughly studied of the lipid kinases and have been shown to be important in tumorigenesis (103). They are heterodimers made up of a p110 catalytic subunit and p85 regulatory subunit (Figure 9). The p110 catalytic subunit has three isoforms, p110α, p110β and p110δ, encoded by the *PIK3CA, PIK3CB* and *PIK3CD* genes respectively. These isoforms are highly homologous and share five distinct evolutionarily conserved domains. The p110 catalytic subunit contains a p85 binding domain that interacts with p85 regulatory subunit forming a heterodimer (105). The RAS binding domain in the p110 catalytic subunit mediates PI3K activation via the GTPase RAS (Figure 9; (106)). The catalytic domain catalyses the transfer of the gamma phosphate from adenosine triphosphate (ATP) to the OH group at the D-3 position of the inositol ring (31).

The p85 regulatory subunit consists of three isoforms, p85α (plus splice variants p55α and p50α), p85β and p55γ (Figure 9) that are encoded for by the *PIK3R1, PIK3R2* and *PIK3R3* genes respectively (107). All the p85 regulatory subunits contain two SH2 domains that recognise specific phosphorylated tyrosine (pY) residues (Figure 9). RTKs are activated by their appropriate ligand causing autophosphorylation and/or transphosphorylation of specific tyrosine residues within the cytoplasmic domain of the receptor which produces a docking site for binding to the SH2 domain in the regulatory subunit (Figure 9). The regulatory subunit acts as an adaptor that co-localises the catalytic subunit and substrate to the plasma membrane (31). The p85α and p85β isoforms both contain an SH3 domain that is involved in protein-protein interactions with proline rich domains and a breakpoint cluster region (BCR) homology domain (BH). The SH3 and BH domains have negative regulatory functions towards the catalytic subunit (108). P85 binds the p110 catalytic domain via the p110 binding domain (also known as inter-Src homology 2 (iSH2) domain (105)) recruiting the PI3K heterodimer to the plasma membrane (Figure 9; (31)).

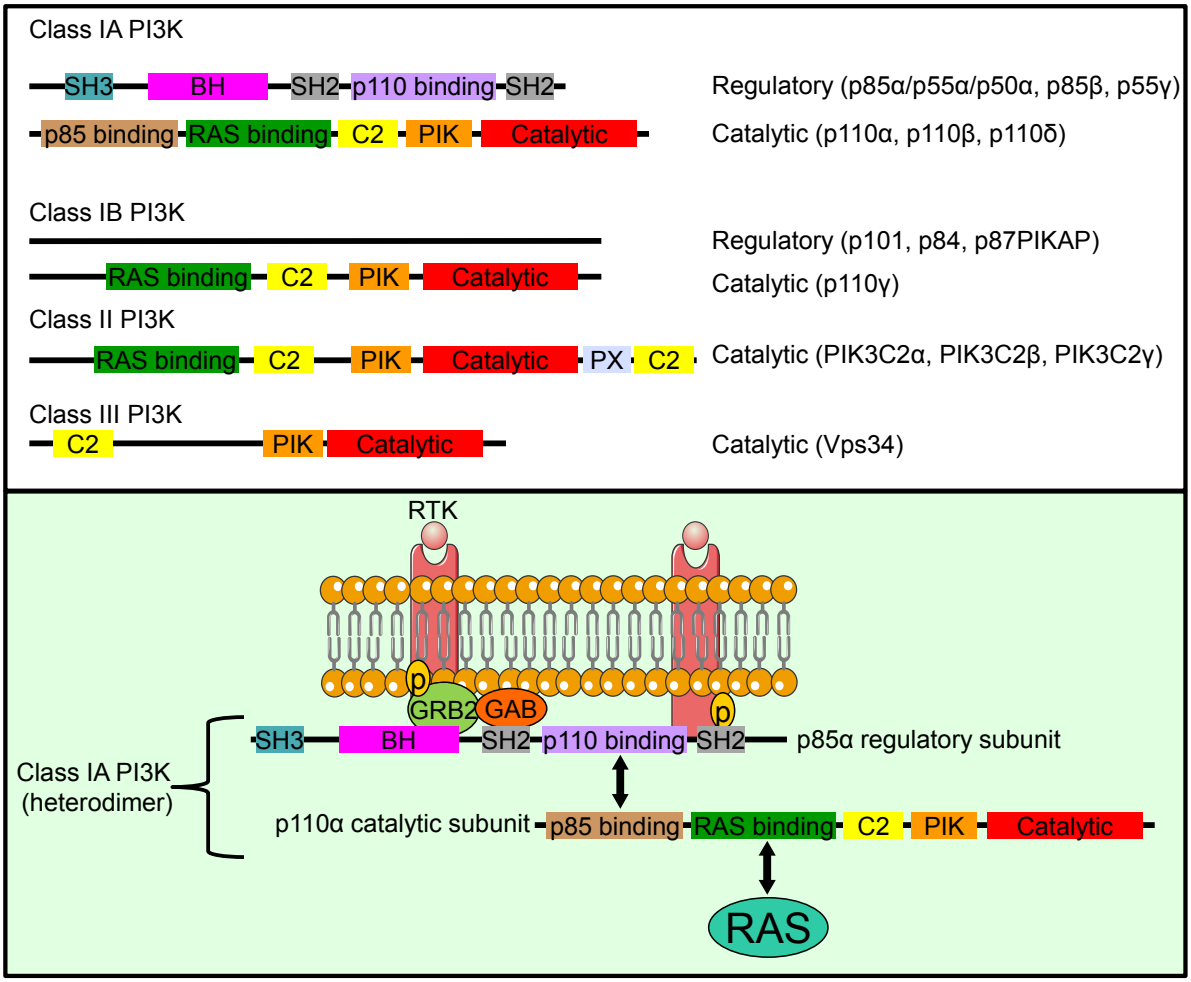

Figure 9: Phosphoinositide 3-kinase family classification. The three main classes of Phosphoinositide 3-kinase (PI3K) are class 1A, class 1B, class II and class III. This is based on their substrate specificity towards phosphoinositides and structure. Class IA are made up of a catalytic domain, p110 that binds the regulatory domains p85 via the p85 binding domain forming a heterodimer. Monomeric G protein RAS binds p110 catalytic subunit via the RAS binding domains (103). p85 binds GAB (GRB2 associated protein) via the SH2 domain. Illustration made using Servier Medical Art.

1.2.3 Class IA PI3K activation and negative regulation

Class IA PI3K are activated by three independent pathways, all of which involve binding of a ligand to an RTK such as EGFR, insulin receptors (for example insulin-like growth factor-1 receptor) or PDGFR (platelet-derived growth factor receptor). In unstimulated cells, the PI3K heterodimer is located in the cytoplasm where via intramolecular interactions the regulatory subunit inhibits the catalytic subunit from accessing its substrate. When a growth factor such as EGF binds to the extracellular domain of EGFR it induces EGFR dimerisation and autophosphorylation of the cytoplasmic domain of several tyrosine residues which

allows SH2 domain containing proteins to interact (Figure 9). The SH2 domains in the regulatory subunit of class IA PI3K recognise a specific phospho-tyrosine motif (YXXM, where X is any amino acid) and binds with high affinity thus interfering with autoinhibitory intramolecular interacting and activating the catalytic subunit (Figure 9). Activated PI3K co-localises with PtdIns(4,5)P2 at the plasma membrane (32, 103, 109, 110).

Other modes of PI3K activation rely on GRB2 (growth factor receptor bound protein 2) adaptor protein that preferentially binds to the phospho-tyrosine motif (YXN). GRB2 binds to other scaffold proteins such as GAB (GRB2 associated protein) which also binds to the PI3K regulatory subunit p85 and results in activation of PI3K catalytic domain as previously described (Figure 9; (111, 112)). Lastly PI3K can be activated via RAS (106). GRB2 can also form a complex with SOS (son of sevenless) which is a GEF (guanine nucleotide exchange factors) that localises RAS to the plasma membrane where RAS is activated, resulting in activation of the RAS/MAPK pathway (113). RAS binds to the PI3K catalytic domain via the RAS binding domain (Figure 9) which activates p110 independently of p85 (114). Active PI3K is then able to phosphorylate PtdIns(4,5)P2 to produce PtdIns(3,4,5)P3 which acts as a secondary messenger by transmitting the signal from the RTK to effectors such as AKT and PDPK1 (PDK1; phosphoinositide dependent protein kinase-1) which contain a PH (Pleckstrin homology) domain (Figure 10 (32, 103, 109, 110)). Currently it is not clear which of these PI3K activation pathways predominates in different physiological situations.

PTEN is a lipid and protein phosphatase that acts as a tumour suppressor (115). It negatively regulates the PI3K pathway through its ability to dephosphorylate the D-3 phosphate on the inositol ring of PtdIns(3,4,5)P3 and converts PtdIns(3,4,5)P3 to PtdIns(4,5)P2. Therefore loss of PTEN results in hyperactivation of the PI3K pathway. Other phosphatases such as SHIP1/2 (SH2 domain-containing inositol 5'-phosphatase) are important in PtdIns(3,4,5)P3 metabolism as they dephosphorylate the D-5 position in the inositol ring and convert PtdIns(3,4,5)P3 into PtdIns(3,4)P2 (31, 110, 116, 117).

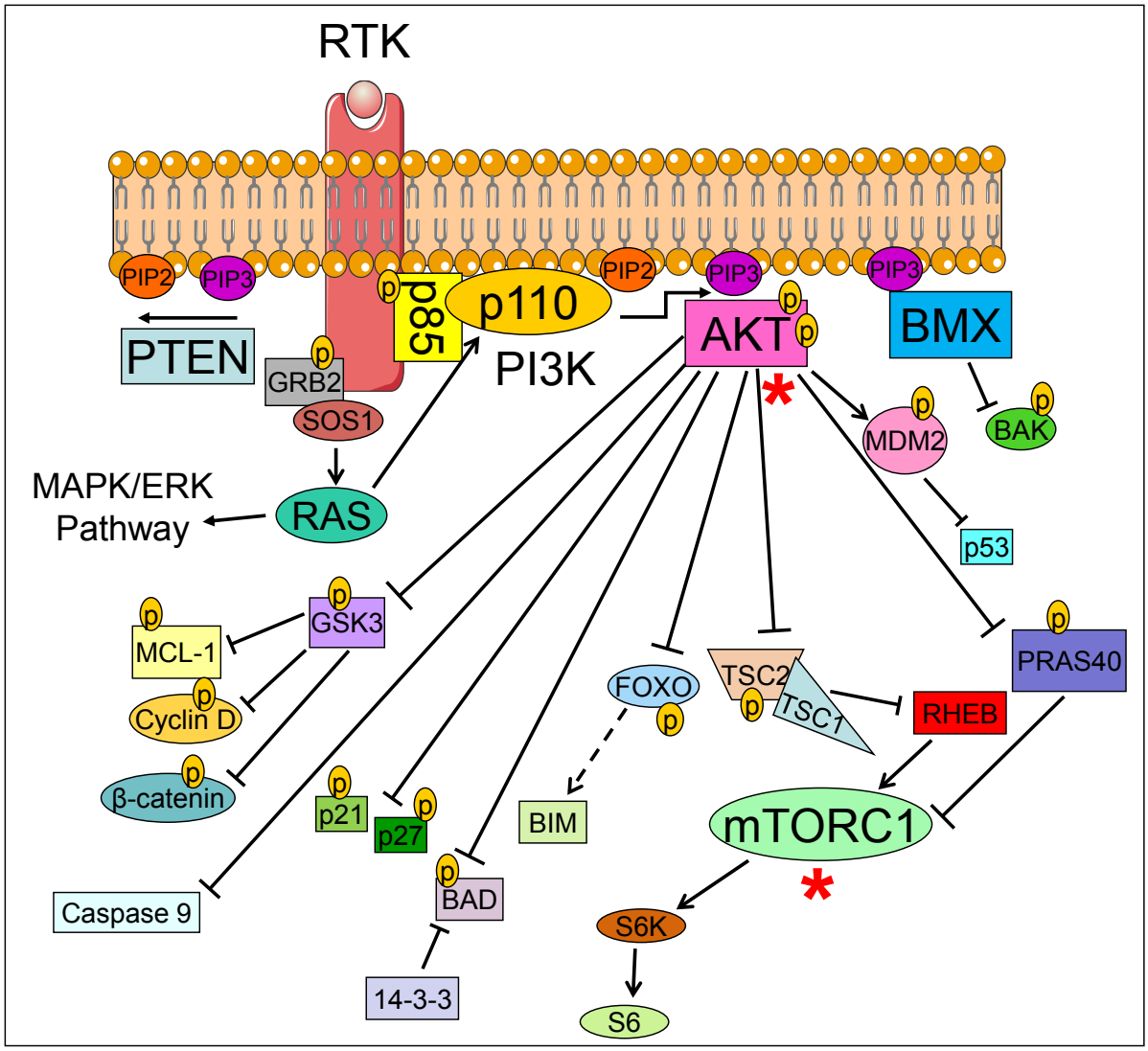

Figure 10: Class IA phosphoinositol 3-kinase signalling. Activated class IA phosphoinositol 3-Kinase (PI3K) phosphorylates PtdIns(4,5)P2 (PIP2) producing PtdIns(3,4,5)P3 (PIP3). PI3K downstream effectors, AKT and BMX bind PIP3 via their Pleckstrin homology domain where they are further activated. AKT and BMX regulate multiple biological processes such as survival and proliferation. *AKT and mTOR are the main known downstream effectors of PI3K (101). Illustration made using Servier Medical Art.

1.2.4 AKT – The main PI3K downstream effector

AKT (also known as PKB (protein kinase B)) is a serine/threonine protein kinase of which there are three distinct isoforms; AKT1, 2 and 3 encoded by the *AKT1, AKT2* and *AKT3* genes respectively (31). The different AKT isoforms appear to target similar effectors (Figure 10; (118)). However, increasing evidence suggests that the three AKT isoforms are non-redundant and function in an isoform specific manner in signal transduction pathways (119, 120). Although *AKT1* and *AKT2* knock-out mice are both small, suggesting some overlap in function, only *AKT2*

knock-out mice display a diabetic phenotype, suggesting a non-redundant function of the two isoforms (120, 121).

Once PI3K activation has resulted in PtdIns(3,4,5)P3, this provides a specific phospholipid surface that the PH domains found in AKT and PDPK1 (another serine/threonine kinase) can recognise, allowing the co-localization of these two proteins at the plasma membrane. PDPK1 was thought to be constitutively active however emerging evidence indicates that PDPK1 is regulated through phosphorylation of multiple serine, threonine and tyrosine residues but the exact mechanism remains unknown (122). Docking of AKT causes a conformational change which exposes two phosphorylation sites on AKT, T308 which is phosphorylated by PDPK1 (123, 124) and S473 which is phosphorylated by mTORC2 (mTOR complex-2) leading to complete activation of AKT (125). mTORC2 is made up of mTOR, mLST8 (GTPase β-subunit like protein GβL), deptor (disheveled, Egl-10, pleckstrin (DEP) domain containing mTOR interacting protein), rictor (rapamycin insensitive companion of TOR), mSIN1 (mammalian stress-activated protein kinase (SAPK)-interacting protein) and PRR5 (Proline-rich protein 5, also known as protor) (126-130). mTORC2 is thought to be activated by PI3K via an unknown mechanism involving mTORC2 associating with ribosomes (131). In addition, AKT can be ubiquitinated by the E3 ligase TRAF6 at lysine 63, which targets AKT to the plasma membrane. This ubiquitination is also important for phosphorylation and activation of AKT (132). Activated AKT regulates a vast number of effectors involved in a variety of biological processes such as cellular survival, metabolism, proliferation and angiogenesis. This regulation occurs via phosphorylation that can either be activating or inhibitory it its effect (31, 32).

AKT promotes cellular survival via multiple mechanisms that regulate apoptosis (Figure 10). BAD is a pro-apoptotic protein that forms a heterodimer with anti-apoptotic BCL-2, BCL-xL and BCL-w proteins, neutralising their anti-apoptotic effect. The phosphorylation of BAD (S146) by AKT causes BAD to be recognised by the phosphoserine binding protein 14-3-3. BAD/14-3-3 interaction blocks the pro-apoptotic function of BAD promoting survival (1, 2, 133). GSK3β is a serine/threonine kinase that phosphorylates the anti-apoptotic Bcl-2 family protein MCL-1 which causes it to be targeted for degradation (134). AKT negatively

regulates GSK3β thus stabilising MCL-1 (135). AKT phosphorylates and antagonises the upstream apoptotic protease caspase 9 by altering its catalytic activity promoting survival (136). AKT negatively regulates members of the forkhead family of transcription factors. FOXO1 (Forkhead box protein O1) promotes transcription of the pro-apoptotic proteins, BIM (Bcl-2 family) and FAS ligand; however AKT mediated phosphorylation results in cytoplasmic sequestering via 14-3-3 (137). When cell stress such as irreparable DNA damage occurs, p53 activates a pro-apoptotic response by both activating transcription of pro-apoptotic Bcl-2 family BH3-only proteins like NOXA and PUMA and inactivating transcription of anti-apoptotic family members like BCL-2. MDM2 (Mouse double minute 2 homolog) is an E3 ubiquitin-protein ligase that negatively regulates p53. AKT phosphorylates MDM2 which promotes nuclear translocation and enhances p53 degradation (138, 139).

In addition to its anti-apoptotic role AKT can also regulate cell proliferation in a number of ways (Figure 10). Cyclin D1, a critical regulator of G1-S phase progression is inhibited by GSK3β via several mechanisms. GSK3β can phosphorylate cyclin D1 and targets it for degradation (135). GSK3β can also promote degradation of β-catenin a transcriptional activator of cyclin D1 (140). Therefore GSK3β inhibition by AKT can elevate cyclin D1 levels both transcriptionally and post-translationally (135, 140). Furthermore AKT promotes cell cycle progression via phosphorylation and inhibition of cyclin dependent kinase inhibitors (CDKI) p27 and p21. CDKIs block cyclin/CDK (cyclin dependent kinase) complexes which are essential for cell cycle progression (141).

mTORC1 (mTOR complex-1) is an important downstream effector of AKT, involved in a variety of cellular processes including cell growth, proliferation, and ribosomal biogenesis. mTORC1 is a multi-subunit complex comprising mTOR, the scaffold protein Raptor (regulatory associated protein of TOR), mLST8 and deptor (142, 143). RHEB (RAS homolog enriched in brain) is a RAS-family small GTPase that activates mTORC1 in its GTP bound form via an incompletely defined mechanism (144-146). TSC2 (tuberous sclerosis complex-2) forms part of the TSC1/TSC2 tumour suppressor complex which has GTPase activating protein (GAP) function that antagonizes the association between RHEB and mTORC1.

AKT promotes mTORC1 activation via an inhibitory phosphorylation event that has been reported to decrease TSC1/TSC2 GAP activity (Figure 10; (147)). PRAS40 (proline-rich AKT substrate of 40 kDa) can form part of the mTORC1 complex inhibiting it. Activated AKT phosphorylates PRAS40 which causes it to be disassociated from the mTORC1 complex and be sequestered by the phospho binding protein 14-3-3 therefore releasing its inhibitory effect (129, 148). The mTOR subunit in mTORC1 is a serine/threonine kinase that regulates multiple effectors involved in mRNA translation. mTORC1 phosphorylates and activates the serine/threonine kinase S6K (Ribosomal Protein S6 Kinase), which in turn phosphorylates and activates the S6 (ribosomal protein S6). Active S6 stimulates the translation of mRNA containing a 5'polypyrimidine tract (104). Another important effector of mTORC1 is 4EBP1, a repressor of CAP-dependent translation. Active mTORC1 phosphorylates 4EBP1 which primes 4EBP1 for further phosphorylation leading to the release of the CAP-binding protein eIF4E and subsequent assembly of the eIF4E/eIF4G complex required for translation initiation (149, 150).

1.2.5 PI3K-dependent, AKT-independent pathway

AKT is one of the major downstream effectors of PI3K, however there are over 560 other proteins in humans with PH domains according to SMART (Simple Modular Architecture Research Tool (151, 152)) although not all these bind phosphoinositides with high affinity and specificity (153). Proteins that have PH domains and bind PtdIns(3,4,5)P3 have the potential to be regulated by PI3K. Proteins that have PH domains are involved in a wide variety of cellular functions from metabolism to signalling and trafficking. Whilst knockout of an activating mutant *PIK3CA* allele in CRC cell lines led to a decrease in AKT phosphorylation (154) it is not clear whether AKT is essential for *PIK3CA*-driven tumorigenesis. Indeed, in a panel of breast cancer and CRC cell lines with *PIK3CA* mutations' PI3K was found to be essential for proliferation, whilst AKT was not essential in a subset of these cell lines including HCT-116 and HT-29 (155). Another AGC (cAMP-dependent protein kinase 1 (PKA), cGMP-dependent protein kinase (PKG) and protein kinase C (PKC)) kinase closely related to AKT (156), SGK3 (serum/glucocorticoid regulated kinase 3), was activated in a PI3K- and PDPK1-

dependent manner, and was essential for cellular proliferation, suggesting the presence of an alternative PI3K signalling pathway in some *PIK3CA* mutant cells (155). A proteomic study demonstrated that upregulation of the STAT (signal transducer and activator of transcription) family transcription factors may be AKT-independent function of PI3K (157). STAT3 is important in mutant *PIK3CA*-induced transformation and that it is phosphorylated in response to PI3K activation by the NRTK (non-receptor tyrosine kinase) BMX (158). Whilst PI3K pathways independent of AKT are poorly studied, they clearly exist in a cell-context dependent manner and understanding mechanism of activation and their downstream effects have the potential to inform on tumorigenesis and future drug targets to treat cancer.

1.2.6 BMX and the PI3K pathway

The role of BMX in CRC and SCLC drug responses is a focus on this thesis. BMX also known as ETK (epithelial and endothelial tyrosine kinase), is a member of the Tec family of NRTK. The Tec family are made up of BMX, BTK (Bruton's tyrosine kinase), ITK (inducible T-cell kinase), TEC and TXK (also known as resting lymphocyte kinase (RLK)). They contain a PH, SH2, SH3, TH (Tec homology) and a tyrosine kinase domain with the exception of BMX that lacks the TH domain and TXK that lacks the PH domain (159). The Tec family of kinases are primarily expressed in the hematopoietic cell linage with the exception of BMX which has a much broader expression profile and has been shown to be expressed in endothelium and in epithelial cells as well as cells of the brain, prostate, lung and heart (160-162).

BMX is targeted to the plasma membrane via the secondary messenger PtdIns(3,4,5)P3 (Figure 10) which interacts with BMX via its N-terminal PH domain (Figure 11). The PH domain in BMX regulates the activation of the protein via intra-molecular interactions with the tyrosine kinase domain having an autoinhibitory effect on the protein in an unstimulated cell. BMX activity is regulated by multiple mechanisms which are likely to be cell context dependent. Multiple studies have reported that BMX is regulated by PI3K via its interaction with PtdIns(3,4,5)P3 (159, 163, 164). The NRTK SRC is then able to

phosphorylate membrane bound BMX on the kinase domain (Y566) leading to BMX activation (159, 164). Alternatively the PH domain of BMX can bind to the NRTK FAK's (focal adhesion kinase) FERM (four-point-one, ezrin, radixin, moesin) domain where is can be activated by SRC. FAK has also been shown to phosphorylate the PH domain (Y40) on BMX which releases its autoinhibitory effect on the tyrosine kinase domain (165). BMX's preferred target motif is pYpY, a site found in many RTKs and NRTKs. Usually the RTK ligand induces autophosphorylation or transphosphorylation but requires a further phosphorylation of the second tyrosine before the receptor is fully activated. BMX has been proposed to be required for this second tyrosine phosphorylation amplifying tyrosine kinase signalling. BMX has shown to increase phosphorylation of multiple tyrosine kinases including MET, FAK, FGFR1 (Fibroblast Growth Factor Receptor 1), ACK1 (Activated CDC42 kinase 1) and InsR (166) suggesting BMX is a key regulator of many biological processes.

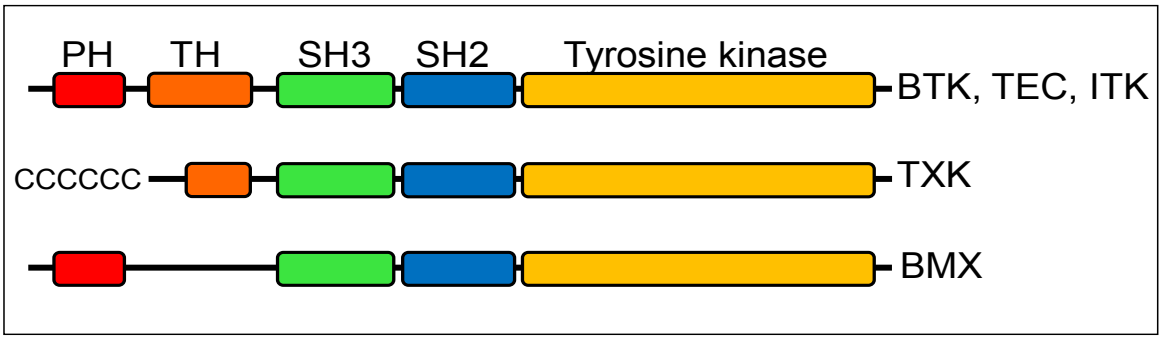

Figure 11: Tec family kinases structure. The Tec family of non-receptor tyrosine kinases are made up of 5 family members. They all contain a tyrosine kinase domain in the C-terminus and a SH2 (SRC homology 2) and SH3 domain. BMX, BTK, TEC and ITK all have a PH (Pleckstrin homology) domain in the N-terminus but TXK lacks this and instead has a cysteine rich motif. BTK, TEC,ITK and TXK contain a TH (Tec homology) domain but BMX lacks this (167).

BMX has been implicated in regulating multiple biological processes including proliferation, differentiation, motility and apoptosis but despite this, direct downstream targets of BMX and the exact mechanism of BMX function remain largely unknown (157, 168-171). Depending on cellular context BMX has been shown to have both pro- and anti-apoptotic functions *in vitro*. For example, expression of BMX protects the LNCAp prostate cells from apoptosis induced by photodynamic therapy or thapsigargin (172), but sensitises mast cells (32D) to apoptosis after treatment with G-CSF (granulocyte-colony stimulating factor; (163))

and in both cases this was PI3K dependent. There is also evidence for a role for BMX in DNA-damage response mediated via p53 via a direct interaction between the SH3 domain of BMX and the proline rich domain of p53. Treatment of LNCaP cells with doxorubicin caused up-regulation of the p53 regulatory protein p21 (cell cycle inhibitor) and down-regulation of survivin (IAP family member that negatively regulates apoptosis). However, the opposite effect was seen when BMX was stably over-expressed in LNCaP cells (LNCaP-BMX) leading to decreased p21 and increased survivin levels, suggesting that BMX inhibits p53 transcriptional activity in these cells. Furthermore, p53 also inhibited BMX activity suggesting a bi-directional regulation between p53 and BMX in LNCaP cells (168).

In a study of 71 patients with SCLC BMX was expressed in 75% (43 patients) of SCLC tumours and BMX expression correlated with expression of the anti-apoptotic BCL-2 family members, BCL-2 and BCL-xL (173). Furthermore, over-expression of BMX in H446 SCLC cells led to a 6-fold decrease in doxorubicin sensitivity and concomitant upregulation of BCL-2 and BCL-xL (173). BMX was also overexpressed in the chemo-resistant SCLC cell line H69AR relative to the chemo-sensitive parental cell line and BMX knockdown re-sensitised H69AR cells to a panel of chemotherapy drugs, potentially via downregulation of BCL-xL (174). These data suggest that BMX has an anti-apoptotic role in SCLC, potentially via BCL-xL and BCL-2 but the molecular mechanism and role of PI3K remains unclear (investigated in Chapter 3 and 5). Up-regulation of BMX correlated with poor prognosis in bladder cancer where BMX localised predominantly to the cytoplasm but was also found in the mitochondria (175). BMX does not contain a mitochondrial localising signal suggesting it localises there through protein-protein interactions. Co-immunoprecipitation studies showed a direct interaction between BMX and BCL-xL and co-localisation at the mitochondria which may suggest that this interaction is responsible for the mitochondrial localisation of BMX (175).

1.2.7 Aberrations in the PI3K pathway

Several components of the PI3K pathway (Figure 10) are frequently mutated in multiple cancers such as CRC and SCLC, causing gain or loss of function which typically leads to increased PI3K pathway signalling and tumour formation. The

PIK3CA gene encoding the catalytic p110α subunit is mutated in a range of cancers such as breast, brain, and of relevance in this thesis in CRC and SCLC (176-178). The *PIK3CA* mutations found in CRC and SCLC tumours are somatic (Figure 12; (75, 76)). Two major hotspot regions in exons 9 and 20 corresponding to the helical (PIK domain) and kinase catalytic domains respectively have been identified in the genome of CRC and SCLC cells (Figure 12). These hot spot point mutations result in missense mutation, indeed no truncating or nonsense mutations have been found. Validation of *PIK3CA* mutations have shown increase in levels of PtdIns(3,4,5)P3 leading to AKT and PDPK1 activation and cellular transformation although the exact molecular mechanism remains unknown (75, 76, 176, 177, 179, 180). The three most frequent *PIK3CA* point mutations found in CRC and SCLC are E542, E545 and H1047, highlighted in red on Figure 12 (75, 76, 180). This indicates the occurrence of non-random, selective mutations resulting in a cellular advantage such as increased proliferation. The helical domain mutations are thought to interfere with the intramolecular interactions between the p110α and p85 subunits that cause inhibition of PI3K in a resting cell, resulting in a constitutively active PI3K. The kinase catalytic domain mutation in located near the activation loop which results in a constitutively active p110 catalytic subunit and therefore constitutively active PI3K signalling (181, 182). The main difference between the *PIK3CA* helical and kinase catalytic domain mutants is highlighted when the RAS binding domain is also mutated. In this situation the helical domain mutant are no longer oncogenic whereas the kinase domain mutants are, confirming they have different mechanism for PI3K activation (183). Depending on cellular context, constitutively active p110α may allow cells to sustain proliferative signals in the absence of growth factors and resist cell death by activating survival signalling pathways such as PI3K/AKT, both of which are hallmarks of cancer (1, 2).

Mutations in *PIK3R1*, which encodes the p85α, p55α and p50α regulatory subunits have been identified in cancers such as ovarian, CRC and SCLC (32, 75, 76, 184, 185). Most mutations were found in the SH2 and p110 binding (iSH2) domains, and crystallographic data suggests these mutations abrogate antagonistic intra-molecular interactions between p85α and p110α and therefore promote constitutive activation of p110α (186). In CRC, mutations in p110 binding domain

rendering it non-functional have been observed. This type of mutation can lead to constitutive activation of the PI3K pathway by releasing the negative regulation of p85α thereby allowing p110 to bind its substrate and activate the PI3K pathway which is independent of RTK regulation and signalling. The frequency of mutations in the other regulatory subunits, p85β and p55γ, is low or absent suggesting an isoform specific function for p85α in cancer (32, 184, 185, 187).

Loss of function mutations in *PTEN* have been found in many cancers such as breast, CRC, SCLC, endometrial, skin and prostate cancer, highlighting the significance of this protein in negatively regulating the PI3K pathway. 9% of CRC (188) and 2-5% of SCLC (74-76) have inactivating PTEN mutations. However, PI3K and PTEN mutations are not mutually exclusive and are found together in 5.6% CRC (188) and 2.5% SCLC (75, 76). Coexistence of these mutations suggests a difference in oncogenic molecular mechanism and implies that their effect provides selective advantage to cells that harbour both mutations (189-191). This could be via PTENs PI3K independent function (115). PTEN can localise to the cytoplasm and the nucleus and has phosphatase independent functions. When PTEN is in the nucleus it regulates double-stranded DNA break repair via induction of RAD51 (192) which is a protein critical for invading the sister chromatid during DNA repair (193). In the nucleus, PTEN is involved in global transcriptional regulation through chromatin remodelling via direct interaction with histone H1 which chromatin condensation and downregulation of transcription in that region of the genome (194). PTEN has also been shown to regulate p53 activity independent of PTENs phosphatase activity. The cross-talk between p53 and PTEN appears complex; stabilised p53 in response to DNA damage can increase PTEN expression through p53 binding PTENs promoter. This is PI3K independent but PTEN also indirectly stabilises p53 via PI3K/AKT/MDM2 pathway (Figure 10; (195)).

In vitro studies revealed other mutations in the PI3K pathway in CRC cells such as mutation in *AKT1* and *AKT2* which results in growth factor independence by allowing ATK1 to translocate to the plasma membrane in the absence of growth factor-induced production of PtdIns(3,4,5)P3 (196-198). This plasma membrane localisation allows AKT1 to be phosphorylated, and activated by mTORC2 and

PDPK1 (199). Three mutations have also been found in *PDPK1*, with two affecting the same residue in the kinase domain (197). Activating mutations in RTK such as EGFR and IGFR-1 and mutations in (30, 75, 76, 180). These mutations activate the PI3K/AKT pathway by activating PI3K directly or indirectly as described previously.

CBioPortal for cancer genomics is a tool developed and maintained by MSKCC (Memorial Sloan-Kettering Cancer Centre) and contains data from 21441 tumour samples from 91 cancer studies (75, 76). This tool was used to analyse the frequency of mutations data of PI3K pathway components in the available studies on CRC (four studies) and SCLC (two studies). The PI3K pathway component genes (*PIK3CA, PIK3CB, PIK3CD, PIK3R1, PIK3R2, PIK3R3, AKT1, AKT2, AKT3, PTEN, MTOR, RPS6KA2, RPS6KA6* and *PDPK1*), were analysed for frequency of mutations in each study (Figure 13). PI3K pathway mutations were frequent and of comparable levels in CRC and SCLC, with between 29-45.8% in CRC (200-202) and 24.1-38.1% in SCLC (66, 67). This suggests that PI3K is an attractive drug target in both cancer types, although with the caveat that a large portion of the mutation data available via cBioPortal has not yet been verified. However, informatics tools such as mutationassessor.org (203) and Polyphen2 (204) are available to assess the likely functional impact of specific mutations on a protein of interest, revealing whether the mutation is likely to be a driver or passenger mutation.

BMX is altered most frequently in prostate cancer with gene amplification found in 19% (205). Of all 91 cancer studies on cBioPortal (75, 76) 52 had documented changes in BMX (mutation, deletion, amplification or multiple alterations). Of the six CRC and SCLC studies available, four of them documented mutations in BMX (three CRC and one SCLC). CRC studies reported mutations in 1.9-2.8% of cases (200-202) and 6.9% in SCLC (66) which was second to prostate with most frequently mutated BMX. In the CRC and SCLC studies, 3/12 studies contained mutations in the PH and tyrosine kinase domains of BMX that had a predicted functional impact score of ‘medium’ using the mutation assessor (203). The other BMX mutations had low or neutral scores. However, the actual effects of any of

these mutations on BMX functions are currently unknown. These data do however implicate a role for BMX in many cancer types including CRC and SCLC.

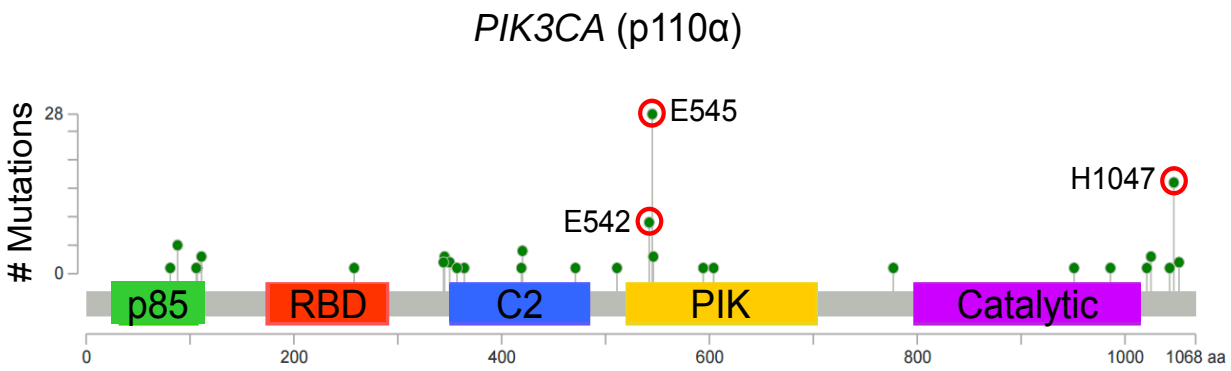

Figure 12: Point mutations found in *PIK3CA* in colorectal and small cell lung cancer. Analysis of the *PIK3CA* gene in colorectal (CRC) and small cell lung cancer (SCLC) tumour samples have identified somatic point mutations in specific exons. The mutations localize to various domains of the p110α primary structure as indicated. The three major hotspot mutations that occur in CRC and SCLC are located at residues E542, E545 and H1047, highlighted in red. Protein domains are p85-binding domain (p85), RAS-binding domain (RBD), protein-kinase-C homology-2 domain (C2), Helical domain (PIK) and a kinase catalytic domain (75, 76).

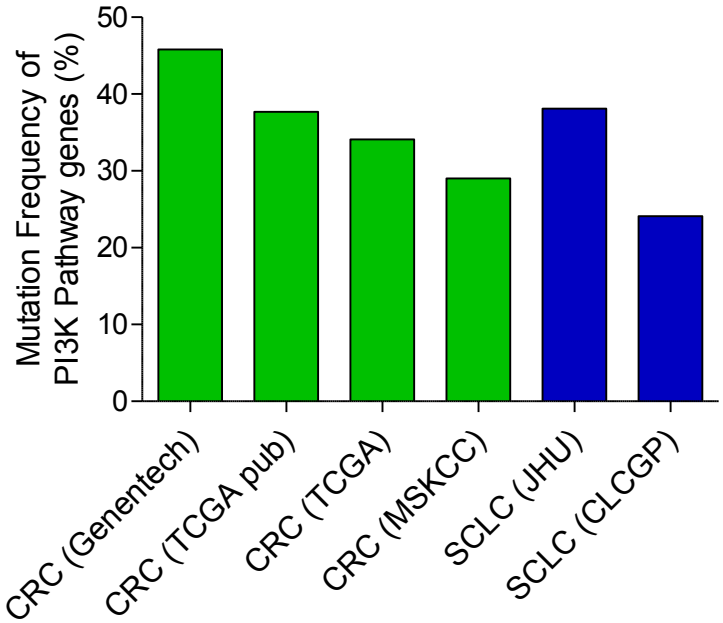

Figure 13: Frequency of mutations in PI3K pathway genes. Analysis of PI3K pathway gene mutations found in colorectal (CRC) and small cell lung cancer (SCLC). Data for CRC (green) and SCLC (blue) using CBioPortal (*PIK3CA, PIK3CB, PIK3CD, PIK3R1, PIK3R2, PIK3R3, AKT1, AKT2, AKT3, PTEN, MTOR, RPS6KA2, RPS6KA6* and *PDPK1* genes analysed; (75, 76)). The CRC studies were carried out by Genentech (200), The Cancer genome Atlas Network (TCGA (206) (201)) and Memorial Sloan-Kettering Cancer Center (MSKCC; (202)) and the SCLC studies were carried out by John Hopkins University (JHU; (67)) and Clinical Lung Cancer Genome Project (CLCGP; (66)).

1.2.8 PI3K pathway inhibitors

The high frequency of mutation in PI3K pathway components found in a broad spectrum of cancers suggests that activation of this pathway is important for transformation and oncogenesis. Thus, the PI3K pathway provides an attractive drug target as inhibition of inappropriate signalling could provide a therapeutic strategy for selectively blocking cell division of cancer cells and therefore tumour growth. As such many pharmaceutical companies and academic laboratories have designed small molecule inhibitors that can be used to target the PI3K pathway (Table 3 and Figure 14).

The first generation of PI3K inhibitors were wortmannin (207) and LY294002 (208). Wortmannin is a natural compound isolated from *Penicillium wortmannin* and binds covalently to the lysine residue essential for catalytic activity in PI3K. This reaction is irreversible and it shows little selectivity within the PI3K family and is toxic to animals. LY294002 the first synthetic PI3K inhibitor, is reversible but again lacks selectivity resulting in high toxicity (209, 210). Despite their clinical limitations they proved invaluable in preclinical studies that contributed to our molecular understanding of the PI3K pathway. Table 3 lists the preclinical PI3K inhibitors, including the dual class I PI3K and mTOR inhibitor PI-103 that were used in this project (PI-103 chemical structure found in Appendix I, Figure 26 (211)).

Dual inhibitors of the p110 catalytic domain of PI3K and mTOR opened up a new cancer therapeutic strategy to inhibit proliferation and sensitise cancer cells to apoptosis. Dual PI3K and mTOR pathway inhibitor drugs are currently in clinical trials and include BEZ235 (Novartis) which is in phase I/II clinical trials in patients with solid tumours such as breast, pancreatic, prostate and renal cell carcinoma (212). BEZ235 causes competitive inhibition of the ATP-binding pocket in the kinase domain of p110 and mTOR thus inhibiting PI3K and mTOR catalytic activity (213). BEZ235 has anti-proliferative activity in tumour xenografts containing either *PIK3CA* activating mutations or inactivating *PTEN* mutations (214).

As previously described, BMX is a Tec family kinase. Ibrutinib (PCI-32765, chemical structure found in Appendix I, Figure 26), is an irreversible Tec family

kinase inhibitor that has recently been granted FDA approval (215) for second line therapy in haematological malignancies such as chronic lymphocytic leukaemia (CLL) and mantle cell lymphoma where Tec family kinase signalling through BTK is a major drivers of oncogenesis (216). PCI-32765 binds covalently to the cysteine residue (Cys-481) in the kinase active site of Tec family kinases and although PCI-32765 binds most strongly to BTK it also binds to BMX, albeit with a 1.6 fold reduction in potency (217). Only 10 kinases contain the Cys-481 residue or analogous cysteine residues in their active site whose activity can also be inhibited by PCI-32765 and five of those are the Tec kinase family members (217, 218).

Type of inhibitor	Name	Target	Specificity	Reference
PI3K	LY294002	p110	Pan PI3Ks	(208)
	Wortmannin	p110	Pan PI3Ks	(208)
	IC87114	p110δ lipid kinase activity	p110δ lipid kinase activity only	(219)
	TG100-115	All class I isoforms	5 to 10 X potency p110δ/p110γ	(220)
	ZSTK474	ATP competitive pan class I	Minimal isoform selectivity but no activity against protein kinase	(221)
	XL147	ATP competitive pan class I	No activity against other kinases	(222)
	PI-103	ATP competitive	All 4 class I PI3Ks and mTOR	(211)
	PI-540	ATP competitive	All 4 class I PI3Ks and mTOR	(223)
	PI-620	ATP competitive	All 4 class I PI3Ks and mTOR	(224)

Table 3: Preclinical phosphoinositol 3-Kinase pathway inhibitors

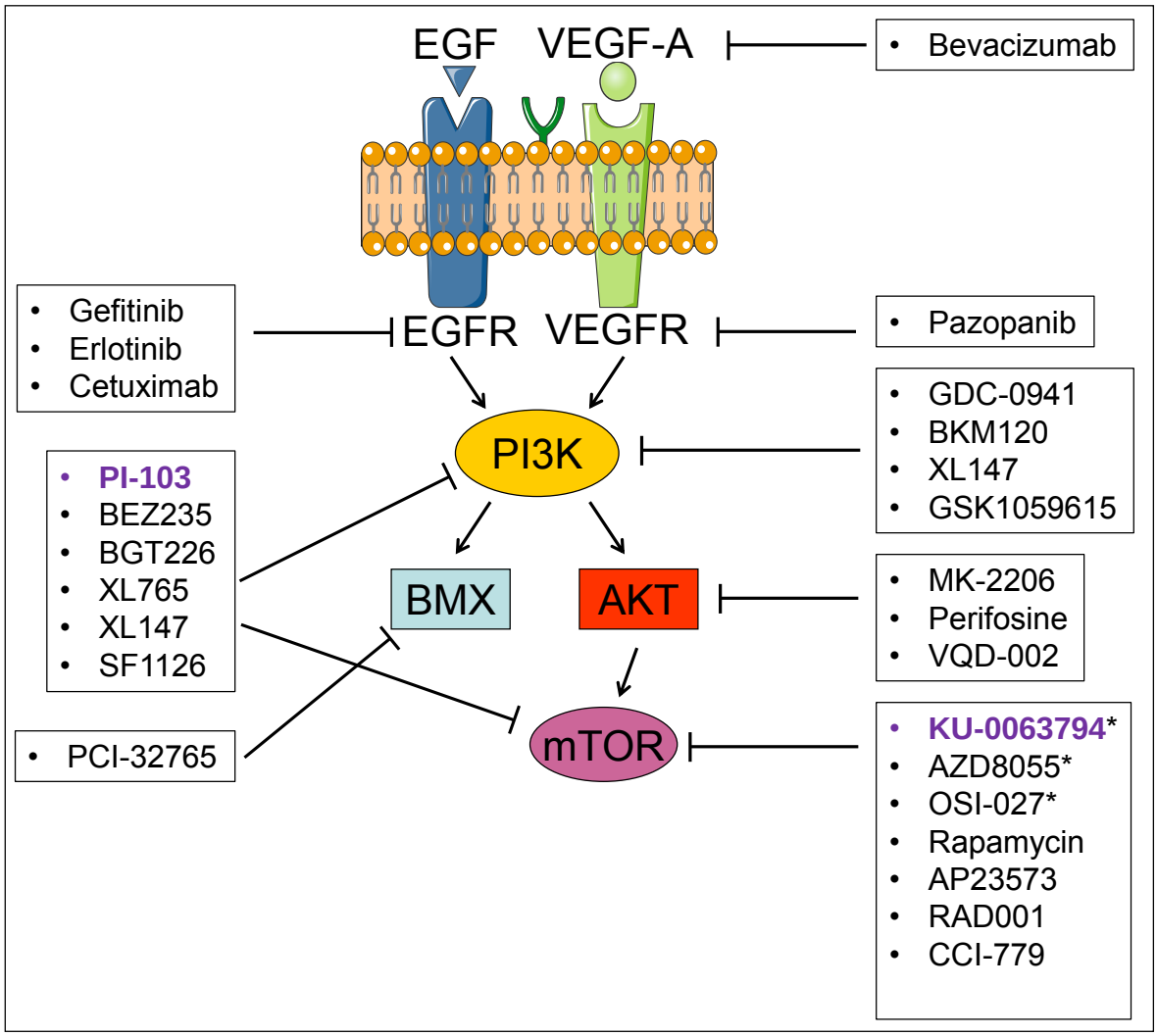

Figure 14: Phosphoinositol 3-kinase (PI3K) pathway inhibitors in clinical trials and their proposed modes of action. (225). These inhibitors can target the PI3K pathway either upstream of PI3K via EGFR (epidermal growth factor receptor), VEGFR (vascular endothelial growth factor receptor) or the VEGFR ligand VEGF-A, the catalytic p110 domain of PI3K or via downstream effectors AKT, BMX or mTOR (31). PI-103 and KU-0063794 shown in purple are not in clinical trials but are shown here because they are used *in vitro* in this project. * KU-0063794, AZD8055 and OSI-027 target mTORC1 and mTORC2. Illustration made using Servier Medical Art.

1.3. Resisting cell death

1.3.1 Apoptosis

Apoptosis is a form of physiological programmed cell death, which is critical during development and throughout the lifespan of an organism, and is therefore tightly regulated (226). Apoptotic cells acquire classical morphological changes such as shrinkage, cytoskeletal collapse, nuclear envelope disassembly and chromatin condensation (1, 227). Resisting apoptosis is a hallmark of cancer and is recognised to result in resistance to anti-cancer therapies (1, 2). The two major apoptotic pathways are the intrinsic pathway which is the focus of this thesis and extrinsic pathways (Figure 15). Both pathways ultimately result in the activation of initiator caspases (cysteinyl aspartate specific protease; caspase 8 and 9) that in turn activate downstream effector caspases (caspase 3 and 7). Activation of effector caspases results in cell-wide specific proteolysis which amplifies the apoptotic signal, decreased ATP production and labelling of the cell with signals recognised by phagocytic cells such as macrophages leading to their engulfment and degradation. This process of dead cell removal maximises recycling of cellular components as well as limiting any resultant immunological response (228-230).

1.3.2 Intrinsic apoptotic pathway and the Bcl-2 family

The intrinsic apoptotic pathway (Bcl-2 pathway or mitochondrial pathway) ultimately results in mitochondrial outer membrane permeabilization (MOMP) which causes the release of pro-apoptotic factors such as cytochrome c and SMAC (second mitochondria derived activator of caspases) from the intermembrane space (231). Once cytochrome c enters the cytosol, it interacts with APAF1 (apoptotic protease activating factor-1), the initiator procaspase 9 and ATP to form a holoenzyme known as the apoptosome (Figure 15). The formation of the apoptosome results in activation of caspase 9. This then cleaves procaspase 3 into caspase 3 (229) and the activated caspase cascade causes cell-wide specific proteolysis, dysfunction, decrease in ATP production and remodelling of the cell surface with ‘molecular flags’ such as externalisation of Phosphatidylserine. This allows the cell to be recognised by phagocytic cells such as macrophages that then engulf the apoptotic cell. This efficient removal of dying

cells allows ‘biological building blocks’ to be recycled, an immune response to dead cells is contained and damage to healthy cells in the vicinity of apoptotic cells is minimised, in contrast to necrotic cell death (228-230).

MOMP is regulated by the Bcl-2 family of proteins and can be activated by various mechanisms such as developmental cues, growth factor deprivation and DNA damage (232-235). The Bcl-2 family of proteins can be grouped into three sub-families, the pro-apoptotic effectors, the anti-apoptotic and the pro-apoptotic BH3-only proteins (Figure 10). The effector subfamily are multi-domain proteins containing BH (BCL-2 homology) domains 1-3, however structure alignment has revealed a conserved BH4 domain (236-238). The members of this subfamily are BAK (BCL2-Antagonist/Killer), BAX (BCL2-Associated X Protein) and BOK (BCL2-Related Ovarian Killer) (232), the latter having restricted expression in reproductive tissue (239). In healthy cells, BAX is mostly cytosolic or lightly attached to the outer mitochondrial membrane (OMM), whereas BAK is an integral mitochondrial protein found on the cytosolic side of the OMM. Before MOMP occurs BAK and BAK undergoes a conformational change in the N-terminus. In BAK this reveals a newly exposed epitope (240) and a change in the BH1 domain that parallels the release of anti-apoptotic Bcl-2 family members such as BCL-xL (B-cell lymphoma-extra Large; (241). A change in BAX conformation is followed by translocation to the OMM (242) where BAK and BAX form homo-oligomers in the OMM (243), forming pores through which intermembrane proteins such as cytochrome c are released (244, 245). BAK and BAX are functionally redundant, however loss of both prevents intrinsic apoptosis, showing BAX and BAK are essential for MOMP (246).

The anti-apoptotic subfamily consists of the multi-domain proteins BCL-2 (B-cell lymphoma 2), BCL-xL, BCL-w, MCL1 (Myeloid Cell Leukemia 1), and A1 (BFL-1) (Figure 15). These conserved proteins share homology in BH1-4 domains and are predominantly located in the OMM, but are also present in the cytosol and endoplasmic reticulum (ER) (247, 248). The Bcl-2 anti-apoptotic members prevent MOMP via antagonising interactions with the pro-apoptotic Bcl-2 family members (249). The BH1-3 domains of the anti-apoptotic family members fold into a globular tertiary structure forming a hydrophobic groove on its surface. The

hydrophobic groove provides a platform for the pro-apoptotic Bcl-2 family members to interact via their amphipathic alpha helix (~24 amino acid residues) in the BH3 domain (249-252).

The pro-apoptotic BH3-only subfamily consists of BAD (BCL2-Associated Agonist of Cell Death), BID (BH3 Interacting Domain Death Agonist), BIK (BCL2-Interacting Killer), BIM (BCL2-Interacting Mediator of Cell Death), BMF (BCL2-Modifying Factor), HRK (Harakiri), NOXA and PUMA (p53 Up-Regulated Modulator of Apoptosis; (232)) (Figure 15). The BH3-only proteins are so-called due to shared homology of BH3 domains and they have little homology with the other Bcl-2 family members (253) (Figure 16). They show specificity in their binding to the anti-apoptotic Bcl-2 family members (Figure 17). BID, BIM and PUMA are antagonists of all the anti-apoptotic proteins and therefore potent inducers of apoptosis. BAD is a BCL-2, BCL-w and BCL-xL antagonist. HRK is a specific BCL-xL antagonist and NOXA is a specific MCL-1 antagonist. BIK and BMF antagonise BCL-2, BCL-w, BCL-xL and MCL-1 (249, 250, 254, 255).

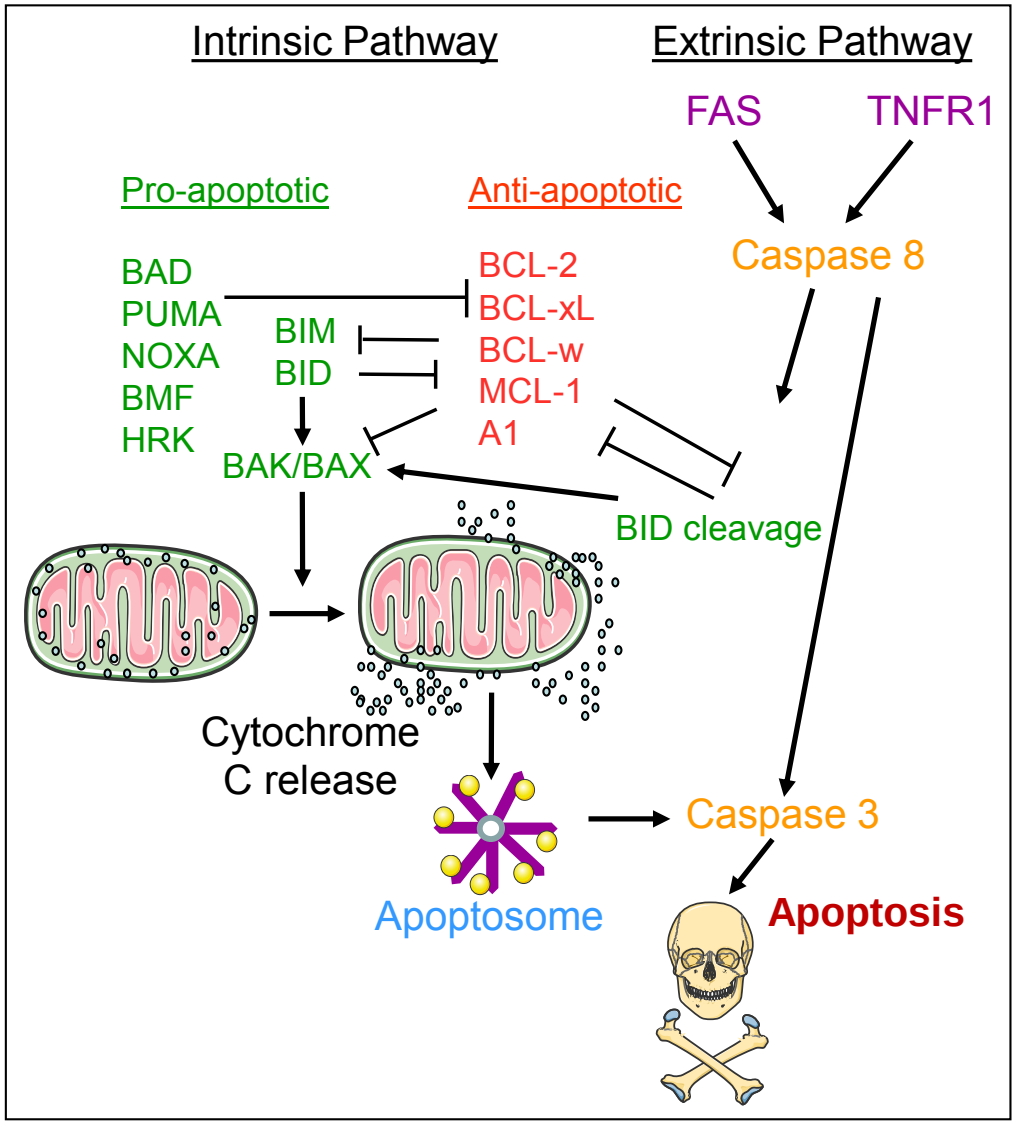

Figure 15: Intrinsic and extrinsic apoptotic pathways. The intrinsic apoptotic pathway can be activated by various factors such as growth factor deprivation and stress (232-235). Apoptotic signals result in an increase in active/available pro-apoptotic Bcl-2 family members (green) and/or decrease in active/available anti-apoptotic Bcl-2 family members (red) shifting the cell survival equilibrium towards apoptosis. This allows the pro-apoptotic effectors BAK and BAX to be released and activated by pro-apoptotic BH3-only proteins BIM or BID resulting in BAX/BAK homo-oligomerization in the outer mitochondrial membrane, mitochondrial outer membrane permeabilization and apoptosis. Cell surface receptors, such as FAS and tumour necrosis factor receptor-1 (TNFR-1) can activate apoptosis, resulting in activation of the extrinsic apoptotic pathway. The extrinsic pathway can feed into the intrinsic pathway via BID cleavage and activation (232). Illustration made using Servier Medical Art.

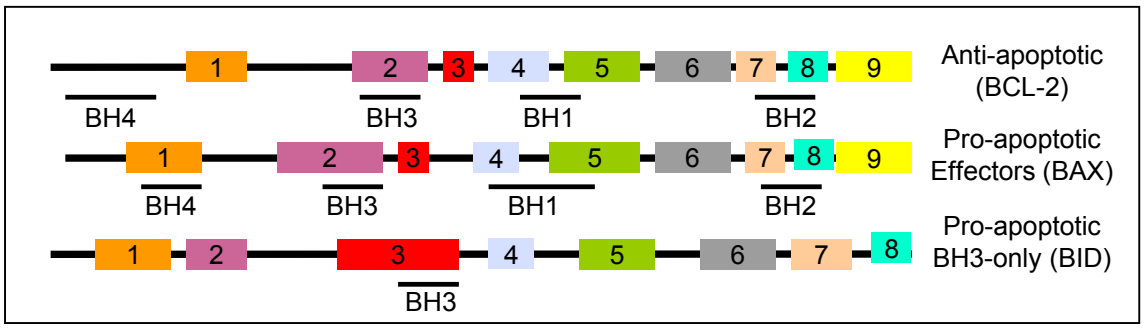

Figure 16: Schematic diagram of Bcl-2 subfamily representative. The Bcl-2 family of proteins contain BCL-2 homology (BH) domains. BCL-2, BAX and BID are examples of the Bcl-2 family members and each one is representative of Bcl-2 three subfamilies, anti-apoptotic, pro-apoptotic effectors and pro-apoptotic BH3-only respectively. BCL-2 is a multi-domain anti-apoptotic protein that contains a BH1, BH2, BH3 and BH4 domain. BAX is a pro-apoptotic effector protein that contains a BH1, BH2, BH3 and BH4 domain. BID is a BH3-only protein that contains just a BH3 domain. The numbered domains represent the alpha-helices within the protein structure (249).

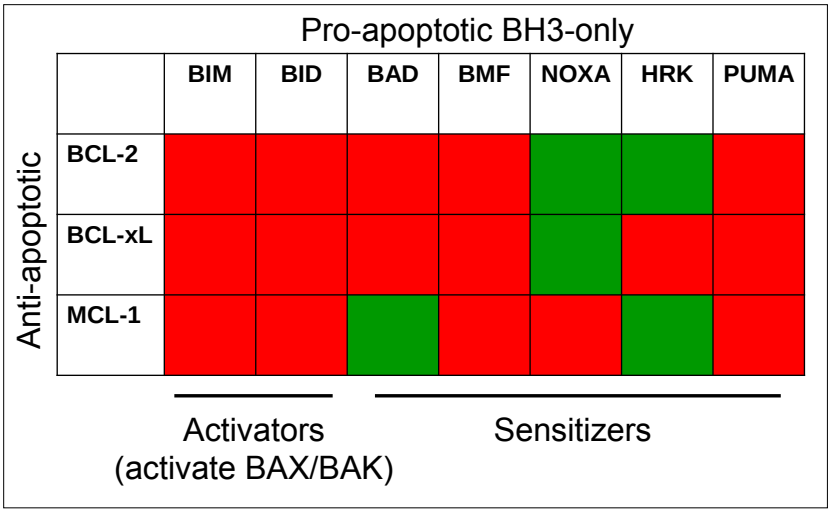

Figure 17: Specificity in binding of the BH3-only proteins to the anti-apoptotic Bcl-2 family members BCL-2, BCL-xL and MCL-1. BH3-only proteins are divided into activator or sensitizers depending on their apoptotic properties. BH3-only peptides bind and antagonise specific anti-apoptotic family members. Red indicates high affinity binding and green indicates no binding (250).

1.3.2.1 Regulation of the Bcl-2 family

The Bcl-2 family are tightly regulated by several transcriptional and post-transcriptional (PTM) mechanisms (256-258). As previously described active AKT regulates multiple members of the Bcl-2 family including stabilisation of anti-apoptotic MCL-1, sequestering of pro-apoptotic BAD blocking pro-apoptotic function and downregulation of pro-apoptotic BIM (Chapter 1.2.4). Under environmental stress BIM can be transcriptionally upregulated by transcription factors such as FOXO3A (forkhead box protein O3; cytokine deprivation) or C/EBPa (CCAAT-enhancer-binding proteins; ER stress) and CHOP (C/EBP homologous protein; ER stress) (259). The transcription factor RUNX3 (runt-related transcription factor 3), can upregulate BIM via its interaction with FOXO3A on the BIM promoter (260, 261). There are three major alternatively spliced isoforms of the *BIM* gene, BIM-S, BIM-L and BIM-EL. The BIM isoforms have distinct sizes and pro-apoptotic function (259, 262). MicroRNAs (miRNA) such as miRNA-17-92, negatively regulate the translation of BIM and over-expression of this miRNA results in a BIM-deficient phenotype (263). BIM activity can also be regulated by PTM. Activation of the MAPK pathway leads to activation of the serine/threonine protein kinase ERK1/2 (extracellular-signal-regulated kinases 1/2) and phosphorylation of BIM-EL (S69; (264)) causing BIM ubiquitination and its degradation by the proteasome (265, 266). Conversely, TGFβ (transforming growth factor beta) signalling through SMAD3 activates the MAPK phosphatase, MKP2 (MAPK phosphatase 2) which dephosphorylates ERK1/2 resulting in the stabilisation and increase in BIM (267).

Cleavage of the large unstructured loop between the N-terminal and C-terminal BH3 domain of BID produces pro-apoptotic tBID, the active form of BID. Cleavage can be carried by extrinsic factors such as caspases 8 (Figure 15), granzyme B (produced by cytotoxic lymphocytes) and caspase 2 (produced during heat shock) (249). There appears to be multiple distinct mechanisms regulating BID cleavage by caspase 8 and 3, which will likely be cellular context-dependent (268). N-myristoylation of tBid has been shown to increase its localisation to the OMM and increase BAK activation (269).

Phosphorylation of anti-apoptotic proteins BCL-2 and BCL-xL occurs at many sites during cell cycle arrest and acts as a sensors for when a cell should switch from cell cycle arrest to apoptosis due to its environment (256, 257, 270). Phosphorylation of BCL-xL (S62) regulates its antagonising function releasing BCL-xL from BAX. A decrease in phospho- BCL-xL promotes anti-apoptotic function by increasing BCL-xL bound to BAX (256). BCL-2 is negatively regulated by phosphorylation at various sites (S70, S87 and T69; (257)). Mutating the phospho-sites to alanine increases the anti-apoptotic activity of both BCL-2 and BCL-xL (256, 257). JNK kinase can phosphorylate BCL-2 and BCL-xL (256, 257) and more recently Terrano *et al*., suggest that CDK1/Cyclin B phosphorylatesBCL-2 and BCL-xL to disable their anti-apoptotic function when cells are in mitotic arrest (270). Over-expression of non-degradable cyclin B causes apoptosis but this can be blocked by a BCL-xL phospho-defective mutant but not by a phospho-mimic mutant suggesting that prolonged mitotic arrest increases phosphorylation of BCL-xL resulting in inactivation of the anti-apoptotic proteins thus linking the cell cycle block to apoptosis (270).

Recently the Tec kinase BMX was identified as the tyrosine kinase that negatively regulates BAK through phosphorylation (Y108) retaining BAK in the inactive confirmation (Figure 10) (258). Only when this tyrosine is dephosphorylated is BAK free (271) to be activated by BH3-only proteins such as BIM (272). Activated BAK can homo- oligomerize creating pores in the OMM resulting in MOMP (Figure 15).

1.3.3 The direct and indirect models for BAK and BAX activation

There are two competing models which attempt to explain how the pro-apoptotic effector proteins, BAK and BAX are activated to cause MOMP (Figure 18). These models are similar in that they both depend upon the pro-apoptotic BH3-only proteins, however their precise roles differ between the two models (273). The direct model divides the BH3-only proteins into two categories, sensitizers (BAD, BIK, HRK, NOXA and PUMA) and activators (BID and BIM). There is some evidence that PUMA can act as an activator (274). In this model the activators can directly interact with and activate BAK and BAX thus promoting homo-

oligomerization and MOMP (Figure 18A-B). BID and BIM are sequestered by binding of their BH3 domains to the hydrophobic cleft of the anti-apoptotic proteins which prevents BID and BIM from directly activating BAK and BAX. The sensitizers compete with BID and BIM for binding to the hydrophobic cleft on the anti-apoptotic proteins displacement of BID and BIM allows them to directly activate BAK and BAX causing a conformational change, leading to the formation of homo-oligomers and MOMP (255, 275-278). This hypothesis is supported by evidence showing that triple knockout Bim/Bid/Puma cells are not able to undergo apoptosis (272) and NMR studies which demonstrated that BIM and BAX interact (279).

The indirect model states that there is no direct activation of pro-apoptotic BAK and BAX by the pro-apoptotic BH3-only proteins. Instead BAK and BAX are constantly inhibited from forming homo-oligomers by their interaction with the Bcl-2 anti-apoptotic proteins (Figure 18C-D). This model does not discriminate between pro-apoptotic BH3-only members as they are all classed as antagonists of the Bcl-2 anti-apoptotic proteins. The BH3-only proteins interact with the Bcl-2 anti-apoptotic family members only and disrupt the Bcl-2 anti-apoptotic-BAK/BAX interaction causing BAK and BAX to be released and therefore free to form homo-oligomers leading to MOMP. This model acknowledges that BAK and BAX must undergo a conformational change to form homo-oligomers but the exact mechanism for this remains unanswered (254, 280-282). As previously mentioned both BAK and BAX have been observed undergoing an N-terminal conformational change before MOMP occurs, induced by apoptotic signals (142, 242).

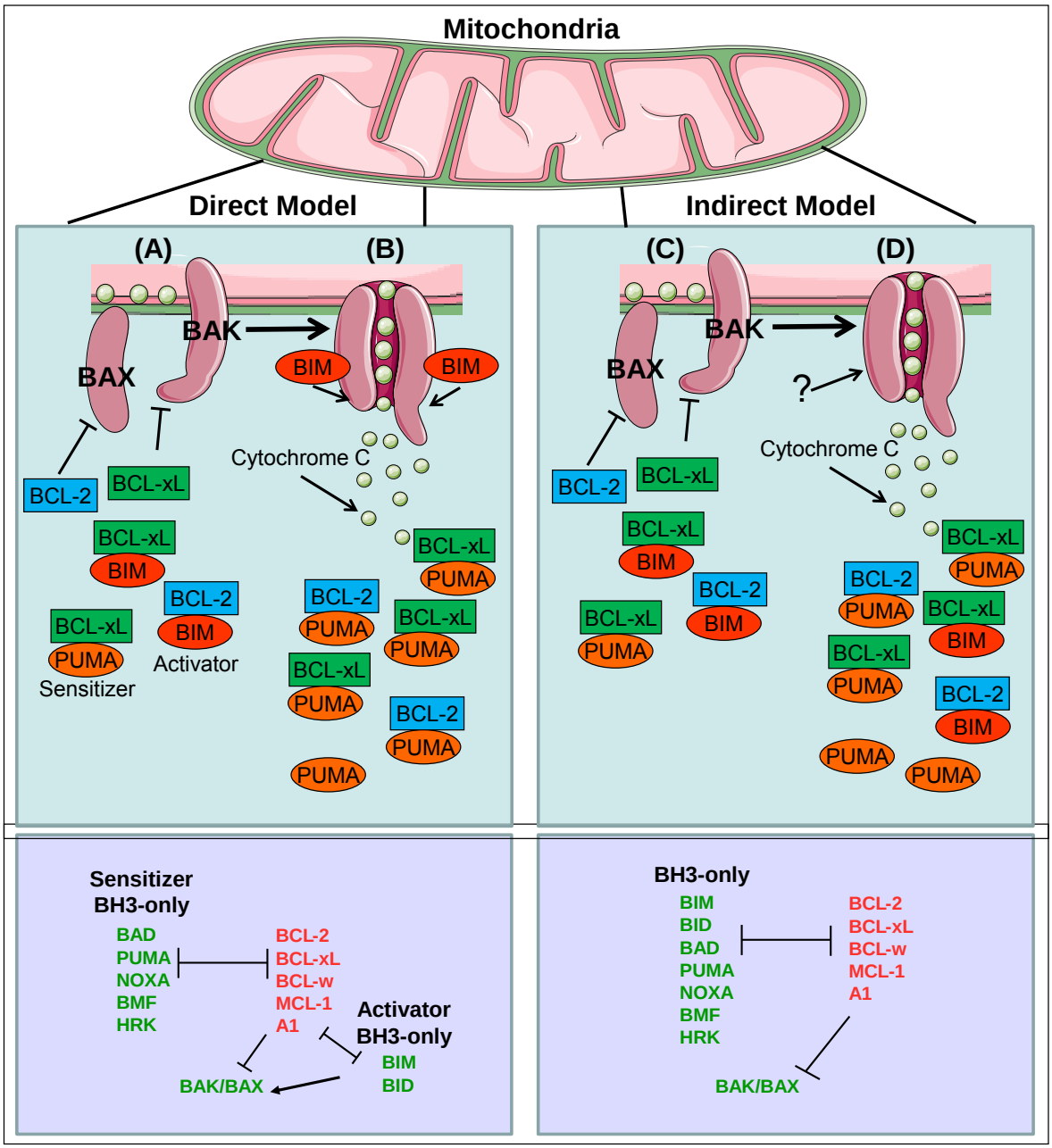

Figure 18: The direct and indirect model for BAK and BAX activation. The direct model splits the pro-apoptotic BH3-only proteins into activators; BIM and BID; and sensitizers BAD, PUMA, NOXA, BMF and HRK. Both activators and sensitizers are anti-apoptotic antagonists. (A) Anti-apoptotic Bcl-2 family members such as BCL-2 and BCL-xL directly inhibit the pro-apoptotic effectors BAX and BAK. (B) When BH3-only proteins are upregulated such as PUMA, they bind the anti-apoptotic members causing then to release their inhibitory effect on pro-apoptotic proteins BAX, BAK and BIM. Activator BIM is now available to directly activate BAX and BAK which causes homo-oligomerization creating pores in the mitochondrial outer membrane and induces mitochondrial outer membrane permeabilization (MOMP) and cytochrome c release leading to apoptosis. According to the indirect model all pro-apoptotic BH3-only proteins are the same (no activator or sensitizer). (C) Anti-apoptotic Bcl-2 family members BCL-2 and BCL-xL directly inhibit the pro-apoptotic effectors BAX and BAK. PUMA and BIM inhibit BCL-2 and BCL-xL. (D) Upregulation of PUMA due to apoptotic signalling causes increase interaction between pro-apoptotic BH3-only proteins and anti-apoptotic proteins releasing their effect of BAX and BAK. BAX and BAK are now free to be activated by an unknown mechanism causing MOMP and apoptosis(249). Illustration made using Servier Medical Art.

1.3.4 BH3 Profiling to interrogate apoptosis

A 'primed' cell has a low apoptotic threshold meaning that apoptosis can be more easily induced by apoptotic drugs such as BH3 mimetics, discussed later (Chapter 1.3.7). To measure 'priming' the BH3 profiling assay was developed by Anthony Letai's group at the Dana Farber Cancer Institute (DFCI, Boston, MA, USA). BH3 profiling uses synthetic BH3 peptides derived from the BH3 domain of the pro-apoptotic BH3-only proteins (activator and sensitizer) to interrogate the propensity of cytochrome c release from mitochondria. Cytochrome c release is used as a surrogate for MOMP because cytochrome c is released from the mitochondria intermembrane space once MOMP occurs. When a carefully selected panel of BH3 peptides are used, BH3 profiling can reveal what apoptotic block cancer cells are likely using to evade apoptosis and thus provide a measure of how 'primed' that cell is (Figure 19). A cell that evades apoptosis via downregulation of pro-apoptotic BH3-only activators will only respond to activator peptides in the BH3 profiling assay (Figure 19A (red bars)). The inability of either activator or sensitizer BH3 peptides to induce cytochrome c release by BH3 profiling would suggest a lack of functional BAX/BAK in those cells (Figure 19B). If both activator and sensitizer BH3 peptides could induce cytochrome c release then a mechanism of evading apoptosis via upregulation of anti-apoptotic Bcl-2 family members would be suggested (Figure 19C (red and green bars). This type of cell would be classed as 'primed' because all the components to induce apoptosis are present but they are neutralised by the anti-apoptotic Bcl-2 family members (Figure 19).

BH3 profiling can also reveal which anti-apoptotic proteins a cell has become reliant on through the response of specific sensitizers BH3 peptides to cause cytochrome c release. This is because sensitizers BH3-only proteins show specificity in their binding to the anti-apoptotic proteins (Figure 17). For example if a BH3 profile revealed that the sensitizer BH3 peptides, PUMA, BAD and BMF caused cytochrome c release but NOXA and HRK didn't, this would suggest that this population of cells are likely dependent on BCL-2 but not BCL-xL or MCL-1. NOXA is a specific antagonist for MCL-1 and HRK is a specific antagonist for BCL-xL so would cause cytochrome c release if cells were dependent on them for evading apoptosis (Figure 19C BH3 profile).

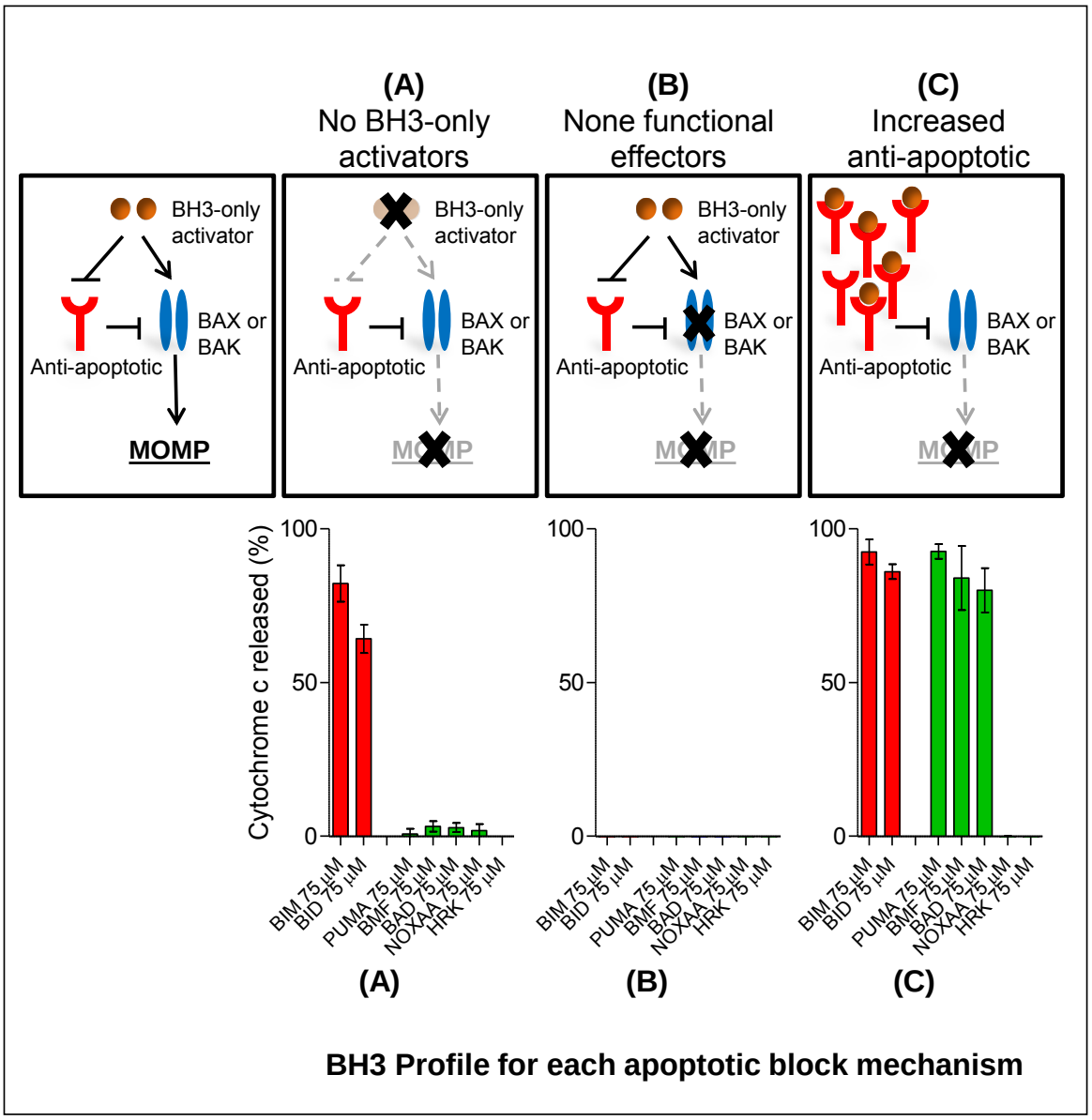

Figure 19: Anti-apoptotic mechanisms in cancer cells. Cancer cells can evade apoptosis via three mechanisms involving the Bcl-2 family and BH3 profiling can distinguish these mechanisms via cytochrome c released after exposure to individual activator or sensitizer BH3 peptides. Cytochrome c release is a surrogate for MOMP (mitochondrial outer membrane permeabilization) because cytochrome c is released from the mitochondria intermembrane space once MOMP has occurred. Downregulation of pro-apoptotic BH3-only activators would evade apoptosis because pro-apoptotic effectors BAX/BAK cannot be activated in the absence of activators and therefore no MOMP and no cytochrome c released. BH3 profiling on this type of cell would be determined because activator peptides (red bars) would release cytochrome c but sensitizer peptides (green bars) would not. The Second mechanism of evading apoptosis is through inactivation or downregulation of BAK/BAX because without BAX/BAK no MOMP and no cytochrome c released. BH3 profiling on a cell that uses this block would be determined when none of the BH3 peptides (activators or sensitizers) cause cytochrome c release. The final mechanism to evade apoptosis is via upregulation of anti-apoptotic Bcl-2 family members as this would neutralise any pro-apoptotic effectors or BH3-only proteins preventing MOMP. BH3 profiling on cells that use this block would be determined when both activator and sensitizer peptides cause cytochrome c release.

1.3.5 The extrinsic pathway

The extrinsic pathway is mediated through interactions of ligands with the death receptors (Figure 15). Death receptors (DR) are members of the tumour necrosis factor (TNF) receptor family and include FAS and TNFR1 (283, 284). Death receptors contain a death domain (DD) within the cytoplasmic region of the receptor. Once the receptor is activated this DD binds the DD of adaptor proteins such as FAS-associated death domain (FADD). This active complex now recruits procaspase 8 where it can be activated. Active caspase 8 then amplifies the caspases signal via activation of other caspase members such as caspase 3, 6 and 7. The extrinsic pathway does not rely on the Bcl-2 family of proteins to elicit apoptosis, however crosstalk between the pathways can occur in some cell types such as hepatocytes, where active caspase 8 can cleave BID, forming truncated Bid (tBID) which translocates to the mitochondria to promote BAX and BAK homo-oligomerization and MOMP (Figure 15; (283, 284)).

1.3.6 Aberrations in apoptotic proteins found in cancer

The original Bcl-2 family member, BCL-2 was discovered because of its involvement in a reciprocal translocation t(14;18), characteristic of follicular B-cell lymphoma (285, 286). This translocation causes a fusion between *BCL-2* and the immunoglobulin heavy chain gene under the regulation of the immunoglobulin heavy chain enhancer region causing high expression of BCL-2 (287). The *BCL-2* gene is also amplified in some cancers such as non-Hodgkin's lymphoma and SCLC (288, 289), whilst BCL-2 is overexpressed in more than 70 % of CLL due to either deletion or inactivation of *miR15* or *miR16* which target BCL-2 mRNA for degradation or hypomethylation of the *BCL-2* promoter (290, 291). Other anti-apoptotic Bcl-2 family members can also be upregulated in cancer, for instance *miR-29* represses the expression of the anti-apoptotic family member MCL-1 and loss of *miR29* has been observed in CRC (292, 293).

Aberrations in the pro-apoptotic Bcl-2 family members such as BAX also occur in cancer. BAX contains a guanosine stretch (8 amino acids) and slippage of the replication folk during S-phase can occur on repetitive DNA sequences. Cancers with defective MMR pathway, such as some CRC, are more prone to mutations

within repetitive regions of DNA which can lead to frame-shift mutations in *BAX* (294). Reduced levels of BIM and/or PUMA are associated with poor prognosis in CRC (295). Mutated *BRAF* and *NRAS* constitutively activate the MAPK pathway leading to BIM degradation (Chapter 1.3.2.1) and melanoma cells have been observed to be resistant to anoikis, a form of apoptosis in anchorage dependent cells via downregulation of BIM (296, 297). Low levels of RUNX3 have been observed in gastric cancer resulting in a decrease in BIM expression discussed previously (Chapter 1.3.2.1; (260, 261)).

The most common oncogenic mutation affecting apoptosis is loss of the tumour suppressor *TP53* (298). The p53 pathway regulates cellular response to environmental stress such as DNA damage or oncogene activation (299, 300). Loss of p53 leads to deregulation of vital checkpoints that cause either cell cycle arrest whilst defects are repaired or induce apoptosis if that damage is too severe (301). Wild type p53 regulates the transcription of various pro-apoptotic Bcl-2 family genes such as BAX, BID, NOXA and PUMA in both a cell-type and environmental stress-dependent manner (302-304). P53 also up-regulates genes involved in apoptosis downstream of the mitochondria such as APAF-1 (305-308) and caspase 8 and 6 (309, 310). p53 has also been shown to have a transcription-independent function in apoptosis regulation at the mitochondria where it can form a complex with anti-apoptotic proteins BCL-xL and BCL-2 thus promoting MOMP and cytochrome c release in response to apoptotic signals (311). The *TP53* gene is commonly mutated in a variety of cancers; specifically mutations are found in 40-50% of CRC (312) and 75-90% of SCLC (72).

According to the cBioPortal, aberrations in the Bcl-2 family genes (*BCL2, BAK1, BAX, BCL2A1, BCL2L11, BCL2L1, BCL2L15, BCL2L13, BCL2L14, BCL2L12, BCL2L10, BCL2L12P1, BCL2L2, BOK, MCL1, BID, BAD, HRK, NOXA1, BBC3* and *BMF*) are found in 74 of the 91 cancer studies available which includes three of four CRC studies and both SCLC studies, highlighting the importance of this anti-apoptotic pathway in cancer.

1.3.7 Apoptotic targeting drugs

Alterations in the function and expression of the Bcl-2 family of proteins contributes to cancer progression (2), highlighting their potential as sensible drug targets. Compared to normal cells cancer cells have increased apoptotic signalling caused by factors such as oncogene activation and changes in the microenvironment (1, 2). To avoid apoptosis these cancer cells upregulate anti-apoptotic proteins such as BCL-2 and/or downregulate pro-apoptotic proteins such as BIM (Figure 19). Cancer cells become reliant on anti-apoptotic signalling in order to survive, known as 'oncogene addiction' and drugs have been developed which target and exploit this. As this effect is specific to cancer cells, normal cells are not targeted by apoptotic-inducing drugs. The first biological therapy designed to target the apoptotic pathway was the antisense DNA agent targeting BCL-2, Oblimersen (Genasense/G3139; Genentech, San Francisco, USA) which was shown to induce apoptosis in cancer cell lines (313). Although single agent clinical trials have not shown promising results Oblimersen combined with chemotherapy agents is more efficacious (314).

An alternative approach is the use of small molecules antagonists that can block interactions between anti-apoptotic and pro-apoptotic Bcl-2 family members, known as BH3 mimetics (87, 315, 316). These are designed based on the BH3 domain of the pro-apoptotic BH3-only Bcl-2 family members and act as competitive inhibitors of the anti-apoptotic Bcl-2 family members. Their binding to anti-apoptotic proteins releases the pro-apoptotic Bcl-2 family members to induce apoptosis (Figure 20; chemical structure found in Appendix I, Figure 26). The first BH3 mimetic, ABT-737 was developed in 2005 (AbbVie, Chicago, IL, USA) and is based on the structure of the BH3 domain of BAD and thus antagonises BCL-2, BCL-xL and BCL-w (317). Preclinical studies demonstrated that ABT-737 has single agent activity in some SCLC, lymphoma and CLL cell lines *in vitro* and *in vivo* (87, 317-319) and acts synergistically with a wide range of conventional chemotherapeutic agents (320) and targeted therapies in a wide range of cancer types (84, 321). ABT-737 has been reported to be more effective under hypoxic conditions (322, 323), which is in contrast to radiotherapy and the majority of chemotherapy agents for which hypoxia drives resistance (324). Cells which rely

on BCL-2, BCL-w or BCL-xL for survival are particularly sensitive to ABT-737. ABT-737 is unable to interact with MCL-1, expression of this Bcl-2 family member is a resistance factor for ABT-737 efficacy (325). Indeed ABT-737 sensitisation caused by other drugs or the tumour microenvironment is often associated with MCL-1 downregulation (84, 322).

The clinical derivative of ABT-737 is Navitoclax (ABT-263; Figure 20; chemical structure found in Appendix I, Figure 26), an orally bioavailable BH3 mimetic. Navitoclax has shown promise in the phase I setting, where biomarkers of apoptotic cell death were detected in patients treated with Navitoclax (326). It is currently in phase I/II clinical trials in SCLC, ALL and CLL patients as a single agent and in combination with chemotherapy (327). Navitoclax showed promising single agent efficacy in phase II clinical trials in CLL (328) but not in in SCLC (326). Combing Navitoclax with targeted agents such as MEK or mTOR inhibitors appears to increase the potency of Navitoclax in preclinical models in NSCLC, pancreatic and SCLC (85, 329, 330), although the clinical impact of these findings remains to be determines.

Another BH3 mimetic currently in clinical trials in haematological malignancies (CLL and lymphoma) is Venetoclax (ABT-199, co-developed by AbbVie and Genentech, San Francisco, CA, USA), a BCL-2 specific antagonist (Figure 20; (331)). Recently it was show that the Tec kinase inhibitor Ibrutinib sensitised to Venetoclax in CLL where Ibrutinib has already been approved for second line treatment. Sensitisation is via inhibition of the Tec family kinase BTK and was associated with a decrease in MCL-1 and BCL-xL levels (332). In another study in CLL, Venetoclax-resistant cells are sensitised to Venetoclax when Venetoclax is combined with the BEZ235 (dual PI3K/mTOR inhibitor) and this is associated with MCL-1 downregulation due to PI3K pathway inhibition (333).

Other BH3 mimetics are being developed which target combinations of Bcl-2 family members. Obatoclax (Cephalon, Frazer, PA, USA) is reported to target all the anti-apoptotic Bcl-2 family (Figure 20) (334) and should therefore be effective in tumours which rely on MCL-1 overexpression for survival. However, the mode of action of Obatoclax is not clear as BAX/BAK-null cells can also be killed by

Obatoclax (335, 336), suggesting an atypical mechanism not dependent on MOMP. Phase II clinical trials in ES and chemo-refractory SCLC with Obatoclax in combination with SOC or second line therapy topotecan were disappointing because Obatoclax failed to improve response to chemotherapy and OS (337, 338). Recently BH3 mimetics targeting BCL-xL (Figure 20; A-1155463, AbbVie) or MCL-1 (Figure 20; Maritoclax (is a natural compound called marinopyrrole A, identified from a species of marine-derived streptomycetes (339)) have been developed/identified but these are still under preclinical testing (340).

Other apoptotic pathway-targeting drugs include SMAC mimetics, otherwise known as IAP antagonists (341, 342). IAPs such as XIAP are a family of proteins that interact with caspases (caspase 9, 7, 3) inhibiting their activation and preventing apoptosis (343). SMAC is a pro-apoptotic protein that is sequestered in the inner mitochondrial membrane. Once MOMP occurs, SMAC is released and binds IAPs blocking them from inhibiting caspases. SMAC mimetics are small molecule antagonist that binds IAP causing the release of caspases which allows them to be activated in the response to apoptotic signals (344, 345). SMAC mimetics are currently in phase I/II clinical trials both as single agents and in combination with chemotherapy in both solid tumours and haematological malignancies (346). Tumour necrosis factor-related apoptosis-inducing ligand (TRAIL) is a cytokine ligand from the TNF family that induces the extrinsic apoptotic pathway by binding to its transmembrane death receptors 4 and 5 (DR4 and 5). This can also cross talk with the intrinsic pathway to activate apoptosis via active caspase 8 cleaving BID to tBID (Figure 15; (347)). A humanised mAb, HGS-ETR1 (Mapatumumab; Human Genome Sciences, Inc, Rockville, MD, USA) recognises DR4 to activate the extrinsic apoptotic pathway (348) and is currently in phase II clinical trials in NSCLC and Non-Hodgkin lymphoma (349).

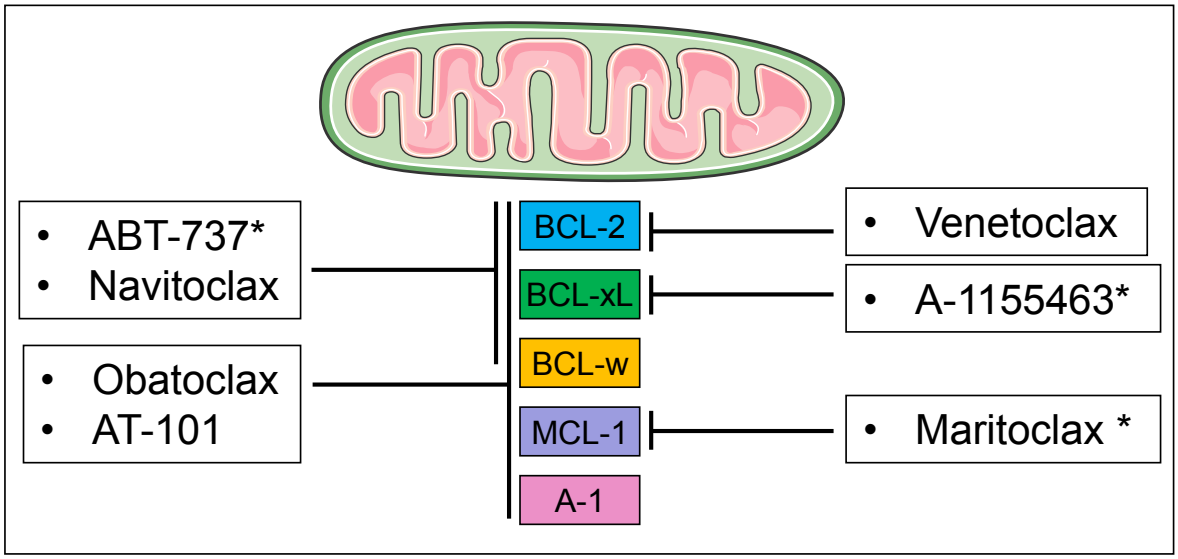

Figure 20: BH3 mimetics that target the intrinsic apoptotic pathway. BH3 mimetics are small molecule antagonists modelled on the pro-apoptotic BH3-only proteins and target specific anti-apoptotic Bcl-2 family members (BCL-2, BCL-xL, BCL-w, MCL-1 and A-1) depending on the specificity of the BH3-only protein modelled. Navitoclax, Obatoclax, AT-101 and Venetoclax are currently being tested in clinical trials (350). * ABT-737, A-1155463 and Maritoclax are preclinical compounds.

1.4 The future direction of cancer treatment

1.4.1 Targeted therapy and precision medicine

Targeted therapies are drugs which are designed to inhibit specific signalling pathways essential for tumour survival, growth and dissemination. The concept of targeted therapy is based on the idea of oncogene addiction (351) which hypothesize that an activated oncogene is essential for the proliferation and/or survival of cancer cells (1, 2, 352). Whereby, inhibition of the oncogene or its essential downstream targets will impede tumour progression (188, 189, 353, 354). Examples of targeted therapies are signal transduction inhibitors, apoptosis inducers, hormone therapies, angiogenesis inhibitors and immunotherapies (355). The great advances in understanding tumour biology over the past 20 years has paralleled advances in cancer drug discovery as new molecular drug targets on which a particular tumour might be dependent upon for one or more of its functions are uncovered. A major strategy for drug discovery is to identify mutated genes that cause deregulation of signalling pathways and drive tumorigenesis and to identify biomarkers that allow stratification of those patients who are most likely to benefit from a particular targeted therapy (356-358). This has led to development of the field of precision medicine (also termed personalised of stratified medicine) in the treatment of cancer whereby treatment is determined at the individual patient level based on the unique molecular pathology of their cancer (356-358). Figure 21 brings together the concept of precision medicine in the treatment of cancer.

The ‘poster child’ of targeted therapy in the treatment of cancer is the tyrosine kinase inhibitor imatinib (Gleevec, Novartis, Basel, Switzerland) in the treatment of chronic myeloid leukaemia (CML; (359, 360)). A subset of CML patients have aberrant activation of the NRTK ABL (Abelson murine leukemia viral oncogene homolog 1) caused by a t(9:22) chromosome translocation that fuses the *ABL* and *BCR* (breakpoint cluster region protein) genes, generating the proto-oncogenic fusion gene, *BCR-ABL* (361, 362). Inhibition of BCR-ABL with imatinib can lead to eradication of the disease in early chronic phase CML (363). However, in more advanced CML (accelerated or blast crisis phase) imatinib is not as effective,

possibly due to the accumulation of additional mutations and increased heterogeneity which allow inhibition of BCR-ABL to be overcome (364). Highlighting one of the main problems with targeted therapies; acquired and innate drug resistance. Another example of targeted therapy is treatment of NSCLC patients with activating *EGFR* mutations with the small molecule EGFR inhibitors erlotinib (Roche, Basel, Switzerland) and gefitinib (AstraZeneca, London, England). However relapse occurs in most patients due to acquired resistance. In some cases this is due to the acquisition of a second mutation in *EGFR* that leads to EGFR inhibitor resistance (365). The next generation EGFR inhibitors, such as AZD9291 (AstraZeneca) and rociletinib (Clovis Oncology, Denver, CO, USA), can overcome resistance to the most common *EGFR* mutation (*EGFR* T790M) and prolong OS (366).

Acquired resistance also occurs in patients with metastatic melanoma carrying the V600E *BRAF* mutation who have been treated with vemurafenib (PLX4032; Daiichi-Sankyo, Tokyo, Japan and Genentech) where a remarkable 80% of patients had partial or complete tumour regression (367). Acquired resistance to vemurafenib does not develop by secondary mutation in *BRAF* but through upregulation of PDGFRβ or *NRAS* mutations which result in reactivation of the MEK/ERK pathway (368).

Despite their proposed precise molecular targets present only in cancer cells, targeted therapies can cause substantial side effects such as high blood pressure, gastrointestinal perforation, problems with blood clotting and skin problems (369, 370). In some cases the more severe side effects can be associated with better patient outcome. For example NSCLC patients with serve skin rash during treatment with the EGFR small molecule inhibitor erlotinib (Tarceva) or gefitinib (Iressa; Figure 14) have a better response than patients that do not develop the rash (370). Better outcomes are also associated with mCRC patients that develop high blood pressure due to bevacizumab treatment ((369); Figure 14).

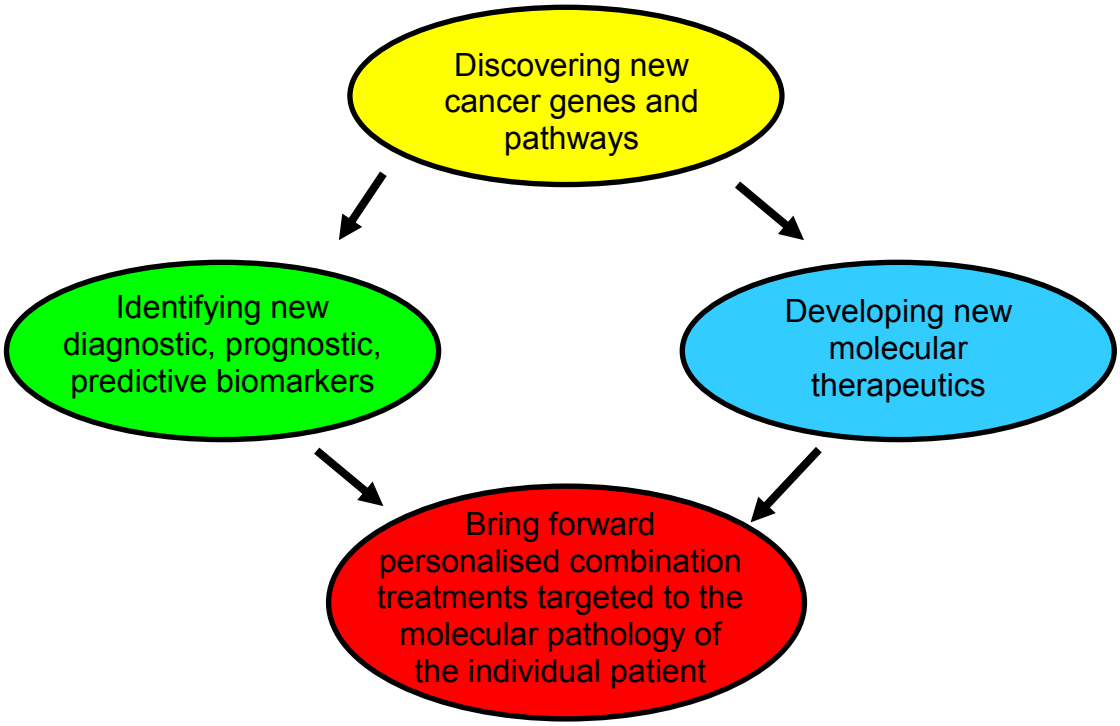

Figure 21: Strategy for exploiting the mechanisms that cause tumorigenesis. This strategy is to exploit our understanding of cancer genes and signalling pathways to develop personalised therapies which target the molecular pathology of the individual patient (357).

Currently there are phase II clinical trials in various cancers including CRC and SCLC where patients are profiled for molecular abnormalities and as a result are assigned to treatment groups whereby they receive given different targeted therapies according to whether they have a mutation in *EGFR* (erlotinib), *KRAS, BRAF, HRAS, NRAS* (AZD6244, MEK inhibitor), *PIK3CA, AKT, PTEN* (MK-2206, allosteric AKT inhibitor), *KIT, PDGFRA* (sunitinib, inhibits multiple RTK such as VEGFR and PDGFR) or *ERBB2* (lapatinib, HER2 and EGFR inhibitor). Targeted therapies are currently used to treat a wide range of cancer, as shown in Table 4. However, a major drawback observed in patients receiving targeted therapies is innate/acquired resistance along with heterogeneity (20, 77, 368, 371). One proposed route to overcome this problem in order to improve clinical outcome is with the use of rational drug combinations which target multiple cellular components simultaneously or sequentially (372).

Cancer Type	FDA Approved Targeted Therapy
Adenocarcinoma of the stomach or gastroesophageal junction	Trastuzumab (Herceptin), ramucirumab (Cyramza)
Basal cell carcinoma	Vismodegib (Erivedge), sonidegib (Odomzo)
Brain cancer	Bevacizumab (Avastin), everolimus (Afinitor)
Breast cancer	Everolimus (Afinitor), tamoxifen, toremifene (Fareston), Trastuzumab (Herceptin), fulvestrant (Faslodex),anastrozole (Arimidex), exemestane (Aromasin), lapatinib (Tykerb), letrozole (Femara), pertuzumab (Perjeta), ado-trastuzumab emtansine (Kadcyla), palbociclib (Ibrance)
Cervical cancer	Bevacizumab (Avastin)
Colorectal cancer	Cetuximab (Erbitux), panitumumab (Vectibix), bevacizumab (Avastin), ziv-aflibercept (Zaltrap),regorafenib (Stivarga), ramucirumab (Cyramza)
Dermatofibrosarcoma protuberans	Imatinib mesylate (Gleevec)
Endocrine/neuroendocrine tumours	Lanreotide acetate (Somatuline Depot)
Head and neck cancer	Cetuximab (Erbitux)
Gastrointestinal stromal tumour	Imatinib mesylate (Gleevec), sunitinib (Sutent), regorafenib (Stivarga)
Giant cell tumour of the bone	Denosumab (Xgeva)
Kaposi sarcoma	Alitretinoin (Panretin)
Kidney cancer	Bevacizumab (Avastin), sorafenib (Nexavar), sunitinib (Sutent), pazopanib (Votrient), temsirolimus (Torisel), everolimus (Afinitor), axitinib (Inlyta)
Leukaemia	Tretinoin (Vesanoid), imatinib mesylate (Gleevec), dasatinib (Sprycel), nilotinib (Tasigna), bosutinib (Bosulif),rituximab (Rituxan), alemtuzumab (Campath)
Liver cancer	Sorafenib (Nexavar)
None Small Cell Lung cancer	Bevacizumab (Avastin), crizotinib (Xalkori), erlotinib (Tarceva), gefitinib (Iressa), afatinib dimaleate (Gilotrif), ceritinib (LDK378/Zykadia), ramucirumab (Cyramza), nivolumab (Opdivo)
Lymphoma	Ibritumomab tiuxetan (Zevalin), denileukin diftitox (Ontak), brentuximab vedotin (Adcetris), rituximab (Rituxan), vorinostat (Zolinza), romidepsin (Istodax), bexarotene (Targretin), bortezomib (Velcade), pralatrexate (Folotyn)
Melanoma	Ipilimumab (Yervoy), vemurafenib (Zelboraf), trametinib (Mekinist), dabrafenib (Tafinlar), pembrolizumab (Keytruda), nivolumab (Opdivo)
Multiple myeloma	Bortezomib (Velcade), carfilzomib (Kyprolis), lenaliomide (Revlimid), pomalidomide (Pomalyst),panobinostat (Farydak)
Myelodysplastic/myeloproliferative disorders	Imatinib mesylate (Gleevec), ruxolitinib phosphate (Jakafi)
Neuroblastoma	Dinutuximab (Unituxin)
Ovarian epithelial/fallopian tube/primary peritoneal cancers	Bevacizumab (Avastin), olaparib (Lynparza)
Pancreatic cancer	Erlotinib (Tarceva), everolimus (Afinitor), sunitinib (Sutent)
Prostate cancer	Cabazitaxel (Jevtana), enzalutamide (Xtandi), abiraterone acetate (Zytiga), radium 223 chloride (Xofigo)
Soft tissue sarcoma	Pazopanib (Votrient)
Systemic mastocytosis	Imatinib mesylate (Gleevec)
Thyroid cancer	Cabozantinib (Cometriq), vandetanib (Caprelsa), sorafenib (Nexavar), lenvatinib mesylate (Lenvima)

Table 4: FDA approved drugs in cancer treatment (373).

1.4.2 Rational drug combinations

Understanding signalling pathways and their interactions along with an enhanced understanding of the hallmarks of cancer, drug resistance and heterogeneity (1, 2, 77) has led to the development of rational drug combinations in the treatment of cancer. Advanced and metastatic tumours display staggering levels of heterogeneity which means a one size fits all therapy will not be curative (77, 371, 374). Heterogeneous tumours which are initially responsive will almost certainly develop drug resistance and a secondary outgrowth of these resistant cells will ultimately cause relapse. Heterogeneity plays a crucial part in resistance to targeted therapy because tumours are made up of subclones (77, 78, 371). For example, a biopsy from a sub-section of tumour reveals wild-type *KRAS* in a mCRC patient so this patient is put on Cetuximab. However, this patient had a *KRAS* mutant subclone and Cetuximab treatment drives selection of this aggressive subclone and resistance to the targeted therapy. Where possible there is a need for multiple tumour biopsies to get as much mutational information on that specific tumour. No targeted therapies have yet been approved in SCLC (Table 4) and this is due to the remarkable heterogeneity of SCLC and lack of prevalent and druggable drive mutations (66-69) (Chapter 1.1.2.2 and 1.1.2.3). The rationale behind drug combinations is that by targeting two driver pathways simultaneously this reduces the cancers ability to become resistant, having a synergistic effect.

A common mechanism of resistance to targeted therapies is due to complex nature of crosstalk between different signal transduction pathways. Targeted inhibition of a specific pathway can cause upregulation of another aspect of the same pathway or other pathways due to feedback loops and crosstalk (375). It is important to understand the molecular mechanism of the drug targets in order to rationally combine two synergistic drugs successfully. An example of drug resistance due to pathway feedback loops in response to targeted therapy was observed in breast and CRC patient tumours treated with the mTORC1 inhibitor, the rapamycin derivative RAD001 (Everolimus, Novartis). RAD001 treatment caused feedback activation of AKT observed by increased phospho-AKT (S473), resulting in resistance. However, rationally combining RAD001 with IGF-1R

reversed the feedback loop by blocking AKT activation (376). An interesting example of feedback activation and pathway crosstalk was observed in CRC where patients harbouring the V600E *BRAF* mutation had a poor response to vemurafenib (377). As previously mentioned vemurafenib initially has excellent single agent efficacy in melanoma patients harbouring this *BRAF* mutation, however, in CRC vemurafenib-induced inhibition of V600E *BRAF* caused feedback activation of EGFR resulting in vemurafenib resistance (377). This is because the mechanism of action downstream of active BRAF/ERK pathway is cell-context dependent and CRC mechanism is different to melanoma. In CRC downstream of active BRAF the phosphatase CDC25C negatively regulates EGFR. Vemurafenib inhibition of BRAF inactivates CDC25C, resulting in continuation of EGFR signalling pathway via PI3K and therefore resistance to vemurafenib. This feedback activation of EGFR suggests that EGFR expression levels may be a useful predictive biomarker for response to therapy in CRC patients with *BRAF* mutation (377). This data also provides strong rationale for combining BRAF and EGFR inhibitors in V600E *BRAF* mutant CRC patients, further strengthened by the finding that combining vemurafenib with the EGFR inhibitors cetuximab, gefitinib or erlotinib caused inhibition of EGFR/PI3K signalling and proved efficacious *in vivo* (377).

Various rational drug combinations are currently in phase II clinical trial in individuals with advanced CRC that have not responded to standard chemotherapy (378). One involves the combination of the MEK inhibitor AZD6244 with the AKT inhibitor MK-2206. The rationale being that simultaneous inhibition of the MEK pathway and PI3K pathway (via AKT) will have a synergistic effect on two of the most commonly altered oncogenic pathways that drive tumorigenesis in CRC. In addition, a phase II clinical trial in advanced solid tumours (NSCLC, CRC, breast cancer, pancreatic cancer and malignant melanoma) with *KRAS*, *NRAS* and/or *BRAF* mutations using BEZ235 (dual PI3K/mTOR inhibitor) in combination with MEK162 (MEK1/2 inhibitor) is also underway (379).

Whilst the results of these trials using rational drug combinations are eagerly awaited much work is still required to understand which combinations will have the greatest efficacy in which tumours and that novel treatments are urgently required,

particularly in aggressive diseases like SCLC in which therapy options are limited. The aim is that future treatment for CRC and SCLC will limit the use of cytotoxic therapies and instead will revolve around the use of less toxic targeted drugs used in a rational combination for maximal effect, in order to reduce the overall drug toxicity in patients which can both limit the patients response and cause significant short and long-term morbidity and even result in death. Mainstay of treatment in CRC and SCLC as discussed revolves around chemotherapy regimens therefore rational drug combinations must be tested alongside SOC until such a day until evidence supports rational drug combinations are more beneficial for the patient over standard of care. The FDA are now considering rational combinations in early phase clinical trials without the necessity for prior single-agent approval as long as the combination proves to increase the efficacy of either drug as a single agent and there is sound scientific rationale for the combination in that specific disease (380).

1.4.3 Rational drug combination of a PI3K pathway inhibitor with ABT-737 or Navitoclax in CRC and SCLC

Current PI3K pathway literature discussed in detail in Chapter 1.2.4 describes the role of active PI3K/AKT pathway in positively regulating survival pathways via regulation of the Bcl-2 family (133, 135, 381), caspases activity (136) and FAS ligand expression (137). However, inhibition of the PI3K pathway does not activate apoptosis in many types of cancer cell lines such as CRC which suggests that the role of PI3K and the activation of survival pathways may be cell-context dependent (223, 382). As previously discussed, components of the PI3K pathway are frequently mutated in both CRC and SCLC making the PI3K pathway an attractive drug target in these cancers (Chapter 1.2.7, Figure 13) and another potential avenue is directly targeting the anti-apoptotic pathways, which is characteristic in cancers (1, 2). In this thesis we hypothesise that combining a PI3K inhibitor (PI3Ki) with a BH3 mimetic in CRC and SCLC is rational because PI3K pathway inhibition will ‘prime’ a cell therefore lowering the apoptotic threshold to potentiates BH3 mimetic efficacy. This ‘double attack’ on cells with the rational combination blocks proliferative signals (PI3K pathway (382)) and survival signals (Bcl-2 family (249, 273)) simultaneously to reduce therapy resistance. The synergistic approach

means lower concentration of drug may prove clinically efficacious therefore lowering the toxic side effects observed with these targeted therapies.

94

1.5 Project aims and objectives

1.5.1 Overall project aims

Metastatic CRC and SCLC patient prognosis is poor and curative surgery is rarely an option. Treatment options are limited, thus representing an area of unmet clinical need in both diseases. 10-30% SCLC patients are chemo-refractory highlighting a need to identify such patients and provide alternative therapies. PI3K pathway genes are frequently mutated in both CRC and SCLC and upregulation of anti-apoptotic pathways are present in the majority of cancers making the PI3K pathway and the anti-apoptotic pathway attractive drug targets. In an attempt to improve the therapeutic strategy for patients with mCRC and SCLC, the rational drug combination of a PI3K inhibitor with a BH3 mimetic was assessed in CRC and SCLC preclinical models. The downstream effectors of PI3K and the molecular mechanism underpinning drug combination effects were investigated. If the therapeutic strategy explored in this thesis is successful, the preclinical data produced could support applications for clinical trials using this combination of drugs for patients with CRC and SCLC.

1.5.2.1 Specific Objectives

1.5.2.2 Chapter 3

Objective 1: To determine the effect of PI3K pathway inhibition with various inhibitors against PI3K, AKT or mTOR on the sensitivity of the BH3 mimetic ABT-737 in CRC cells lines and whether the drug combination increase apoptosis compared to single agent drug.

Objective 2: To determine the effect of PI3K pathway inhibitors on Bcl-2 family protein expression levels in CRC cell lines.

Objective 3: To investigate the effect of the Bcl-2 anti-apoptotic protein MCL-1 on ABT-737 sensitivity in CRC cell lines and determine whether MCL-1 is regulated by the PI3K pathway in these cells.

Objective 4: To carry out a siRNA library screen to identify PI3K downstream effectors and determine whether knock down of candidate mRNA sensitises CRC cell lines to ABT-737. The siRNA screen will focus on targeting mRNA of proteins with a PH domain as they are have potential to be regulated by PI3K.

Objective 5: To validate any potential siRNA hits from the siRNA screen that sensitise CRC cells to ABT-737 to determine sensitisation is due to on-target effects. Use individual siRNA that make up the SMARTpool siRNA to knock down target and determine whether knock-down significantly sensitises to ABT-737 compared to the non-targeting siRNA control. Further investigate targets in other CRC cells and use pharmacological inhibitors available (if any) inhibit and does this sensitise to ABT-737.

1.5.2.3 Chapter 4

Objective 6: To determine what cancer cell lines express the highest levels of BMX using the cancer cell line encyclopaedia (CCLE).

Objective 7: To investigate the role of PI3K/BMX pathway in cell lines that express BMX. To determine whether inhibition of the PI3K/BMX pathway inhibitors sensitises SCLC cells to ABT-737 and whether this increases levels of apoptosis compared to single agent drugs.

Objective 8: To investigate the role of BMX in SCLC cell lines by knocking down BMX and whether this sensitises to ABT-737. Determine if BMX is acting downstream of PI3K in these cells. To treat SCLC BMX RNAi cells with PI3Ki and analyse the effect on ABT-737 efficacy.

Objective 9: To investigate the role of AKT and mTOR on SCLC cell lines sensitivity to ABT-737 using AKT and mTOR inhibitors in combination with ABT-737.

Objective 10: To determine the effect of PI3K, BMX, AKT and mTOR inhibitors on Bcl-2 family protein expression levels in SCLC cell lines.

Objective 11: To investigate the downstream effectors of BMX in SCLC cell lines using a phospho-kinase array on cells that have BMX knocked down by RNAi or treated with the Tec kinase inhibitor Ibrutinib.

Objective 12: To interrogate SCLC preclinical *in vivo* models to assess the rational drug combination of a PI3K inhibitor and BH3 mimetic using the clinically relevant class I PI3K inhibitor GDC-0941 and the ABT-737 oral derivative Navitoclax. Use cell line xenograft and CDX models with the aim to show proof of mechanism of drug.

1.5.2.4 Chapter 5

Objective 13: To determine whether BH3 profiling on CDX tumours is feasible and optimise a workflow.

Objective 14: To BH3 profile CDX models with known response to SOC (cisplatin/etoposide) retrospectively. To determine whether chemo-sensitive and chemo-refractory CDX models respond differently to BH3-only peptides and whether this information can be used to predict of CDX response to standard of care.

Objective 15: To BH3 profile CDX models derived at baseline and again at relapse prospectively to further validate the process for prediction of response to SOC and to clarify whether BH3 profiles can be used as predictive biomarkers for chemotherapy responses in SCLC.

Chapter 2

Materials and Methods

2. Materials and methods

2.1 Materials

All materials were purchased from Sigma Aldrich (Poole, UK) unless otherwise specified

2.1.1 BH3 profiling reagents

DTEB Buffer (kept at 4°C for 6 months and no freeze thawing)

DTEB buffer contained 135 mM Trehalose, 10 mM HEPES (pH 7.5 with KOH), 20 µM EDTA (pH 7.5 with KOH), 20 µM EGTA (pH 7.5 with KOH), 5 mM Succinate acid, 0.1% BSA and 50 mM KCl in sterile ddH_2O and sterile filter (pH 7.5 +/- 0.1 with KOH).

BH3 peptide buffer (made freshly on day of use)

BH3 peptide buffer contained DTEB and 0.002% digitonin (5% stock digitonin in DMSO (dimethylsulfoxide), kept at -20°C).

Extracellular staining buffer (kept sterile and stored at 4°C)

Extracellular staining buffer contained 2% FBS (fetal bovine serum, BioWest, Nuaillé, France) and 1X HBSS (Hank's Balanced Saline Solution; Life Technologies, Inc, Paisley, UK) in sterile ddH_2O.

Neutralising Buffer (kept at room temperature)

Neutralising buffer contained 1.7 M Tris (Trizma base) and 1.25 M glycine (pH 9.1 with KOH).

Intracellular Staining Buffer 10X (kept sterile and stored at 4°C)

Intracellular staining buffer contained 1% Saponin, 10% BSA, 20% FBS and 15 mM sodium azide in PBS (Phosphate-buffered saline, made in house by laboratory services) and sterile filtered.

Formaldehyde

Formaldehyde is diluted to 4% (vol/vol) with PBS.

2.1.2 Drugs

ABT-737 (a kind gift from AbbVie, Chicago, IL, USA), PI-103, rapamycin, Akti1/2, KU-0063794 (Merck, Nottingham, UK), GDC-0941 (*in vitro* use), MK-2206, and Ibrutinib (Selleck Chemicals, Houston, TX, USA) were all dissolved to 10 mM in DMSO and stored as single use aliquots at −20°C/−80°C. Navitoclax (a kind gift from AbbVie) was stored at 4°C and formulated in 10% ethanol, 30% polyethylene glycol 400, and 60% Phosal 50 PG (American Lecithin Company, Oxford, CT, USA). GDC-0941 (Lancrix Chemicals, Shanghai, China) was stored at -20°C and formulated in 10% DMSO, 5% Tween 20, and 85% sterile saline (Fresenius Kabi, Cheshire, UK). Once formulated, Navitoclax and GDC-0941 were stored at room temperature for up to 7 days. All drug structures are in Appendix I Figure 26 (383).

2.1.3 Cell line freezing media (kept at -20°C)

Cell line freezing media contained 90% FBS and 10% DMSO.

2.1.4 HITES medium (kept at 4°C)

HITES medium contained 5 µg/mL insulin, 10 µg/mL transferrin, 10 nM β-estradiol, 30 nM sodium selenite and 10 nM hydrocortisone in RPMI phenol red free media (Roswell Park Memorial Institute; Life Technologies, Inc).

2.2 *In vitro* methods

2.2.1 Cell culture

HCT116, DLD-1 (American Type Culture Collection (ATCC) Manassas, VA, USA) cells were cultured in McCoy's 5A media (Life Technologies, Inc) supplemented with 10% FBS. SW620 (ATCC) cells were cultured in Dulbecco's modified Eagle's medium (Life Technologies, Inc) supplemented with 10% FBS and 2 mmol/L L-glutamine (Life Technologies, Inc). NCI-H146, NCI-H526, NCI-H1048 and

DMS114 (ATCC) cells were cultured in RPMI 1640 media supplemented with 10% FBS. CRC and SCLC cell lines were authenticated using the AmpFISTR system (Applied Biosystems, Paisley, UK). SU-DHL-4 and BBDL (BAX/BAK deficient lymphoma; originally misreported as SU-DHL-10 by the Letai laboratory DFCI. Recently identified as distinct from SU-DHL-10) lymphoma cells were cultured in RPMI 1640 media supplemented with 10% FBS and used as BH3 profiling positive controls. SU-DHL-4 and BBDL cells were authenticated using the Promega *GenePrint*® 10 System (DFCI molecular biology core facility). All cell lines were incubated in a humidified atmosphere at 37°C and 5% CO_2.

2.2.2 Concentration response

Cells were seeded into 96 well plate(s). DLD-1 cells were seeded at 500 cells per well, HCT-116 cells were seeded at 1000 cells per well, and SW620 cells were seeded at 5000 cells per well. H1048 and DMS114 cells were seeded at 7300 cells per well, H526 cells were seeded at 14000 cells per well and H146 cells were seeded at 15000 cells per well. 24 hours after seeding cells were treated with the indicated concentration of drug(s) and cultured for a further 72 hours. Adherent cells (DLD-1, HCT-116, SW620, H1048 and DMS114) were then subjected to a SRB (sulforhodamine B) assay and suspension cells (H146 and H526) were subjected to a resazurin assay. To determine logGI50, log drug concentration was plotted against raw absorbance, and nonlinear curve fit analysis was performed (GraphPad Prism; GraphPad Software, Inc, La Jolla, CA, USA). For display purposes only, drug concentration (log scale) has been plotted against normalized absorbance. Statistical analysis was carried out on three independent logGI50 readings and transformed to growth inhibition 50 (GI_{50}).

2.2.2.1 Sulforhodamine B (SRB) assay

SRB assay (adherent cells) was carried out on cells after drug treatment for 72 hours. SRB is an aminoxanthene dye that binds to cellular protein and once the dye is resuspended the absorbance of the dye is directly proportional to the mass thereby enabling a determination of cellular biomass. Adherent cells were washed in PBS and then fixed with ice cold 10% TCA (trichloroacetic acid) for 60 minutes at 4°C. Cells were then washed with PBS and left to air dry. Fixed cells were then

stained with 0.4% SRB (wt/vol) for 15 minutes and washed with 1% acetic acid (vol/vol). Stained protein was then resuspended with 100 µL 1.5 M Tris-HCl (pH 8.8) to release the dye and the absorbance was read at OD_{540} nm on a 96-well plate spectrophotometer (Labsystems, Original multiskan EX, Vienna, VA, USA).

2.2.2.2 Resazurin assay

Resazurin assay (suspension cells) was carried out after drug treatment for 72 hours and measures the metabolic activity of living cells. Bioreduction of the resazurin dye by viable cells increases the fluorescent intermediate and this can be used as an indication of compound toxicity. Suspension cells were removed from incubator into sterile tissue culture hood. Resazurin solution 10X stock (2 mM) was added to culture media and returned to incubator for 4 hours. The 96 well plate was lightly shaken and the fluorescence (λex 530 nm, λem 590 nm) was recorded using a fluorescence spectrophotometer (FLUOstar, BMG LABTECH, Ortenberg, Germany).

2.2.3 Measurement of apoptosis

2.2.3.1 Annexin V/7-aminoactinomycin D (7-AAD) assay

Annexin V/7-AAD assay is used to distinguish viable cells from early or late apoptotic cells and was performed in HCT-116 and SW620 cells after indicated drug treatment. Cells were harvested by trypsinization and resuspended in Annexin Binding Buffer (BD Biosciences) and incubated with 7-AAD (BD Bioscience) and/or Annexin V-APC (BD Bioscience) in the dark for 15 minutes at room temperature. Cells were then analysed by flow cytometry on a BD FACSArray Bioanalyzer (BD Bioscience).

2.2.3.2 Cytochrome c release assay

The cytochrome c release assay was performed in H526, H1048 and DMS114 cells to measure the percentage of cells that retained cytochrome c in the mitochondria after indicated drug treatment. A cell that is cytochrome c negative suggests that MOMP has occurred releasing the cytochrome c and therefore the cytochrome c release assay is used as a surrogate for apoptosis. Cells ($5x10^5$–

$1x10^6$) were pelleted after indicated drug treatment and resuspend in 100 µL of DTEB and 0.002% digitonin in a clean tube and incubated for 15 minutes at room temperature. Cells were fixed in formaldehyde (1% final concentration) for 15 minutes at room temperature in the dark and tubes were gently flicked. Cells were diluted with 3X neutralising buffer for 15 minutes at room temperature in the dark. Cells were stained with cytochrome c antibody 1:400 (Alexa 488, clone 6h2.b4, BD biosciences) in intracellular staining buffer overnight at 4°C. The next day cells were analysed by flow cytometry (BD LSRFortessa™ analyzer) using Diva software (BD Biosciences). Cytochrome c released was calculated from cytochrome c positive cells minus 100%. Cytochrome c released was normalised to DMSO and no antibody control. Statistical analysis was carried out on three independent raw cytochrome c released readings.

2.2.3.3 BAK conformational change assay

Before MOMP occurs BAK undergoes a conformational change in the N-terminus (Chapter 1.3.2). This reveals a new epitope in BAK that can be detected by immunofluorescence. For assessment of BAK conformational change, cells were cultured in a 96 well plate and treated with the indicated drug(s) for 24 hours. Cells were fixed with 1% formaldehyde and sent to Imagen Biotech (Cheshire, UK) where immunofluorescence staining for conformation changed BAK and high-content analysis were carried out using proprietary protocols using BAK conformation–specific antibodies (BAK Ab-1 (#AM03) raised against a peptide corresponding to N-terminal residues 1-52 amino acids; BAK Ab-3 (#AM15) raised against an epitope encompassing the BH-1 domain (amino acids 82-135); BAK (#66026E) all from Calbiochem).

2.2.3.4 Caspase 3/7 assay

Effector Procaspases 3 and 7 are cleaved and activated to caspase 3 and 7 in response to pro-apoptotic signals (Chapter 1.3.2, Figure 15). Real time assessment of cells with activated caspase 3/7 was carried out using the CellPlayer apoptosis caspase 3/7 reagent (Essen BioScience, Ann Arbor, MI, USA) following manufacturer's recommendations. Cells were placed in an IncuCyte (Essen BioScience) and imaged every 2 hours. The number of

fluorescent cells per field of view was determined using IncuCyte software (Essen BioScience) following manufacturer's recommendations.

2.2.4 BCA assay

The Pierce BCA (bicinchoninic acid assay) protein assay kit (Thermo Scientific, IL, USA) was used to determine protein concentration of a cell lysate sample. Samples were diluted 10X in sterile ddH_2O to ensure protein concentration was below 1 mg/mL. Protein standards (2 mg/mL BSA) were diluted with a 1:1 serial dilution in sterile ddH_2O to get a range from 1 mg/mL to 0.0625 mg/mL. Lysis buffer was diluted 10X in sterile ddH_2O and used as a 0 mg/mL control. 20 µL of each protein standard and diluted lysate sample were added to duplicate wells of a 96 well plate. The BCA reagents were made up 1 part reagent B to 50 parts reagent A (1:50) and mixed together. 200 µL of the mixed BCA reagents was added to each well and the plate was incubated at 37ºC for 30 minutes. The plate absorbance was read at OD_{540} nm on a 96-well plate spectrophotometer. The protein standard readings were used to make a line of best fit and then the protein concentration for each lysate sample was calculated using the BCA assay equation shown in Table 5.

Line equation	y=mx+c
Protein concentration	x=y-c/m
BCA assay	x=((mean of duplicate readings-c)/m)*10(sample dilution factor)

Table 5: Equations for BCA assay

2.2.5 Western Blotting

Cells were washed with ice cold PBS and lysed directly into 10% cell lysis buffer (Cell Signalling Technology, MA, USA) supplemented with 1% Protease Inhibitor Cocktail and 1% Phosphatase Inhibitor Cocktail I and II. Protein concentrations were determined using a Pierce BCA Protein Assay Kit (Chapter 2.2.4). Protein samples were separated on, 4-12% (gradient), 10% or 12% NuPAGE Novex Bis-Tris Gels (Thermo Fisher Scientific, Waltham, MA, USA) with NuPAGE MES or MOPS SDS Running Buffer (Thermo Fisher Scientific) depending on protein size (Figure 22) and gels were run for ~90 minutes at 120V. Polyvinylidene fluoride

membranes (Perkin Elmer, MA, USA) were activated in methanol for 1 minute prior to use. Proteins were transferred to polyvinylidene fluoride membranes for 1 hour by electroblotting at 30V using NuPAGE transfer buffer (Thermo Fisher Scientific) with 20% methanol. Membranes were blocked in 10% dried milk (Marvel, Ireland) in PBST (PBS containing 1% Tween-20) for 30 minutes at room temperature on a rocking platform. Membranes were washed 3 times in PBST (10 minutes each) and incubated overnight at 4°C with appropriate primary antibody. Membranes were washed 3 times in PBST (10 minutes each) then re-incubated with an appropriate species specific secondary antibody conjugated to horseradish peroxidise for 1 hour at room temperature. Membranes were then washed an additional 3 times in PBST (10 minutes each). Proteins were detected using electrochemical luminescence reagents, Western Lightning (Perkin Elmer, UK). Protein weights were determined using Colour Prestained Protein Standard (New England BioLabs, Ipswich, MA, USA). Bands were visualised using a Fujifilm LAS 1000 Luminescence Image Analyser (Fujifilm, Tokyo, Japan). All primary and secondary antibodies used for Western blotting are in Table 6.

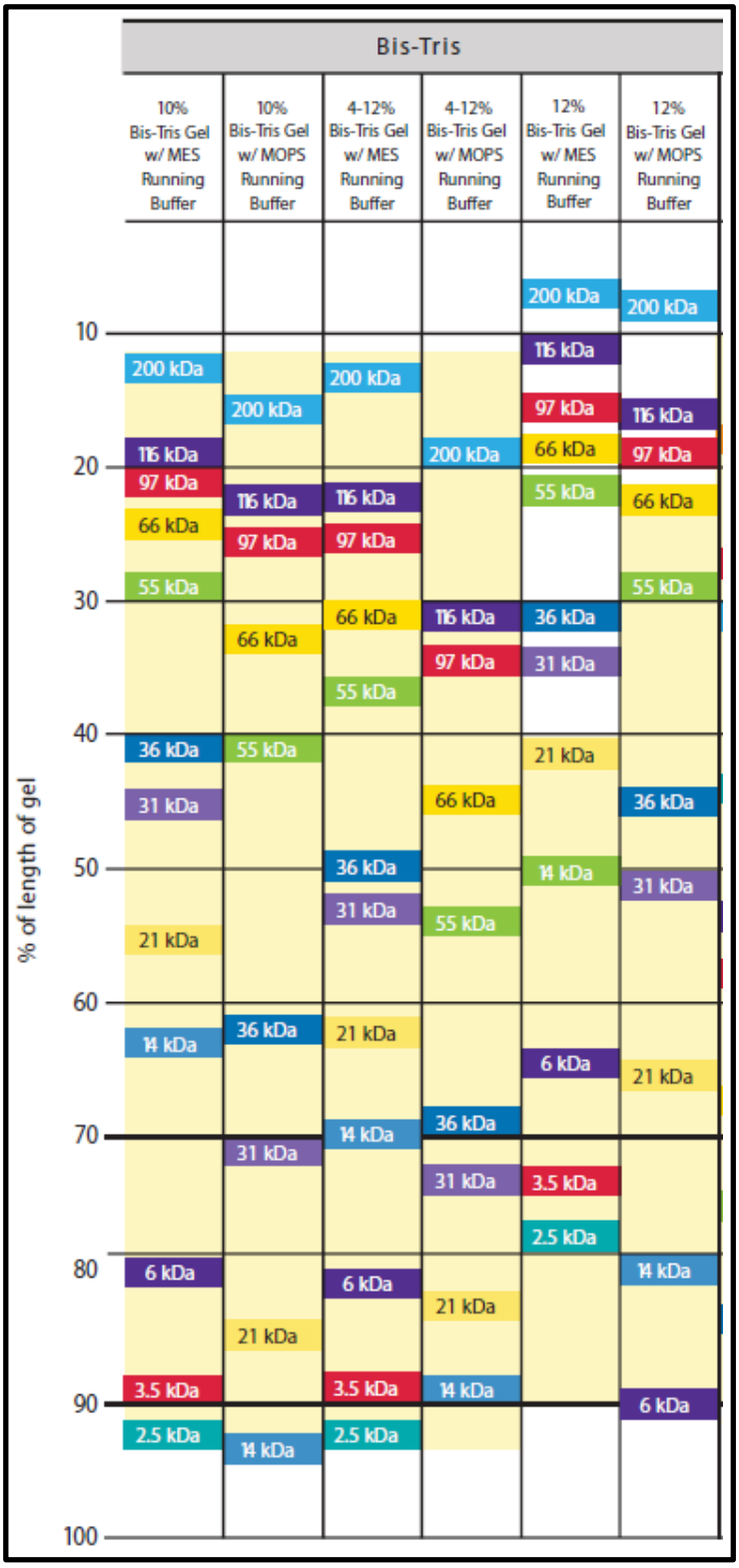

Figure 22: NuPAGE Bis-Tris gel migration chart. Figure adapted from NuPAGE technical guide. The migration pattern of protein standards according to size, percentage gel and buffer used. The chart was used to select the appropriate gel for separating proteins of interest based on size.

Antibody	Species	Dilution	Source
Anti- human Actin	Mouse	1:2000	Sigma
Anti- human GAPDH	Mouse	1:2000	Sigma
Anti- human α-tubulin	Mouse	1:2000	Merck
Anti-human BCL-2	Mouse	1:1000	Dako
Anti-human BCL-xL	Rabbit	1:1000	Becton Dickinson
Anti-human MCL-1	Mouse	1:1000	Becton Dickinson
Anti-human PUMA	Rabbit	1:1000	Sigma
Anti-human BAK	Mouse	1:1000	Calbiochem
Anti-human BAX	Rabbit	1:1000	Cell signalling
Anti-human BAD	Rabbit	1:500	R&D Systems
Anti-human BID	Goat	1:1000	R&D Systems
Anti-human BIM	Rabbit	1:1000	Cell signalling
Anti-human BMX	Mouse	1:1000	Becton Dickinson
Anti-human pS473 AKT	Rabbit	1:1000	Cell signalling
Anti-human pT308 AKT	Rabbit	1:1000	Cell signalling
Anti-human total AKT	Rabbit	1:1000	Cell signalling
Anti-human pT246 PRAS40	Rabbit	1:1000	Cell signalling
Anti-human total PRAS40	Rabbit	1:1000	Cell signalling
Anti-human pS235/236 S6	Rabbit	1:1000	Cell signalling
Anti-human pS240/244 S6	Rabbit	1:1000	Cell signalling
Anti-human total S6	Rabbit	1:1000	Cell signalling
Anti-human cleaved caspase 3	Rabbit	1:1000	Cell signalling
Anti-human PARP	Rabbit	1:1000	Cell signalling
Anti-mouse horseradish peroxidase	Goat	1:2000	Dako
Anti-rabbit horseradish peroxidase	Goat	1:2000	Dako
Anti-goat horseradish peroxidase	Mouse	1:2000	Dako

Table 6: Antibodies used for Western blotting

2.2.6.1 RNA interference (forward transfection with siRNA)

SMARTpool small interfering RNA (siRNA) or individual oligos (Thermo Fisher Scientific) were transfected into SW620 or HCT116 cells using DharmaFECT 2 (Thermo Fisher Scientific) and H1048 cells using RNAiMAX (Thermo Fisher Scientific) according to manufacturer's instructions. All siRNAs were resuspended in 1X siRNA buffer (5X siRNA buffer (Thermo Fisher Scientific) diluted to 1X in RNase-free water (Thermo Fisher Scientific)) to 20 μM stock. All cells were transfected in a 6 well plate. In HCT-116 and SW620 cells, 2.5 μL (20 μM siRNA stock) was mixed with 197.5 μL OptiMEM (Thermo Fisher Scientific; 50 pmol siRNA) by inversion and incubated for 5 minutes. In HCT-116 cells 1 μL, or SW620 cells 3 μL, of DharmaFECT 2 was mixed with 199 μL or 197 μL OptiMEM respectively by inversion and incubated for 5 minutes. Then the siRNA and transfection reagent were mixed together and incubated at room temperature for

20 minutes. $4x10^5$ HCT116 and $1x10^6$ SW620 cells were seeded in 1.6 mL of media and the siRNA-lipid complex was added to the cells. In H1048 cells, 1.5 µL (20 µM siRNA stock) was mixed with 148.5 µL OptiMEM by inversion. 9 µL of RNAiMAX was mixed with 141 µL OptiMEM by inversion and both solutions were diluted 1:1 and incubated for 5 minutes. 250 µL of the siRNA-lipid (25 pmol siRNA) complex was added to $1x10^6$ H1048 cells seeded the previous day in 1.75 mL of media. The next day cells were reseeded into appropriate culture vessels depending on the experiment (drug treatment (SRB), Western blotting or qPCR (quantitative or real time Polymerase Chain Reaction). Non-targeting, BMX SMARTpool and MCL-1 SMARTpool siRNAs target sequence can be found in Appendix II Table 13.

2.2.6.2 siRNA library screen (reverse transfection)

The siRNA library screen was to identify potential PI3K downstream effectors that sensitise to ABT-737 when knocked down by RNA interference (RNAi). The siRNA library consisted of 65 SMARTpool siRNA candidates (Table 7). The majority of the candidate siRNAs targeted the mRNA of proteins with a PH domain because they have the potential to be regulated by PI3K (via interacting with PtdIns(3,4,5)P3, Chapter 1.2.5). SW620 cells were reverse transfected with 5 pmol of each SMARTpool siRNA candidate from the mother plate 1 and 2, in 1 well of a 96-well plate (6 replicate daughter plates). Then 48 hours later 3 replicate daughter plates were treated with 4 µM ABT-737, and 3 were treated with DMSO equivalent. Then 72 hours later cells were subjected to a SRB assay (Chapter 2.2.2.1). Each of the candidate siRNAs target sequence and the layout of the siRNA screen mother plate 1 and 2 are in Appendix III Table 14 and Appendix IV Figure 27 respectively.

SOS1	CYTH2	GAB1	MCF2	PLEKHB2	AKAP13	FGD6
PLCXD2	DOCK2	PIK3CA	GAB2	CYTH1	RASA1	BMX
CYTH4	TEC	RASA3	VAV1	PLEKHA2	BTK	PTPN9
VAV3	ARAP3	RASA2	PHLDB1	ARAP1	GAB3	GSK3A
TIAM1	PREX1	DOCK1	SWAP70	AKT2	AKT1	PIK3R2
SGK1	ARAP2	PIK3CD	MTOR	PREX2	PHLDB3	
PIK3R1	PLCL2	PIK3CB	AKT3	MYO10	RPTOR	
ITK	SBF1	PDPK1	CYTH3	RICTOR	DAPP1	
ARHGEF4	GSK3B	SGK2	PLEKHA1	ARHGEF6	SH3BP2	
VAV2	SGK3	ADAP1	ARHGAP1	PLEK2	ADAP2	

Table 7: siRNA library screen candidates

2.2.6.3 ABT-737 sensitivity of each siRNA candidate in the siRNA screen library

SW620 cells sensitivity to ABT-737 after transfection with each siRNA SMARTPool was assessed by calculating the surviving fraction following treatment for 72 hours with 4 μM ABT-737 (Table 7). Surviving fraction = replicate well with ABT-737 / (average of three replicate wells with DMSO). The robust Z-score was used to analyse siRNA screen data. Robust Z-score is the number of median absolute deviations a value is from the median value of the data set. The robust Z-score is used because it reduces the effect of outliers on the results and prevents missing potential significant changes in sensitivity to ABT-737. Firstly the new surviving fractions are calculated. New surviving fraction = median surviving fraction for all 65 siRNAs – individual surviving fraction. New negative surviving fractions are converted to positive values and the median absolute deviation (MAD) is then calculated. MAD = Standard deviation (new surviving fractions) x 1.4826. The robust Z-score for each individual replicate can be calculated. Robust Z-score = ((survival fraction – median survival fraction) / MAD) x 1.4826. A threshold of median +/- 2 standard deviations is usually defined as a screen hit.

Unpaired two tailed t-test was used to calculate the P-value for each siRNA compared to non-targeting siRNA (negative control). A P-value below 0.05 would show a significant difference between that specific candidate siRNA and the non-targeting siRNA. P-values were plotted against Robust Z-scores to identify the most likely ABT-737 sensitizers because no Z-scores reached +/- 2 standard deviations.

2.2.7.1 Reverse transcription

Levels of BMX, SGK1 or SOS1 mRNA were assessed in SW620 RNAi cells. qPCR was performed on cDNA reverse transcribed from RNA isolated from SW620 RNAi cells. RNA was isolated from cells using RNeasy kit according to manufacturer's instructions (Qiagen, Limburg, Netherlands). Isolated RNA was stored at -20°C. 2 µg RNA was made up to 13 µL in sterile ddH_2O and 2µL Oligo dT (Thermo Fisher Scientific) was added to this and then heated at 70°C for 5 minutes. Then the sample was cooled on ice for 5 minutes, after a quick spin down. A reverse transcription master mix was made up with the following components: 90 µL 5X RT reaction buffer (Promega, Madison WI, USA), 22.5 µL dNTP (Thermo Fisher Scientific), 18 µL RNasin (Thermo Fisher Scientific), 18 µL M-MLV RT (Promega) and 301.5 µL sterile ddH_2O and gently mixed. 25 µL of the master mix was added to each RNA sample with a gentle flick to mix and quick spin down, and then incubated at 42°C for 60 minutes. The cDNA samples were stored at -20°C until qPCR was carried out.

2.2.7.2 Quantitative polymerase chain reaction (qPCR)

qPCR was carried out on cDNA, reverse transcribed from RNA, isolated from SW620 cells. qPCR assays for BMX, SOS1, and SGK1 were designed with the Universal Probe Library-Assay Design Centre (Roche; West Sussex, UK) (Table 8). 18S (18S ribosomal RNA) and TFRC (Transferrin Receptor) were selected as housekeeper genes to normalise qPCR data (Table 8). 5 µL cDNA at 1 ng/µL was mixed with 6 µL qPCR mater mix (Promega), left and right primers and probe (5.25 µL master mix, 0.25 µL of each primer (100 µM) and probe (100 µM)) were added to a well (in triplicate). The plate was run on a 384 well qPCR machine (7900 Real-Time PCR system; Applied Biosystems, Waltham, MA, USA) and data was analysed using SDS 2.1 software (Applied Biosystems).

Oligo name	Sequence (5'-3')	Probe #
BMX qPCR left	TGATTCCATTCCAAAGCTTATTC	50
BMX qPCR right	CCTTGTTGGCCTTTGTTGAC	50
SGK1 qPCR left	GACAGGACTGTGGACTGGTG	24
SGK1 qPCR right	TTTCAGCTGTGTGTTTCGGCTA	24
SOS1 qPCR left	GCAATGATACCGTCTTTATCCAA	43
SPS1 qPCR right	CACTTCATCAGTGCCTTTGGT	43
18S (housekeeper) left	GCAATTATTCCCARGAACG	48
18S (housekeeper) right	GGGACTTAATCAACGCAAGC	48
TFRC (housekeeper) left	TGAAGAGAAAGTTGTCGGAGAAA	56
TFRC (housekeeper) right	CAGCCTCGAGGGACATA	56

Table 8: Left and right oligo primer sequence and probe used for qPCR

2.2.8 Drug treatment

All cell lines were seeded into 6 well plates at 10^6 cells per well. After 24 hours, cells were treated with the indicated (on Figure) concentration of drug(s) for either 4 or 24 hours. Cells were harvested and washed with ice cold PBS then lysed directly into 10% cell lysis buffer (supplemented with 1% Protease Inhibitor Cocktail and 1% Phosphatase Inhibitor Cocktail I and II). Protein concentrations were assessed using BCA assay (Chapter 2.2.4) and proteins of interest were analysed by Western blotting analysis (Chapter 2.2.5).

2.2.9 Phospho-kinase array

Drug treatment (Ibrutinib 4 hours) or RNAi (BMX SMARTpool and non-targeting control siRNA) was conducted as previously described in Chapter 2.2.8 and Chapter 2.2.6.1 respectively. BMX knock-down and inhibition of the PI3K pathway was determined by Western blotting analysis using antibodies against BMX and the pharmacodynamic biomarkers of the PI3K pathway, phospho-AKT and phospho-S6 (antibodies found in Table 6; PI3K pathway discussed in Chapter 2.2.5). Lysates from non-targeting RNAi, BMX RNAi or Ibrutinib treated cells were then used in a phospho-kinase array according to manufacturer's instructions (Catalogue Number ARY003B, R&D Systems, Minneapolis, MN, USA).

2.2.10 Statistical analysis

Statistical analysis of *in vitro* preclinical studies was carried out using unpaired, two-tailed t tests to compare treated and control groups. T-tests were performed in Excel (Microsoft, Redmond, WA) to determine significance. $P < 0.05$ was considered statistically significant.

2.3 Patient recruitment, ethics and consent

Between August 2012 and December 2013, 35 patients were recruited through The Christie Hospital NHS Trust to our SCLC biomarker research program. Patients had histologically or cytologically confirmed SCLC and were chemotherapy-naïve. These patients provided additional informed consent that specified samples collected could be used for *in vivo* studies and genetic analysis in accordance with UK regulatory requirements. Patients were selected and approached for inclusion in the CDX study as their clinic appointments matched the capacity within the *in vivo* research team for blood processing and enriched CTC implantation in mice. Of the 35 patients 30 had the additional clinical feature of ES disease. The study was prospectively approved by the NHS NorthWest 9 Research Ethical Committee and included the collection of clinical and demographic data.

2.3.1 Patient blood collection and response to chemotherapy

Blood (10 mL) was drawn into CellSave Presevative tubes (Janssen Diagnostics, NJ, USA) for CTC enumeration using the CellSearch platform (385). CTCs thus defined expressed EpCAM and cytokeratins (cytokeratins, 8, 18 and 19), were >4 μm in diameter and had an intact DAPI stained nucleus. A paired blood sample (10 mL) was drawn into EDTA vacutainers (Becton Dickinson, Oxford, UK). Patients' subsequent response to treatment was evaluated by computed tomography (CT) imaging performed before and following 4 cycles of chemotherapy, or earlier if clinically indicated. Patients who had a radiological response to chemotherapy that was sustained for greater than 3 months following completion of therapy were classified as chemo-sensitive. Patients with

progressive disease within 3 months following completion of therapy were classified as chemo-refractory (384).

A second paired blood sample ((10 mL) CellSave preservative tubes for CTC enumeration and (10 mL) EDTA vacutainers for CDX study) were drawn from patient 3 and patient 8 after initial response to first line therapy and relapse with progressive disease (the first paired blood sample from patients 3 and 8 produced CDX3 and CDX8 (chemotherapy-naïve) respectively). Routine clinical practice was to perform a reassessment CT upon completion of chemotherapy. Patients were followed up every 3 months with chest x-rays and clinical review. Repeat CT was performed if there were clinical and radiological (chest x-ray) findings consistent with progressive disease.

2.4 *In vivo* methods

2.4.1 *In vivo* ethics

All *in vivo* procedures were carried out in accordance with Home Office Regulations (UK) and the UK Coordinating Committee on Cancer Research guidelines and by approved protocols (Home Office Project Licence no. 70/8252 which was reviewed by Cancer Research UK Manchester Institute Animal Welfare and Ethical Review Body). *In vivo* work was reported according to the ARRIVE (Animal Research Reporting of *In Vivo* Experiments) guidelines (2010).

2.4.2 Circulating tumour cell (CTC) enrichment before implantation into mice

An EDTA blood sample from a patient with SCLC was mixed with 500 µL RosetteSep Human Circulating Epithelial Tumour Cell Cocktail (Stem Cell Technology, Vancouver, Canada) and incubated for 20 minutes at room temperature with constant mixing. This was diluted with 10 mL 9:1 1X HBSS: HITES medium in a 50 mL tube layered over 15 mL Ficoll-Plaque Plus (GE Heathcare, Little Chalfont, UK) and centrifuged at 1,200 x *g* for 20 minutes. Cells at the medium-Ficoll boundary were collected, washed with 30 mL 9:1 HBSS:HITES and centrifuged at 250 × *g* for 5 minutes. The cell pellet was

resuspended in 100 µL ice cold HITES and mixed with 100 µL Matrigel (BD Biosciences) and kept on ice.

2.4.3 Growth of CDX tumours in immunocompromised mice

Enriched CTC sample/HITES/Matrigel (100–200 µL) was injected subcutaneously into one, or both, mid-dorsal flanks of 8 week old female NOD.Cg-*Prkdc*^{scid}*Il2rg*^{tm1Wjl}/SzJ (NSG) mice (Charles River, Edinburgh, UK). Mice were housed together in vented caging systems in a 12 hour light/12 hour dark environment and maintained at uniform temperature and humidity. Mice were monitored twice weekly for signs of tumour growth. Once a palpable tumour was detected, measurements were taken twice a week with callipers. Tumour volume was calculated using the formula 0.5 x (longest measurement) x (shortest measurement)^2. When the total tumour burden reached 1,000 mm^3 or there were demonstrable signs of ill health, the animal was sacrificed and tumour fragments were passaged into NSG mice.

2.4.4 Growth of CDX tumours in immunocompromised mice for BH3 profiling

CDX models were generated as described above in Chapter 2.4.3. For each CDX model tumour fragments, from passage 4, were subcutaneously implanted into the mid-dorsal flank of 8 week old female NSG mice. Six mice per CDX model were housed, maintained and tumour growth monitored as previously described in Chapter 2.4.3. When each individual tumour reached 400 mm^3 the animal was sacrificed and the tumour processed. The BH3 profiling method can be found in the *ex vivo* methods, Chapter 2.5.1 and 2.5.2.

2.4.5 *In vivo* tolerance of combined GDC-0941 and Navitoclax

Three 8 weeks old female SCID-beige mice (C.B-17/IcrHsd-*Prkdc*^{scid}*Lyst*$^{bg-J}$; Harlan Laboratories, UK) were treated for 21 days by oral gavage with 75 mg/kg GDC-0941 followed one hour later with 100 mg/kg Navitoclax. For the duration of the dosing mice were monitored twice daily for any changes in weight and appearance. Monitoring was continued for a further two weeks after which the animals were sacrificed.

2.4.6 *In vivo* efficacy of GDC-0941 and Navitoclax

H1048 xenografts were grown by subcutaneous injection of $5x10^6$ cells in 0.2 mL of 1:1 RPMI:Matrigel into the mid-dorsal flank of 8 week old female SCID-beige mice. CDX2 were generated as described in Chapter 2.4.3. CDX2 passage 4 tumour fragments were subcutaneously implanted into the mid-dorsal flank of 8 week old female SCID-beige mice. These mice were housed (6 mice to a cage), maintained and tumour growth monitored as previously described in Chapter 2.4.3. Seven days after implantation mice bearing H1048 xenograft tumours measuring between 150-250 mm^3 were randomized, using the deterministic method, into four groups of 10 mice. Eleven weeks after implantation of the CDX2 fragments, mice were put onto a randomized (sequential) rolling recruitment over 4 weeks when CDX2 tumours reached between 150-250 mm^3. They were allocated into 4 groups of 7 mice. H1048 xenograft and CDX2 tumour bearing mice were split into the following treatment groups; vehicle only, 75 mg/kg GDC-0941 only, 100 mg/kg Navitoclax only or 75 mg/kg GDC-0941 followed one hour later with 100 mg/kg Navitoclax. Treatments were administered by oral gavage for 21 days. Tumour measurements were continued three times a week until the tumour reached four times initial tumour volume (4xITV) or the mouse had been on study for 6 months after which the mouse was sacrificed.

2.4.7.1 *In vivo* pharmacodynamics biomarkers of GDC-0941 and Navitoclax activity

H1048 xenografts or CDX2 were generated as described above in Chapter 2.4.6 and Chapter 2.4.3 respectively. Mice with H1048 xenografts were allocated into 8 groups of five mice and CDX2 tumour bearing mice into 8 groups of four mice. Each group was treated with either, vehicle only, 75 mg/kg GDC-0941 only, 100 mg/kg Navitoclax only or 75 mg/kg GDC-0941 followed one hour later with 100 mg/kg Navitoclax by oral gavage. Animals were sacrificed at either 4 hours or 24 hours post dose. Tumours were fixed in 4% formalin for 24 hours and then placed in 70% ethanol.

2.4.7.2 Immunohistochemistry pharmacodynamics biomarkers of GDC-0941 and Navitoclax activity

Immunohistochemistry (IHC) was performed on formalin fixed paraffin embedded tissue from CDX2 tumours and H1048 derived xenograft. Sections (4 μm) were stained using antibodies against cleaved caspase 3 (CC3) (Cell Signaling Technology, Danvers, MA, USA; product number 9661; 1:200 dilution) and Phospho-S6 Ribosomal Protein (Ser235/236; pS6) (Cell Signaling Technology; product number 4857; 1:200 dilution). Both IHC assays were performed on LEICA Bond Max Platform. Deparaffinization was performed automatically in the autostainer with BondDewax solution at 72 °C for 30 minutes followed by 3 rinses in reagent alcohol and BondWash solution. CC3 antibody staining was performed following antigen retrieval in Bond Epitope Retrieval Solution 1 (HIER1) (Leica Microsystems, Wetzlar, Germany) for 20 minutes. Optimal pS6 antibody staining required Epitope Retrieval Solution 2 for 10 minutes. Control tissue for CC3 staining was MDA-231 XG4 breast carcinoma cells ± 1 μM staurosporin (untreated was negative control and treated was positive). Control tissue for pS6 staining was the SCLC cell lines DMS114 (positive) and DMS79 (negative). Staining was quantified using the following workflow. Digital images of whole-tissue sections were acquired using a Leica SCN400 histology scanner (Leica Microsystems, Milton Keynes, UK). Images were subsequently analysed using Definiens Developer XD version 2.0.4 and the Tissue Studio (Definiens AG, Munich, Germany). Regions of interest (ROIs) within the tissue sections were first identified using Definiens Tissue Studio which utilised machine learning technology across several samples to ensure that the full range of intensity was determined. Within these ROIs, cytoplasmic and nuclear protein expression was measured and classified as either positive or negative based on the haematoxylin and IHC staining thresholds. Thresholds were fixed across all tissue sections analysed.

2.4.8 Statistical analysis

Statistical analysis, to determine significance, of *in vivo* preclinical studies was carried out using unpaired, two-tailed t tests, performed in Excel, unless otherwise specified. Overall Survival rates were assessed using Kaplan-Meier analysis, while

a log-rank test was used for comparison of the survival distributions. In addition, 1-way ANOVA multiple comparisons analysis was used to compare multiple drug treatment groups effect on tumour doubling time. These analyses were conducted using GraphPad Prism software. $P < 0.05$ was considered statistically significant.

2.5 *Ex vivo* methods

2.5.1 CDX tumour dissociation

CDX tumours were dissociated using the gentleMACS dissociator and human tumour dissociation kit according to manufacturer's instructions (Miltenyi Biotec Ltd, Surrey, UK). This works through both enzymatic action and mechanic force to break down the extracellular matrix, leaving a single cell suspension. CDX tumours were cut into small pieces (2-4 mm) and transferred into a gentleMACS C tube containing an enzyme mix in media (4.7 mL RPMI media, 200 µL of Enzyme H, 100 µL of Enzyme R and 25 µL of Enzyme A; Miltenyi Biotec Ltd). The tube was then attached to the gentleMACS dissociator and the appropriate programs run followed by 30 minute incubation at 37°C under continuous rotation using the MACSmix Tube Rotator (Miltenyi Biotec Ltd). This was completed three times as follows; first run (program h_tumor_01), followed by 30 minutes incubation, second run (program h_tumor_02), followed by 30 minutes incubation and then the third run (program h_tumor_03) twice. Sample was then added to a 70 µm cell strainer (Corning, Wiesbaden, Germany), placed on a sterile 50 mL tube for collection of single cells. Red blood cells were lysed with RBC lysis buffer (G-Biosciences, USA). A cell viability check trypan blue exclusion preceded incubation of the suspension with dead cell removal beads (Miltenyi Biotec Ltd) and with anti-mouse IgG2a + b microBeads (Miltenyi Biotec Ltd) with anti-mouse MHCI (H-2kd/H-2Dd) antibody (eBiosciences, San Diego, CA, USA) for 15 minutes at room temperature. The cell suspension was diluted in binding buffer (Miltenyi Biotec Ltd) and added to LS-column to remove dead and mouse cells from the cell suspension where upon cell viability was reassessed.

2.5.2.1 Staining of CDX dissociated cells

Disaggregated CDX tumour cells were stained to identify viable, human SCLC cells using live/dead dye (1:1000; near-IR (NIR) fluorescent reactive dye, #L10119; Invitrogen) and the following cell surface antibodies: anti-human CD56 to identify human neuroendocrine (SCLC) cells (1:10; PE mouse anti-human CD56, #555516; BD Biosciences) and anti-mouse CD45 (1:50; BV421 rat anti-mouse CD45, #563890; BD Biosciences) to identify mouse cells for 30 minutes on ice. Amine reactive live/dead dye works by crossing the cell membranes of dead cells, and reacting with free amines within the cell. Live cells do not take up this reactive dye because their cell membranes are intact. This causes differential fluorescence between the live/dead cell populations. After staining CDX tumour cells were then subjected to BH3 profiling.

2.5.2.2 BH3 Profiling on CDX tumours

BH3 peptides were diluted in BH3 peptide buffer to the concentrations shown in Table 9. Digitonin in the BH3 peptide buffer lightly permeabilized the plasma membrane but keeps the organelles intact. Approximately 10^5 CDX tumour cells were diluted in DTEB and added to the tubes containing diluted BH3 peptide. This was incubated for 1 hour in the dark at room temperature. SU-DHL-4 and BBDL cells were BH3 profiled as a positive and negative control respectively. Cells were then fixed with formaldehyde (1% final concentration) at room temperature for 15 minutes in the dark. After fixation cells were diluted 2:1 with neutralising buffer and incubated at room temperature for 15 minutes in the dark. Fixed cells were then stained with cytochrome c antibody (1:400; Alexa 488, Clone 6h2.b4 mouse anti-human cytochrome c, #560263; BD Biosciences) diluted in intracellular staining buffer overnight at 4°C. Cells were analysed the next day by flow cytometry (BD LSRFortessa™ analyzer) using FACSDiva software (BD Biosciences). The flow cytometry gating strategy is shown in Figure 23 and 24. The laser filter and voltage used for each antibody is summarised in Table 10. Cells were initially gated based on forward and side scatter characteristics. Dead cells were then excluded using a side scatter vs Live/Dead NIR gating strategy. Human SCLC cells were distinguished from viable mouse cells via a hCD56 vs mCD45 gate before

cytochrome c fluorescent human CDX tumour cells were enumerated using a PUMA2A peptide treated sample as negative control. A no cytochrome c antibody (FMO (fluorescence minus one)) control was used to set the staining threshold. PUMA2A is a mutant PUMA peptide with a non-functional BH3 domain so cannot activate MOMP. After optimisation of the gating strategy samples were batch analysed to determine the percentage of CDX tumour cells in the cytochrome c positive gate and determine the percentage of cells with cytochrome c released (Figure 24). BH3 peptide sequence is shown in Table 11 and each BH3 peptide, expected behaviour towards MOMP activation and therefore cytochrome c release is shown in Table 12.

2.5.3 Generation of CDX2 and drug treatment

CDX2 tumours were generated as described in Chapter 2.4.3. CDX2 tumours were dissociated immediately after sacrifice of the mouse host when the tumour reached 400 mm^3 as described in Chapter 2.5.1. CDX2 tumour cells were subsequently cultured in RPMI 1640 media supplemented with 10% FBS and seeded into a 96 well plate at 5000 cells per well and incubated in a humidified atmosphere at 37°C and 5% CO_2. After 24 hours cells were treated with the indicated (on Figure) concentration of drug(s) and cultured for a further 72 hours after which they were subjected to a resazurin assay (Chapter 2.2.2.2).

BH3 Peptide	Concentrations (µM)
BIM	75, 7.5, 0.75 and 0.075
BID	75, 7.5 and 0.75
PUMA	75, 7.5 and 0.75
BMF	75, 7.5 and 0.75
BAD	75 and 7.5
NOXA A	75 and 7.5
HRK	75 and 7.5
PUMA2A	75

Table 9: BH3 peptides and concentrations used to run a full BH3 profile

Variable	Voltage	[laser] filter
FSC		500
SSC		200
mCD45-BV421	350	[405] 450/50
hCD56-PE	600	[561] 586/15
Cytochrome c-Alexa488	450	[488] 525/50
Live/Dead NIR	400	[640] 780/60

Table 10: Voltage and filter for BD LSRFortessa™ analyser

Peptide	Sequence	BH3-only class
BIM	MRPEIWIAQELRRIGDEFNA	Activator
BID	EDIIRNIARHLAQVGDSMDRY	Activator
PUMA	EQWAREIGAQLRRMADDLNA	Sensitizer
BMF	HQAEVQIARKLQLIADQFHRY	Sensitizer
BAD	LWAAQRYGRELRRMSDEFEGSFKGL	Sensitizer
NOXAA	AELPPEFAAQLRKIGDKVYC	Sensitizer
HRK	WSSAAQLTAARLKALGDELHQ	Sensitizer
PUMA2A	EQWAREIGAQARRMAADLNA	Control

Table 11: BH3 peptide sequence and BH3-only class

Peptide	Expected peptide behaviour
BIM	Rapid MOMP when BAX and BAK are present/functional
BID	
PUMA	MOMP primed cells (Pan-sensitizers)
BMF	
BAD	MOMP if dependent on BCL-2, BCL-w or BCL-xL
NOXA	MOMP only if dependent on MCL1
HRK	MOMP only if dependent on BCL-xL
PUMA2A	Mutant control peptide. No depolarization

Table 12: BH3 peptide expected behaviour towards mitochondria outer membrane permeabilization (MOMP)

A

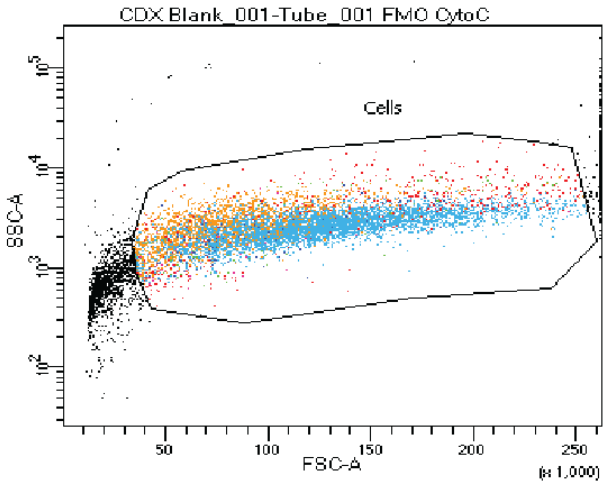

B

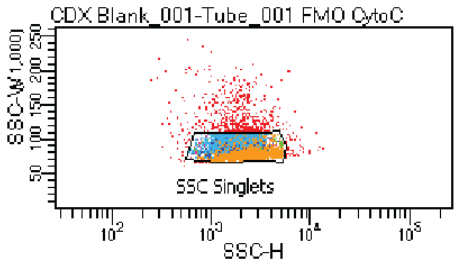

C

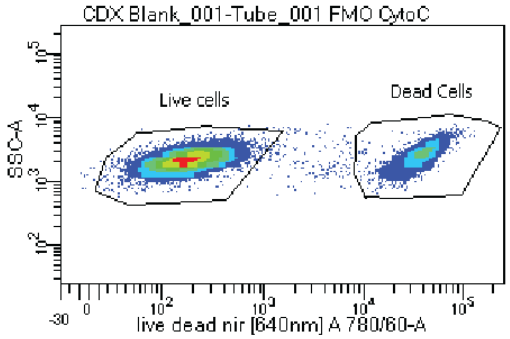

D

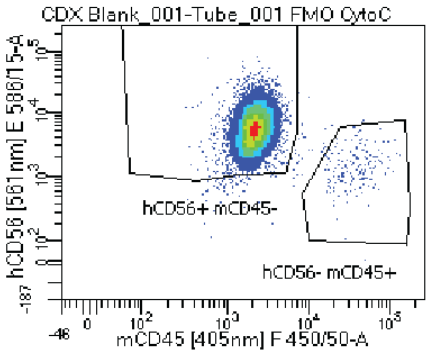

E

Experiment N...	CDX 3 n2 19-6...	Record Date:	Jan 30, 2015 5...
Specimen Na...	CDX Blank_001	$OP:	Cytometry
Tube Name:	Tube_001 FM...	GUID:	12552069-704...

Population	#Events	%Parent	CytoC [4... Median	CytoC [4... rSD
All Events	9,806	####	1,283	571
Cells	7,987	81.5	1,331	441
SSC Singlets	7,265	91.0	1,299	400
Live cells	5,625	77.4	1,341	361
hCD56+ mCD45-	5,372	95.5	1,354	349
hCD56+ Cytochrome C+	5	0.1	2,045	126
hCD56- mCD45+	162	2.9	895	386
Dead Cells	1,449	19.9	1,042	452

Figure 23: BH3 profiling gating strategy for SCLC CDX. Flow cytometry was used to analyse cells (LSRFortessa™ analyzer) and then batch analysis was carried out on all BH3 peptides and controls. (A) Cells were gated based on side scatter area vs forward scatter area. (B) Cell singlets were gated from doublets by side scatter width vs side scatter height. (C) Live cells were gated away from dead cells by side scatter area vs live/dead NIR [640 nm]. (D) Human SCLC cells (hCD56+) were gated away from mouse cells (mCD45+) by hCD56 [561 nm] vs mCD45 [405 nm]. This is the final parent population of live, human SCLC cells. (E) Statistics table of events in each group, percentage parent population and median events.

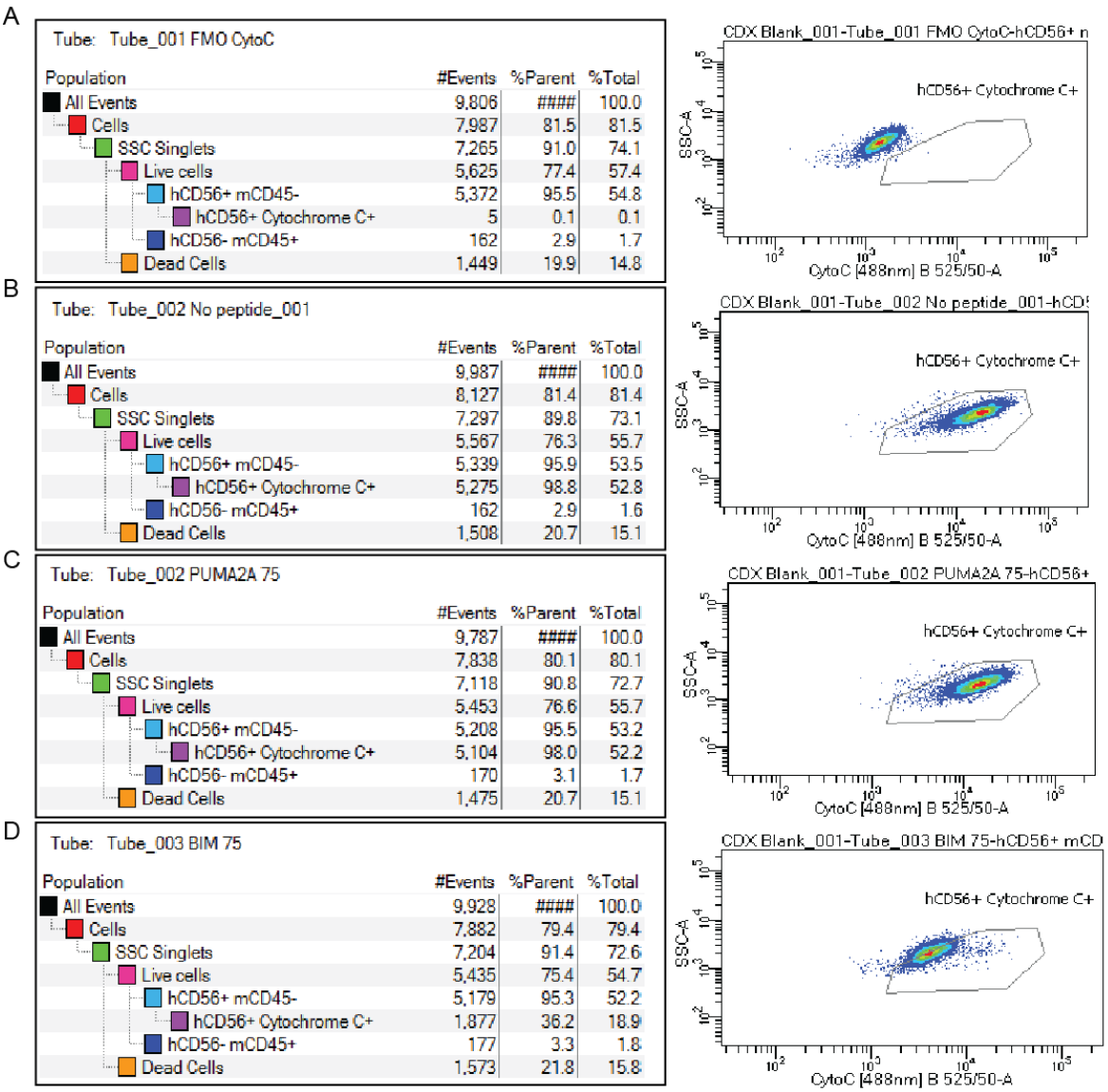

Figure 24: BH3 profiling gating strategy for cytochrome *c* positive SCLC CDX cells. Cytochrome *c* positive cells are identified within the parent population of viable human SCLC cells from Figure 23. Within this parent population the percentage of cells that stain positive for cytochrome *c* can be determined using side scatter area vs human cytochrome *c* [488]. The percentage parent population within each gate was set using the gating strategy shown in Figure 23. This is shown here for the (A) FMO control (no cytochrome *c* antibody), No peptide control (B), 75 μM PUMA2A peptide negative control (C) and 75 μM BIM (D). The percentage cytochrome *c* positive cells within the final parent population can be converted to percentage cytochrome *c* released (cytochrome *c* positive percentage minus 100). This was then put into a bar chart for each peptide to make the BH3 profile shown in Figure 2, 3 and 4.

Chapter 3

Paper 1:

BMX Acts Downstream of PI3K to Promote Colorectal Cancer Cell Survival and Pathway Inhibition Sensitizes to the BH3 Mimetic ABT-737

NEOPLASIA
www.neoplasia.com

Volume 16 Number 2 February 2014 pp. 147–157 147

BMX Acts Downstream of PI3K to Promote Colorectal Cancer Cell Survival and Pathway Inhibition Sensitizes to the BH3 Mimetic ABT-737[1,2]

Danielle S. Potter[*], Paul Kelly[*], Olive Denneny[*], Veronique Juvin[†], Len R. Stephens[†], Caroline Dive[*,3] and Christopher J. Morrow[*,3]

*Clinical and Experimental Pharmacology Group, Cancer Research UK Manchester Institute, University of Manchester, Manchester, United Kingdom; [†]Inositide Laboratory, Babraham Institute, Babraham Research Campus, Cambridge, United Kingdom

Abstract

Evasion of apoptosis is a hallmark of cancer, and reversing this process by inhibition of survival signaling pathways is a potential therapeutic strategy. Phosphoinositide 3-kinase (PI3K) signaling can promote cell survival and is upregulated in solid tumor types, including colorectal cancer (CRC), although these effects are context dependent. The role of PI3K in tumorigenesis combined with their amenability to specific inhibition makes them attractive drug targets. However, we observed that inhibition of PI3K in HCT116, DLD-1, and SW620 CRC cells did not induce apoptotic cell death. Moreover, these cells were relatively resistant to the Bcl-2 homology domain 3 (BH3) mimetic ABT-737, which directly targets the Bcl-2 family of apoptosis regulators. To test the hypothesis that PI3K inhibition lowers the apoptotic threshold without causing apoptosis *per se*, PI3K inhibitors were combined with ABT-737. PI3K inhibition enhanced ABT-737–induced apoptosis by 2.3- to 4.5-fold and reduced expression levels of MCL-1, the resistance biomarker for ABT-737. PI3K inhibition enhanced ABT-737–induced apoptosis a further 1.4- to 2.4-fold in CRC cells with small interfering RNA–depleted MCL-1, indicative of additional sensitizing mechanisms. The observation that ABT-737–induced apoptosis was unaffected by inhibition of PI3K downstream effectors AKT and mTOR, implicated a novel PI3K-dependant pathway. To elucidate this, an RNA interference (RNAi) screen of potential downstream effectors of PI3K signaling was conducted, which demonstrated that knockdown of the TEC kinase BMX sensitized to ABT-737. This suggests that BMX is an antiapoptotic downstream effector of PI3K, independent of AKT.

Neoplasia (2014) 16, 147–157

Introduction

Single-agent treatments rarely prove sufficient for cancer cure. This is in part due to a variety of innate or acquired, drug-specific, or pleiotropic drug resistance mechanism(s), one of which is suppression of drug-induced cell death. Consequently, there is considerable motivation to overcome drug resistance mechanisms by identifying rational combinations of molecular targeted drugs. To aid this, the US Food and Drug Administration (FDA) is considering early-phase drug combination trials without the necessity for prior single-agent approval [1]. Historically, choice of drug combinations is predicated

Abbreviations: CRC, colorectal cancer; PI3K, phosphoinositide 3-kinase; PtdIns(3,4,5)P_3, phosphatidylinositol-3,4,5-triphosphate; PH, pleckstrin homology; siRNA, small interfering RNA; SRB, sulforhodamine B

Address all correspondence to: Christopher J. Morrow, PhD, or Caroline Dive, PhD, Cancer Research UK Manchester Institute, University of Manchester, Wilmslow Road, Manchester, M20 4BX, United Kingdom. E-mail: christopher.morrow@cruk.manchester.ac.uk, caroline.dive@cruk.manchester.ac.uk

[1]This work was supported by Cancer Research UK (CR-UK) core funding to the CR-UK Manchester Institute (grant No. C147/A12328). O.D. was supported through funding from the Cancer Research UK Experimental Cancer Medicine Centre grant to the Manchester Cancer Research Centre.

[2]This article refers to supplementary materials, which are designated by Tables W1 to W8 and Figures W1 to W9 and are available online at www.neoplasia.com.

[3]These authors contributed equally to this work.

Received 23 July 2013; Revised 12 December 2013; Accepted 17 January 2014

DOI 10.1593/neo.131376

on nonoverlapping drug toxicities; however, the concept of targeting multiple different hallmarks of cancer is an emerging approach [2]. Two such hallmarks are sustained inappropriate proliferative signaling and suppression of apoptotic cell death [2]. Molecular features that contribute to these hallmarks in several human tumors, including colorectal cancer (CRC), are aberrations in the phosphoinositide 3-kinase (PI3K) signaling pathway and up-regulation of antiapoptotic Bcl-2 family proteins. This study examines the combined effect of inhibiting PI3K signaling and interrupting the protein-protein interactions between proapoptotic and antiapoptotic members of the Bcl-2 family in CRC cells.

PI3K phosphorylates the 3-hydroxy group of phosphatidylinositol lipid rings to generate a secondary messenger that is implicated in many intracellular signaling pathways. The most studied are the class I PI3Ks, which phosphorylate phosphatidylinositol-4,5-bisphosphate generating phosphatidylinositol-3,4,5-triphosphate [PtdIns(3,4,5)P_3] [3]. PtdIns(3,4,5)P_3 is a docking site for a number of proteins that contain PtdIns(3,4,5)P_3-binding motifs such as pleckstrin homology (PH) domains, frequently leading to activation of the docked protein. The best characterized effectors of the pathway are phosphoinositide-dependent kinase 1 (PDK1) and AKT (AKA protein kinase B). PDK1 and AKT bind to PtdIns(3,4,5)P_3, allowing PDK1 to phosphorylate and activate AKT [4]. Activation of AKT has multiple cell fate outcomes including increased cell survival, sustained cell proliferation, and enhanced cell migration, all of which have potential to promote oncogenesis [5]. Aberrant PI3K signaling is implicated in many cancer types. For example, loss of the PI3K antagonistic phosphatase PTEN and activating mutations in *PIK3CA*, the gene encoding the catalytic PI3K subunit p110α, are among the most common genetic aberrations in cancer [6]. Consequently, the PI3K signaling pathway is a major focus of drug discovery programs, with multiple small-molecule inhibitors targeting PI3K, AKT, and other PI3K pathway components undergoing clinical trials [6]. Multiple lines of preclinical evidence suggest that PI3K signaling acts to suppress apoptosis through mechanisms including the modulation of Bcl-2 family proteins that control the release of potent apoptogens from mitochondria [5]. However, despite this body of evidence, apoptosis is not induced in many cancer cell lines after specific inhibition of PI3K pathway signaling [7,8]. Furthermore, emerging evidence shows that, whereas in some cell types, combining PI3K inhibition with conventional chemotherapeutic agents induces apoptosis [9,10], this is not the case with CRC cells [7], a disease where aberrant PI3K activation is common.

Drug development efforts to disrupt interactions between proapoptotic and antiapoptotic proteins of the Bcl-2 family yielded the Bcl-2 homology domain 3 (BH3) mimetic class of drugs [11]. The "poster-child" BH3 mimetic ABT-737 and its related clinical candidate navitoclax readily induce apoptosis in small cell lung cancer *in vitro* and *in vivo* as a single agent [12] and kill lymphoma cell lines and primary lymphoma cells *ex vivo* [12,13], and navitoclax has demonstrated promising results in a phase I clinical trial in patients with chronic lymphocytic leukemia [14]. However, in several cancer cell types, including CRC, ABT-737 treatment alone does not induce apoptosis at clinically relevant concentrations [15]. In a broad range of cancer cell types, ABT-737 acts synergistically with a variety of conventional and novel chemotherapeutic agents [16], including agents that target the PI3K pathway [17,18]. This suggests that a lowering of the apoptotic threshold by ABT-737 facilitates the coupling of drug-induced damage and/or the interruption of survival signaling events to the commitment to apoptotic cell death. Therefore, the hypothesis tested in this study was that PI3K pathway ablation using small-molecule inhibitors could "prime" CRC cells for apoptosis but that cell death would only be realized if the actions of antiapoptotic Bcl-2 family proteins were negated by a BH3 mimetic.

Materials and Methods

Cell Culture and Drugs

HCT116, DLD-1 [American Type Culture Collection (ATCC), Manassas, VA], and isogenic pairs of HCT116 and DLD-1 expressing only wild-type or mutant PIK3CA (a kind gift from B. Vogelstein) were cultured in McCoy's 5A media (Life Technologies, Inc, Paisley, United Kingdom) supplemented with 10% FBS (BioWest, Nuaillé, France). SW620 (ATCC) were cultured in Dulbecco's modified Eagle's medium supplemented with 10% FBS and glutamine (Life Technologies, Inc). All cells were maintained in a humidified atmosphere at 37°C and 5% CO_2. Cell lines were authenticated using the AmpFlSTR system (Applied Biosystems, Paisley, United Kingdom) during the study. ABT-737 (a kind gift from AbbVie, Chicago, IL), PI-103, rapamycin, Akti1/2, KU-0063794 (Merck, Nottingham, United Kingdom), GDC-0941, MK-2206, and PCI-32765 (Selleck Chemicals, Houston, TX) were all dissolved to 10 mM in DMSO (Sigma, Dorset, United Kingdom) and stored as single use aliquots at −20°C/−80°C (Figure W1).

Concentration Response

Cells were seeded into 96-well plates. After 24 hours, cells were treated with the indicated concentration of drug(s) and cultured for a further 72 hours in the presence of drug(s). Plates were stained with sulforhodamine B (SRB) and processed as previously described [7] to give an indication of cellular biomass. To determine logGI_{50}, log drug concentration was plotted against raw absorbance, and nonlinear curve fit analysis was performed (GraphPad Prism; GraphPad Software, La Jolla, CA). Statistical analysis was carried out on three independent logGI_{50} readings and transformed to growth inhibition 50 (GI_{50}) for presentation. For display purposes only, drug concentration (log scale) has been plotted against normalized absorbance.

Western Blot Analysis

Cell lysis and Western blot analysis were carried out as previously described [7]. The following primary antibodies were used: rabbit anti-pS473AKT (No. 4058), rabbit anti-AKT (No. 9297), rabbit anti-pT246 40-kDa proline-rich AKT substrate (PRAS40) (No. 2997), rabbit anti-PRAS40 (No. 2691), pS240/244S6 (No. 4838), rabbit anti-S6 (No. 2217), rabbit anti–cleaved caspase 3 (No. 9661), rabbit anti-PARP (No. 9542), rabbit anti-Bax (No. 2774; all from Cell Signaling Technology, Danvers, MA), mouse anti–Bcl-2 (M0887; Dako, Glostrup, Denmark), rabbit anti–BCL-XL (No. 610211; Becton Dickinson, Oxford, United Kingdom), mouse anti-human MCL-1 (No. 559027; Becton Dickenson), rabbit anti–MCL-1 (sc819; Santa Cruz Biotechnology, Inc, Dallas, TX), rabbit anti-Bad (AF819; R&D Systems, Minneapolis, MN), rabbit anti-Bim (No. 202000; Merck), mouse anti-Bak (AM03; Merck), mouse anti–α-tubulin (CP06; Merck), and mouse anti-GAPDH (G9545; Sigma).

Measurement of Apoptosis

Annexin V/7-aminoactinomycin D (7AAD) flow cytometry was performed as previously described [7]. For assessment of Bak conformational change, cells were cultured in a 96-well plate and

treated with the indicated drug(s) for 24 hours. Cells were fixed with 1% formaldehyde and sent to Imagen Biotech (Cheshire, United Kingdom) where immunofluorescent staining for conformationally changed Bak and high-content analysis were carried out using proprietary protocols using Bak conformation–specific antibodies. Real-time assessment of cells with activated Caspase 3/7 was carried out using the CellPlayer apoptosis Caspase 3/7 reagent (Essen BioScience, Ann Arbor, MI) following manufacturer's recommendations. Cells were placed in an IncuCyte (Essen BioScience) and imaged every 2 hours. The number of fluorescent cells per field of view was determined using IncuCyte software (Essen BioScience) following manufacturer's recommendations.

RNA Interference (RNAi)

siRNA SMARTpools or individual oligos (Thermo Scientific, Leicestershire, United Kingdom) were transfected into SW620 or HCT116 cells using DharmaFECT 2 (Thermo Scientific) according to manufacturer's instructions. For the small interfering RNA (siRNA) library screen, cells were reverse transfected with 5 pmol of siRNA in 6 wells of a 96-well plate per SMARTpool and left for 48 hours, 3 wells were treated with 4 μM ABT-737, and 3 wells were treated with DMSO equivalent. For other siRNA experiments, siRNA were transfected in six-well plates, reseeded into appropriate culture vessels 24 hours later, and drug treated after another 24 hours. Calculation of robust z score is described in Supplemental Materials and Methods section.

Real-Time Quantitative Polymerase Chain Reaction

Quantitative polymerase chain reaction (qPCR) was carried out as previously described [19]. Assays for *bone marrow tyrosine kinase* gene in chromosome X protein (*BMX*), SOS1, and SGK1 were designed with the Roche (West Sussex, United Kingdom) Universal ProbeLibrary Assay Design Center.

Statistical Analysis

Unpaired, two-tailed t tests were performed in Excel (Microsoft, Redmond, WA) to determine significance. $P < .05$ was considered significant.

Results

PI-103 Sensitized CRC Cell Lines to ABT-737

The purpose of this study was to investigate the effect of combining ABT-737 with PI3K pathway inhibitors in CRC cell lines. The lines used were HCT116 and DLD-1, which carry oncogenic activating mutations in *PIK3CA*, and SW620 cells that are wild type for *PIK3CA* [20]. All three cell lines also harbor mutant *KRAS* (www.sanger.ac.uk/genetics/CGP/cosmic/), which can activate the PI3K signaling pathway [4]. All cell lines were responsive to the PI3K/mammalian target of rapamycin (mTOR) inhibitor PI-103 in the SRB assay, which measures cellular biomass, with GI_{50} values of 288 nM in HCT116 [95% confidence interval (CI) = 255-325 nM], 184 nM in DLD-1 (95% CI = 132-256 nM), and 636 nM in SW620 cells (95% CI = 508-797 nM) (Figure W2*A*). The phosphorylation of PI3K and/or mTOR effectors AKT, PRAS40, and S6 was inhibited by PI-103 in all cell lines (Figure W2*B*), confirming that PI-103 inhibited PI3K and mTOR. To determine whether PI-103 treatment affected CRC cell sensitivity to ABT-737, HCT116, SW620, and DLD-1 cells were treated concomitantly with PI-103 and/or ABT-737 (Figure 1*A* and Table 1). All cell lines exhibited a concentration-dependent response to ABT-737 alone, and the ABT-737 GI_{50} was reduced significantly in a concentration-dependent manner by PI-103. This is consistent with PI3K inhibition sensitizing CRC cells to ABT-737. The observation that PI-103 increased the sensitivity toward ABT-737 irrespective of *PIK3CA* mutation status suggests that *PIK3CA* mutation is not essential for this effect.

PI-103 Enhanced ABT-737–Induced Apoptosis

The effect of PI-103 on the levels of ABT-737–induced apoptosis was determined by several methods. First, the effect of ABT-737 and/or PI-103 on caspase 3 and PARP cleavage was determined by Western blot analysis (Figure 1*B*). ABT-737 alone induced some caspase 3 and PARP cleavage, whereas PI-103–only treatment had no effect. Combining the two agents increased caspase 3 and PARP cleavage, suggesting that the combination caused more apoptosis than either agent alone. The effect of ABT-737 and PI-103 on the externalization of phosphatidylserine, another classic biomarker of apoptosis, was determined by flow cytometry in HCT116 and SW620 cells (Figure 1*C*). In both cases, neither PI-103 nor ABT-737 alone caused a significant level of apoptosis compared to untreated cells, whereas combining ABT-737 and PI-103 gave significantly more apoptosis than any other condition.

PI3K signaling can promote numerous antiapoptotic mechanisms that act upstream or downstream of cytochrome *c* release from mitochondria, for example, Bad sequestration and caspase 9 inhibition, respectively [21,22]. To determine whether the PI-103–induced ABT-737 sensitization was upstream of cytochrome *c* release, the percentage of HCT116 cells exhibiting the early activating N-terminal conformational change in the multidomain proapoptotic protein Bak [23] was assessed by immunofluorescence. The combination of PI-103 and ABT-737 resulted in a significantly higher proportion of cells with activated Bak than either agent alone (Figure 1*D*). This confirmed that PI-103 sensitized CRC cells to ABT-737–induced apoptosis and that this effect was mediated upstream of cytochrome *c* release.

ABT-737 Sensitization Was Not Solely due to MCL-1 Down-Regulation

There is precedence for PI3K inhibition affecting several Bcl-2 family members including Bad, Bim, Bcl-2, MCL-1, and Bax [5]. When the effect of PI-103 on expression levels of 10 Bcl-2 family members was assessed by Western blot analysis in HCT116 and SW620 cells, the only observed change was a reduction in MCL-1 level (Figure 2*A*). MCL-1 is an established resistance biomarker for ABT-737, due to the poor affinity of ABT-737 for this antiapoptotic Bcl-2 family member [24,25]. Moreover, MCL-1 stability is known to be decreased by PI3K inhibition due to activation of GSK3β [26]. To test the hypothesis that PI-103–induced sensitivity to ABT-737 was solely due to a reduction of MCL-1 levels, MCL-1 was depleted by siRNA (Figure 2*B*), and the effect of PI-103 on ABT-737 sensitivity was reassessed. If the effect of PI3K inhibition on ABT-737 sensitivity is mediated only through MCL-1 down-regulation, treatment with PI-103 should not further sensitize MCL-1–depleted cells to ABT-737. MCL-1 knockdown significantly sensitized both HCT116 and SW620 to ABT-737, reducing the GI_{50} to a similar extent to that in cells transfected with nontargeting siRNA and treated with PI-103

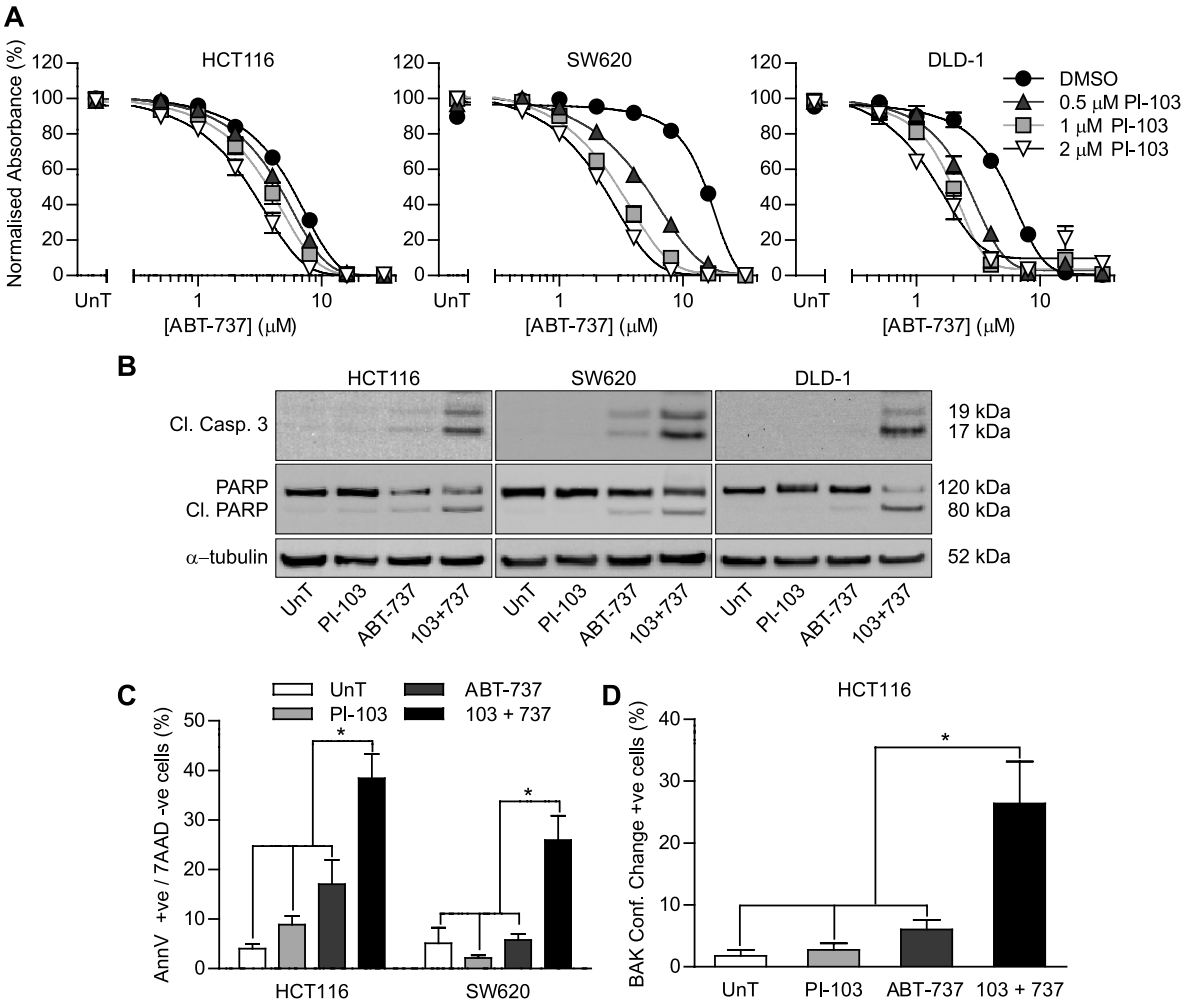

Figure 1. PI-103 sensitized CRC Cell Lines to ABT-737–induced apoptosis. (A) Cells were exposed to DMSO or the indicated concentration of PI-103 and the indicated concentration of ABT-737 for 3 days. Cells were fixed and stained with SRB, and the absorbance relative to untreated (UnT) cells was determined relative to DMSO or PI-103 only–treated cells as appropriate for individual concentration response curves. (B–D) Cells were treated with the indicated combinations of 4 μM ABT-737 (A and B) or 8 μM ABT-737 (C) and 2 μM PI-103 for 24 hours. (A) The level of cleaved caspase 3, full-length PARP, cleaved PARP, and α-tubulin was assessed by Western blot analysis. Results are representative of three independent experiments. (B) Cells were stained with allophycocyanin (APC)-conjugated annexin V and 7AAD, and the percentage of annexin V–positive/7AAD-negative cells was determined by flow cytometry. (C) Cells were fixed and stained for conformationally changed BAK, and the percentage of positive cells was determined by immunofluorescence. All graphs represent the means of three independent experiments carried out in triplicate (A) or duplicate (C and D) ± SEM. *$P < .05$ according to two-tailed unpaired *t* test.

(Figure 2*C* and Table W1). However, PI-103 significantly increased sensitivity to ABT-737 in MCL-1 knockdown cells. To determine whether this additional increase in ABT-737 sensitivity was due to apoptosis, cells were transfected with nontargeting siRNA or MCL-1–specific siRNA, treated with combinations of ABT-737 and/or PI-103, and analyzed by annexin V/7AAD flow cytometry (Figure 2*D*). This confirmed that, in MCL-1–depleted HCT116 and SW620 cells, PI-103 treatment increased ABT-737–induced apoptosis. One experimental caveat is that, whereas MCL-1 was clearly depleted by siRNA, a detectable level remained, and PI-103 could be reducing the MCL-1 levels further (beyond the resolution of the assay). Thus, the increased apoptosis observed could still be MCL-1 dependent. To address this, similar studies were performed in MCL-1$^{-/-}$ mouse embryonic fibroblasts (MEFs). MCL-1 knockout was confirmed (Figure W3*A*), and combining ABT-737 and PI-103 gave a significantly greater decrease in colony formation than either agent alone (Figure W3*B*). Furthermore, the combination gave enhanced cell death in parental and MCL-1$^{-/-}$ MEFs (Figure W3*C*). Although the mechanism of PI-103–induced sensitization to ABT-737 may be different between CRC cell lines and MEFs, this further demonstrates that MCL-1 is not essential for PI-103–induced sensitization. Taken together, these data suggest that, although reduced levels of MCL-1 in PI-103–treated cells caused

Table 1. Effect of PI-103 Treatment on ABT-737 GI_{50}.

Cell Line	Treatment	ABT-737 GI_{50} (μM ± 95% CI)	Significance*
HCT116	DMSO	5.80 (5.16-6.52)	
	0.5 μM PI-103	4.70 (4.30-5.15)	0.0495
	1 μM PI-103	4.39 (3.78-5.09)	0.0439
	2 μM PI-103	3.11 (2.26-4.29)	0.0231
SW620	DMSO	15.5 (14.2-16.8)	
	0.5 μM PI-103	5.07 (3.75-6.84)	0.0022
	1 μM PI-103	2.88 (2.14-3.88)	0.0004
	2 μM PI-103	2.22 (1.86-2.66)	<0.0001
DLD-1	DMSO	5.35 (5.15-5.55)	
	0.5 μM PI-103	2.44 (2.19-2.71)	0.0002
	1 μM PI-103	1.82 (1.60-2.07)	0.0001
	2 μM PI-103	1.36 (0.99-1.87)	0.0011

*Two-tailed unpaired *t* test *versus* DMSO-treated GI_{50} for same cell line.

sensitization to ABT-737, there are additional MCL-1–independent events that influence the response to ABT-737.

ABT-737 Sensitization Was due to Inhibition of PI3K but Not AKT or mTOR

PI-103 is a dual PI3K/mTOR inhibitor; therefore, it was investigated whether the effect of PI-103 on ABT-737 sensitivity was due to PI3K inhibition, mTOR inhibition, and/or off-target effects. To assess this, PI3K signaling was genetically altered. This was achieved using HCT116 and DLD-1 cells, both of which normally express one mutant and one wild-type *PIK3CA* allele (labeled Parental). In the isogenic cell lines, one allele had been silenced by insertion of an adeno-associated virus (AAV)–targeting system into exon 1 of either the wild-type or mutant *PIK3CA* [27]. If the AAV inserted into the wild-type *PIK3CA* allele, only the mutant protein was expressed, resulting in higher PI3K activity compared to parental cells (labeled Mutant). Conversely, if the AAV inserted into the mutant *PIK3CA* allele, only the wild-type protein was expressed, resulting in lower PI3K activity (labeled Wild-Type). This was confirmed by assessing the level of AKT and PRAS40 phosphorylation in the isogenic cells (Figure 3*A*). HCT116 and DLD-1 cells that only expressed wild-type *PIK3CA* (low PI3K activity) were significantly more sensitive to ABT-737 than corresponding parental cells (Figure 3*B* and Table W2). HCT116 cells that only expressed mutant *PIK3CA* (high PI3K activity) were significantly more resistant to ABT-737 than HCT116 parental cells, and DLD-1 cells with mutant *PIK3CA* were as resistant as parental cells. These data demonstrate that reduced PI3K activity correlates with increased ABT-737 sensitivity, suggesting that the observed effect of PI-103 was not due to off-target effects. However, as both targets of PI-103 are components of the PI3K signaling pathway, it remained unclear which target of PI-103 was responsible for the enhanced ABT-737 sensitivity. To investigate this further, the effect of a panel of PI3K pathway inhibitors on ABT-737 sensitivity was assessed in HCT116 and SW620 cells, specifically GDC-0941, a class I PI3K-specific inhibitor [28], rapamycin, an mTOR complex 1 (mTORC1)-specific inhibitor [29], KU-0063794, an ATP-competitive mTOR inhibitor that inhibits mTORC1 and mTORC2 but not PI3K [30], and AKTi1/2 and MK-2206, two allosteric AKT inhibitors [31,32]. All agents were used at concentrations that demonstrably inhibited their primary targets: GDC-0941 and KU-0063794 inhibited phosphorylation of AKT, PRAS40, and S6; rapamycin inhibited S6 phosphorylation but increased AKT and PRAS40 phosphorylation; and AKTi1/2 and MK-2206 inhibited AKT and PRAS40 but not S6 phosphorylation (Figure 3*C*). In HCT116 and SW620 cells, GDC-0941 significantly sensitized to ABT-737, whereas rapamycin and KU-0063794 were without effect (Figure 3*D* and Table 2), suggesting that PI3K inhibition, rather than mTORC1/2 inhibition, was responsible for ABT-737 sensitization. Contrary to expectations, KU-0063794 did not sensitize to ABT-737 despite the fact that AKT is a target of mTORC2 (Figure 3*C*) and AKT is considered the main downstream effector of PI3K [6]. To explore this further, the effect of AKT inhibition on ABT-737 sensitivity was investigated. In both cell lines, neither AKTi1/2 nor MK-2206 had a significant effect on the sensitivity to ABT-737 (Figure 3*D* and Table 2), strongly suggesting that the downstream target of PI3K responsible for ABT-737 sensitization is AKT independent and implicating a novel, antiapoptotic PI3K-dependent, AKT-independent signaling pathway. The ABT-737 concentration-response data were verified by combining ABT-737 with each of the PI3K pathway inhibitors and monitoring caspase activation in SW620 cells (Figure 3*E*). Only PI-103 and GDC-0941 when combined with ABT-737 caused a significant increase in the number of cells with activated caspase compared to ABT-737 alone, consistent with the ABT-737 concentration-response data. Furthermore, the PI-103–induced down-regulation of MCL-1 was not observed with Akti1/2 or rapamycin treatment (Figure W4), and neither Akti1/2 nor rapamycin was able to further sensitize MCL-1–depleted SW620 cells to ABT-737 (Figure W5 and Table W3). These data are consistent with at least two antiapoptotic AKT/mTOR-independent pathways acting downstream of PI3K, only one of which affects MCL-1 levels.

BMX Down-Regulation Sensitized to ABT-737

The secondary messenger generated by class I PI3K, PtdIns(3,4,5)P_3, has the potential to regulate many proteins in addition to AKT. Indeed, there are reported to be >50 proteins that can bind to PtdIns(3,4,5)P_3 [3]. To determine whether any of these proteins may be involved in the PI3K inhibition–induced sensitization to ABT-737, a SMARTpool siRNA library targeting mRNA for each of 52 proteins containing a PH domain that interacts with PtdIns(3,4,5)P_3 and other core PI3K pathway proteins was designed (Table W4). SW620 cells, which exhibited the greatest degree of sensitization to ABT-737 when PI3K signaling was inhibited, were transfected with each siRNA, and the effect of ABT-737 treatment determined relative to non-targeting siRNA–transfected cells (Figure 4*A*, *left panel*). Four siRNAs were shown to induce a significant ($P < .05$; robust z score < −0.9) increase in ABT-737 sensitivity (Figure 4*A*, *right panel*, and Table W4). Of these four siRNAs, BMX, SOS1, and SGK1 were chosen for further analysis. A complete ABT-737 concentration response was carried out on cells transfected with each of the individual siRNA oligos that made up the SMARTpool with some oligos demonstrating a degree of sensitization for all three targets (Figures 4*B* and W6). However, only oligos 1 and 3 targeting BMX produced a significant sensitization to ABT-737 ($P = .041$ and .022, respectively; Table W5). Furthermore, when the association between the level of mRNA knockdown for each oligo set and the sensitization toward ABT-737 was assessed, only knockdown of BMX significantly correlated with ABT-737 efficacy ($P = .0015$; Figures 4*C* and W6*B*). The BMX siRNA oligos that gave the greatest degree of ABT-737 sensitization, SMARTpool, oligos 1 and 3, also caused the greatest reduction of BMX protein expression (Figure W7). BMX knockdown in HCT116 cells also sensitized to ABT-737 (Figure 4*D* and Table W6). Moreover, pharmacological inhibition of BMX with the TEC family

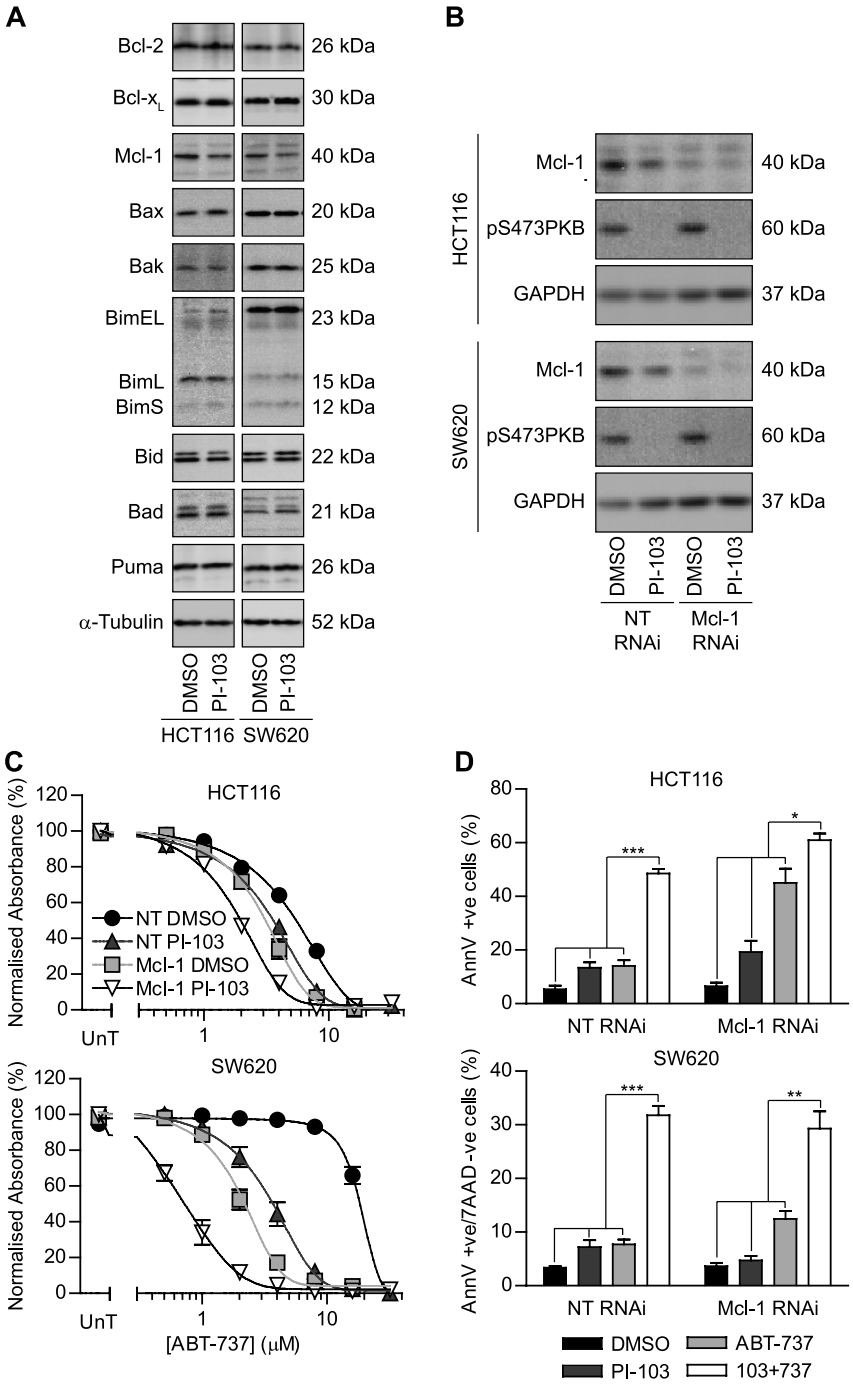

Figure 2. Reduced MCL-1 level is not solely responsible for increased ABT-737 sensitivity. (A) HCT116 and SW620 cells were treated with DMSO equivalent or 2 μM PI-103 for 24 hours, and the level of Bcl-2, BCL-XL, MCL-1, Bax, Bak, Bim, Bid, Puma, Bad, and Noxa was determined by Western blot analysis. (B–D) HCT116 and SW620 cells were transfected with nontargeting siRNA (NT RNAi) or siRNA targeting MCL-1 (MCL-1 RNAi) and plated for experiments 24 hours later. Cells were treated with 2 μM PI-103 for 24 hours, and the effect on levels of MCL-1, pS473 AKT, and GAPDH was determined by Western blot analysis (B). RNAi cells were treated with 2 μM PI-103 or DMSO equivalent and the indicated concentration of ABT-737 for 3 days and processed as in Figure 1*A* (C). RNAi cells were treated with 2 μM PI-103 and/or 4 μM ABT-737 (NT RNAi), 2 μM ABT-737 (HCT116 MCL-1 RNAi), or 1 μM ABT-737 (SW620 MCL-1 RNAi) for 24 hours. Cells were stained with APC-conjugated annexin V and 7AAD and analyzed by flow cytometry (D). All blots are representative of three independent experiments, and all graphs represent the means of three independent experiments carried out in triplicate (C) or duplicate (D) ± SEM. *$P < .05$, **$P < .01$, and ***$P < .001$ according to two-tailed unpaired t test.

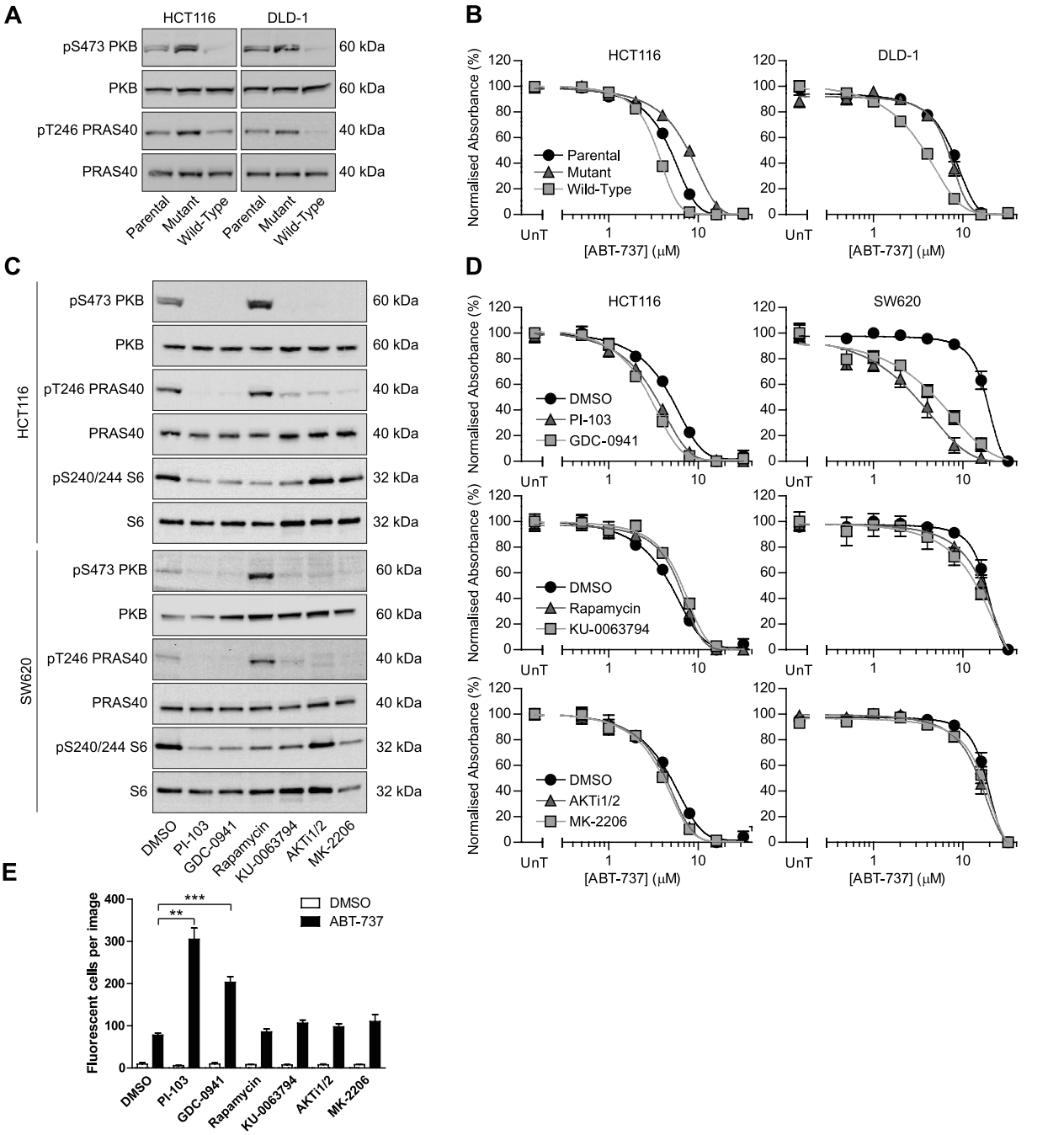

Figure 3. ABT-737 sensitization was PI3K dependent but AKT and mTOR independent. (A and B) Parental HCT116 and DLD-1 cells or cells expressing only the mutant or wild-type *PIK3CA* allele were assessed for the level of pS473 AKT, total AKT, pT246 PRAS40, or total PRAS40 by Western blot analysis (A) or exposed to the indicated concentrations of ABT-737 and processed as in Figure 1*A* (B). (C) HCT116 and SW620 cells were exposed to 2 μM PI-103, 2 μM GDC-0941, 10 nM rapamycin, 2 μM KU-0063794, 1 μM AKTi1/2, or 1 μM MK-2206 for 4 hours, and the effect on level of pS473 AKT, total AKT, pT246 PRAS40, total PRAS40, pS240/244 S6, and total S6 was determined by Western blot analysis. (D) HCT116 and SW620 cells were treated with the same concentrations of PI3K pathway inhibitors as in C and the indicated concentrations of ABT-737 for 3 days and processed as in Figure 1*A*. (E) SW620 cells were treated with the same concentrations of PI3K pathway inhibitors as in C with or without 4 μM ABT-737 plus CellPlayer Caspase 3/7 reagent, which fluoresces after cleavage by caspases. Number of fluorescent cells was determined 8 hours after start of treatment. All blots are representative of three independent experiments, and all graphs represent the means of three independent experiments carried out in triplicate (B and D) or duplicate (E) ± SEM. $^{**}P < .01$ and $^{***}P < .001$ according to two-tailed unpaired *t* test.

Table 2. Effect of PI3K Pathway Inhibitors on ABT-737 GI_{50}.

Cell Line	Treatment	ABT-737 GI_{50} (μM ± 95% CI)	Significance*
HCT116	DMSO	4.95 (4.15-5.90)	
	2 μM PI-103	3.33 (2.88-3.84)	0.0268
	2 μM GDC0941	2.73 (2.54-2.93)	0.0036
	1 μM AKTi1/2	4.32 (4.17-4.46)	0.2092
	1 μM MK2206	4.06 (3.72-4.43)	0.1189
	10 nM rapamycin	6.19 (5.77-6.64)	0.0821
	2 μM KU0063794	6.57 (6.10-7.07)	0.0441
SW620	DMSO	16.9 (15.4-18.5)	
	2 μM PI-103	3.15 (2.45-4.05)	0.0002
	2 μM GDC0941	6.09 (3.10-11.9)	0.0424
	1 μM AKTi1/2	14.5 (11.4-18.5)	0.3140
	1 μM MK2206	20.0 (10.6-37.6)	0.6317
	10 nM rapamycin	15.3 (12.8-18.4)	0.4049
	2 μM KU0063794	16.4 (12.9-20.8)	0.8369

*Two-tailed unpaired *t* test *versus* DMSO-treated GI_{50} for same cell line.

kinase inhibitor PCI-32765 (ibrutinib [33]) in SW620, HCT116, and DLD-1 cells sensitized to ABT-737 (Figures 4*E* and W8, and Table W7). To determine whether BMX acted downstream of PI3K with regard to ABT-737 sensitization, the effect of BMX knockdown and PI-103 treatment on ABT-737 sensitivity was assessed. Knockdown of BMX did not further sensitize PI-103–treated SW620 cells to ABT-737 (Figure 4*F* and Table W8), suggesting that BMX-induced sensitization to ABT-737 is downstream of PI3K. BMX inhibition, either by RNAi or treatment with PCI-32765, did not affect expression of MCL-1 (Figure W9), suggesting that sensitization to ABT-737 is through an MCL-1–independent mechanism. Together, these data suggest that inhibition of BMX activity, either through knockdown or pharmacological inhibition, can sensitize CRC cell lines to ABT-737. This indicates that this PH domain–containing protein may represent a key AKT-independent effector downstream of PI3K that is responsible for PI3K inhibition–induced ABT-737 sensitization.

Discussion

In this study, we presented evidence that the inhibition of PI3K signaling increased the sensitivity of CRC cells to ABT-737–induced apoptosis. This effect was shown to be independent of AKT inhibition and in part due to factors additional to the observed MCL-1 down-regulation. Furthermore, we present data demonstrating that inhibition of the TEC kinase BMX also sensitizes to ABT-737. This raises the possibility that BMX is a key downstream target of PI3K signaling mediating ABT-737 sensitivity and suggests that the PI3K/BMX axis may have antiapoptotic activity in CRC cells.

Other studies in non–small cell lung cancer [18] and lymphoma cell lines [17] have demonstrated that canonical PI3K pathway inhibition downstream of PI3K increased apoptosis in response to ABT-737 (or navitoclax). BCL-XL prevented PI3K inhibition–induced apoptosis in non–small cell lung cancer cells, and this was overcome by ABT-737; however, PI3K inhibition was phenocopied in AKT-depleted cells, suggesting that the antiapoptotic effect of PI3K signaling was AKT dependent [18]. Rapamycin increased navitoclax-induced apoptosis in lymphoma cells *in vitro* and *in vivo*, although the mechanism of action was not investigated [17]. Taken together, these three studies suggest that there are different mechanisms downstream of PI3K signaling to suppress ABT-737–induced apoptosis and that these mechanisms are context dependent. In support of this, a study investigating the importance of AKT in cellular proliferation/survival across a panel of human tumor cell lines revealed that a subset of cell lines (including HCT116 and DLD-1) was dependent on PI3K but not on AKT for proliferation and survival [34]. The lack of an absolute requirement for AKT in CRC cells has also been reported. When either *PDK1* or *AKT1* and *AKT2* were knocked out in both HCT116 and DLD-1 cells [35], the cells were able to survive in standard culture conditions. However, inhibition of PI3K signaling by pharmacological intervention or expression of a dominant negative PI3K subunit in the same cell lines ([7] and Figure W2) caused a profound proliferation delay. Overall, there are clearly cell line–dependent differences in signaling downstream of PI3K, and this emphasizes the need to broaden our understanding of this important signaling pathway beyond AKT and its known downstream targets.

The TEC family of kinases is the second largest family of nonreceptor protein tyrosine kinases, comprising five members, namely, TEC, BTK, ITK, TXK, and BMX (also known as ETK). Whereas TEC kinases are primarily expressed in hematopoietic cells, BMX and TEC have a broader expression profile. Specifically, BMX is expressed in endothelial linages as well as epithelial cancers such as breast and prostate [36]. All TEC kinases except TXK have a PH domain that interacts with PtdIns(3,4,5)P_3 and can be activated by PI3K signaling [37–39]. Furthermore, BMX has recently been implicated in mutant PIK3CA transformation [40]. BMX has been suggested to have an antiapoptotic function in prostate cancer cell lines [41], where expression of dominant negative BMX enhances chemotherapy- and radiotherapy-induced apoptosis. The downstream targets of BMX are not fully elucidated; although research has demonstrated that BMX can activate STAT3 [42] and also bind to and activate PAK1 [43], whether these targets are responsible for the antiapoptotic effect of BMX is unclear. BMX has been reported to bind to BCL-XL in bladder cancer cell lines [44], although the functional consequences of this interaction and how it is regulated have not been investigated. In the study reported here, we were unable to detect any change in phosphorylation of STAT proteins after treatment with PI3K or TEC kinase inhibitors (data not shown), and further investigation is now required to understand the antiapoptotic role of BMX in CRC better.

In addition to BMX, the RNAi library screen identified three other potential sensitizers to ABT-737, namely, SOS1, SGK1, and PLEKHB2. Further study with deconvolved SMARTpool siRNA oligos (Figures 4*C* and W5) suggested that the efficacy of SOS1 and SGK1 RNAi was probably due to off-target effects of some of the oligos, rather than knockdown of the intended target. PLEKHB2 was not investigated further as PLEKHB2's PH domain has recently been suggested to bind preferentially to phosphatidylserine rather than PtdIns(3,4,5)P_3 [45], and therefore, it is unlikely that PLEKHB2 is a downstream target of PI3K signaling. It is also interesting to note that knockdown of two PI3K subunits, PIK3CB and PIK3R1, was implicated in causing resistance to ABT-737 (Figure 4*A*). One possibility is that down-regulation of specific PI3K subunits (e.g., PIK3CB) leads to a compensatory up-regulation of other subunits (e.g., PIK3CA), and it is the upregulated subunit that drives ABT-737 resistance, a hypothesis that will be tested in future studies.

From a clinical perspective, the data presented here suggest that combining navitoclax with PI3K inhibitors or TEC kinase inhibitors may prove beneficial to patients with metastatic CRC, a population of patients with a 6% chance of 5-year survival (Colorectal Cancer Survival by Stage—NCIN Data Briefing 2009, http://tinyurl.com/pf5hl45), exemplifying the clinical need for improved therapy.

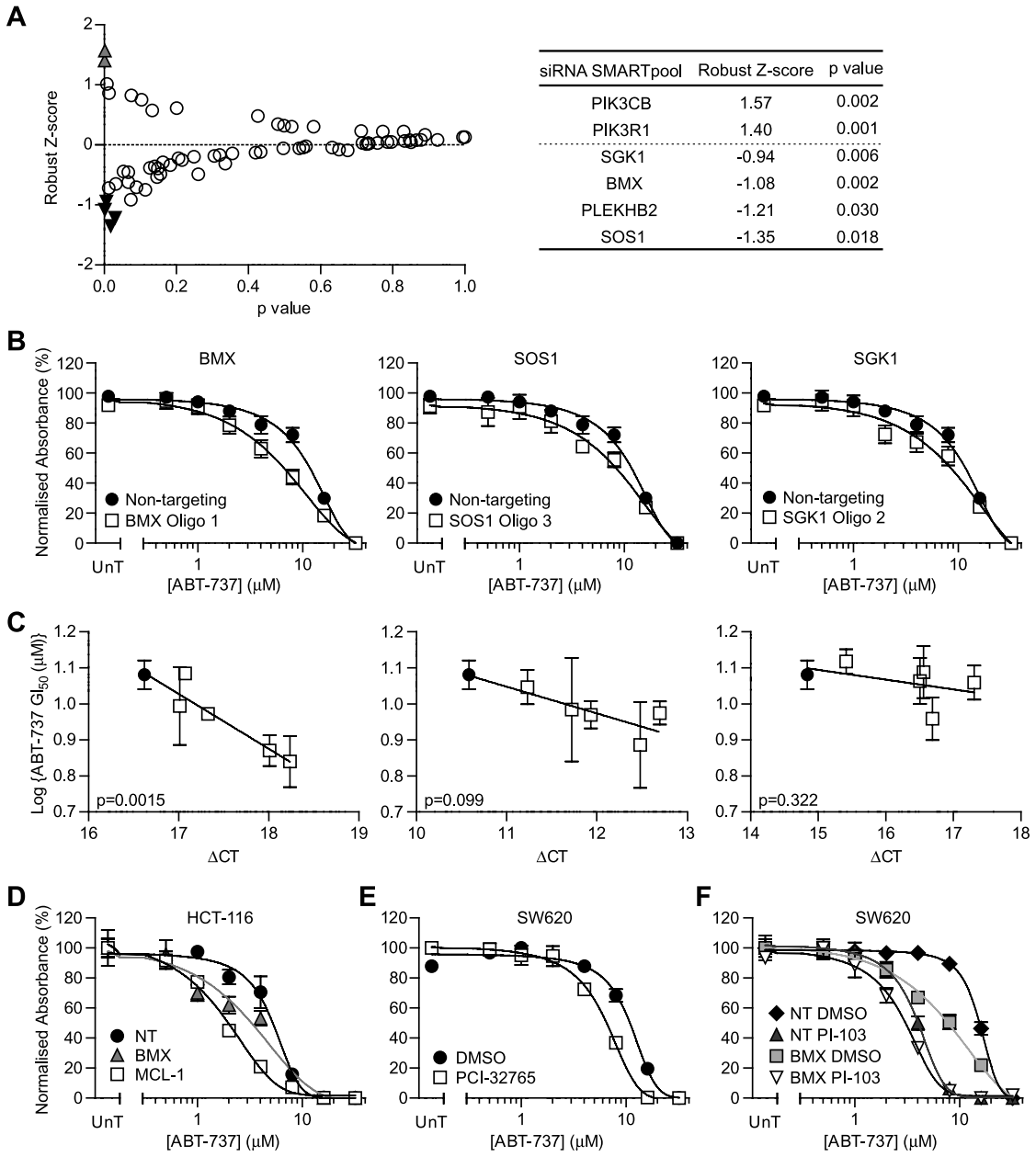

siRNA SMARTpool	Robust Z-score	p value
PIK3CB	1.57	0.002
PIK3R1	1.40	0.001
SGK1	-0.94	0.006
BMX	-1.08	0.002
PLEKHB2	-1.21	0.030
SOS1	-1.35	0.018

Figure 4. BMX knockdown and inhibition sensitized to ABT-737. (A) SW620 cells were transfected with an siRNA SMARTpool targeting 1 of 65 mRNA that encode proteins potentially involved in PI3K signaling or a nontargeting control. Forty-eight hours later, cells were treated with 4 μM ABT-737 or DMSO equivalent for 72 hours, and cellular biomass was determined by SRB staining. Robust *z* score of ABT-737–treated cells compared to DMSO control cells was calculated, and the *P* value for each SMARTpool compared to nontargeting control was determined by two-tailed unpaired *t* test. Values for SMARTpool that induce ABT-737 resistance (▲) and sensitivity (▼) are shown in right-hand table. (B and C) SW620 cells were transfected with nontargeting siRNA (●), SMARTpool siRNA, or individual oligos targeting BMX, SOS1, or SGK1 (□), and an ABT-737 concentration response was carried out, or the appropriate mRNA level was determined by qPCR. B shows the concentration response curve for the most effective siRNA oligo, and C shows the correlation between knockdown efficiency and ABT-737 efficacy. (D) HCT116 cells were transfected with nontargeting siRNA, BMX siRNA, or MCL-1 siRNA and the indicated concentration of ABT-737 for 3 days and processed as in Figure 1*A*. (E) SW620 cells were treated with 4 μM PCI-32765 or DMSO equivalent and the indicated concentration of ABT-737 for 3 days and processed as in Figure 1*A*. (F) SW620 cells were transfected with nontargeting siRNA or BMX oligo 1, treated with 2 μM PI-103 or DMSO equivalent and the indicated concentration of ABT-737 for 3 days, and processed as in Figure 1*A*. All graphs represent the means of three independent experiments carried out in triplicate ± SEM.

However, more research is needed to identify phenotypic and/or genotypic traits that predict for combinatorial efficacy. The data presented here demonstrate that PI3K inhibition increased apoptosis induced by ABT-737 more in SW620 cells (*PIK3CA* wild type) than in DLD-1 or HCT116 cells (*PIK3CA* mutant). However, we lack sufficient statistical power to conclude that these differences are due to *PIK3CA* status due to the plethora of other genetic differences between the cell lines. Therefore, to develop predictive biomarkers for this drug combination expansion to a larger panel of CRC cell lines with known genetic aberrations is required.

Acknowledgments

The authors thank John Brognard for advice on data interpretation and manuscript preparation and Becky Bola and Matthew Lancashire for editorial advice.

References

[1] FDA (2011). Regulatory watch: FDA guidance on co-developing investigational drugs. *Nat Rev Drug Discov* **10**, 86.
[2] Hanahan D and Weinberg RA (2011). Hallmarks of cancer: the next generation. *Cell* **144**, 646–674.
[3] Stephens L and Hawkins P (2010). Signalling via class IA PI3Ks. *Adv Enzyme Regul* **51**, 27–36.
[4] Vivanco I and Sawyers CL (2002). The phosphatidylinositol 3-kinase–AKT pathway in human cancer. *Nat Rev Cancer* **2**, 489–501.
[5] Manning BD and Cantley LC (2007). AKT/PKB signaling: navigating downstream. *Cell* **129**, 1261–1274.
[6] Engelman JA (2009). Targeting PI3K signalling in cancer: opportunities, challenges and limitations. *Nat Rev Cancer* **9**, 550–562.
[7] Martin-Fernandez C, Bales J, Hodgkinson C, Welman A, Welham MJ, Dive C, and Morrow CJ (2009). Blocking phosphoinositide 3-kinase activity in colorectal cancer cells reduces proliferation but does not increase apoptosis alone or in combination with cytotoxic drugs. *Mol Cancer Res* **7**, 955–965.
[8] Raynaud FI, Eccles S, Clarke PA, Hayes A, Nutley B, Alix S, Henley A, Di-Stefano F, Ahmad Z, Guillard S, et al. (2007). Pharmacologic characterization of a potent inhibitor of class I phosphatidylinositide 3-kinases. *Cancer Res* **67**, 5840–5850.
[9] Guillard S, Clarke PA, Te Poele R, Mohri Z, Bjerke L, Valenti M, Raynaud F, Eccles SA, and Workman P (2009). Molecular pharmacology of phosphatidylinositol 3-kinase inhibition in human glioma. *Cell Cycle* **8**, 443–453.
[10] Opel D, Westhoff MA, Bender A, Braun V, Debatin KM, and Fulda S (2008). Phosphatidylinositol 3-kinase inhibition broadly sensitizes glioblastoma cells to death receptor– and drug-induced apoptosis. *Cancer Res* **68**, 6271–6280.
[11] Chonghaile TN and Letai A (2008). Mimicking the BH3 domain to kill cancer cells. *Oncogene* **27**(suppl 1), S149–S157.
[12] Oltersdorf T, Elmore SW, Shoemaker AR, Armstrong RC, Augeri DJ, Belli BA, Bruncko M, Deckwerth TL, Dinges J, Hajduk PJ, et al. (2005). An inhibitor of Bcl-2 family proteins induces regression of solid tumours. *Nature* **435**, 677–681.
[13] Del Gaizo Moore V, Schlis KD, Sallan SE, Armstrong SA, and Letai A (2008). BCL-2 dependence and ABT-737 sensitivity in acute lymphoblastic leukemia. *Blood* **111**, 2300–2309.
[14] Wilson WH, O'Connor OA, Czuczman MS, LaCasce AS, Gerecitano JF, Leonard JP, Tulpule A, Dunleavy K, Xiong H, Chiu YL, et al. (2010). Navitoclax, a targeted high-affinity inhibitor of BCL-2, in lymphoid malignancies: a phase 1 dose-escalation study of safety, pharmacokinetics, pharmacodynamics, and antitumour activity. *Lancet Oncol* **11**, 1149–1159.
[15] Harrison LR, Micha D, Brandenburg M, Simpson KL, Morrow CJ, Denneny O, Hodgkinson C, Yunus Z, Dempsey C, Roberts D, et al. (2011). Hypoxic human cancer cells are sensitized to BH-3 mimetic-induced apoptosis via downregulation of the Bcl-2 protein Mcl-1. *J Clin Invest* **121**, 1075–1087.
[16] Cragg MS, Harris C, Strasser A, and Scott CL (2009). Unleashing the power of inhibitors of oncogenic kinases through BH3 mimetics. *Nat Rev Cancer* **9**, 321–326.
[17] Ackler S, Xiao Y, Mitten MJ, Foster K, Oleksijew A, Refici M, Schlessinger S, Wang B, Chemburkar SR, Bauch J, et al. (2008). ABT-263 and rapamycin act cooperatively to kill lymphoma cells *in vitro* and *in vivo*. *Mol Cancer Ther* **7**, 3265–3274.
[18] Qian J, Zou Y, Rahman JS, Lu B, and Massion PP (2009). Synergy between phosphatidylinositol 3-kinase/Akt pathway and Bcl-xL in the control of apoptosis in adenocarcinoma cells of the lung. *Mol Cancer Ther* **8**, 101–109.
[19] Klymenko T, Brandenburg M, Morrow C, Dive C, and Makin G (2011). The novel Bcl-2 inhibitor ABT-737 is more effective in hypoxia and is able to reverse hypoxia-induced drug resistance in neuroblastoma cells. *Mol Cancer Ther* **10**, 2373–2383.
[20] Morrow CJ, Gray A, and Dive C (2005). Comparison of phosphatidylinositol-3-kinase signalling within a panel of human colorectal cancer cell lines with mutant or wild-type PIK3CA. *FEBS Lett* **579**, 5123–5128.
[21] Cardone MH, Roy N, Stennicke HR, Salvesen GS, Franke TF, Stanbridge E, Frisch S, and Reed JC (1998). Regulation of cell death protease caspase-9 by phosphorylation. *Science* **282**, 1318–1321.
[22] Datta SR, Dudek H, Tao X, Masters S, Fu H, Gotoh Y, and Greenberg ME (1997). Akt phosphorylation of BAD couples survival signals to the cell-intrinsic death machinery. *Cell* **91**, 231–241.
[23] Griffiths GJ, Dubrez L, Morgan CP, Jones NA, Whitehouse J, Corfe BM, Dive C, and Hickman JA (1999). Cell damage-induced conformational changes of the pro-apoptotic protein Bak *in vivo* precede the onset of apoptosis. *J Cell Biol* **144**, 903–914.
[24] Konopleva M, Contractor R, Tsao T, Samudio I, Ruvolo PP, Kitada S, Deng X, Zhai D, Shi YX, Sneed T, et al. (2006). Mechanisms of apoptosis sensitivity and resistance to the BH3 mimetic ABT-737 in acute myeloid leukemia. *Cancer Cell* **10**, 375–388.
[25] van Delft MF, Wei AH, Mason KD, Vandenberg CJ, Chen L, Czabotar PE, Willis SN, Scott CL, Day CL, Cory S, et al. (2006). The BH3 mimetic ABT-737 targets selective Bcl-2 proteins and efficiently induces apoptosis via Bak/Bax if Mcl-1 is neutralized. *Cancer Cell* **10**, 389–399.
[26] Faber AC, Li D, Song Y, Liang MC, Yeap BY, Bronson RT, Lifshits E, Chen Z, Maira SM, Garcia-Echeverria C, et al. (2009). Differential induction of apoptosis in HER2 and EGFR addicted cancers following PI3K inhibition. *Proc Natl Acad Sci USA* **106**, 19503–19508.
[27] Samuels Y, Diaz LA Jr, Schmidt-Kittler O, Cummins JM, Delong L, Cheong I, Rago C, Huso DL, Lengauer C, Kinzler KW, et al. (2005). Mutant PIK3CA promotes cell growth and invasion of human cancer cells. *Cancer Cell* **7**, 561–573.
[28] Folkes AJ, Ahmadi K, Alderton WK, Alix S, Baker SJ, Box G, Chuckowree IS, Clarke PA, Depledge P, Eccles SA, et al. (2008). The identification of 2-(1H-indazol-4-yl)-6-(4-methanesulfonyl-piperazin-1-ylmethyl)-4-morpholin-4-yl-thieno[3,2-d]pyrimidine (GDC-0941) as a potent, selective, orally bioavailable inhibitor of class I PI3 kinase for the treatment of cancer. *J Med Chem* **51**, 5522–5532.
[29] Sarbassov DD, Ali SM, Kim DH, Guertin DA, Latek RR, Erdjument-Bromage H, Tempst P, and Sabatini DM (2004). Rictor, a novel binding partner of mTOR, defines a rapamycin-insensitive and raptor-independent pathway that regulates the cytoskeleton. *Curr Biol* **14**, 1296–1302.
[30] Garcia-Martinez JM, Moran J, Clarke RG, Gray A, Cosulich SC, Chresta CM, and Alessi DR (2009). Ku-0063794 is a specific inhibitor of the mammalian target of rapamycin (mTOR). *Biochem J* **421**, 29–42.
[31] Barnett SF, Defeo-Jones D, Fu S, Hancock PJ, Haskell KM, Jones RE, Kahana JA, Kral AM, Leander K, Lee LL, et al. (2005). Identification and characterization of pleckstrin-homology-domain-dependent and isoenzyme-specific Akt inhibitors. *Biochem J* **385**, 399–408.
[32] Hirai H, Sootome H, Nakatsuru Y, Miyama K, Taguchi S, Tsujioka K, Ueno Y, Hatch H, Majumder PK, Pan BS, et al. (2010). MK-2206, an allosteric Akt inhibitor, enhances antitumor efficacy by standard chemotherapeutic agents or molecular targeted drugs *in vitro* and *in vivo*. *Mol Cancer Ther* **9**, 1956–1967.
[33] Honigberg LA, Smith AM, Sirisawad M, Verner E, Loury D, Chang B, Li S, Pan Z, Thamm DH, Miller RA, et al. (2010). The Bruton tyrosine kinase inhibitor PCI-32765 blocks B-cell activation and is efficacious in models of autoimmune disease and B-cell malignancy. *Proc Natl Acad Sci USA* **107**, 13075–13080.
[34] Vasudevan KM, Barbie DA, Davies MA, Rabinovsky R, McNear CJ, Kim JJ, Hennessy BT, Tseng H, Pochanard P, Kim SY, et al. (2009). AKT-independent signaling downstream of oncogenic PIK3CA mutations in human cancer. *Cancer Cell* **16**, 21–32.
[35] Ericson K, Gan C, Cheong I, Rago C, Samuels Y, Velculescu VE, Kinzler KW, Huso DL, Vogelstein B, and Papadopoulos N (2010). Genetic inactivation of

AKT1, AKT2, and PDPK1 in human colorectal cancer cells clarifies their roles in tumor growth regulation. *Proc Natl Acad Sci USA* **107**, 2598–2603.

[36] Cenni B, Gutmann S, and Gottar-Guillier M (2012). BMX and its role in inflammation, cardiovascular disease, and cancer. *Int Rev Immunol* **31**, 166–173.

[37] August A, Sadra A, Dupont B, and Hanafusa H (1997). Src-induced activation of inducible T cell kinase (ITK) requires phosphatidylinositol 3-kinase activity and the Pleckstrin homology domain of inducible T cell kinase. *Proc Natl Acad Sci USA* **94**, 11227–11232.

[38] Li Z, Wahl MI, Eguinoa A, Stephens LR, Hawkins PT, and Witte ON (1997). Phosphatidylinositol 3-kinase-γ activates Bruton's tyrosine kinase in concert with Src family kinases. *Proc Natl Acad Sci USA* **94**, 13820–13825.

[39] Qiu Y, Robinson D, Pretlow TG, and Kung HJ (1998). Etk/Bmx, a tyrosine kinase with a pleckstrin-homology domain, is an effector of phosphatidylinositol 3′-kinase and is involved in interleukin 6-induced neuroendocrine differentiation of prostate cancer cells. *Proc Natl Acad Sci USA* **95**, 3644–3649.

[40] Hart JR, Liao L, Yates JR III, and Vogt PK (2011). Essential role of Stat3 in PI3K-induced oncogenic transformation. *Proc Natl Acad Sci USA* **108**, 13247–13252.

[41] Xue LY, Qiu Y, He J, Kung HJ, and Oleinick NL (1999). Etk/Bmx, a PH-domain containing tyrosine kinase, protects prostate cancer cells from apoptosis induced by photodynamic therapy or thapsigargin. *Oncogene* **18**, 3391–3398.

[42] Tsai YT, Su YH, Fang SS, Huang TN, Qiu Y, Jou YS, Shih HM, Kung HJ, and Chen RH (2000). Etk, a Btk family tyrosine kinase, mediates cellular transformation by linking Src to STAT3 activation. *Mol Cell Biol* **20**, 2043–2054.

[43] Bagheri-Yarmand R, Mandal M, Taludker AH, Wang RA, Vadlamudi RK, Kung HJ, and Kumar R (2001). Etk/Bmx tyrosine kinase activates Pak1 and regulates tumorigenicity of breast cancer cells. *J Biol Chem* **276**, 29403–29409.

[44] Guo S, Sun F, Guo Z, Li W, Alfano A, Chen H, Magyar CE, Huang J, Chai TC, Qiu S, et al. (2011). Tyrosine kinase ETK/BMX is up-regulated in bladder cancer and predicts poor prognosis in patients with cystectomy. *PLoS One* **6**, e17778.

[45] Uchida Y, Hasegawa J, Chinnapen D, Inoue T, Okazaki S, Kato R, Wakatsuki S, Misaki R, Koike M, Uchiyama Y, et al. (2011). Intracellular phosphatidylserine is essential for retrograde membrane traffic through endosomes. *Proc Natl Acad Sci USA* **108**, 15846–15851.

Supplemental Materials and Methods

Robust Z Score Calculation

Sensitivity to ABT-737 for each siRNA SMARTPool was assessed calculating the surviving fraction following treatment with 4 μM ABT-737 for 72 hours for each siRNA target. Surviving fraction = replicate well with ABT-737/(average of three replicate wells with DMSO). The robust *z* score was used to analyze siRNA screen data. Robust *z* score is the number of median absolute deviations (MADs); a value is from the median value of the data set. The robust *z* score is used because it reduces the effect of outliers on the results and prevents missing potential significant changes in sensitivity to ABT-737. First, the new surviving fractions are calculated. New surviving fraction = median surviving fraction for all 65 siRNAs – individual surviving fraction. Negative new surviving fractions are converted to positive values, and the MAD is then calculated. MAD = SD (new surviving fractions) × 1.4826. The robust *z* score for each replicate can be calculated. Robust *z* score = [(surviving fraction – median surviving fraction)/MAD] × 1.4826.

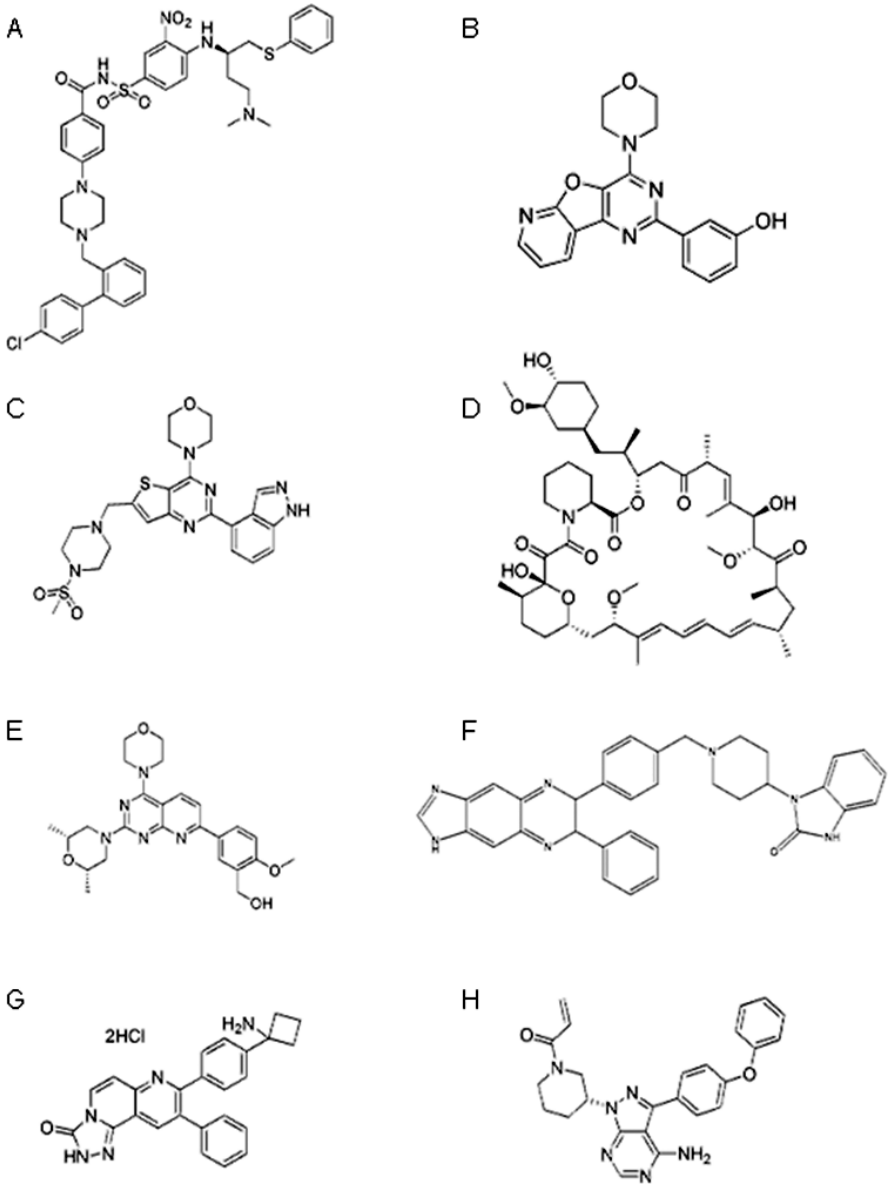

Figure W1. Structures of inhibitors used in study. (A) ABT-737, (B) PI-103, (C) GDC-0941, (D) rapamycin, (E) KU-0063794, (F) AKTi1/2, (G) MK-2206, and (H) PCI-32765.

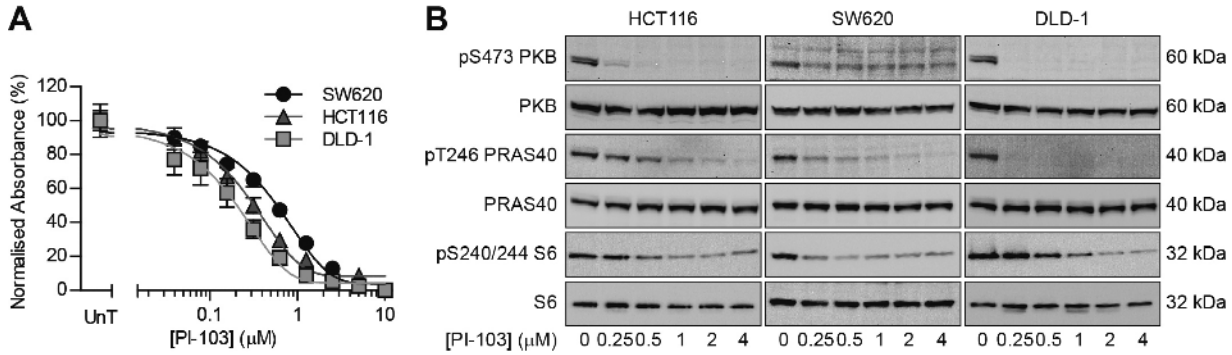

Figure W2. PI-103 inhibited cell proliferation and PI3K and mTOR signaling. (A) Cells were exposed to the indicated concentration of PI-103 for 3 days. Cells were fixed and stained with SRB, and the absorbance relative to untreated (UnT) cells was determined. Data represent the means of three independent experiments carried out in triplicate ± SEM. (B) Cells were exposed to the indicated concentration of PI-103 for 4 hours, and the effect on level of pS473 PKB, total PKB, pT246 PRAS40, total PRAS40, pS240/244 S6, and total S6 was determined by Western blot analysis. Results are representative of three independent experiments.

Table W1. Effect of MCL-1 RNAi on ABT-737 GI_{50}.

Cell Line	Treatment*	ABT-737 GI_{50} (μM ± 95% CI)	Significance†	
			vs NT DMSO	*vs* MCL-1 DMSO
HCT116	NT DMSO	5.83 (5.39-6.31)		
	NT PI-103	3.64 (3.20-4.15)	0.0037	
	MCL-1 DMSO	3.07 (2.59-3.65)	0.0027	
	MCL-1 PI-103	1.90 (1.75-2.06)	<0.0001	0.0079
SW620	NT DMSO	18.0 (17.1-19.0)		
	NT PI-103	3.54 (2.75-4.55)	0.0002	
	MCL-1 DMSO	2.09 (1.76-2.48)	<0.0001	
	MCL-1 PI-103	0.71 (0.56-0.92)	<0.0001	0.0022

The table relates to Figures 4*B*, *C*, and W6.
*Cells were transfected with either nontargeting siRNA (NT) or MCL-1 targeting siRNA (MCL-1). Cells were also treated with 2 μM PI-103 or a DMSO equivalent.
†Two-tailed unpaired *t* test *versus* indicated treatment for the same cell line.

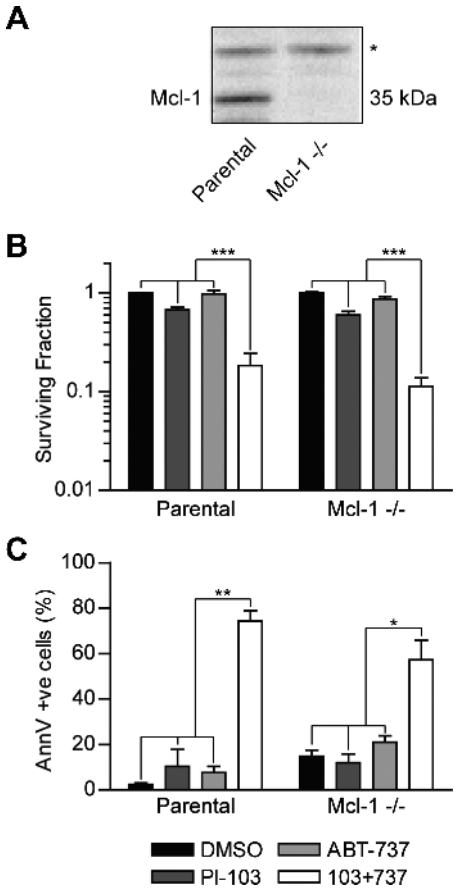

Figure W3. MCL-1$^{-/-}$ MEFs were sensitized to ABT-737–induced apoptosis by PI-103. (A) The level of MCL-1 in parental and MCL-1$^{-/-}$ MEFs was determined by Western blot analysis. *, nonspecific background band that acts as a loading control. (B) Parental and MCL-1$^{-/-}$ MEFs seeded at a low density were exposed to 2 μM PI-103 and/or 10 μM ABT-737 (parental) or 0.15 μM ABT-737 (MCL-1$^{-/-}$) for 3 days. Drugs were removed, and cells were left for 1 week for colonies to form. The number of colonies were counted and expressed as a surviving fraction relative to DMSO control. (C) Parental and MCL-1$^{-/-}$ MEFs were exposed to the same concentrations of PI-103 and ABT-737 as in B for 24 hours and stained with APC-conjugated annexin V. All graphs represent the means of three independent experiments carried out in duplicate ± SEM.

Table W2. Effect of PI3K Activity on ABT-737 GI_{50}.

Cell Line	PIK3CA Status	ABT-737 GI_{50} (μM ± 95% CI)	Significance*
HCT116	Parental	4.89 (4.55-5.24)	
	Mutant	8.16 (7.18-9.26)	0.0023
	Wild-type	3.40 (3.13-3.71)	0.0031
DLD-1	Parental	7.92 (7.29-8.61)	
	Mutant	6.97 (5.37-9.04)	0.4085
	Wild-type	3.76 (2.96-4.76)	0.0043

The table relates to Figure 3*B*.
*Two-tailed unpaired *t* test *versus* GI_{50} of parental cells for same cell line.

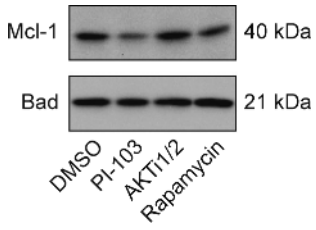

Figure W4. AKT and mTORC1 inhibition did not effect MCL-1 expression. HCT116 cells were treated with DMSO equivalent, 2 μM PI-103, 1 μM AKTi1/2, or 10 nM rapamycin for 24 hours, and the level of MCL-1 and Bad was determined by Western blot analysis.

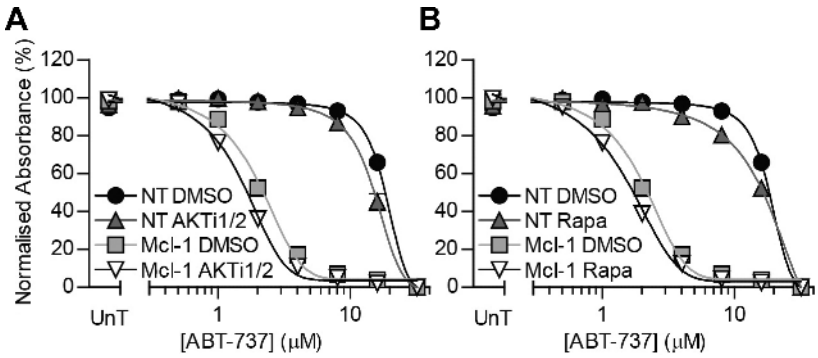

Figure W5. Neither AKTi1/2 nor rapamycin further sensitized MCL-1 knockdown SW620 cells to ABT-737. SW620 cells were transfected with NT RNAi or MCL-1 RNAi and plated for experiments 24 hours later. Cells were treated with 1 μM AKTi1/2 (A), 10 nM rapamycin (Rapa; B), or DMSO equivalent and the indicated concentration of ABT-737 for 3 days and processed as in Figure 1*A*. All graphs represent the means of three independent experiments carried out in triplicate ± SEM.

Table W3. Effect of MCL-1 RNAi on ABT-737 GI_{50}.

Cell Line	Treatment*	ABT-737 GI_{50} (μM ± 95% CI)	Significance†	
			vs NT DMSO	*vs* MCL-1 DMSO
SW620	NT DMSO	17.7 (17.3-18.2)		
	NT AKTi1/2	15.1 (13.0-17.7)	0.12	
	NT rapamycin	16.2 (14.5-18.1)	0.20	
	MCL-1 DMSO	2.1 (1.8-2.5)	<0.0001	
	MCL-1 AKTi1/2	1.6 (1.3-2.0)	<0.0001	0.11
	MCL-1 rapamycin	1.6 (1.3-2.1)	<0.0001	0.17

The table relates to Figure W5.
*Cells were transfected with either nontargeting siRNA (NT) or MCL-1 targeting siRNA (MCL-1). Cells were also treated with 1 μM AKTi1/2 or 10 nM rapamycin or a DMSO equivalent.
†Two-tailed unpaired *t* test *versus* indicated treatment for the same cell line.

Table W4. Results of siRNA Screen.

siRNA SMARTpool	Robust *Z* Score	*P* Value
MCL1	−4.669	4.66E-15
SOS1	−1.348	.018
PLEKHB2	−1.213	.030
BMX	−1.080	.002
SGK1	−0.944	.006
PIK3R2	−0.915	.074
AKT1	−0.746	.114
PHLDB3	−0.718	.013
PLEKHA2	−0.706	.089
SGK3	−0.649	.032
PIK3CD	−0.619	.067
AKT2	−0.535	.147
MCF2	−0.488	.261
DAPP1	−0.484	.156
FGD6	−0.456	.067
PREX2	−0.444	.054
ARAP3	−0.393	.149
VAV2	−0.382	.127
VAV1	−0.359	.140
ARHGEF4	−0.338	.183
DOCK1	−0.311	.336
GSK3B	−0.290	.163
PLEKHA1	−0.250	.216
TIAM1	−0.224	.206
PHLDB1	−0.197	.249
ADAP2	−0.186	.305
MTOR	−0.169	.320
GAB3	−0.141	.355
PIK3CA	−0.127	.419
ARAP1	−0.119	.434
SH3BP2	−0.079	.651
NT	−0.077	.539
SGK2	−0.056	.497
ARHGAP1	−0.055	.541
ADAP1	−0.045	.632
RASA2	−0.043	.552
VAV3	−0.025	.559
GSK3A	0.015	.726
SBF1	0.023	.733
PLCXD2	0.029	.732
CYTH4	0.031	.716
PLEK2	0.032	.758
ITK	0.046	.851
TEC	0.049	.796
PTPN9	0.067	.833
GAB1	0.078	.848
ARHGEF6	0.080	.865
SWAP70	0.083	.924
GAB2	0.084	.879
RASA3	0.131	.995
PREX1	0.167	.890
RICTOR	0.223	.830
PDPK1	0.224	.773
DOCK2	0.230	.712
CYTH2	0.301	.519
AKT3	0.303	.580
CYTH1	0.318	.498
ARAP2	0.345	.482
MYO10	0.482	.426
RASA1	0.572	.133
CYTH3	0.612	.201
BTK	0.751	.104
RPTOR	0.825	.075
AKAP13	0.861	.013
PLCL2	1.015	.008
PIK3R1	1.404	.001
PIK3CB	1.571	.002

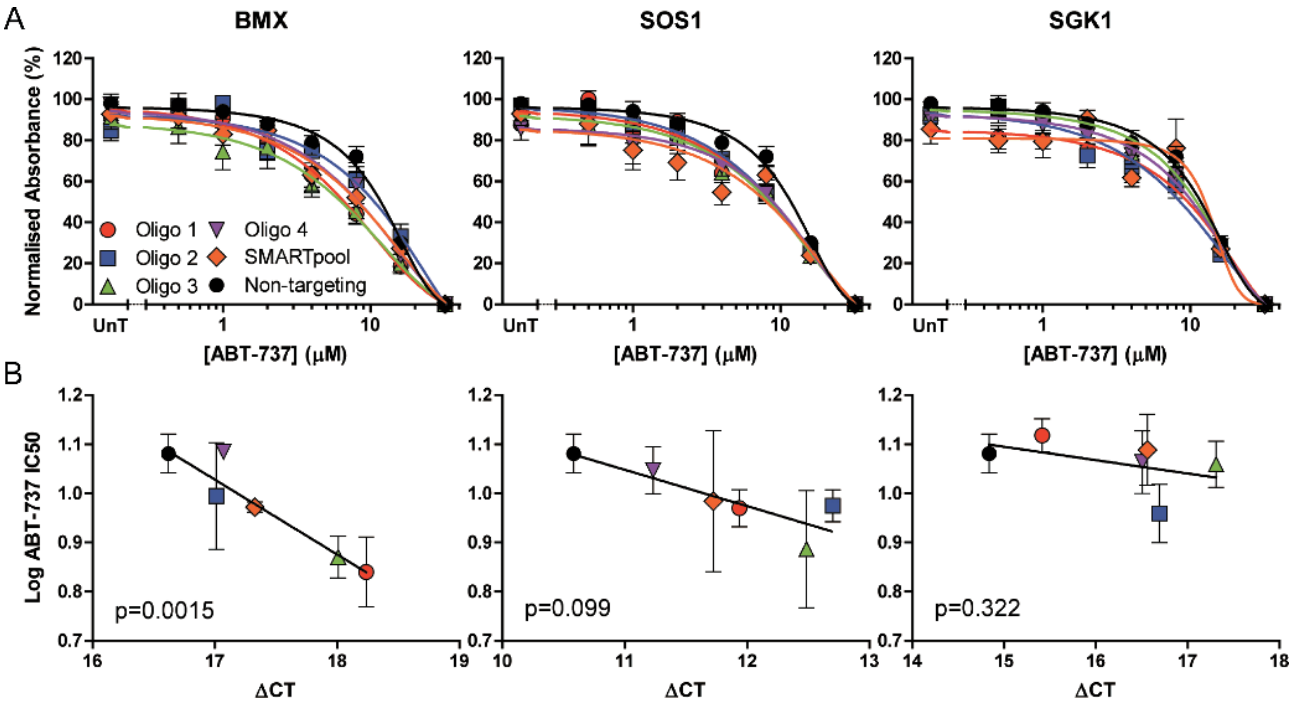

Figure W6. Deconvolution of BMX, SOS1, and SGK1 SMARTpool. SW620 cells were transfected with nontargeting siRNA, SMARTpool siRNA, or individual oligos targeting BMX, SOS1, or SGK1, and an ABT-737 concentration response was carried out, or the appropriate mRNA level was determined by qPCR. (A and B) A shows the concentration response curves, and B shows the correlation between knock-down efficiency and ABT-737 efficacy. All graphs represent the means of three independent experiments carried out in triplicate ± SEM.

Table W5. ABT-737 GI_{50} from Deconvolved siRNA Transfection.

RNAi Target	Oligo	ABT-737 GI_{50} (μM ± 95% CI)	Significance*
Nontargeting	SMARTpool	12.04 (10.07-14.10)	
BMX	1	6.92 (5.02-9.52)	0.041
	2	9.87 (6.06-16.08)	0.496
	3	7.42 (6.13-8.99)	0.022
	4	8.80 (4.68-16.56)	0.402
	SMARTpool	9.38 (8.95-9.83)	0.057
SOS1	1	9.33 (7.87-11.06)	0.113
	2	9.42 (8.16-10.91)	0.107
	3	7.70 (4.49-13.20)	0.198
	4	11.13 (8.98-13.81)	0.613
	SMARTpool	9.64 (5.04-18.44)	0.552
SGK1	1	13.11 (11.26-15.26)	0.516
	2	9.10 (6.96-11.89)	0.163
	3	11.46 (9.26-14.17)	0.744
	4	11.58 (8.69-15.44)	0.832
	SMARTpool	12.25 (8.85-16.96)	0.931

The table relates to Figures 4, *B* and *C*, and W4.
*Two-tailed unpaired *t* test *versus* nontargeting siRNA ABT-737 GI_{50}.

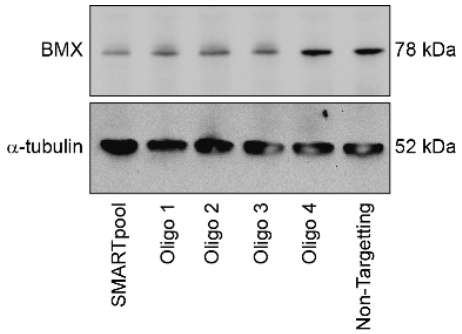

Figure W7. BMX RNAi reduced levels of BMX protein. SW620 cells were transfected with BMX siRNA SMARTpool, individual BMX siRNA oligos, or nontargeting control siRNA SMARTpool. After 48 hours, cells were harvested, and the level of BMX was assayed by Western blot analysis. Tubulin was used as a loading control. Blots are representative of three independent experiments.

Table W6. ABT-737 GI_{50} from HCT116 BMX RNAi.

RNAi Target	ABT-737 GI_{50} (μM ± 95% CI)	Significance*
Nontargeting	5.32 (4.40-6.43)	
BMX	2.94 (2.83-3.05)	0.027
MCL-1	1.70 (1.28-2.24)	0.022

The table relates to Figure 4*D*.
*Two-tailed unpaired *t* test *versus* nontargeting siRNA ABT-737 GI_{50}.

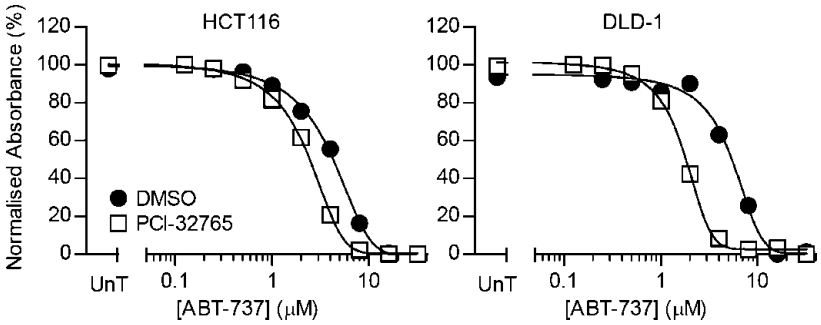

Figure W8. PCI-32765 increased the sensitivity of HCT116 and DLD-1 cells to ABT-737. HCT116 and DLD-1 cells were treated with 4 μM PCI-32765 or DMSO equivalent and the indicated concentration of ABT-737 for 3 days and processed as in Figure 1*A*. All graphs represent the means of three independent experiments carried out in triplicate. SEM error bars are not visible due to being smaller than the symbols.

Table W7. ABT-737 GI_{50} from SW620, HCT116 and DLD-1 PCI-32765 Treatment.

Cell Line	Treatment	ABT-737 GI_{50} (μM ± 95% CI)	Significance*
SW620	DMSO	10.8 (10.3-11.2)	
	4 μM PCI-32765	6.4 (5.9-6.9)	0.0005
HCT116	DMSO	4.2 (3.8-4.7)	
	4 μM PCI-32765	2.3 (2.0-2.7)	0.005
DLD-1	DMSO	5.4 (5.1-5.8)	
	4 μM PCI-32765	1.8 (1.7-1.8)	>0.0001

The table relates to Figures 4*E* and W8.
*Two-tailed unpaired *t* test *versus* nontargeting DMSO-treated ABT-737 GI_{50}.

Table W8. ABT-737 GI_{50} from SW620 BMX RNAi +/– PI-103.

Treatment*	ABT-737 GI_{50} (μM ± 95% CI)	Significance†	
		vs NT DMSO	*vs* NT PI-103
NT DMSO	15.4 (14.3-16.6)		
NT PI-103	3.79 (3.02-4.76)	0.0003	
BMX oligo 1 DMSO	8.0 (7.2-8.87)	0.0006	
BMX oligo 1 PI-103	2.93 (2.4-3.57)	0.0001	0.171

The table relates to Figure 4*F*.
*Cells were transfected with either nontargeting siRNA (NT) or BMX oligo 1. Cells were also treated with 2 μM PI-103 or a DMSO equivalent.
†Two-tailed unpaired *t* test *versus* indicated treatment for the same cell line.

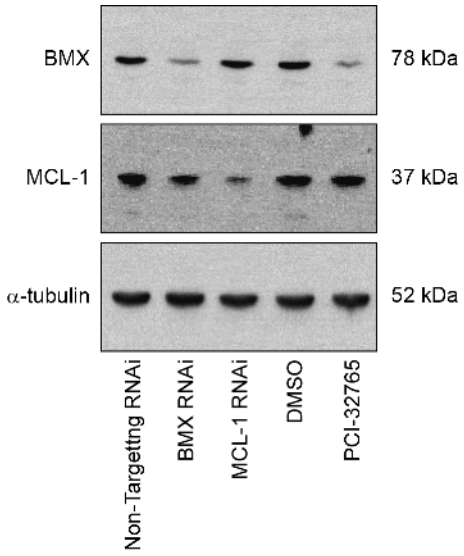

Figure W9. Neither BMX RNAi nor inhibition affected levels of MCL-1. SW620 cells were transfected with nontargeting siRNA, BMX siRNA, or MCL-1 siRNA SMARTpool and harvested 48 hours later to be treated with 4 μM PCI-32765 or DMSO equivalent and harvested 24 hours later. The level of BMX and MCL-1 was assayed by Western blot analysis. Tubulin was used as a loading control. Blots are representative of three independent experiments.

Chapter 4

Paper 2:

Inhibition of PI3K/BMX Cell Survival Pathway Sensitizes to BH3 mimetics in SCLC

Inhibition of PI3K/BMX Cell Survival Pathway Sensitizes to BH3 mimetics in SCLC

Danielle S Potter[1], Melanie Galvin[1], Stewart Brown[1], Cassandra Hodgkinson[1], Fiona Blackhall[2,3], Christopher J Morrow[1] and Caroline Dive[1]

[1]Clinical and Experimental Pharmacology Group, Cancer Research UK Manchester Institute and [2]Institute of Cancer Sciences, University of Manchester, [3]Christie NHS Foundation Trust, Manchester UK.

Abstract

Most Small Cell Lung Cancer (SCLC) patients are initially responsive to cytotoxic chemotherapy but almost all undergo fatal relapse with progressive disease, highlighting urgent need for improved therapies and better patient outcomes. The pro-apoptotic BH3 mimetic ABT-737, targeting BCL-2 family proteins demonstrated good single agent efficacy in preclinical SCLC models. Clinical trials of the BH3 mimetic Navitoclax were disappointing. We previously demonstrated that inhibition of a PI3K/BMX cell survival signalling pathway sensitised colorectal cancer cells to the ABT-737. Here we show that SCLC cell lines, which express high levels of BMX, become sensitized to ABT-737 upon inhibition of PI3K *in vitro*, and this is dependent on inhibition of the PI3K-BMX-AKT/mTOR signalling pathway in SCLC cells. Consistent with cell line data, combined BH3 mimetic and PI3K inhibition suppressed tumor growth in both an established SCLC xenograft model and in a newly circulating tumor cell derived explant (CDX) model generated from chemorefractory SCLC patient's blood sample. These data show for the first time that a PI3K/BMX pathway plays a role in survival signalling in SCLC and that combined BH3 mimetic and PI3K inhibition causes prolonged tumor regressions in a chemorefractory SCLC patient derived model *in vivo*. The data add to a body of evidence that this combination should move towards the clinic.

Keywords

Apoptosis, Bcl-2 family, BH3 mimetic, BMX, CDX models, PI3K, Tec family non-receptor tyrosine kinases

Introduction

Small cell lung cancer (SCLC), an aggressive neuroendocrine tumor, accounts for ~15% of newly diagnosed lung cancer cases and ~200,000 deaths worldwide each year (1). Patients with SCLC are commonly elderly and either heavy or ex-smokers (2) with only rare cases of never smokers (3). SCLC is classified as either limited stage (LS; confined to one hemithorax) or extensive stage (ES; more widespread (4)). LS and ES patients have a 5 year survival rate of between 8-31% and 2% respectively (5). Surgery is performed on <5% SCLC patients and standard of care (SOC) is cytotoxic chemotherapy +/- radiation (6). First line treatment is cisplatin or carboplatin combined with etoposide and LS patients may also receive sequential or concomitant thoracic radiotherapy (4). Patients with brain metastases are also offered prophylactic cranial irradiation as a palliative treatment (7).

Without any treatment the median overall survival (OS) of SCLC patients is 2-4 months (8). LS and ES SCLC patients have a median OS of 15-20 months and 8-13 months respectively, following the recommended first and second line therapy (9). Although 80-90% of LS and 70-80% of ES patients initially respond to therapy, virtually all patients eventually relapse with progressive disease within 3-18 months (9-11) and response rates to second line therapy are far lower than first line therapies with only 20% response rate (10). The molecular mechanism(s) underlying acquired drug resistance at relapse have yet to be elucidated and current research focuses on a potential selection of pre-existing chemo-resistant clones (12). Approximately 10-30% patients are classified as chemo-refractory with disease progression within 90 days of chemotherapy (9, 11).

Multiple targeted therapies have been tested in SCLC, yet none have improved patient outcomes (13) and platinum-based chemotherapy combined with etoposide remains SOC, three decades after its introduction. A better understanding of the biology of SCLC, improved preclinical models, discovery of druggable targets and biomarker led clinical trials are clearly warranted in this dismal disease.

The hallmark genetic aberrations in SCLC involve the tumor suppressors *TP53* (mutated in 75-90% of cases; (14)) and *RB1* (lost in 60-90% of cases; (1, 15)), consistent with the observed rapid tumor proliferation. Other common aberrations in SCLC is amplification of *MYC* family genes (in 18-31% of patients (14)) and amplification of BCL-2 (in ~40% patients (16, 17)). Commonly recurring and druggable oncogenic drivers of SCLC have yet to be identified, although mutually exclusive mutations are observed in genes within the PI3K (phosphoinositide 3-kinase) pathway in 36% of SCLC patients (18). Three landmark studies comprehensively characterised the genomic landscape of SCLC cell lines and tumor samples, identifying alterations in genes encoding histone modifying proteins and transcription factors including *SOX2* and the *NOTCH* family genes (19-21). These studies also revealed a mutation rate of 5.5-7.4 coding mutations per Mb, second only to melanoma amongst human cancers (22). These data report only 22 of 8000 protein coding mutations were observed in more than one SCLC tumor, indicating a high degree of diversity in SCLC (20). Consequently, identifying novel anti-cancer strategies for the treatment of SCLC is challenging. Given the overexpression of anti-apoptotic BCL-2 protein in SCLC (16, 17), one rational drug combination approach under investigation in SCLC is to target the Bcl-2 family core machinery that regulates commitment to apoptosis, together with putative survival signals such as those delivered via PI3K and mTOR that can modulate the threshold for apoptotic cell death (23, 24).

The intrinsic apoptotic pathway, regulated by the balance of pro- and anti-apoptotic Bcl-2 family proteins, is frequently modulated during tumor development allowing enhanced tumor cell survival in hostile nutrient and oxygen deprived tumor microenvironments (25, 26). The Bcl-2 family is subdivided into anti-apoptotic proteins, pro-apoptotic effectors and the pro-apoptotic BH3-only proteins. Pro-apoptotic effectors such as BAX and BAK, once activated, form homo-oligomers that create pores in the outer mitochondrial membrane causing mitochondrial outer membrane permeabilization (MOMP) and release of apoptotic factors such as cytochrome c (27). The anti-apoptotic subfamily (BCL-2, BCL-x_L, BCL-w, MCL-1, and A1) prevent MOMP via interactions with pro-apoptotic family members. Pro-apoptotic BH3-only proteins are further sub-divided into activators (BIM and BID) or sensitizers (BAD, BMF, HRK, NOXA and PUMA). Activators

directly activate effector proteins BAX and BAK and are potent initiators of apoptosis. Both activators and sensitizers antagonise anti-apoptotic family members, releasing pro-apoptotic effectors for activation (28-31). BH3 mimetic drugs were modelled on BH3-only protein structure and block anti- and pro-apoptotic Bcl-2 family member interactions. ABT-737, the first BH3 mimetic developed by Abbvie was modelled on BAD and binds BCL-2 and BCL-x_L but has poor affinity for MCL-1. *In vitro* ABT-737 showed good single agent efficacy within a panel of SCLC cell lines and in several cell line derived xenograft models (32-35). SCLC cell lines that were most sensitive to ABT-737 expressed higher levels of BCL-2, BCL-x_L, BIM and NOXA with low levels of MCL-1 (33), conversely high expression of MCL-1 was considered to be one mechanism of ABT-737 resistance (32, 33). Despite promising preclinical data (32, 36), clinical trials of Navitoclax (ABT-263, the clinical candidate analogue of ABT-737) as a single agent in SCLC were disappointing (37) and rational combination strategies are considered critical to make progress.

Phosphoinositide 3-kinases are a conserved family of lipid kinases split into three classes that catalyse the phosphorylation of the D-3 hydroxyl position on the inositol ring of phosphatidlyinositol (PtdIns) species. Class I PI3K preferentially utilise PtdIns(4,5)P_2 as a substrate, producing PtdIns(3,4,5)P_3. PI3K class IA are the most thoroughly studied of the lipid kinases and have been shown to be important in tumorigenesis (38). Class IA PI3Ks are heterodimers composed of a p110 catalytic subunit and p85 regulatory subunit and once activated serve as signal transducers in pathways involved in cellular metabolism, cytoplasmic rearrangement, proliferation, polarity and cell survival (39, 40). Recently, we demonstrated that BMX, a seldom studied PI3K downstream effector, has anti-apoptotic function in colorectal cancer (CRC) cell lines and inhibition of PI3K/BMX pathway resulted in sensitisation to ABT-737 (41) in CRC cell line that were insensitive to ABT-737.

BMX, a member of the TEC family of non-receptor tyrosine kinases (NRTK) is expressed in endothelium, epithelial and hematopoietic cells (42, 43). BMX plays a role in the activation of many tyrosine kinases signalling pathways by phosphorylation of proteins such as MET, FAK, FGFR1, ACK1 and Insulin

receptor (44), suggesting a role in many biological processes. BMX is targeted to the plasma membrane via its Pleckstrin homology (PH) domain interacting with the PI3K product PtdIns(3,4,5)P_3. BMX was detected in 75% of SCLC patient samples where its expression correlated with that of BCL-2 and BCL-x_L (45). Furthermore, over-expression of BMX in the SCLC cell line H446, lead to a 6-fold decrease in doxorubicin sensitivity and upregulation of BCL-2 and BCL-x_L, suggesting an anti-apoptotic role for BMX in this disease (45). BMX was over-expressed in the chemo-resistant SCLC cell line H69AR relative to its parental cell line and BMX knockdown in these cells re-sensitised the cells to a panel of chemotherapy drugs (including cisplatin and etoposide), potentially via downregulation of BCL-x_L (46).

Here we set out to establish preclinical evidence for the combination of BH3 mimetics and PI3K inhibitors in SCLC and examined the role of BMX downstream of PI3K signalling in setting the threshold for apoptosis using traditional cell line models and a novel patient derived Circulating tumor cell Derived eXplant (CDX) model (47).

Materials and methods

Cell culture and drugs

NCI-H146, NCI-H526, NCI-H1048 and DMS114 (American Type Culture Collection (ATCC) Manassas, VA, USA) cells were cultured in RPMI media (Life Technologies, Inc, Paisley, UK) supplemented with 10% FBS (fetal bovine serum, BioWest, Nuaillé, France). All cell lines were incubated in a humidified atmosphere at 37°C and 5% CO_2. Cell lines were authenticated using the AmpFlSTR system (Applied Biosystems, Paisley, UK). ABT-737 (a kind gift from AbbVie, Chicago, IL, USA), PI-103, KU-0063794 (Merck, Nottingham, UK), MK-2206, and Ibrutinib (Selleck Chemicals, Houston, TX, USA) were all dissolved to 10 mM in DMSO (Sigma, Poole, UK) and stored as single use aliquots at −20°C/−80°C. Navitoclax (a kind gift from AbbVie) was stored at 4°C and formulated in 10% ethanol, 30% polyethylene glycol 400 (Sigma), and 60% Phosal 50 PG (American Lecithin Company, Oxford, CT, USA). GDC-0941 (Lancrix Chemicals, Shangai, China) was stored at -20°C and formulated in 10% DMSO, 5% Tween 20 (Sigma), and 85%

sterile saline. Once formulated, Navitoclax and GDC-0941 were stored at room temperature for up to 7 days.

Generation of CDX2 and CDX tumor dissociation

CDX2 tumors were generated as previously described (47). CDX2 tumors were disaggregated using the gentleMACS dissociator and human tumor dissociation kit, according to manufacturer's instructions (Miltenyi Biotec Ltd, Surrey, UK), immediately after sacrifice of the mouse host when the tumor reached 400 mm^3. Red blood cells were lysed with RBC lysis buffer (G-Biosciences, USA) and remaining cells were filtered through a 70 μm cell strainer (Corning, Wiesbaden, Germany). Cell viability was checked by trypan blue exclusion. CDX2 cells were maintained in the same culture conditions as described above for established SCLC cell lines.

Drug concentration responses and drug treatments

Cells were seeded into 96 well plates. H1048 and DMS114 cells were seeded at 7300 cells per well, H526 cells were seeded at 14000 cells per well, H146 cells were seeded at 15000 cells per well and disaggregated CDX2 tumor cells were seeded at 5000 cells per well. 24 hours after seeding, cells were treated with the indicated (on Figure) concentration of drug(s) and cultured for a further 72 hours in the presence of drug(s). Adherent cells H1048 and DMS114 were stained with sulforhodamine B (SRB) as previously described (48) and suspension cells H146, H526 and CDX2 were assessed using the resazurin assay as previously described (49). To determine logGI50, log drug concentration was plotted against raw absorbance, and nonlinear curve fit analysis was performed (GraphPad Prism, GraphPad Software, Inc, La Jolla, CA, USA). For display purposes only, drug concentration (log scale) has been plotted against normalized absorbance. Statistical analysis was carried out on three independent logGI50 readings and transformed to growth inhibition 50 (GI_{50}).

To assess Bcl-2 family expression levels, PI3K or apoptotic pharmacodynamic biomarkers after drug treatment, 10^6 cells were seeded into a 6 well plate (per

well). 24 hours later cells were treated with indicated concentration of drug (on Figure, GI_{50}) for either 4 hours or 24 hours.

Measurement of apoptosis

Apoptosis was measured as a function of mitochondrial cytochrome *c* release in H526, H1048 and DMS114 cells. Cells (10^6) were pelleted and washed in PBS after indicated drug treatment(s). Cells were resuspend and incubated in DTEB buffer (135 mM trehalose, 10 mM HEPES, 20 µM EDTA, 20 µM EGTA, 5 mM succinate acid, 0.1 % BSA and 50 mM KCl in sterile ddH_2O at pH 7.5 (KOH)) and 0.002% digitonin for 15 minutes at room temperature. Cells were fixed with formaldehyde (1% final concentration) at room temperature for 15 minutes in the dark and then diluted with 2:1 with neutralising buffer (1.7 M Tris and1.25 M glycine at pH 9.1) at room temperature for 15 minutes in the dark. Fixed cells were stained with cytochrome *c* antibody (1:400, Alexa 488, Clone 6h2.b4, BD Biosciences) diluted in staining buffer (1% saponin and 10% bovine serum albumins (Sigma) in sterile ddH_2O) overnight at 4°C and analysed the next day by flow cytometry (BD LSRFortessa™ analyzer) using Diva software (BD Biosciences).

***In vivo* efficacy of GDC-0941 and Navitoclax**

All *in vivo* procedures were carried out in accordance with Home Office Regulations (UK) and the UK Coordinating Committee on Cancer Research guidelines and by approved protocols (Home Office Project Licence no. 70/8252 which was reviewed by Cancer Research UK Manchester Institute Animal Welfare and Ethical Review Body, and *in vivo* work reported according to the ARRIVE (Animal Research Reporting of *In Vivo* Experiments) guidelines (2010)). H1048 xenografts were grown by *s.c* injection of $5x10^6$ cells in 0.2 mL of 1:1 RPMI:Matrigel (BD Biosciences) into the mid-dorsal flank of 8 week old female SCID-beige mice (C.B-17/IcrHsd-*Prkdc*^{scid}*Lyst*$^{bg-J}$; Harlan Laboratories, UK). CDX2 were generated as previously described (47). CDX2 (passage 4) tumor fragments were implanted *s.c.* into 8 week old female SCID-beige mice. Six mice were housed together in vented caging systems in a 12-hours light/12-hours dark environment and maintained at uniform temperature and humidity. Mice were

monitored twice weekly for signs of tumor growth, and once a palpable tumor was present, this was measured twice a week by callipers and tumor volume calculated as 0.5 x (longest measurement) x (shortest measurement)^2. Seven days after implantation mice bearing H1048 xenograft tumors of 150-250 mm^3 were randomized into 4 groups of 10 mice. Eleven weeks after implantation of CDX2 fragments, mice were put onto a randomized rolling recruitment over 4 weeks when CDX2 tumors reached between 150-250 mm^3 they were allocated into 4 groups of 7 mice. The treatment groups for both H1048 xenograft and CDX2 bearing mice were; vehicle only, 75 mg/kg GDC-0941 only, 100 mg/kg Navitoclax only, 75 mg/kg GDC-0941 and one hour later 100 mg/kg Navitoclax. Treatments were administered by oral gavage for 21 days. Tumor measurements were continued three times a week until the tumor reached four times initial tumor volume (4xITV) or the mouse had been on study for 6 months and then the mouse was sacrificed.

In vivo pharmacodynamics biomarkers of GDC-0941 and Navitoclax activity

H1048 xenografts or CDX2 were generated as described above. Mice with H1048 xenografts were allocated into 8 groups of 5 mice and CDX2 explant bearing mice into 8 groups of 4 mice. Each group were treated with either, vehicle only, 75 mg/kg GDC-0941 only, 100 mg/kg Navitoclax only, 75 mg/kg GDC-0941 and one hour later 100 mg/kg Navitoclax by oral gavage and sacrificed at 4 hours or 24 hours after dosing. Tumors were fixed in 4% formalin for 24 hours and then placed in 70% ethanol. Immunohistochemistry staining was carried out as previously described (50) to assess the percentage of apoptosis (cleaved caspase 3) and PI3K inhibition (phospho-S6). The following primary antibodies were used, cleaved Caspase 3 (D175) and pS235/236S6 (91B2) from Cell Signaling. Staining was quantitated as follows: digital images of whole-tissue sections were acquired using a Leica SCN400 histology scanner (Leica Microsystems, Milton Keynes, UK). Images were analysed using Definiens Developer XD version 2.0.4 and the Tissue Studio (Definiens AG, Munich, Germany).

In vivo tolerance of combined GDC-0941 and Navitoclax

Three 8 weeks old female SCID-beige mice were treated with 75 mg/kg GDC-0941 and one hour later 100 mg/kg Navitoclax by oral gavage for 21 days. Mice were monitored twice daily for any changes in weight and appearance for the duration of the dosing and for two weeks after and then sacrificed.

RNA interference (RNAi)

siRNA SMARTpools or individual oligos (Table 1; Thermo Scientific, Leicestershire, United Kingdom) were transfected into H1048 cells using Lipofectamine RNAiMAX (Life Technologies) according to the manufacturer's instructions. Cells were transfected in six-well plates and reseeded into appropriate culture vessels 24 hours later, and then drug treated 24 hours after that.

Target	Target sequence
BMX	GUACCAGUCUAGCGCAAUA
	GAAGAUACCUCGGGCAGUU
	GAAGAGAGCCGAAGUCAGU
	GAGCAUUUAUGGUUAGAAA
MCL-1	GGUUUGGCAUAUCUAAUAA
	GAAGGUGGCAUCAGGAAUG
	GAUUAUCUCUCGGUACCUU
	CGAAGGAAGUAUCGAAUUU
Non-targeting	UGGUUUACAUGUCGACUAA

Table 1: BMX, MCL-1 and non-targeting siRNAs target sequence.

Western blotting

Cell lysis, protein quantification and Western blotting analysis were carried out as previously described (48). The following primary antibodies were used: rabbit anti-AKT, rabbit anti-pS473AKT, rabbit anti-pT308AKT, rabbit anti-BAX, rabbit anti-BIM, rabbit anti-cleaved caspase 3, rabbit anti-PARP, rabbit anti-S6, rabbit anti-pS235/236S6 (Cell Signaling Technology, Danvers, MA), mouse anti-BCL-2 (Dako, Glostrup, Denmark), rabbit anti–BCL-x_L, mouse anti-BMX, mouse anti-MCL-1 (Becton Dickenson, Oxford, United Kingdom), rabbit anti-BAD (R&D Systems, Minneapolis, mouse anti-BAK (Merck), mouse anti–α-tubulin (Merck), mouse anti-Actin and rabbit anti-PUMA (Sigma).

Phospho-kinase array

Drug treatment (Ibrutinib 4 hours) or RNAi (BMX SMARTpool and non-targeting (control) siRNA) was conducted as previously described in Chapter 2.2.8 and Chapter 2.2.6.1 respectively. BMX knock-down and inhibition of the PI3K pathway was determined by Western blotting analysis using the pharmacodynamic biomarkers of the PI3K pathway, phospho-AKT and phospho-S6 (antibodies found in Table 6; PI3K pathway discussed in Chapter 2.2.5). Lysates from non-targeting RNAi, BMX RNAi or Ibrutinib treated cells were then used in a phospho-kinase array according to manufacturer's instructions (catalogue number ARY003B, R&D Systems, Minneapolis, MN, USA).

Statistical analysis

Statistical analysis, to determine significance, of preclinical experiments comparing treated and control groups, was carried out using unpaired, two-tailed t tests, performed in Excel, unless otherwise specified. Overall Survival rates were assessed using Kaplan-Meier analysis, while a log-rank test was used for comparison of the survival distributions. In addition, 1-way ANOVA multiple comparisons analysis was used to compare multiple drug treatment groups effect on tumor doubling time. These analyses were conducted using GraphPad Prism software. $P < 0.05$ was considered statistically significant

Results

BMX expression in SCLC

The PI3K/BMX pathway is implicated as having anti-apoptotic function in CRC cells where its inhibition sensitises to the BH3 mimetic ABT-737 (41). We hypothesised that other cancer cell types that express relatively high levels of BMX may use this PI3K/BMX anti-apoptotic pathway where combined PI3K inhibitor and BH3 mimetics would prove beneficial. BMX mRNA expression data (~1000 cancer cell lines) was obtained from the Broad institute's Cancer Cell Line Encyclopaedia (CCLE). BMX mRNA was expressed at relatively low levels in the majority of cancer cell lines, although some cancer types had examples of specific cell lines with high BMX expression. Most notable was the SCLC cell line group, which contained the top three BMX expressing cell lines (H211, H526 and CORL311 – Supplementary Figure 1A). To confirm the data obtained from the CCLE, the level of BMX protein expression was determined by Western blot across a panel of 9 SCLC cell lines. Five of the SCLC cell lines expressed BMX (H526, H1048, DMS114, H82 and DMS79; Supplementary Figure 1B). The combination of PI3K/BMX inhibitors with ABT-737 was assessed in 3 BMX expressers (H526, H1048 and DMS114) and one non-expresser (H146). H1048 and DMS114 grow as adherent monolayers whereas H146 and H526 grown as loose clusters in suspension. The H1048 SCLC cell line harbours an oncogenic activating mutation in *PIK3CA* and the rest are wildtype for *PIK3CA* (51).

PI3K/BMX pathway inhibition sensitised SCLC cell lines to ABT-737

PI-103, a dual class I PI3K/mTOR (mammalian target of rapamycin) inhibitor was used in inhibit PI3K signalling (52). The Tec kinase inhibitor Ibrutinib (PCI-32765 (53)) was used to inhibit BMX (which it inhibits with similar potency to the Tec kinase BTK (Bruton's Tyrosine Kinase, its primary target). PI-103 and Ibrutinib were assessed in combination with ABT-737. All 4 SCLC cell lines were responsive to PI-103 in either an SRB assay (adherent cells) which measures cellular biomass or a resazurin assay (suspension cells) which measures cellular viability through metabolic activity of live cells. The GI_{50} of PI-103 was 175 nM in H1048, 300 nM in H526, 330 nM in DMS114 and 30 nM in H146 cells

(Supplementary Figure 2). As pharmacodynamic biomarkers, phosphorylation of AKT and S6 was observed in response to GI_{50} concentrations of PI-103 confirming PI3K pathway inhibition in H1048, H526 and DMS114 cells. This was not observed in H146 cells which had less phospho-AKT but more phospho-S6 compared to untreated (DMSO) indicating incomplete inhibition of the PI3K pathway (Figure 1A).

SCLC cell lines were less sensitive to Ibrutinib with GI_{50} values of 4 μM in H1048, 15 μM in H526, 12 μM in DMS114 and 8 μM in H146 cells (supplementary Figure 2). Ibrutinib treatment inhibited phosphorylation of AKT and S6 in H1048 and H526 but had a similar effect to PI-103 in H146 cells which had less phospho-AKT but more phospho-S6 compared to untreated (DMSO) (Figure 1A). Ibrutinib had no effect on phospho-AKT and phospho-S6 levels compared to untreated (DMSO) in DMS114 (Figure 1A).

To determine whether PI3K/BMX pathway inhibition affected SCLC cell sensitivity to ABT-737, H1048, H526, DMS114 and H146 cells were treated concomitantly with PI-103 and/or ABT-737, or with Ibrutinib and/or ABT-737. All cell lines exhibited a concentration dependent response to ABT-737 alone (Figure 1B) consistent with previous studies (32, 33). In H1048 and H526 cells, the ABT-737 GI_{50} was significantly reduced in a concentration dependent manner by PI-103 or Ibrutinib but not in DMS114 and H146 (Figure 1B and supplementary Figure 3). This suggests that PI3K pathway inhibition sensitises to ABT-737 in a cell context dependent manner as not all SCLC cell lines were sensitised to ABT-737 when the PI3K pathway was inhibited. The observation that PI3K pathway inhibition sensitised towards ABT-737 in H1048 and H526 was irrespective of PIK3CA mutation status confirming the findings observed in CRC cell lines (41).

PI3K pathway inhibition enhanced ABT-737-induced apoptosis

We sought to confirm that increased sensitivity to ABT-737 in H1048 and H526 cells treated with PI-103 or Ibrutinib was due to increased apoptosis. DMS114 cells (which showed no combination response below 10μM) were included as a negative control. The effect of PI-103 only, Ibrutinib only, ABT-737 only, PI-103 plus ABT-737 or Ibrutinib plus ABT-737 on cytochrome c release was determined

by flow cytometry (Figure 2A). As single agents, neither PI-103 or Ibrutinib caused significant mitochondrial cytochrome c release in H1048 and H526 compared to untreated (DMSO) cells, ABT-737 caused cytochrome c release in 20% of H1048 cells (P = 0.011) and 11% of H526 cells (P = 0.0007). ABT-737-induced apoptosis was significantly increased when combined with either PI-103 or Ibrutinib compared to ABT-737 treatment alone in H1048 and H526 cells (Figure 2B). Cytochrome c release was not detected in DMS114 cells with any single agent or combination treatment (Figure 2A).

Consistent with these data, PI-103 and Ibrutinib treatment alone did not increase the cellular levels of cleaved Caspase 3 or cleaved Poly ADP-ribose polymerase (PARP) in H1048 and H526 cells. ABT-737 as a single agent did increase levels of these apoptosis biomarkers that were further increased when ABT-737 was combined with either PI-103 or Ibrutinib (Figure 2C). No cleaved Caspase 3 and cleaved PARP were observed with any treatment of DMS114 (Figure 2C). Taken together these data suggest that the increased ABT-737 sensitivity caused by PI-103 or Ibrutinib treatment in H1048 and H526 cells is due to increased ABT-737-induced apoptosis.

PI-103 sensitize to ABT-737 independent of MCL-1

The PI3K pathway regulates multiple Bcl-2 family members including BIM (54), BAD (55) and MCL-1 (56). We hypothesised that changes in expression of these proteins could represent the molecular mechanism underlying ABT-737 sensitisation. Therefore, the effect of PI-103, Ibrutinib, MK-2206 (allosteric AKT inhibitor) and KU-0063794 (ATP competitive mTORC1/2 inhibitor) treatment on expression levels of 8 Bcl-2 family members including BIM, BAD and MCL-1 was assessed after 24 hours of treatment in H1048, H526 and DMS114 cells. There were no changes in expression of any of these Bcl-2 family members after treatment with any of the PI3K pathway inhibitors suggesting sensitisation to ABT-737 is not due to regulating the expression levels of these Bcl-2 family members (supplementary Figure 4A).

MCL-1 is an established resistance factor for ABT-737 and Navitoclax efficacy (33, 36) and has been shown by others to be downregulated by mTOR pathway

leading to Navitoclax sensitisation (23). Although PI3K pathway inhibitors did not downregulate MCL-1 in H1048 cells (Figure 2D), others have shown that the mTOCR1/2 inhibitor AZD8055 downregulates MCL-1 in these cells. So we investigated whether PI-103 treatment could further sensitise MCL-1 RNAi cells to ABT-737. Further sensitisation would suggest that inhibition of the PI3K pathway sensitises to ABT-737 independently of MCL-1 downregulation. As expected, MCL-1 RNAi sensitised H1048 cells to ABT-737. However, PI-103 caused a 4.1 fold sensitisation to ABT-737 in control cells and a 9.1 fold sensitisation to ABT-737 in MCL-1 RNAi cells (Figure 2E-F and Supplementary Figure 4B) confirming that MCL-1 downregulation does not underlie PI-103 induced ABT-737 sensitisation in this cellular context.

PI-103 does not further sensitise BMX RNAi cells to ABT-737

To determine whether BMX inhibition sensitised to ABT-737 downstream of PI3K, the effect of BMX RNAi combined with PI-103 treatment on ABT-737 sensitivity was assessed in H1048 cells. Cells were transfected with SMARTpool siRNA targeting BMX mRNA and the individual siRNA oligos that make up the SMARTpool. BMX RNAi cells were treated with ABT-737 (Figure 3A) and BMX knockdown was confirmed by western blot (Figure 3B). SMARTpool siRNA and oligos 1 and 3 caused a significant sensitisation to ABT-737 (Supplementary Figure 5A, P = 0.033, 0.006 and 0.037 respectively) and gave the greatest degree of BMX knockdown (consistent with our previous observations in CRC cells (41)). If BMX is acting downstream of PI3K then BMX RNAi should not significantly further sensitise PI-103 treated cells to ABT-737. H1048 cells were transfected with either siRNA targeting BMX or non-targeting control siRNA and treated concomitantly with PI-103 and/or ABT-737 (Figure 3C). As expected BMX RNAi and PI-103 treatment alone significantly sensitised to ABT-737. PI-103 treated cells were not significantly further sensitised to ABT-737 by knock-down of BMX (Figure 3D and Supplementary Figure 5B). These data suggest that BMX acts downstream of PI3K in a pro-survival signalling pathway. A phospho-kinase array carried out in BMX RNAi cells or Ibrutinib treated cells confirm that BMX regulates the AKT/mTOR pathway in H1048 cells (Figure 3E-F). This array also revealed

that BMX may regulate STAT3 in these cells (Figure 3E-F) which is consistent with the literature (57).

ABT-737 sensitisation by PI3K pathway inhibition is AKT and mTOR dependent in SCLC

BMX was identified as a downstream effector of PI3K in CRC and inhibition of this pathway sensitised to ABT-737 independently of the canonical PI3K downstream effectors AKT and mTOR (41). In H1048 and H526 SCLC cell lines that were sensitised by the PI3K inhibitor and BH3 mimetic combination, Ibrutinib inhibited the AKT/mTOR pathway (Figure 1A) and the phospho-kinase array confirmed this observation (Figure 3E-F). We next investigated AKT/mTOR pathway signalling to determine whether inhibition sensitises to ABT-737 in SCLC. Cell lines showed mixed sensitivity to the allosteric AKT inhibitor MK-2206 but were all responsive to the ATP competitive mTORC1/2 inhibitor KU-0063794 (Supplementary Figure 2). The GI_{50} of MK-2206 was 500 nM in H1048, 250 nM in H526, 8.8 μM in DMS114 and 12.8 μM in H146 cells. The GI_{50} of KU-0063794 was 200 nM in H1048, 400 nM in H526, 400 nM in DMS114 and 350 nM in H146 cells. A decrease in the phosphorylation of AKT and S6 confirmed inhibition of the PI3K pathway with MK-2206 and KU-0063794 treatment in H1048, H526 and DMS114 cells (Figure 4A). KU-0063794 treatment inhibited the PI3K pathway in H146 cells but MK-2206 treatment caused a decrease in phospho-AKT and an increased phospho-S6 (Figure 4A) consistent with what was observed with PI-103 and Ibrutinib inhibitors (Figure 1A).

All cell lines were treated concomitantly with MK-2206 and/or ABT-737, or with KU-0063794 and/or ABT-737. In H1048 and H526 cells the ABT-737 GI_{50} was significantly reduced in a concentration dependent manner by MK-2206 or KU-0063794 but not in DMS114 and H146 (Figure 4B and Supplementary Figure 3). Taken together the data suggest that PI3K pathway inhibition can sensitise H1048 and H526 cells to ABT-737 via both BMX (Figure 1B, 2A-C and 3A-C) and AKT/mTOR dependent (Figure 4B) mechanisms and this is cell context dependent.

Effect of combined PI3K inhibition and BH3 mimetic *in vivo*

Next, we assessed the efficacy of the drug combination of a PI3K inhibitor and BH3 mimetic *in vivo.* PI-103 and ABT-737 are not orally bioavailable compounds so GDC-0941, a clinically relevant class I PI3K inhibitor (currently in various clinical trials in solid tumors (58)), and Navitoclax (tested in phase II trials in SCLC (37)) were used for the *in vivo* studies. The combination was well tolerated in SCID-beige mice with an average body weight decrease of 5.3% after 21 days of treatment which rapidly recovered after cessation of treatment (Supplementary Figure 6). The efficacy of the combination was assessed in mice bearing H1048 xenografts, the cell line which exhibited the highest degree of sensitisation *in vitro* (Figure 1B). Mice bearing H1048 xenograft reached 4xITV in 9 days (vehicle group) and single agent GDC-0941 or Navitoclax in 14 days. When GDC-0941 and Navitoclax were combined there was a significant increase in days taken for tumor to reach the specified end point (32 days) compared to either drug as a single agent or the vehicle group (Vehicle, P = 0.0001; GDC-0941, P = 0.001; Navitoclax, P = 0.001 according to log-rank test; Figure 5A-C). GDC-0941 and Navitoclax in combination significantly increased tumor doubling time compared to vehicle and either drug as a single agent (Figure 5D). Navitoclax alone caused increased level of apoptosis compared to vehicle control after 24 hours which was further enhanced by combining with GDC-0941 (Figure 5E and F). GDC-0941, as a single agent or in combination with Navitoclax, caused downregulation of phospho-S6 after 4 hours of treatment, consistent with its primary pharmacology (Figure 5E and G).

The clinical relevance of long established SCLC cell lines are open to question (59) and SCLC patient derived xenografts (PDX) have been demonstrated to better reflect the underwhelming clinical results seen with single agent Navitoclax (60). Therefore, to expand our results to a mouse model that more accurately effects tumors in patients, we assessed efficacy of GDC-0941 and Navitoclax in a SCLC patient derived CDX (47). This is considered to be a high hurdle for drug development as the SCLC cells that derived the model have already invaded tissue and were disseminating, and proved tumorigenic in the host mouse. We previously demonstrated that CDX mouse models, derived from CTCs enriched

prior to donor patient's chemotherapy, mirror the subsequent chemotherapy response of the donor patient (47). CDX2 was derived from a chemo-refractory patient, whose disease progressed throughout treatment. Treatment of CDX2 with cisplatin and etoposide only delayed tumor growth by 19 days (47).

Initial *ex vivo* culture experiments suggested that disaggregated CDX2 cells were sensitive to ABT-737 and that sensitivity was enhanced by co-treatment with PI-103 (Figure 6A). Therefore, the efficacy of GDC-0941 and Navitoclax alone and in combination was assessed in mice bearing CDX2. The combination caused the greatest effect compared to either drug as a single agent or vehicle (Vehicle, P = 0.0002; GDC-0941, P = 0.0003; Navitoclax, P = 0.033 according to log-rank test; Figure 6B-D). In the combination group, no tumors reached 4xITV over the experimental time course and mean maximum tumor regression was 94%. Navitoclax single agent had a significant effect on tumor growth compared to vehicle and GDC-0941 single agent (vehicle, P = 0.0005; GDC-0941, P = 0.010 according to log-rank test; Figure 6D) although only one tumor failed to reach 4xITV over the experimental time course. Mean maximum tumor regression was 80%, but tumors began to regrow as soon as the Navitoclax treatment was ceased whereas in the combination group tumors began to regrow only after ~30 days post treatment cessation (Figure 6B) and one mouse treated with the combination had no detectable tumor at end of the experiment (Figure 6C). As in the H1048 xenograft model, GDC-0941 caused a significant decrease in phospho-S6 at 4 hours and the combination caused more apoptosis than single agent Navitoclax at 24 hours after treatment (Figure 6E-G). Taken together, these data suggest that combined GDC-0941 and Navitoclax is more efficacious *in vivo* than either drug alone and could prove a beneficial rational combination in SCLC patients, including chemo-refractory patients.

Figure 1:

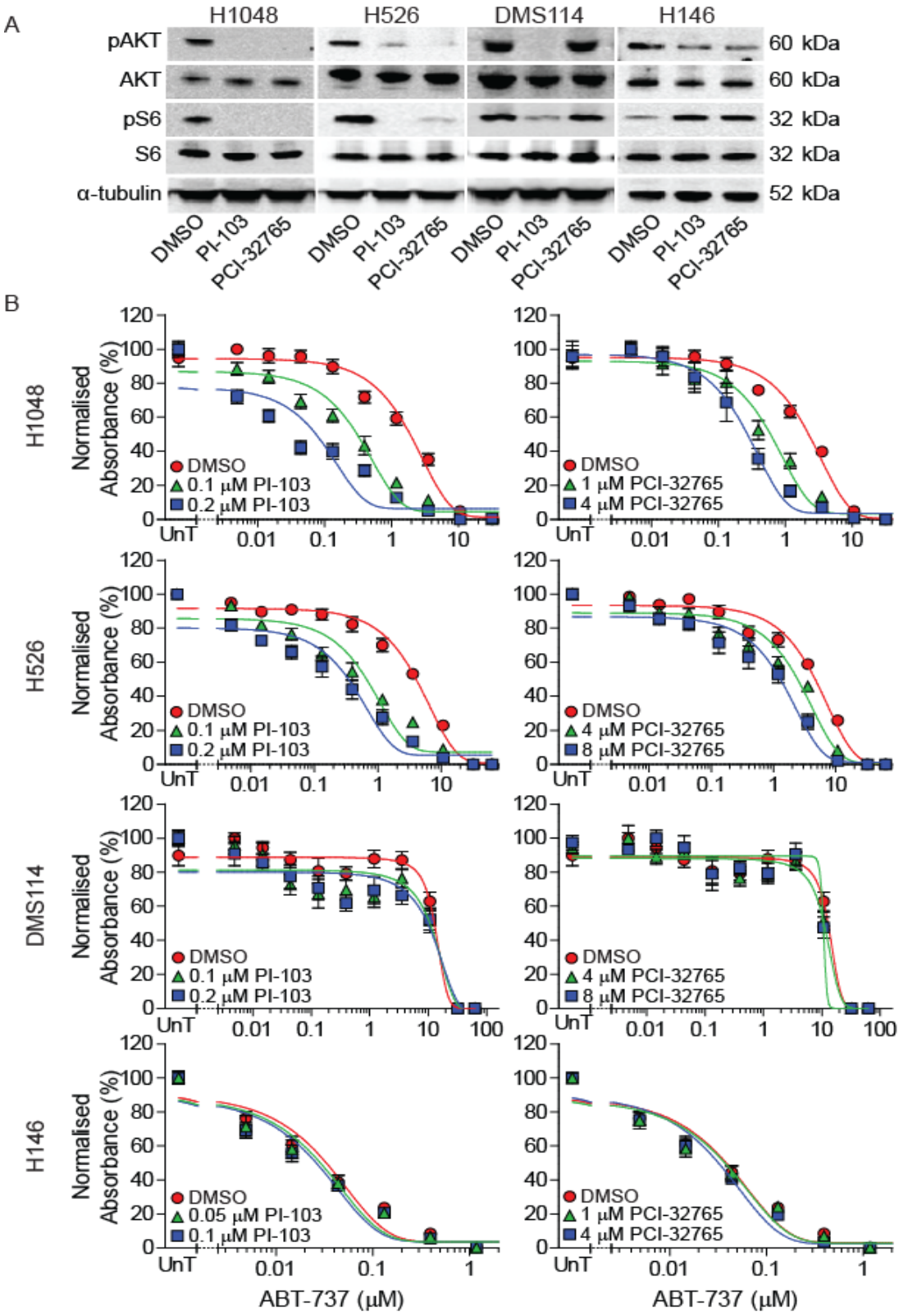
A
H1048
H526
DMS114
H146
pAKT
AKT
pS6
S6
α-tubulin
60 kDa
60 kDa
32 kDa
32 kDa
52 kDa
DMSO
PI-103
PCI-32765
B
H1048
H526
DMS114
H146
Normalised Absorbance (%)
DMSO
0.1 μM PI-103
0.2 μM PI-103
1 μM PCI-32765
4 μM PCI-32765
8 μM PCI-32765
0.05 μM PI-103
UnT
ABT-737 (μM)

Figure 1: PI3K/BMX pathway inhibition sensitized H1048 and H526 cells to ABT-737. (A) H1048 cell were treated with 0.1 μM PI-103 or 4 μM Ibrutinib; H526 and DMS114 were treated with 0.25 μM PI-103 or 8 μM Ibrutinib; H146 were treated with 0.025 μM PI-103 or 8 μM Ibrutinib; or DMSO equivalent for 4 hours, and the effect on levels of pS473 AKT, total AKT, pS235/236 S6 and total S6 was determined by Western blotting. Western blot is a representative of three independent experiments. (B) H1048, H526, DMS114 and H146 cells were exposed to the indicated concentration of either, PI-103, Ibrutinib or DMSO equivalent and the indicated concentration of ABT-737 for 3 days. H1048 and DMS114 cells were fixed and stained with SRB. H526 and H146 stained with resazurin for 4 hours. Absorbance (SRB, 540 nm) or fluorescence (resazurin) relative to untreated (UnT) cells was determined relative to PI-103, Ibrutinib, or DMSO only treated cells as appropriate for individual concentration response curves. Data represents the mean of three independent experiments carried out in triplicate ± SEM.

Figure 2:

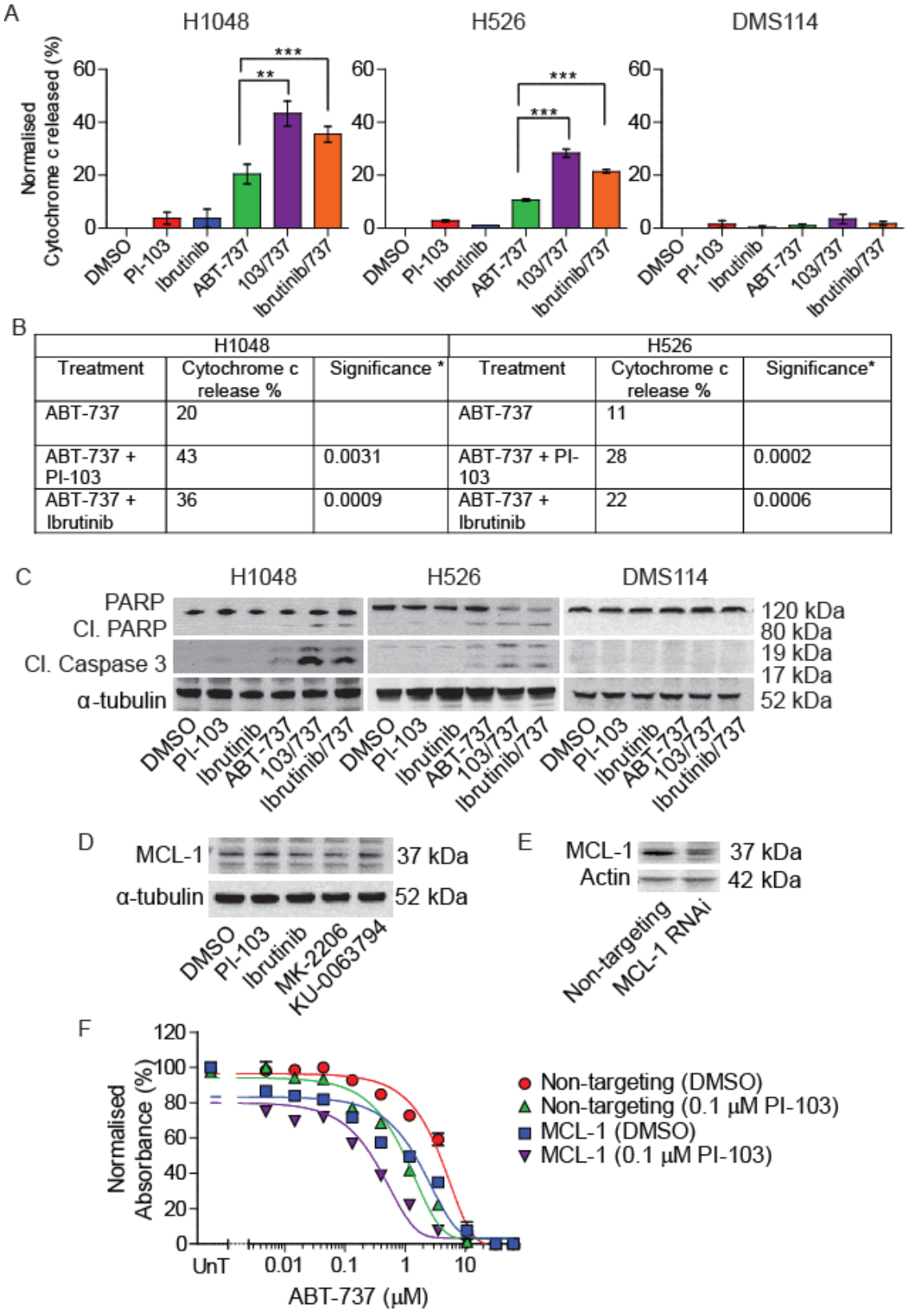

B

H1048			H526		
Treatment	Cytochrome c release %	Significance *	Treatment	Cytochrome c release %	Significance*
ABT-737	20		ABT-737	11	
ABT-737 + PI-103	43	0.0031	ABT-737 + PI-103	28	0.0002
ABT-737 + Ibrutinib	36	0.0009	ABT-737 + Ibrutinib	22	0.0006

Figure 2: PI3K/BMX inhibition increases ABT-737-induced apoptosis in sensitive SCLC cell lines. (A-C) H1048 cells were treated with 0.1 μM PI-103, 4 μM Ibrutinib or 2 μM ABT-737 alone; H526 and DMS114 were treated with to 0.25 μM PI-103, 8 μM Ibrutinib or 4 μM ABT-737 alone; or ABT-737 in combination with PI-103 or Ibrutinib at the same concentration as single agent for 4 hours. (A) Cells were fixed and stained with cytochrome c antibody and analysed using flow cytometry the next day to measure the percentage of cytochrome c positive cells within total population of cells. Cytochrome c positive cells were converted to percentage cytochrome c released (cytochrome c positive -100) and normalised to the controls (DMSO treated = 0%) and FMO (fluorescence minus one, no cytochrome c antibody = 100%). All graphs represent the means of three independent experiments ± SEM. *P < .05, **P < .01, and ***P < .001 according to two-tailed unpaired t test. (B) Table to show the percentage cytochrome c release from part (A) in H1048 and H526 cells. *Two-tailed unpaired t test versus cytochrome c release ABT-737-treated for same cell line. (C) Protein levels of cleaved Caspase 3 and cleaved PARP (poly ADP-ribose polymerase) was determined by Western blotting in H1048, H526 and DMS114 cells. Results are representative of three independent experiments. (D) H1048 cells were treated with 0.1 μM PI-103, 4 μM Ibrutinib, 0.5 μM MK-2206 and 0.25 μM KU-0063794 or DMSO equivalent for 24 hours, and the protein level of MCL-1 and α-tubilin (loading control) was determined by Western blotting. (E-F) H1048 cells were transfected with SMARTpool siRNA targeting MCL-1 mRNA or non-targeting control. (E) 48 hours post transfection MCL-1 protein levels were determined by Western blotting. Results are representative of three independent experiments. (F) 48 hours post transfection cells were treated with 0.1 μM PI-103 or DMSO equivalent and the indicated concentration of ABT-737 for 3 days. Cells were processed as in Figure 1B. Data represents the mean of three independent experiments carried out in triplicate ± SEM.

Figure 3:

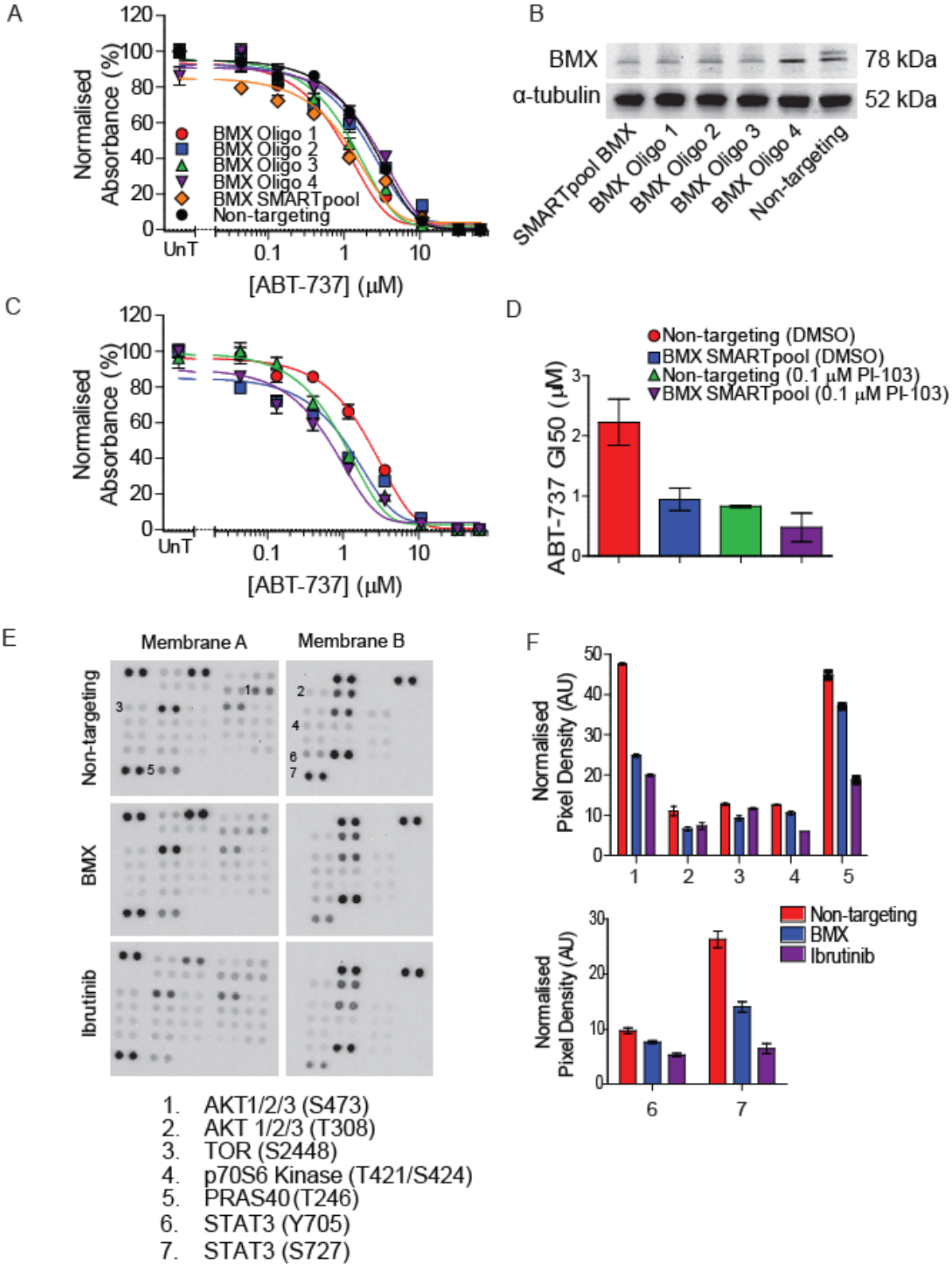

1. AKT1/2/3 (S473)
2. AKT 1/2/3 (T308)
3. TOR (S2448)
4. p70S6 Kinase (T421/S424)
5. PRAS40 (T246)
6. STAT3 (Y705)
7. STAT3 (S727)

Figure 3: BMX RNAi does not further sensitise PI-103 treated cells to ABT-737. (A-B) H1048 cells were transfected with SMARTpool siRNA or individual siRNA oligos targeting BMX mRNA or non-targeting control (NT). (A) 48 hours post transfection cells were treated with indicated concentration of ABT-737 for 3 days. Cells were processed as in Figure 1B. Data represents the mean of three independent experiments carried out in triplicate ± SEM. (B) 48 hours post transfection BMX protein levels were determined in BMX and NT RNAi by Western blotting. Results are representative of three independent experiments. (C) H1048 cells were transfected with SMARTpool siRNA targeting BMX mRNA or NT control. 48 hours post transfection cells were treated with 0.1 μM PI-103 or DMSO equivalent and the indicated concentration of ABT-737 for 3 days. Cells were processed as in Figure 1B. Data represents the mean of three independent experiments carried out in triplicate ± SEM. (D) ABT-737 GI_{50} from Figure 3C carried out in triplicate ± SEM.

Figure 4:

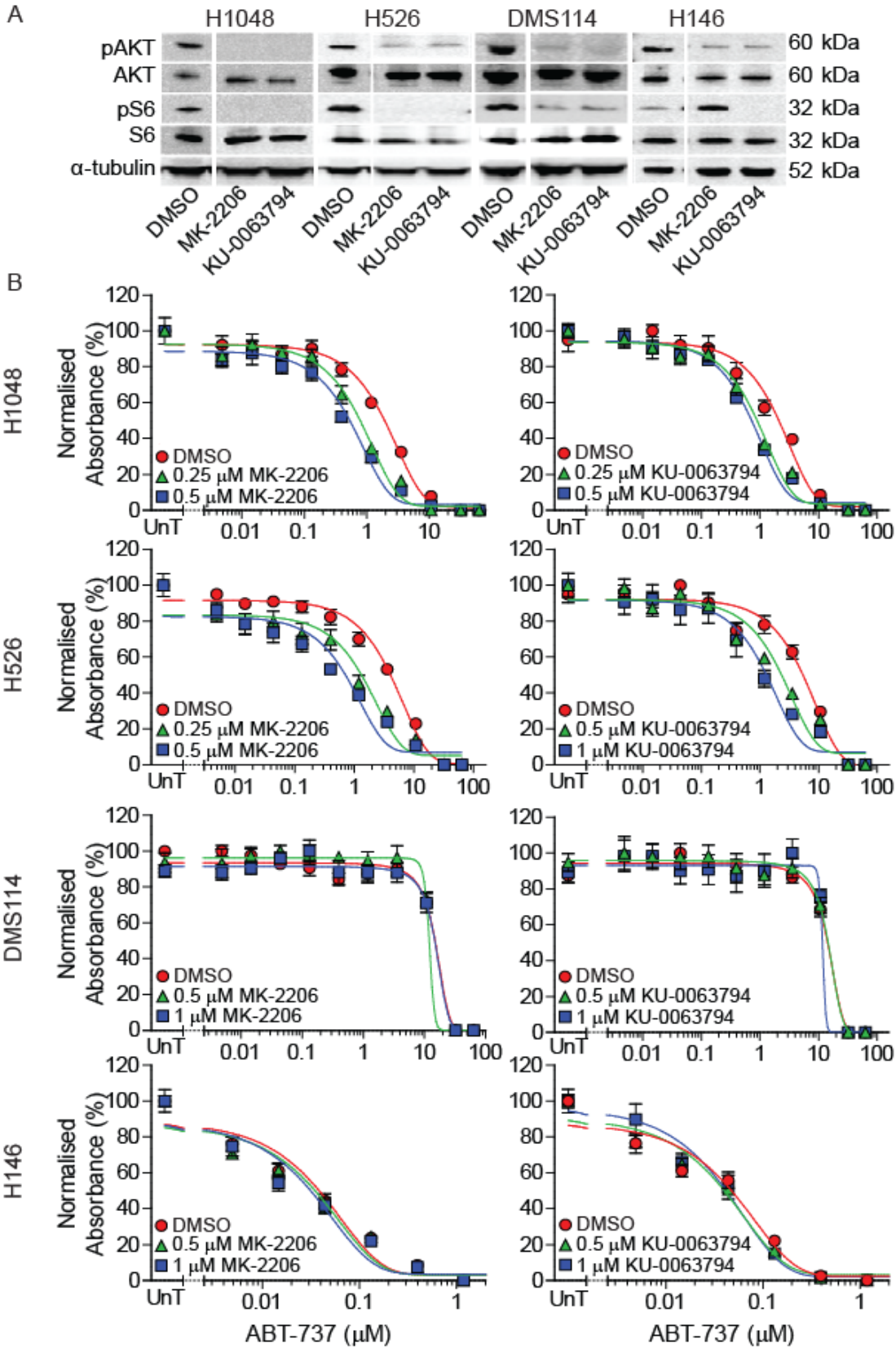
A
H1048
H526
DMS114
H146
pAKT
AKT
pS6
S6
α-tubulin
60 kDa
60 kDa
32 kDa
32 kDa
52 kDa
DMSO
MK-2206
KU-0063794
B
H1048
H526
DMS114
H146
Normalised Absorbance (%)
DMSO
0.25 μM MK-2206
0.5 μM MK-2206
0.25 μM KU-0063794
0.5 μM KU-0063794
1 μM MK-2206
1 μM KU-0063794
UnT
ABT-737 (μM)

Figure 4: AKT/mTOR pathway inhibition sensitized H1048 and H526 cells to ABT-737. (A) H1048 cells were treated with to 0.5 μM MK-2206 and 0.25 μM KU-0063794; H526 cells were treated with to 0.25 μM MK-2206 and 0.4 μM KU-0063794; DMS114 cells were exposed to 8 μM MK-2206 and 0.4 μM KU-0063794 and H146 cells were exposed to 8 μM MK-2206 and 0.4 μM KU-0063794; or DMSO equivalent for 4 hours. DMSO blot is from the same gel but PI-103 and Ibrutinib treatment from Figure 1A was removed for display purpose. Effect on levels of pS473 AKT, total AKT, pS235/236 S6 and total S6 was determined by Western blotting. Blot is representative of three independent experiments. (B) H1048, H526, DMS114 and H146 cells were exposed to the indicated concentration of either, MK-2206, KU-0063794 or DMSO equivalent and the indicated concentration of ABT-737 for 3 days. Cells were processed as in Figure 1B. Data represents the mean of three independent experiments carried out in triplicate ± SEM.

Figure 5:

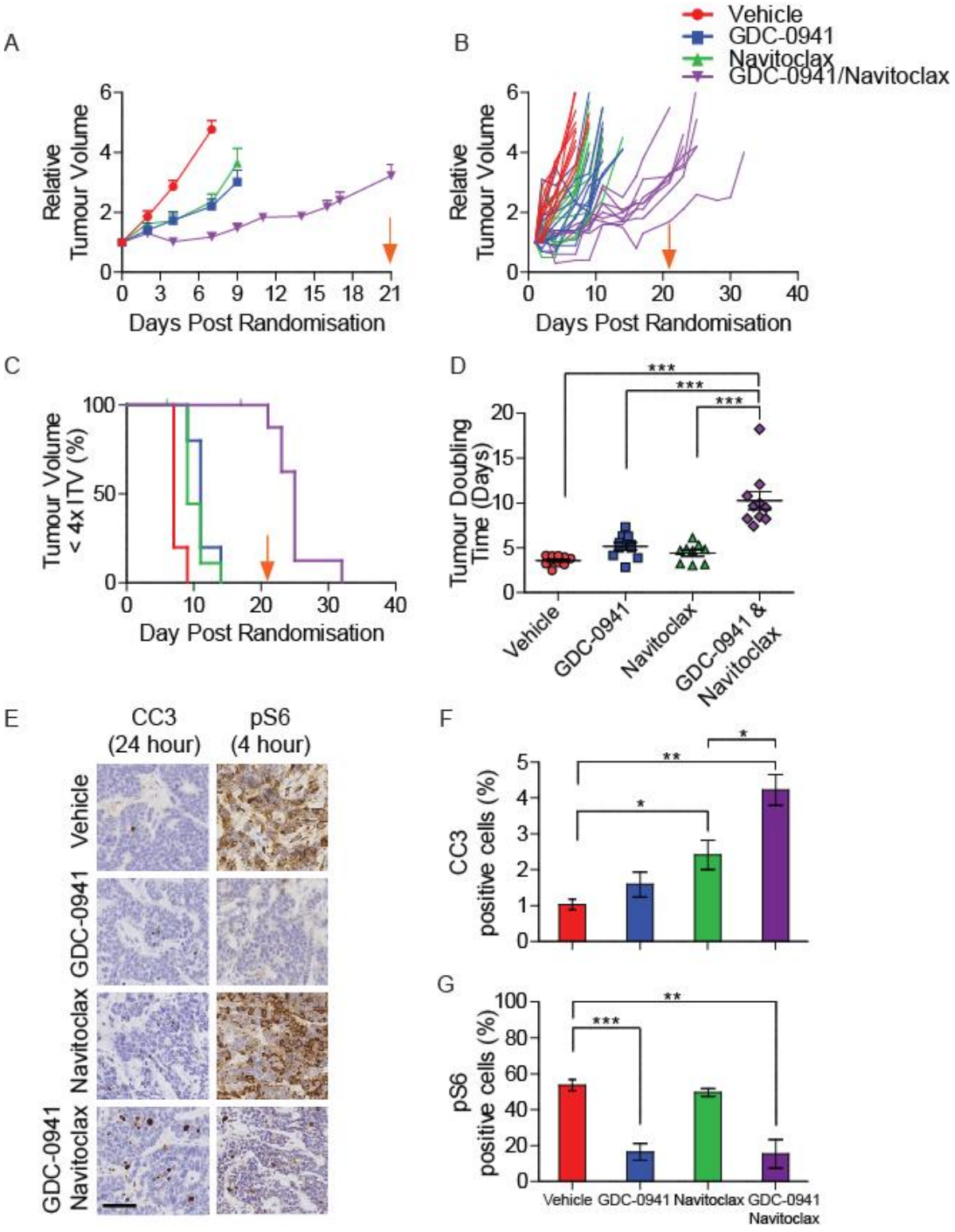
A
Relative Tumour Volume
Days Post Randomisation
B
Vehicle
GDC-0941
Navitoclax
GDC-0941/Navitoclax
Relative Tumour Volume
Days Post Randomisation
C
Tumour Volume < 4x ITV (%)
Day Post Randomisation
D
Tumour Doubling Time (Days)
Vehicle
GDC-0941
Navitoclax
GDC-0941 & Navitoclax
E
CC3 (24 hour)
pS6 (4 hour)
Vehicle
GDC-0941
Navitoclax
GDC-0941 Navitoclax
F
CC3 positive cells (%)
G
pS6 positive cells (%)
Vehicle
GDC-0941
Navitoclax
GDC-0941 Navitoclax

Figure 5: GDC-0941 and Navitoclax in combination proves efficacious *in vivo* in H1048 xenograft. (A-D) 40 SCID-beige mice were implanted with $5x10^6$ H1048 cells and randomised into 4 groups of 10 mice when tumors size reached between 150-250 mm^3. Group 1 was vehicle only, group 2 was 75 mg/kg GDC-0941 only, group 3 was treated 100 mg/kg Navitoclax only and group 4 was treated with 75 mg/kg GDC-0941 and one hour later 100 mg/kg Navitoclax. All groups were treated every day for 21 days (orange arrow indicates last day of dosing), unless tumors reached the end point of 4 x initial tumor volume (4xITV) early. All mice were monitored until tumors reached the end point. (A) Mean relative tumor growth (10 animals per treatment group). Line stops on day the first animal in that treatment group reached the 4xITV endpoint. (B) Relative tumor volumes for individual animal within each treatment group (C) Kaplan-Meier survival curve where animal was sacrificed when reached 4xITV endpoint. GDC-0941/Navitoclax combination was significant compared to all other treatment groups, $P < 0.0001$ calculated by log-rank test. (D) Tumor doubling time for vehicle, GDC-0941, Navitoclax and GDC-0941/Navitoclax groups. GDC-0941/Navitoclax combination tumor doubling time is significant compared to all other treatment groups ***$P < 0.0001$ according to 1way ANOVA multiple comparisons. (E) 20 SCID-beige mice were implanted with $5x10^6$ H1048 cells and randomised into 8 groups of 5 mice when tumors size reached between 150-250 mm^3. Group 1/5 was vehicle only, group 2/6 was 75 mg/kg GDC-0941 only, group 3/7 was treated 100 mg/kg Navitoclax only and group 4/8 was treated with 75 mg/kg GDC-0941 and one hour later 100 mg/kg Navitoclax. Groups 1-4 were culled 4 hours after dosing and groups 5-8 were culled 24 hours after dosing. Tumors were stained for either cleaved Caspase 3 (CC3, 24 hours) or phosphoS235/236-S6 (pS6, 4 hours) and percentage positive (F) CC3 and (G) pS6 was determined. Scale bar, 50µm. *P < 0.05, **P < 0.01, and ***P < 0.001 according to two-tailed unpaired t test.

Figure 6:

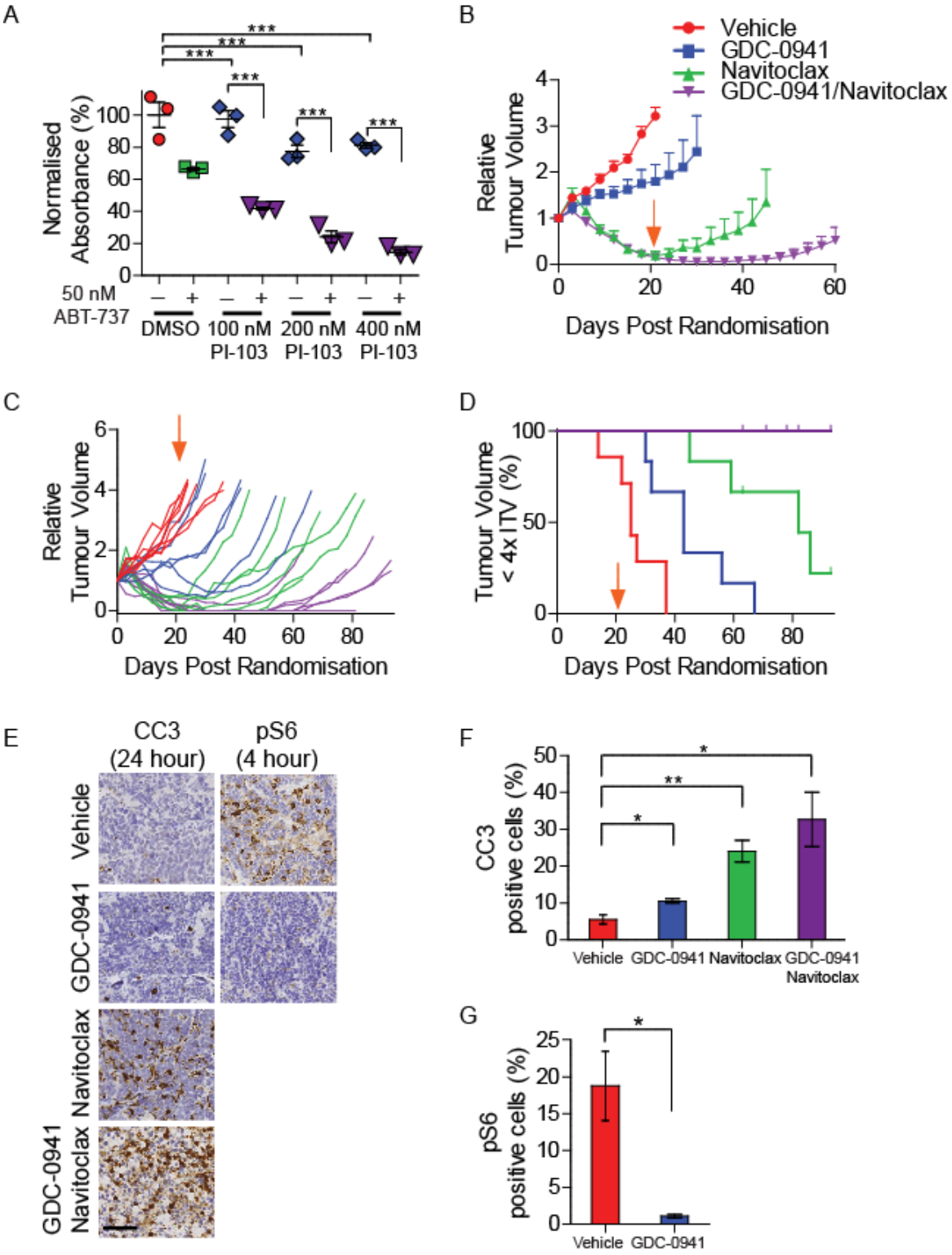
A
Normalised Absorbance (%)
50 nM ABT-737
DMSO
100 nM PI-103
200 nM PI-103
400 nM PI-103
B
Vehicle
GDC-0941
Navitoclax
GDC-0941/Navitoclax
Relative Tumour Volume
Days Post Randomisation
C
Relative Tumour Volume
Days Post Randomisation
D
Tumour Volume < 4x ITV (%)
Days Post Randomisation
E
CC3 (24 hour)
pS6 (4 hour)
Vehicle
GDC-0941
Navitoclax
GDC-0941 Navitoclax
F
CC3 positive cells (%)
Vehicle
GDC-0941
Navitoclax
GDC-0941 Navitoclax
G
pS6 positive cells (%)
Vehicle
GDC-0941

Figure 6: GDC-0941 and Navitoclax in combination proves efficacious *in vivo* in CDX2. (A) CDX2 tumors were disaggregated and 24 hours later drug treated with indicated concentration of drug for 3 days and cells were processed as in Figure 1B. Data represents the mean of three independent experiments ± SEM. (B-D) 24 SCID-beige mice were implanted with CDX2 tumor fragments and randomised into 4 groups of 6 mice when tumors reached between 150-250 mm^3. Four treatment groups were the same as Figure 5A. All groups were treated every day for 21 days (orange arrow indicates last day of dosing) and tumor end point was 4 x initial tumor volume (4xITV) or when the mouse had been on study for 6 months. (B) Mean relative tumor growth curve (6 animals per treatment group). Line stops on day the first animal in that treatment group reached the 4xITV endpoint. No animals reached 4xITV in the GDC-0941/Navitoclax combination group (C) Relative tumor volumes for individual animal within each treatment group (D) Kaplan-Meier survival curve where animal was sacrificed when reached 4xITV endpoint or had been on the study for 6 months. GDC-0941/Navitoclax combination was significant compared to all other treatment groups (Vehicle, $P < 0.0002$; GDC-0941, $P < 0.0003$; Navitoclax, $P < 0.033$ according to log-rank test). (E) Eight treatment groups were the same as Figure 5E. Tumors were stained for either cleaved Caspase 3 (CC3, 24 hours) or phosphoS235/236-S6 (pS6, 4 hours) and percentage positive (F) CC3 and (G) pS6 was determined. Scale bar, 50μm. *$P < 0.05$, **$P < 0.01$, and ***$P < 0.001$ according to two-tailed unpaired t test.

Supplementary Figure 1:

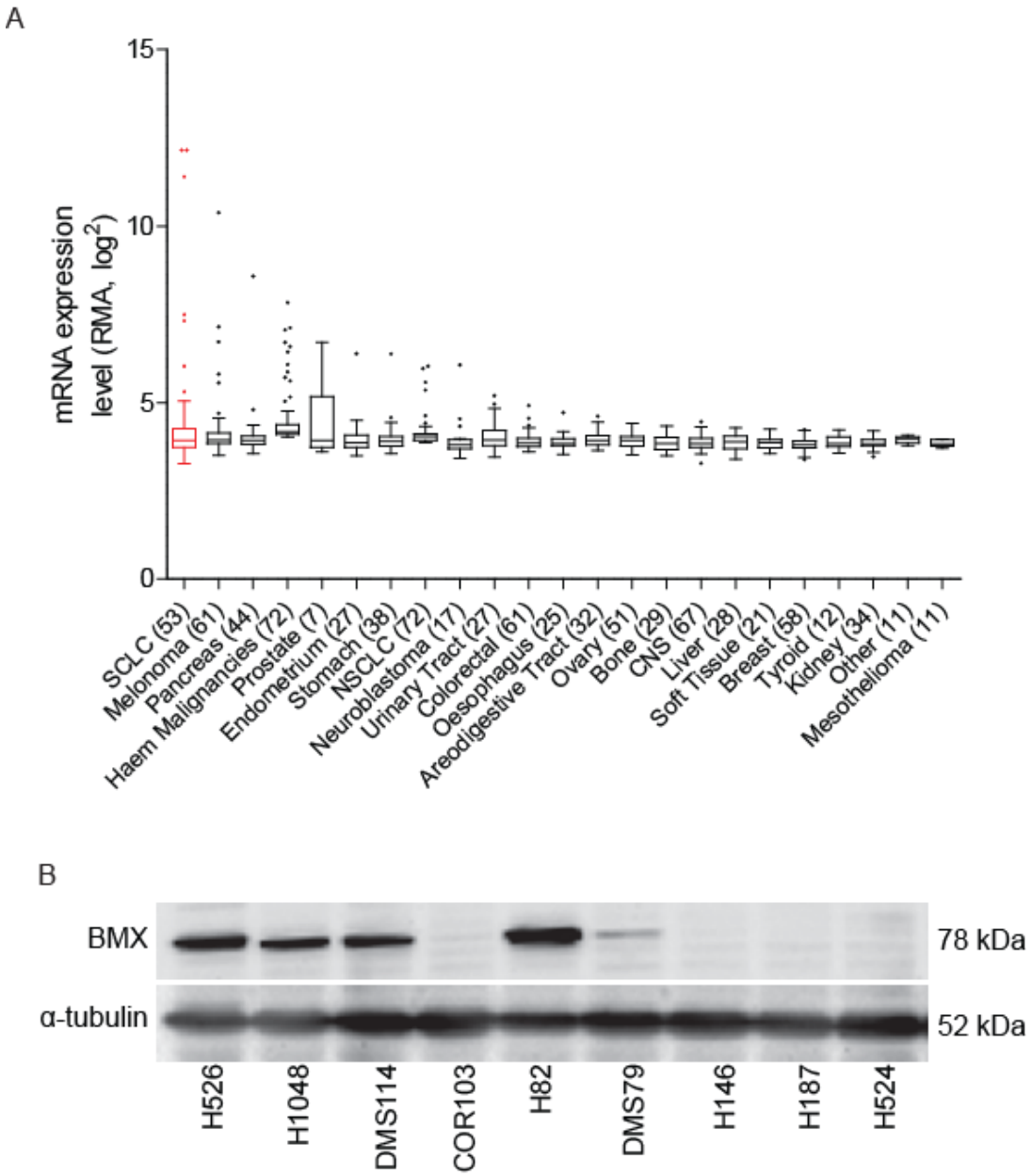

Supplementary Figure 1: BMX expression in SCLC. (A) Box-and-whisker plot of BMX mRNA expression across a panel of 1000 cell lines grouped by cancer type. mRNA data obtained from the Broad Institutes cancer cell line encyclopaedia (68). The Red Box identifies the SCLC cell lines in the plot. (B) BMX and α-tubulin (loading control) protein levels were determined by Western blotting of a panel of 9 SCLC cell lines. This western blot is a representative of three independent experiments.

Supplementary Figure 2:

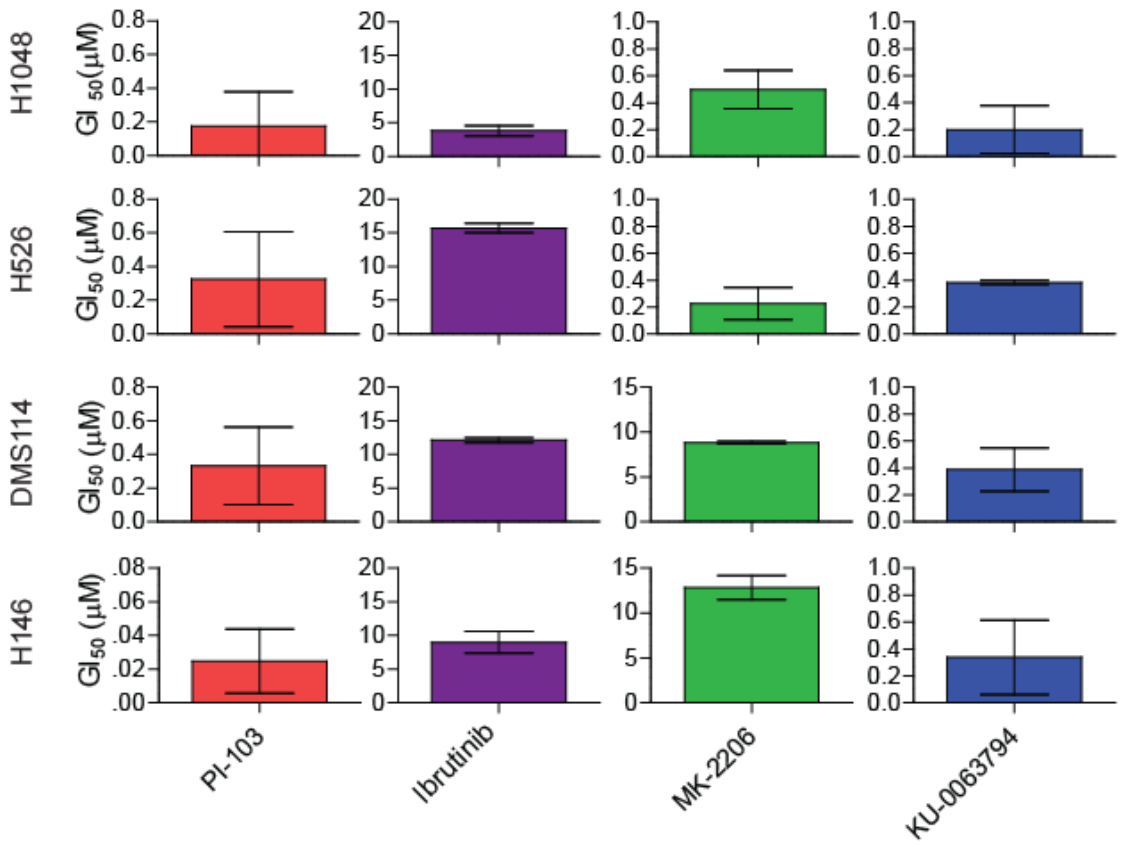

Supplementary Figure 2: PI3K pathway inhibitors GI_{50} in SCLC cell lines. H1048, H526, DMS114 and H146 cells were treated with increasing concentration of either, PI-103 (up to 5 μM), Ibrutinib (up to 32 μM), MK-2206 (up to 32 μM), or KU-0063794 (up to 32 μM), for 3 days. Cell were processed as in Figure 1B. Data represents the mean GI_{50} of three independent experiments carried out in triplicate ± SEM.

Supplementary Figure 3:

(A) H1048

Treatment	ABT-737 GI50 (μM ± 95% CI)	Significance*
DMSO	1.91 (1.32-2.77)	
0.1 μM PI-103	0.23 (0.08-0.70)	0.024
0.2 μM PI-103	0.004 (0.0001-0.2)	0.032
DMSO	2.19 (1.85-2.58)	
1 μM PCI-32765	0.54 (0.21-1.36)	0.043
4 μM PCI-32765	0.19 (0.04-0.84)	0.033
DMSO	2.63 (1.94-3.55)	
0.25 μM MK2206	0.82 (0.69-0.97)	0.003
0.5 μM MK2206	0.57 (0.45-0.72)	0.001
DMSO	2.30 (1.56-3.38)	
0.25 μM KU0063794	0.87 (0.52-1.45)	0.026
0.5 μM KU0063794	0.72 (0.42-1.25)	0.017

(B) H526

Treatment	ABT-737 GI50 (μM ± 95% CI)	Significance*
DMSO	7.95 (6.41-8.52)	
0.1 μM PI-103	0.55 (0.16-1.81)	0.003
0.2 μM PI-103	0.19 (0.03-1.42)	0.002
DMSO	7.44 (6.28-8.82)	
4 μM PCI-32765	3.37 (3.10-3.66)	0.0001
8 μM PCI-32765	0.92 (0.31-2.70)	0.001
DMSO	7.95 (6.41-8.52)	
0.25 μM MK2206	2.61 (1.73-3.94)	0.049
0.5 μM MK2206	1.21 (0.43-3.42)	0.013
DMSO	7.44 (6.28-8.82)	
0.5 μM KU0063794	3.80 (2.64-5.47)	0.003
1 μM KU0063794	1.78 (1.21-2.61)	<0.0001

Supplementary Figure 3: PI3K pathway inhibitors effect on ABT-737 GI_{50} in SCLC cell lines. (A) H1048 and (B) H526 cells were treated as described in Figure 1B and 4B. This table shows the effect of PI-103, Ibrutinib, MK-2206 and KU-0063794 on ABT-737 GI_{50}. *Two-tailed unpaired t test versus DMSO-treated GI_{50} for same cell line

Supplementary Figure 3 (continued):

(C) DMS114

Treatment	ABT-737 GI50 (μM ± 95% CI)	Significance*
DMSO	12.4 (11.0-14.3)	
0.1 μM PI-103	13.7 (11.4-16.5)	0.404
0.2 μM PI-103	14.1 (12.5-15.3)	0.302
DMSO	12.4 (10.7-14.5)	
4 μM PCI-32765	11.4 (9.26-13.9)	0.522
8 μM PCI-32765	10.2 (8.29-12.5)	0.210
DMSO	13.3 (12.9-13.7)	
0.5 μM MK2206	13.1 (12.6-13.6)	0.480
1 μM MK2206	12.8-12.0-13.8)	0.428
DMSO	13.3 (12.2-14.5)	
0.5 μM KU0063794	14.9 (12.0-18.5)	0.390
1 μM KU0063794	13.5 (12.5-14.6)	0.847

(D) H146

Treatment	ABT-737 GI50 (μM ± 95% CI)	Significance*
DMSO	0.017 (0.006-0.046)	
0.1 μM PI-103	0.007 (0.001-0.034)	0.389
0.2 μM PI-103	0.011 (0.003-0.036)	0.598
DMSO	0.017 (0.006-0.046)	
1 μM PCI-32765	0.017 (0.008-0.038)	0.969
4 μM PCI-32765	0.020 (0.016-0.024)	0.772
DMSO	0.017 (0.006-0.046)	
0.5 μM MK2206	0.016 (0.009-0.028)	0.939
1 μM MK2206	0.007 (0.005-0.011)	0.296
DMSO	0.029 (0.013-0.061)	
0.5 μM KU0063794	0.032 (0.027-0.037)	0.804
1 μM KU0063794	0.023 (0.005-0.103)	0.818

Supplementary Figure 3 (continued): PI3K pathway inhibitors effect on ABT-737 GI_{50} in SCLC cell lines. (C) DMS114 and (D) H146 cells were treated as described in Figure 1B and 4B. This table shows the effect of PI-103, Ibrutinib, MK-2206 and KU-0063794 on ABT-737 GI_{50}. *Two-tailed unpaired t test versus DMSO-treated GI_{50} for same cell line.

Supplementary Figure 4

A

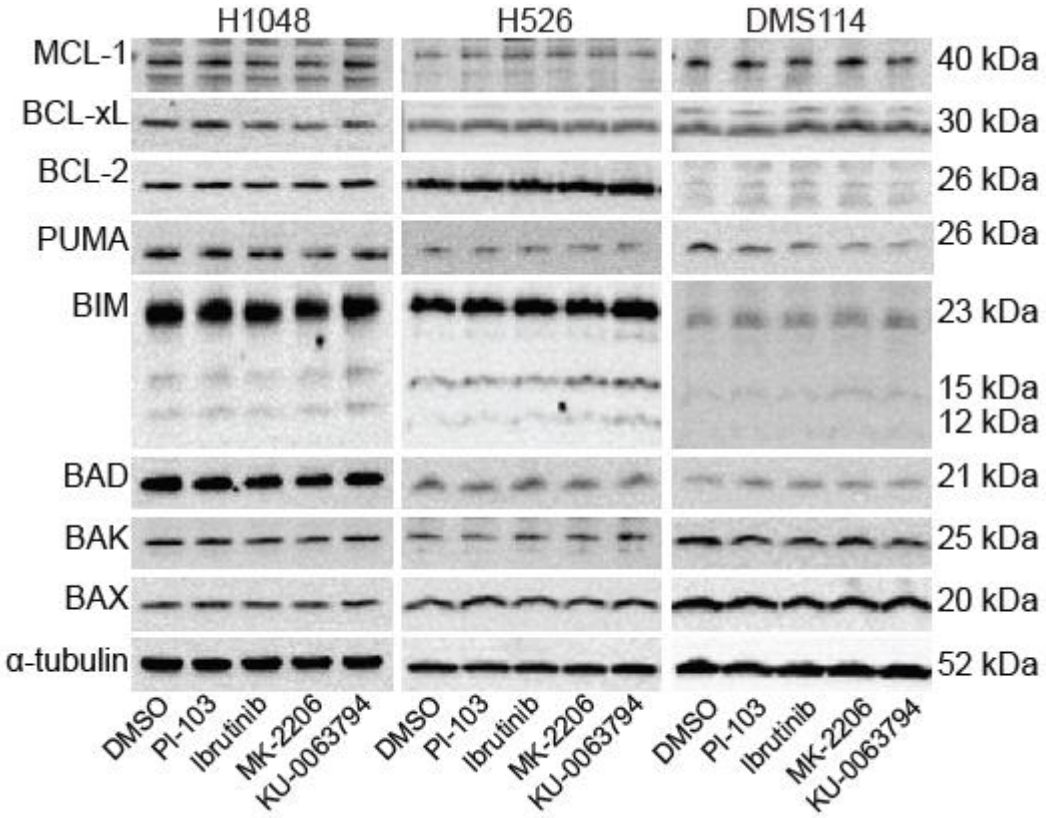

B

siRNA	Treatment	ABT-737 GI50 (μM ± 95% CI)	Significance *
MCL-1	0.1 μM PI-103	0.25 (0.17-0.34)	
Non-targeting	0.1 μM PI-103	0.96 (0.88-1.04)	0.0016
MCL-1	DMSO	2.27 (2.16-2.38)	0.0002
Non-targeting	DMSO	3.96 (3.24-4.85)	0.0002

Supplementary Figure 4: Bcl-2 family expression after treatment with PI3K pathway inhibitors. H1048, H526 and DMS114 cells were treated with the same concentration of PI-103, Ibrutinib, MK-2206 and KU-0063794 as described in Figure 1A and 4A or DMSO equivalent for 24 hours. Protein level of MCL-1, BCL-xL, BCL-2, PUMA, BIM, BAD, BAK, BAX and α-tubilin (loading control) was determined by Western blotting. (B) H1048 cells ABT-737 GI_{50} ± 95 % CI (confidence interval) from Figure 2F carried out in triplicate ± SEM. *Two-tailed unpaired t test versus 0.1 μM PI-103-treated MCL-1 RNAi on GI_{50} for same cell line

Supplementary Figure 5:

A

siRNA	Oligo	ABT-737 GI_{50} (μM ± 95% CI)	Significance*
NT	SMARTpool	2.16 (1.58-2.97)	
BMX	1	0.80 (0.65-0.97)	0.006
	2	1.69 (0.83-3.44)	0.567
	3	1.13 (0.86-1.48)	0.037
	4	2.26 (2.12-3.11)	0.417
	SMARTpool	0.90 (0.58-1.40)	0.033

B

siRNA	Treatment	ABT-737 GI_{50} (μM ± 95% CI)	Significance*
BMX SMARTpool	0.1 μM PI-103	0.38 (0.15-0.94)	
Non-targeting	0.1 μM PI-103	0.83 (0.79-0.87)	0.165
BMX SMARTpool	DMSO	0.90 (0.58-1.40)	0.166
Non-targeting	DMSO	2.16 (1.58-2.97)	0.024

C

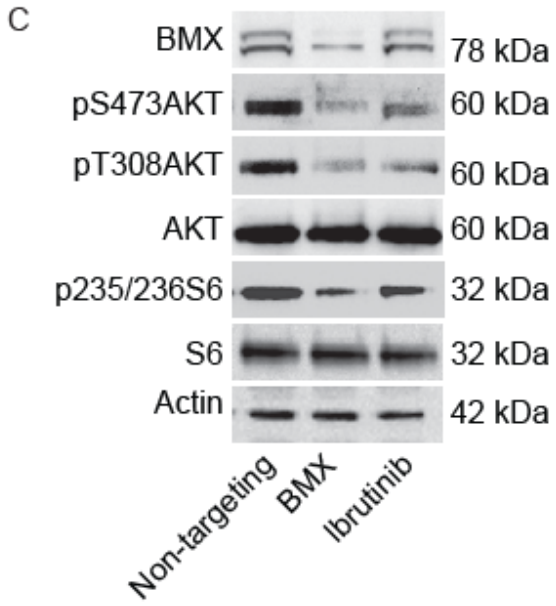

Supplementary Figure 5: BMX RNAi effect on ABT-737 GI_{50}. (A) H1048 cell ABT-737 GI_{50} ± 95 % CI (confidence interval) in H1048 from Figure 4A. Significance* calculated using two-tailed unpaired t test versus non-targeting (NT) RNAi GI_{50} for same cell line. (B) H1048 cell ABT-737 GI_{50} ± 95 % CI (confidence interval) in H1048 from Figure 4C.Table shows the effect of BMX RNAi and/or 0.1 μM PI-103 treatment on cells ABT-737 GI_{50} ± 95 % CI (confidence interval). Significance* is calculated using a two-tailed unpaired t test versus 0.1 μM PI-103 treated NT RNAi GI_{50} for same cell line. (C) H1048 cells were transfected with either siRNA targeting BMX or NT control and 48 hours post transfection cells were harvested. H1048 cells were treated with 4 μM Ibrutinib for 4 hours and then cells were harvested. Protein level of BMX, pS473AKT, pT308AKT, AKT, pS235/236S6, S6 and Actin (loading control) was determined by Western blotting.

Supplementary Figure 6:

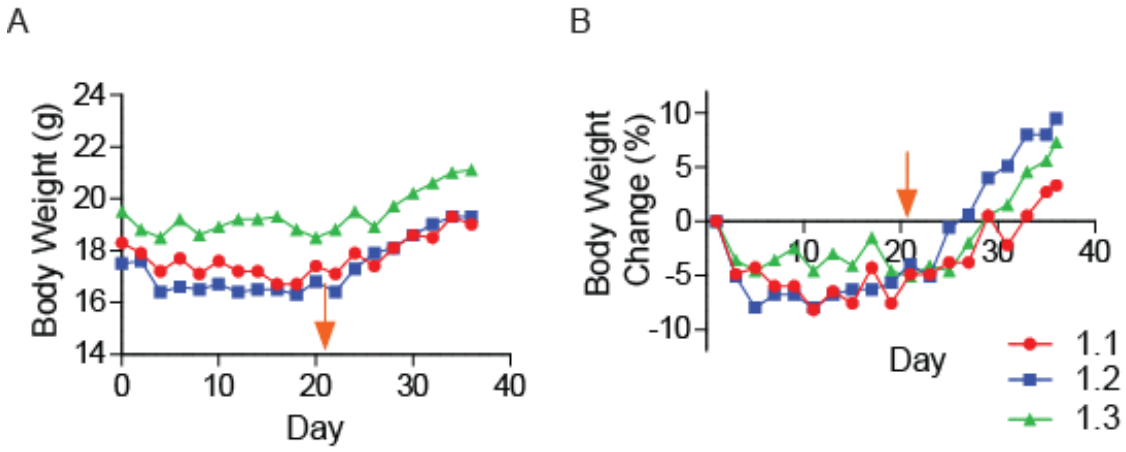

Supplementary Figure 6: GDC-0941 and Navitoclax tolerance *in vivo*. Three mice were treated with 75 mg/kg GDC-0941 and one hour later 100 mg/kg Navitoclax for 21 days (orange arrow indicates last day of dosing). (A) Individual mouse weights during dosing of combination and for two weeks after. (B) Percentage body weight change for each mouse calculated using body weight of animal on day zero.

Supplementary Figure 7:

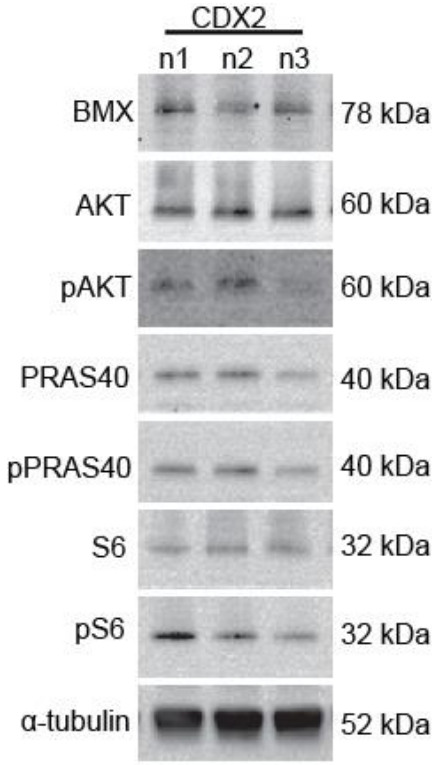

Supplementary Figure 7: PI3K Pathway expression in CDX2. PI3K pathway components were determined in three CDX2 tumors from different host mice. Protein level of BMX, pS473AKT, AKT, pT246PRAS40, PRAS40, S6 pS235/236S6, S6 and α-tubulin (loading control) was determined by Western blotting.

Discussion

Improved outcomes for SCLC patients remain elusive, despite numerous clinical trials of targeted therapeutics. New approaches that extend progression free survival after initially successful chemotherapy and alternatives to chemotherapy in chemorefractory SCLC are urgently required. Here we demonstrate that inhibition of PI3K pathway signalling can increase the sensitivity of SCLC cells (H1048 and H526) to a BCL-2/BCLx_L targeting BH3 mimetic by lowering the threshold for apoptosis. Our data in SCLC cell lines *in vitro* is recapitulated *in vivo* in the H1048 xenograft and in a newly developed patient CDX from a chemorefractory patient. These data provide additional weight to an increasing body of evidence that suggests SCLC clinical trials of combined PI3K/mTOR pathway inhibitors and BH3 mimetics are warranted. There appear to be however, multiple PI3K downstream effector signalling networks and modulation of different Bcl-2 family proteins that affect PI3K/mTOR inhibitor/BH3 mimetic synergy that are cell-context dependent.

In our study, the increased sensitivity to combined PI3K inhibition and BH3 mimetic was dependent on activities of BMX, AKT and mTOR downstream of PI3K. Our data suggest that BMX can regulate AKT/mTOR pathway activity in SCLC, the first time this has been observed. Both inhibition of BMX activity using the small molecule inhibitor Ibrutinib (Figure 1B and Supplementary Figure 5C) and reduction of BMX level by RNAi (Figure 3E-F Supplementary Figure 5C) reduced activation of pathways downstream of BMX including AKT and mTOR, consistent with on target effects. The mechanism by which BMX regulates AKT/mTOR signalling in SCLC is not yet clear, but precedents that link BMX to AKT/mTOR signalling have been reported in other cell types (61, 62). Active BMX mediates TNF-induced recruitment of the p85 subunit of PI3K resulting in AKT activation in human umbilical vein endothelial cells (HUVEC), whilst knock-out of BMX in mouse lung endothelial cells blocks TNF-induced activation of AKT compared to wild type (61). BMX has also been implicated in a positive feed-forward mechanism, where active BMX upregulates VEGF, which when secreted binds its receptors and further activates BMX resulting in AKT activation in endothelial and epithelial cells (62).

We observed a significant increase in apoptosis 4 hours after combined drug treatment *in vitro* suggesting that drug synergy most likely involves post-translational modification(s) (PTM) due to PI3K inhibition. Recently BMX was identified as the tyrosine kinase that phosphorylates BAK, keeping it in the inactive conformation (63). BMX inactivation by PI3K/BMX inhibitors could therefore lead to BAK dephosphorylation in SCLC. In this theoretical model, addition of ABT-737 by antagonism of BCL-2, BCL-x_L or BCL-w would release BIM to activate available dephosphorylated BAK, resulting in BAK homo-oligomerisation, MOMP, cytochrome c release and apoptosis. This putative mechanism now warrants further investigation.

Depending on cellular context, upregulation of PI3K signalling, for instance by *PIK3CA* mutation or *PTEN* deletion, may allow cells to sustain proliferation in the absence of growth factors and resist cell death by activation of survival signalling, two hallmarks of cancer (25, 26). Of the two cell lines which were sensitized to ABT-737 by PI3K or BMX inhibition, only H1048 has a known activating PI3K pathway mutation (although we cannot rule out that H526 cells have activated PI3K signalling via a mechanism yet to be determined). Whilst CDX2 does not harbour known PI3K pathway mutations, one copy of chromosome 10 has been lost (47), which could decrease PTEN expression and increase PI3K signalling (Supplementary Figure 7 shows CDX2 expression of BMX and PI3K/AKT pathway components). BMX is important in mutant *PIK3CA*-induced transformation via phosphorylation (on Y705) and activation of STAT3 causing homo- and hetero-dimerization to activate STAT3 transcriptional regulator function (57). Consistent with this function of BMX, we observed decreased phospho-STAT3 (Y705 and S727) in BMX depleted and Ibrutinib treated H1048 cells (Figure 3E-F). mTOR can phosphorylate and activate STAT3 (on S727) (64). One hypothesis therefore is that PI3K/BMX/mTOR inhibition sensitises to ABT-737 via repression of STAT3. STAT3 is a key regulator of BCL-x_L expression, a key target of ABT-737 (65). However, this mechanism is unlikely to explain our data, as we see no treatment effects on BCL-x_L at 24 hours (Supplementary Figure 4A).

PI3K pathway inhibition mediated sensitization to ABT-737 has been shown in other cancer types, including our study in CRC cell lines, which showed this

occurs via a PI3K/BMX pathway dependent but AKT/mTOR independent route (41). PI3K/AKT/mTOR pathway dependent sensitisation to ABT-737/ Navitoclax has also been reported in NSCLC (66) and lymphoma (67) cell lines. Two recent studies demonstrate that PI3K/mTOR pathway inhibition sensitises to BH3 mimetics in SCLC, consistent with our observations. There are both similarities and differences in the mechanism(s) underpinning the combination synergies observed between the two prior studies and the results we present here.

Gardner *et al.,* showed that the mTOCR1 inhibitor rapamycin increased the efficacy of ABT-737 in H146 cells and in several PDX models (24). In the Gardner *et al*., study, rapamycin prevented ABT-737 mediated down-regulation of BAX resulting in increased BAX dependent apoptosis. BAX protein levels were not decreased in H1048, H526 or DMS114 cells after treatment with PI3K pathway inhibitors (PI-103, MK-2206 or KU-0063794) in our study (Supplementary Figure 4A), consistent with the observations of Faber *et al*., in H1048 cells and in a PDX model using the TORC1/2 inhibitor AZD8055 (23). Moreover, we saw no synergy in H146 cells treated with ABT-737 plus any of the PI3K pathway inhibitors we examined. In our hands PI-103 and Ibrutinib resulted in mTOR pathway activation (increased pS6) in H146.

Faber *et al*., report a different mechanism to explain how AZD8055 sensitises to Navitoclax in SCLC cell lines, xenografts, a PDX and a genetically engineered model (51). They demonstrated in H1048 cells that AZD8055 sensitises to Navitoclax, consistent with our finding for all PI3K pathway inhibitors in the same cell line (Figure 1B and 4B). However, they showed that sensitization was via MCL-1 down-regulation, which was not observed in H1048 cells or any cell line used in our study (Figure 2D and Supplementary Figure 4A), nor in the cell line panel and PDX studied by Gardner *et al*. Faber *et al*., address this issue suggesting that as an mTORC1/2 ATP competitive inhibitor AZD8055 is uniquely capable of downregulating MCL-1, unlike rapamycin. This explanation does not reconcile our data using KU-0063794 which is also an mTORC1/2 ATP competitive inhibitor but did not decrease MCL-1 levels in H1048 cells (at the concentration used and time-point studied). We show that enforced downregulation of MCL-1 with RNAi does indeed sensitise to ABT-737 in H1048

cells, but that sensitivity was significantly further increased by PI-103, suggesting a MCL-1 independent element for this effect (Figure 2E-F and Supplementary Figure 4B).

Approximately 25-30% of LS and 70-80% of ES patients are classified as chemorefractory, where disease progression occurs within 3 months of SOC treatment (9, 10). We assessed the combination of the class I PI3K inhibitor GDC-0941 and Navitoclax in CDX2 to set a 'high hurdle' for this combination. CDX2 was derived from CTCs enriched at baseline from a patient subsequently shown to be chemorefractory. We previously showed that cisplatin (5mg/kg day 1) plus etoposide (8mg/kg, days 1,2,3) administered to mice bearing CDX2 tumors (at 200-250mm^3) regressed to ~50%, but regrew within the subsequent 10 days at a rate not dissimilar to vehicle treated controls, mirroring the response and rapid relapse of the patient. Here we show, dosing CDX2 bearing mice up to 21 days, that GDC-0941 alone slowed CDX2 growth and Navitoclax alone caused tumor regression during the dosing period, but with immediate regrowth after treatment ceased. However, combination resulted in a durable regression beyond 30 days after treatment. These data from a chemorefractory model of SCLC provide some optimism that the PI3K pathway/BH3 mimetic combination may have impact in the most resistant cases of SCLC.

Taken together, our study and that of Gardner *et al*., (24) and Farber *et al*., (23) suggest that there are different mechanisms downstream of PI3K signalling that suppress BH3 mimetic-induced apoptosis and we introduce a new component, BMX, within the complex signalling networks downstream of PI3K and upstream of the Bcl-2 family gatekeepers of an apoptotic cell fate. Overall, despite cell line and pathway inhibitor dependent differential mechanisms, the efficacy of GDC-0941 and Navitoclax in a CDX model derived from a chemo refractory patient highlights the potential clinical utility of this combination and strongly supports initiation of a clinical trial with a BH3 mimetic and a PI3K pathway inhibitor in SCLC patients.

Acknowledgements

CRUK Core funding to CRUK MI code C5759/A20971. The authors thank John Brognard, Kristopher Frese and Stuart Williamson for editorial advice.

References

1. Arriola E, Canadas I, Arumi M, Rojo F, Rovira A, Albanell J. Genetic changes in small cell lung carcinoma. Clin Transl Oncol. 2008;10:189-97.
2. Devesa SS, Bray F, Vizcaino AP, Parkin DM. International lung cancer trends by histologic type: male:female differences diminishing and adenocarcinoma rates rising. Int J Cancer. 2005;117:294-9.
3. Antony GK, Bertino E, Franklin M, Otterson GA, Dudek AZ. Small cell lung cancer in never smokers: report of two cases. J Thorac Oncol. 2010;5:747-8.
4. Thatcher N, Faivre-Finn C, Lorigan P. Management of small-cell lung cancer. Ann Oncol. 2005;16 Suppl 2:ii235-9.
5. http://www.cancer.org/cancer/lungcancer-smallcell/detailedguide/small-cell-lung-cancer-survival-rates
6. Hansen HH, Dombernowsky P, Hirsch FR. Staging procedures and prognostic features in small cell anaplastic bronchogenic carcinoma. Seminars in oncology. 1978;5:280-7.
7. van Meerbeeck JP, Fennell DA, De Ruysscher DK. Small-cell lung cancer. Lancet. 2011;378:1741-55.
8. Kato Y, Ferguson TB, Bennett DE, Burford TH. Oat cell carcinoma of the lung. A review of 138 cases. Cancer. 1969;23:517-24.
9. Lally BE, Urbanic JJ, Blackstock AW, Miller AA, Perry MC. Small cell lung cancer: have we made any progress over the last 25 years? Oncologist. 2007;12:1096-104.
10. Huisman C, Postmus PE, Giaccone G, Smit EF. Second-line chemotherapy and its evaluation in small cell lung cancer. Cancer Treat Rev. 1999;25:199-206.
11. Fujii M, Hotta K, Takigawa N, Hisamoto A, Ichihara E, Tabata M, et al. Influence of the timing of tumor regression after the initiation of chemoradiotherapy on prognosis in patients with limited-disease small-cell lung cancer achieving objective response. Lung Cancer. 2012;78:107-11.
12. De Ruysscher D, Pijls-Johannesma M, Bentzen SM, Minken A, Wanders R, Lutgens L, et al. Time between the first day of chemotherapy and the last day of chest radiation is the most important predictor of survival in limited-disease small-cell lung cancer. J Clin Oncol. 2006;24:1057-63.
13. Arcaro A. Targeted therapies for small cell lung cancer: Where do we stand? Critical reviews in oncology/hematology. 2015;95:154-64.
14. Wistuba, II, Gazdar AF, Minna JD. Molecular genetics of small cell lung carcinoma. Semin Oncol. 2001;28:3-13.
15. Mori N, Yokota J, Akiyama T, Sameshima Y, Okamoto A, Mizoguchi H, et al. Variable mutations of the RB gene in small-cell lung carcinoma. Oncogene. 1990;5:1713-7.
16. Ikegaki N, Katsumata M, Minna J, Tsujimoto Y. Expression of bcl-2 in small cell lung carcinoma cells. Cancer Res. 1994;54:6-8.
17. Jiang SX, Sato Y, Kuwao S, Kameya T. Expression of bcl-2 oncogene protein is prevalent in small cell lung carcinomas. J Pathol. 1995;177:135-8.
18. Umemura S, Mimaki S, Makinoshima H, Tada S, Ishii G, Ohmatsu H, et al. Therapeutic priority of the PI3K/AKT/mTOR pathway in small cell lung cancers as revealed by a comprehensive genomic analysis. J Thorac Oncol. 2014;9:1324-31.
19. Peifer M, Fernandez-Cuesta L, Sos ML, George J, Seidel D, Kasper LH, et al. Integrative genome analyses identify key somatic driver mutations of small-cell lung cancer. Nat Genet. 2012;44:1104-10.
20. Rudin CM, Durinck S, Stawiski EW, Poirier JT, Modrusan Z, Shames DS, et al. Comprehensive genomic analysis identifies SOX2 as a frequently amplified gene in small-cell lung cancer. Nat Genet. 2012;44:1111-6.
21. authors Alo, affiliations appears at the end of the p. Comprehensive genomic profiles of small cell lung cancer. Nature. 2015.

22. Watson IR, Takahashi K, Futreal PA, Chin L. Emerging patterns of somatic mutations in cancer. Nat Rev Genet. 2013;14:703-18.
23. Faber AC, Farago AF, Costa C, Dastur A, Gomez-Caraballo M, Robbins R, et al. Assessment of ABT-263 activity across a cancer cell line collection leads to a potent combination therapy for small-cell lung cancer. Proc Natl Acad Sci U S A. 2015;112:E1288-96.
24. Gardner EE, Connis N, Poirier JT, Cope L, Dobromilskaya I, Gallia GL, et al. Rapamycin rescues ABT-737 efficacy in small cell lung cancer. Cancer Res. 2014;74:2846-56.
25. Hanahan D, Weinberg RA. The hallmarks of cancer. Cell. 2000;100:57-70.
26. Hanahan D, Weinberg RA. Hallmarks of cancer: the next generation. Cell. 2011;144:646-74.
27. Letai AG. Diagnosing and exploiting cancer's addiction to blocks in apoptosis. Nat Rev Cancer. 2008;8:121-32.
28. Chen L, Willis SN, Wei A, Smith BJ, Fletcher JI, Hinds MG, et al. Differential targeting of prosurvival Bcl-2 proteins by their BH3-only ligands allows complementary apoptotic function. Mol Cell. 2005;17:393-403.
29. Chipuk JE, Moldoveanu T, Llambi F, Parsons MJ, Green DR. The BCL-2 family reunion. Mol Cell. 2010;37:299-310.
30. Chonghaile TN, Letai A. Mimicking the BH3 domain to kill cancer cells. Oncogene. 2008;27 Suppl 1:S149-57.
31. Kuwana T, Bouchier-Hayes L, Chipuk JE, Bonzon C, Sullivan BA, Green DR, et al. BH3 domains of BH3-only proteins differentially regulate Bax-mediated mitochondrial membrane permeabilization both directly and indirectly. Mol Cell. 2005;17:525-35.
32. Oltersdorf T, Elmore SW, Shoemaker AR, Armstrong RC, Augeri DJ, Belli BA, et al. An inhibitor of Bcl-2 family proteins induces regression of solid tumours. Nature. 2005;435:677-81.
33. Tahir SK, Yang X, Anderson MG, Morgan-Lappe SE, Sarthy AV, Chen J, et al. Influence of Bcl-2 family members on the cellular response of small-cell lung cancer cell lines to ABT-737. Cancer Res; 2007 Feb 1. p. 1176-83.
34. Del Gaizo Moore V, Schlis KD, Sallan SE, Armstrong SA, Letai A. BCL-2 dependence and ABT-737 sensitivity in acute lymphoblastic leukemia. Blood. 2008;111:2300-9.
35. Mason KD, Vandenberg CJ, Scott CL, Wei AH, Cory S, Huang DC, et al. In vivo efficacy of the Bcl-2 antagonist ABT-737 against aggressive Myc-driven lymphomas. Proc Natl Acad Sci U S A. 2008;105:17961-6.
36. Shoemaker AR, Mitten MJ, Adickes J, Ackler S, Refici M, Ferguson D, et al. Activity of the Bcl-2 family inhibitor ABT-263 in a panel of small cell lung cancer xenograft models. Clin Cancer Res. 2008;14:3268-77.
37. Rudin CM, Hann CL, Garon EB, Ribeiro de Oliveira M, Bonomi PD, Camidge DR, et al. Phase II study of single-agent navitoclax (ABT-263) and biomarker correlates in patients with relapsed small cell lung cancer. Clin Cancer Res. 2012;18:3163-9.
38. Engelman JA, Luo J, Cantley LC. The evolution of phosphatidylinositol 3-kinases as regulators of growth and metabolism. Nat Rev Genet. 2006;7:606-19.
39. Engelman JA. Targeting PI3K signalling in cancer: opportunities, challenges and limitations. Nat Rev Cancer. 2009;9:550-62.
40. Vanhaesebroeck B, Guillermet-Guibert J, Graupera M, Bilanges B. The emerging mechanisms of isoform-specific PI3K signalling. Nat Rev Mol Cell Biol. 2010;11:329-41.
41. Potter DS, Kelly P, Denneny O, Juvin V, Stephens LR, Dive C, et al. BMX acts downstream of PI3K to promote colorectal cancer cell survival and pathway inhibition sensitizes to the BH3 mimetic ABT-737. Neoplasia. 2014;16:147-57.
42. Chott A, Sun Z, Morganstern D, Pan J, Li T, Susani M, et al. Tyrosine kinases expressed in vivo by human prostate cancer bone marrow metastases and loss of the type 1 insulin-like growth factor receptor. Am J Pathol. 1999;155:1271-9.

43. Rajantie I, Ekman N, Iljin K, Arighi E, Gunji Y, Kaukonen J, et al. Bmx tyrosine kinase has a redundant function downstream of angiopoietin and vascular endothelial growth factor receptors in arterial endothelium. Mol Cell Biol. 2001;21:4647-55.
44. Chen S, Jiang X, Gewinner CA, Asara JM, Simon NI, Cai C, et al. Tyrosine Kinase BMX Phosphorylates Phosphotyrosine-Primed Motif Mediating the Activation of Multiple Receptor Tyrosine Kinases. Sci Signal. 2013;6:ra40.
45. Guo L, Chen P, Zhou Y, Sun Y. Non-receptor tyrosine kinase Etk is involved in the apoptosis of small cell lung cancer cells. Exp Mol Pathol. 2010;88:401-6.
46. Guo L, Zhou Y, Sun Y, Zhang F. Non-receptor tyrosine kinase Etk regulation of drug resistance in small-cell lung cancer. Eur J Cancer. 2010;46:636-41.
47. Hodgkinson CL, Morrow CJ, Li Y, Metcalf RL, Rothwell DG, Trapani F, et al. Tumorigenicity and genetic profiling of circulating tumor cells in small-cell lung cancer. Nat Med. 2014.
48. Martin-Fernandez C, Bales J, Hodgkinson C, Welman A, Welham MJ, Dive C, et al. Blocking phosphoinositide 3-kinase activity in colorectal cancer cells reduces proliferation but does not increase apoptosis alone or in combination with cytotoxic drugs. Mol Cancer Res. 2009;7:955-65.
49. Harrison LR, Micha D, Brandenburg M, Simpson KL, Morrow CJ, Denneny O, et al. Hypoxic human cancer cells are sensitized to BH-3 mimetic-induced apoptosis via downregulation of the Bcl-2 protein Mcl-1. J Clin Invest. 2011;121:1075-87.
50. Barraclough J, Hodgkinson C, Hogg A, Dive C, Welman A. Increases in c-Yes expression level and activity promote motility but not proliferation of human colorectal carcinoma cells. Neoplasia. 2007;9:745-54.
51. Forbes SA, Beare D, Gunasekaran P, Leung K, Bindal N, Boutselakis H, et al. COSMIC: exploring the world's knowledge of somatic mutations in human cancer. Nucleic acids research. 2015;43:D805-11.
52. Hayakawa M, Kaizawa H, Kawaguchi K, Ishikawa N, Koizumi T, Ohishi T, et al. Synthesis and biological evaluation of imidazo[1,2-a]pyridine derivatives as novel PI3 kinase p110alpha inhibitors. Bioorg Med Chem. 2007;15:403-12.
53. Honigberg LA, Smith AM, Sirisawad M, Verner E, Loury D, Chang B, et al. The Bruton tyrosine kinase inhibitor PCI-32765 blocks B-cell activation and is efficacious in models of autoimmune disease and B-cell malignancy. Proc Natl Acad Sci U S A. 2010;107:13075-80.
54. Brunet A, Bonni A, Zigmond MJ, Lin MZ, Juo P, Hu LS, et al. Akt promotes cell survival by phosphorylating and inhibiting a Forkhead transcription factor. Cell. 1999;96:857-68.
55. Datta SR, Dudek H, Tao X, Masters S, Fu H, Gotoh Y, et al. Akt phosphorylation of BAD couples survival signals to the cell-intrinsic death machinery. Cell. 1997;91:231-41.
56. Letai A. Growth factor withdrawal and apoptosis: the middle game. Mol Cell. 2006;21:728-30.
57. Hart JR, Liao L, Ueno L, Yates JR, 3rd, Vogt PK. Protein expression profiles of C3H 10T1/2 murine fibroblasts and of isogenic cells transformed by the H1047R mutant of phosphoinositide 3-kinase (PI3K). Cell Cycle. 2011;10:971-6.
58. clinicaltrials.gov
59. Daniel VC, Marchionni L, Hierman JS, Rhodes JT, Devereux WL, Rudin CM, et al. A primary xenograft model of small-cell lung cancer reveals irreversible changes in gene expression imposed by culture in vitro. Cancer Res. 2009;69:3364-73.
60. Hann CL, Daniel VC, Sugar EA, Dobromilskaya I, Murphy SC, Cope L, et al. Therapeutic efficacy of ABT-737, a selective inhibitor of BCL-2, in small cell lung cancer. Cancer Res. 2008;68:2321-8.
61. Zhang R, Xu Y, Ekman N, Wu Z, Wu J, Alitalo K, et al. Etk/Bmx transactivates vascular endothelial growth factor 2 and recruits phosphatidylinositol 3-kinase to mediate the tumor necrosis factor-induced angiogenic pathway. J Biol Chem. 2003;278:51267-76.
62. Chau CH, Chen KY, Deng HT, Kim KJ, Hosoya K, Terasaki T, et al. Coordinating Etk/Bmx activation and VEGF upregulation to promote cell survival and proliferation. Oncogene. 2002;21:8817-29.

63. Fox JL, Storey A. BMX Negatively Regulates BAK Function, Thereby Increasing Apoptotic Resistance to Chemotherapeutic Drugs. Cancer Res. 2015;75:1345-55.
64. Yokogami K, Wakisaka S, Avruch J, Reeves SA. Serine phosphorylation and maximal activation of STAT3 during CNTF signaling is mediated by the rapamycin target mTOR. Curr Biol. 2000;10:47-50.
65. Lesina M, Kurkowski MU, Ludes K, Rose-John S, Treiber M, Kloppel G, et al. Stat3/Socs3 activation by IL-6 transsignaling promotes progression of pancreatic intraepithelial neoplasia and development of pancreatic cancer. Cancer Cell. 2011;19:456-69.
66. Qian J, Zou Y, Rahman JS, Lu B, Massion PP. Synergy between phosphatidylinositol 3-kinase/Akt pathway and Bcl-xL in the control of apoptosis in adenocarcinoma cells of the lung. Mol Cancer Ther. 2009;8:101-9.
67. Ackler S, Xiao Y, Mitten MJ, Foster K, Oleksijew A, Refici M, et al. ABT-263 and rapamycin act cooperatively to kill lymphoma cells in vitro and in vivo. Mol Cancer Ther. 2008;7:3265-74.
68. Barretina J, Caponigro G, Stransky N, Venkatesan K, Margolin AA, Kim S, et al. The Cancer Cell Line Encyclopedia enables predictive modelling of anticancer drug sensitivity. Nature. 2012;483:603-7.

Chapter 5

Paper 3:

Mitochondrial Priming for Chemotherapy-induced Apoptosis in Chemosensitive, Chemorefractory and Relapsed, Progressive Small Cell Lung Cancer

Mitochondrial Priming for Chemotherapy-induced Apoptosis in Chemosensitive, Chemorefractory and Relapsed, Progressive Small Cell Lung Cancer

Danielle Potter[1], Jeremy Ryan[2], Christopher Morrow[1], Melanie Galvin[1], Cassandra Hodgkinson[1], Becky Bola[1], Lynsey Priest[1], Fiona Blackhall[3,4], Anthony Letai[2] and Caroline Dive[1]

[1]Clinical and Experimental Pharmacology Group, Cancer Research UK Manchester Institute, Manchester University, Manchester UK, [2]Dana-Farber Cancer Institute, Harvard Medical School, Boston, MA, USA, [3]Insitute of Cancer Sciences, University of Manchester, Manchester UK,[4]Christie NHS Foundation Trust, Manchester UK.

Small cell lung cancer (SCLC) is an aggressive tumor that accounts for 200,000 deaths each year. Although 70-90% of patients initially respond to standard of care (SOC) chemotherapy, virtually all relapse with progressive disease within 3-18 months. Currently, there is a lack of predictive biomarkers to identify chemorefractory patients and poor preclinical models to study disease progression. We have developed a unique model to study SCLC, called circulating tumor cell derived explant (CDX). CDX are generated from circulating tumor cells isolated from patient blood and we demonstrated that CDX chemotherapy response mirror donor patient response. Moreover, blood samples can be easily taken at any stage throughout disease progression, allowing the generation of 'matched pair' CDXs. Here for the first time, we provide 'matched pair' of CDX models from a patient at baseline (chemotherapy naïve) and again when the patient had relapsed with progressive disease, after initial response to chemotherapy. BH3 profiling assay was developed to measure cellular 'priming' to apoptosis, using BH3 peptides derived from the BH3 domain of the pro-apoptotic BH3-only proteins. BH3 peptides interrogate the propensity of cytochrome *c* release from mitochondria of cancer cells, revealing likely response to cytotoxic therapies. We use BH3 profiling on disaggregated CDX tumors cells *ex vivo,* to predict response to chemotherapy. Prospectively, we are able to define a CDXs as chemosensitive or chemorefractory by how 'primed' the model was.

Keywords

Apoptosis, BH3 profiling, Chemotherapy, Bcl-2 family, CDX models.

Introduction

Small Cell Lung Cancer (SCLC) is an exceptionally aggressive tumor of neuroendocrine origin and accounts for 15% of newly diagnosed lung cancer cases, causing 220,000 deaths each year [1]. It is commonly diagnosed in heavy or former smokers [2] and is clinically classified as two stages, limited stage (LS, confined to one hemithorax) and extensive stage (ES, more widespread). Approximately 70% of SCLC patients present with ES disease [3] and only 5% of patients at presentation are eligible for surgery due to late diagnosis accompanied with widespread distant metastases [4]. Without treatment, median overall survival (OS) is just 2-4 months [5] and LS and ES SCLC patients experience a median OS of 15-20 months and 8-13 months, respectively, following first and second line chemotherapy [6]. Platinum combined with etoposide remains the mainstay treatment since its introduction in the 1980s [7].

Although 10-30% of SCLC patients are defined as chemorefractory and progress within 90 days after first line chemotherapy [6, 8], the majority are initially extremely chemosensitive and experience either a partial or complete radiologic response. Unfortunately most of these patients relapse with progressive disease within 3-18 months and only 20% respond to chemotherapy rechallenge if they are able to tolerate further treatment [9]. Chemotherapy may select for resistant subpopulations and a SCLC ‘stem cell’ hypothesis has been posited to explain the rapid relapse [10-12]. Characterisation of tumor-initiating SCLC subclones at progression has proven elusive thus far and preclinical models to study relapsing human SCLC are scarce.

A number of targeted therapies have been clinically tested in SCLC, but none have been successful. Nevertheless, burgeoning knowledge of SCLC biology has suggested promising new therapeutic strategies including DNA damage repair inhibitors [13, 14], epigenetic targeted agents [15-18] and immunotherapies [19, 20]. As the therapeutic landscape for SCLC expands and rational therapy combinations are evaluated, biomarkers to anticipate backbone chemotherapy responses at baseline and at progression would inform clinical trial design and assist future treatment decision making.

After melanoma, SCLC has the highest frequency of genetic aberrations of any human cancer [21] leading to considerable inter- and intra-patient tumor heterogeneity. The genomic landscape of SCLC was recently comprehensively defined in three landmark papers [22-24]. Clinically applicable insight of the molecular mechanisms that underpin whether or not a SCLC patient will respond to a particular treatment is confounded by this profound genetic instability and resultant tumor heterogeneity [25]. A number of pathway- and drug-specific resistance mechanisms together with microenvironmental factors are likely to be involved [26]. Complex interactions between pro- and anti-apoptotic Bcl-2 family proteins regulate the 'coupling' of upstream drug-induced cellular damage to the downstream engagement of apoptosis via the intrinsic pathway [27-29]. Cisplatin and etoposide activate the intrinsic apoptotic pathway in SCLC [30], where the anti-apoptotic BCL-2 protein is overexpressed in ~40% cases [31, 32]. Bcl-2 family-targeted BH3 mimetic drugs that interrupt binding of pro- and anti-apoptotic family members showed great promise in established SCLC cell lines [33, 34] and xenograft models [35] but failed to improve OS in Phase II clinical trials [36, 37]. However, impressive preclinical studies combining BH3 mimetics with inhibitors of PI3K/mTOR signalling in SCLC patient derived explant models (PDX) demonstrate that this combination merits evaluation in the clinic [38, 39].

Until recently, one significant hurdle to improving the treatment of SCLC has been a lack of relevant preclinical models. Novel therapeutics will most likely be evaluated after standard chemotherapy has failed, and preclinical models of this relapsed stage of disease are needed to best assess their merit. Whilst genetically engineered mouse models are instrumental contributors to the emerging knowledge of the biology of SCLC [40-42], they are rarely used to test novel therapies because they do not represent the true nature of SCLC genetic instability and complexity [43, 44]. PDX models better capture tumor heterogeneity and are amenable to precision medicine-based strategies, but require fresh biopsies that are difficult to obtain, particularly at relapse. Circulating tumor cells (CTCs) are relatively prevalent in SCLC [45] and we took advantage of this non-invasive 'liquid biopsy' approach to develop SCLC CTC derived explant (CDX) mouse models that mimic patient's response to chemotherapy [46]. One main advantage of CDX is the ability to generate models from patients with progressive

disease where tumor biopsy is rarely performed. Here we describe the first 'matched pairs' of CDX derived from 2 patients at baseline and again at progression after an initial response to first line chemotherapy (CDX3 and 3P, CDX8 and 8P).

Resistance to conventional chemotherapeutics in SCLC cell lines has been linked to high expression of BCL-2 [30] although this is cell context dependent [47]. Simple measurement of Bcl-2 family protein expression is insufficient to predict their propensity for drug-induced apoptosis as a highly regulated series of protein-protein interactions between Bcl-2 family members situated on intracellular membranes dictates whether or not a drug-treated cell will undergo apoptosis. The Bcl-2 family is subdivided into functional subgroups; anti-apoptotic proteins (e.g., BCL-2, $BCLx_L$, MCL-1), pro-apoptotic effectors (e.g., BAX, BAK) and the activator or sensitizer pro-apoptotic BH3-only proteins (e.g., BIM, BID or BAD, NOXA respectively). The anti-apoptotic subfamily prevents mitochondrial outer membrane permeabilization (MOMP) via antagonistic interactions with pro-apoptotic effector and BH3-only proteins [48]. BH3-only activators directly activate effectors and are potent initiators of apoptosis. Both BH3-only activators and sensitizers can antagonise anti-apoptotic family members and some show great specificity in their binding [48-51]. Activated pro-apoptotic effectors form homo-oligomers that create pores in the outer mitochondrial membrane causing MOMP, cytochrome *c* release and activation of 'executioner' caspases [52].

Mechanisms by which cancer cells avoid intrinsic apoptosis are subdivided into three categories: downregulation of the pro-apoptotic BH3-only activator proteins, inactivation/downregulation of BAK/BAX and upregulation of anti-apoptotic Bcl-2 family members (Figure 1A; [50, 53]). Therapies that upregulate pro-apoptotic proteins or reduce levels of any anti-apoptotic Bcl-2 family members would shift the apoptotic regulatory equilibrium toward apoptosis. We have previously shown that, in haematological and ovarian cancers, it is possible to predict patient responses to chemotherapy using an approach termed BH3 profiling that reports how 'primed' a tumor cell is for apoptosis. 'Priming' is measured by either MOMP or mitochondrial release of cytochrome *c* after addition of synthetic BH3 peptides, derived from the BH3 domain of BH3-only proteins, to tumor cells [54, 55].

As a step towards prediction of SCLC patient responses to chemotherapy and mechanisms of apoptosis evasion, we tested retrospectively whether BH3 profiling of disaggregated CDX tumors predicted clinical response. We then set out to prospectively anticipate the chemotherapy responses from tumor cells disaggregated from unique matched CDX models derived at disease progression from patients 3 and 8.

Patient Selection and Blood Collection

The ethical approval, selection and consent of SCLC patients into our CDX programme is detailed in Hodgkinson *et al* [46]. Briefly, enrolled patients had histologically or cytologically confirmed chemotherapy-naïve SCLC and clinical and demographic data were collected. Blood was drawn at CDX study entry before administration of chemotherapy and immediately transferred to the laboratory for processing. Blood (10 ml) was drawn into CellSave preservative tubes (Janssen Diagnostics, NJ, USA) for CTC enumeration using the CellSearch platform [45]. A paired blood sample (10 ml) was drawn into EDTA vacutainers (Becton Dickinson, Oxford, UK). Patients' subsequent response to treatment was evaluated by computed tomography (CT) imaging performed before and following 4 cycles of chemotherapy, or earlier if clinically indicated. Patients who had a radiological response to chemotherapy that was sustained for greater than 3 months following completion of therapy were classified as chemosensitive. Patients with no evidence of response to therapy or progression within 3 months following completion of therapy were classified as chemorefractory [56].

A second paired blood sample (CellSave preservative tubes for CTC enumeration [45] and EDTA vacutainers for CDX study) was drawn from patient 3 and patient 8 after initial response to first line therapy and relapse with progressive disease (the first paired blood sample from patients 3 and 8 produced CDX3 and CDX8 (chemotherapy-naïve) respectively). Routine clinical practice was to perform a reassessment CT upon completion of chemotherapy. Patients were followed up every 3 months with chest x-rays and clinical review. Repeat CT was performed if there were clinical and radiological (chest x-ray) findings consistent with progressive disease.

Methods and Materials

Cell Culture

SU-DHL-4 and BBDL (BAX/BAK deficient lymphoma; originally misreported as SU-DHL-10 by the Letai laboratory. Recently identified as distinct from SU-DHL-10) lymphoma cells were cultured in RPMI 1640 media (Life Technologies, Inc,

Paisley, UK) supplemented with 10% FBS (BioWest, Nuaillé, France) and used as positive and negative controls respectively. Both cell lines were incubated in a humidified atmosphere at 37°C and 5% CO_2. Cell lines were authenticated using the Promega *GenePrint*® 10 System (Promega Corporation, WI, USA; authenticated at Dana-Farber Cancer Institute, Molecular Biology Core Facility).

Growth of CDX Tumors in Immunocompromised Mice

All procedures were carried out in accordance with Home Office Regulations (UK) and the UK Coordinating Committee on Cancer Research guidelines and by approved protocols (Home Office Project Licence no. 70/8252, which was reviewed by Cancer Research UK Manchester Institute Animal Welfare and Ethical Review Body, and *in vivo* work reported according to the ARRIVE (Animal Research Reporting of *In Vivo* Experiments) guidelines (2010)).

CDX models were generated as previously described [46]. For each CDX model, passage four CDX tumor fragments were implanted subcutaneously into mid-dorsal flank of 8 week old female NOD.Cg-*Prkdc*^{scid}*Il2rg*^{tm1Wjl}/SzJ (NSG) mice (Charles River, Edinburgh, UK). 30 mice were implanted for each cisplatin/etoposide study and 6 mice were implanted for each model for *ex vivo* BH3 profiling. Mice were housed in vented caging systems in a 12hour light/12 hour dark environment and maintained at uniform temperature and humidity. Mice were monitored twice weekly for signs of tumor growth. Once a palpable tumor was detected measurements were taken twice a week using calipers and tumor volume calculated using the formula 0.5 x (longest measurement) x (shortest measurement)^2. For BH3 profiling, when each individual tumor reached 400 mm^3 the animal was sacrificed and tumor was processed. For cisplatin/etoposide efficacy study, when mice reached 200-250 mm^3 they were randomised by sequential assignment to cisplatin/etoposide or vehicle group. Mice were treated by intraperitoneal injection with 5 mg mg/kg cisplatin (Sigma) dissolved in 0.9% saline solution on day 1, and 8 mg/kg etoposide (Sigma) dissolved in 12.5:1 0.9% saline solution:0.1% citric acid in 1-methyl-2-pyrrolidinone on days 1, 2 and 3, or corresponding vehicle only. Tumor measurements were continued three times a week until the tumor reached four times initial tumor volume (4xITV) or until animal

health deteriorated (censored in survival analysis). Survival analysis was performed in Graphpad Prism software with comparison of survival curves by log-rank test.

CDX Tumors Dissociation and Staining

CDX tumors were dissociated using the gentleMACS dissociator and human tumor dissociation kit according to manufacturer's instructions (Miltenyi Biotec Ltd; Surrey, UK). Red blood cells were lysed with RBC lysis buffer (G-Biosciences, USA) and remaining cells were filtered through a 70 μm cell strainer (Corning, Wiesbaden, Germany). A cell viability check via trypan blue exclusion preceded incubation of the suspension with dead-cell removal beads (Miltenyi Biotec Ltd) and with anti-mouse IgG2a + b microBeads (Miltenyi Biotec Ltd) with anti-mouse MHCI (H-2kd/H-2Dd) antibody (eBiosciences, San Diego, USA) for 15 minutes at room temperature. The cell suspension was diluted in binding buffer (Miltenyi Biotec Ltd) and added to LS-column (Miltenyi Biotec Ltd) to remove dead and mouse cells from the cell suspension whereupon cell viability was reassessed. The resultant cell suspension was stained with live/dead dye (1:1000; near-IR (NIR) fluorescent reactive dye, #L10119; Invitrogen) and the following cell surface antibodies: anti-human CD56 (1:10; PE mouse anti-human CD56, #555516; BD Biosciences) and anti-mouse CD45 (1:50; BV421 rat anti-mouse CD45, #563890; BD Biosciences) for 30 minutes on ice.

BH3 Profiling

BH3 peptides (listed in Supplementary Table 1, peptide sequence found in Ryan *et al.,* [57]) were diluted in DTEB buffer (135 mM trehalose, 10 mM HEPES, 20 µM EDTA, 20 µM EGTA, 5 mM succinate acid, 0.1% BSA and 50 mM KCl at pH 7.5 +/- 0.1 with KOH in sterile ddH_2O) and 0.002% digitonin which lightly permeabilizes the plasma membrane but keeps the organelles intact. Then 10^5 cells diluted in DTEB were added to each tube containing diluted BH3 peptide and incubated for 1 hour in the dark at room temperature. Cells were then fixed with formaldehyde (1% final concentration) at room temperature for 15 minutes in the dark and then diluted with 2:1 neutralising buffer (1.7 M Tris and1.25 M glycine at pH 9.1) at room temperature for 15 minutes in the dark. Fixed cells were then

stained with cytochrome *c* antibody (1:400; Alexa 488, Clone 6h2.b4 mouse anti-human cytochrome *c*, #560263; BD Biosciences) diluted in intracellular staining buffer (1% Saponin (Sigma) and 10% BSA (Sigma) in sterile ddH_2O) overnight at 4°C and analysed by flow cytometry (BD LSRFortessa™ analyzer) using Diva software (BD Biosciences) the next day. The flow cytometry gating strategy applied is detailed in Supplementary Figures 1-2. Initially cells were gated based on forward and side scatter characteristics. Dead cells were then excluded using a side scatter vs Live/Dead NIR gating strategy. Human SCLC cells were distinguished from viable mouse cells via a hCD56 vs mCD45 gate before cytochrome *c* fluorescent human CDX cells were enumerated using a PUMA2A peptide treated sample as negative control and a no cytochrome *c* antibody (FMO (fluorescence minus one)) control to set the staining threshold. With the gating strategy optimised, samples were batch analysed to determine the percentage of CDX cells in the cytochrome c positive gate and determine the percentage of cells with cytochrome c released.

Western Blotting

Tumor/cell lysis, protein quantification and Western blotting analysis were carried out as previously described [58]. The following primary antibodies were used: rabbit anti-BAX (No. 2774) and rabbit anti-BIM (34C5; Cell Signaling Technology, Danvers, MA, USA), mouse anti-BCL-2 (M0887; Dako, Glostrup, Denmark), rabbit anti–BCL-x_L (No. 610211; Becton Dickinson, Oxford, UK), mouse anti-human MCL-1 (No. 559027; Becton Dickenson), rabbit anti-BAD (AF819; R&D Systems, Minneapolis), mouse anti-BAK (AM03; Merck), mouse anti–α-tubulin (CP06; Merck), and mouse anti-Actin (Sigma).

Results

Derivation of Matched Pairs of SCLC CDX at Patient Presentation and at Relapse

BH3 profiling was performed on six CDX models (disaggregated CDX tumor cells). Characteristics and therapy responses of CDX donor patients 2, 3 and 4 together with the derivation of CDX2, CDX3, CDX4 at baseline (chemotherapy-naïve) and their *in vivo* responses to cisplatin/etoposide are as previously described [46].

Here, we report the derivation of the three new CDX models: CDX3P derived after initial response to chemotherapy and relapse with progressive disease from patient 3 (also produced CDX3), CDX8 and CDX8P, a second matched pair of CDX at baseline (chemotherapy-naïve) and after initial response to chemotherapy and relapse with progressive disease from patient 8. Patient 3 and 8, response to chemotherapy, OS and progression free survival (PFS) are shown in Table 1. CTC count (10 ml) using the CellSearch platform is shown in Table 2 for baseline sample (produced CDX3 and CDX8) and progression sample (produced CDX3P and CDX8P). CDX3 and CDX3P had comparable CTC numbers, 507 and 463 respectively. However, CDX8P had a 4.6 fold increase in CTCs compared to CDX8. CDX progression sample from patient 3 and 8 were taken on day 241 and 161 respectively, from day of consent (Table 2).

BH3 Profiling vs Patients Clinical Response to Chemotherapy

The BH3 profiling workflow for SCLC CDX tumors is shown in Figure 1B and to our knowledge this constitutes the first study to directly explore the mechanisms of engagement of the intrinsic pathway in SCLC tumors *ex vivo*. CDX tumors at 400 mm^3 were disaggregated for BH3 profiling as this tumor volume provides 2-4x10^6 cells that are sufficient to run a full BH3 profile (Supplementary Table 1) and tumors above this size display a greater degree of necrosis confounding the assay. The response of CDX3, 2 and 4 to cisplatin/etoposide *in vivo* mirrored the donor patient response to cisplatin/etoposide [46]. CDX3 was sensitive to cisplatin/etoposide with 95% median tumor regression upon treatment followed by tumor regrowth. CDX2 and CDX4 exhibited with minimal or no tumor regression, respectively, after treatment and were classified as chemorefractory [46].

BH3 profiling of baseline CDX3, 2 and 4 was used to assess whether chemosensitive and chemorefractory CDX models display the predicted difference in cytochrome *c* release in response to addition of activator and sensitizer BH3 peptides. First, to confirm that the BH3 profiling workflow performed reliably, we applied it to the lymphoma cell line SU-DHL-4, which is known to be dependent on BCL-2, and the BBDL cell line, which is BAX/BAK deficient. A BCL-2 dependent cell line should show high response to activator BH3 peptides BIM and BID and sensitizer BH3 peptides such as PUMA, BMF, and BAD, as they can interact and

antagonise BCL-2 releasing BIM and BID to activate BAX and BAK, to induce MOMP. A BAX/BAK-deficient cell line should be resistant to all activator and sensitizer BH3 peptides as MOMP cannot be activated via the intrinsic apoptotic pathway. As expected, SU-DHL-4 cells showed high percentage cytochrome *c* released after addition of activator (BIM and BID) and sensitizer (PUMA, BMF, and BAD) BH3 peptides but not after addition of NOXA or HRK BH3 peptides as these family members do not antagonise BCL-2 (Figure 2A). Furthermore BBDL cells did not release cytochrome *c* in response to any of the added BH3 peptides (Figure 2B).

We next tested whether BH3 profiling retrospectively discriminated between samples from patients who subsequently had either a response or no response to chemotherapy. CDX3, CDX2 and CDX4 tumors with known chemotherapy responses [46] were disaggregated and incubated with either activator or sensitizer BH3 peptides. The CDX3 BH3 profile showed activator BH3 peptides BIM and BID caused a concentration-dependent cytochrome *c* release suggesting functional BAK and/or BAX (Figure 2C). Sensitizer BH3 peptides PUMA, BMF, BAD and HRK but not NOXA caused cytochrome *c* release (Figure 2C). As NOXA is a specific MCL-1 antagonist, these data indicate that CDX3 is not reliant on MCL-1 [59]. The high response to activator and sensitizer BH3 peptides suggests that CDX3 is a ‘primed’ model that likely evades apoptosis via upregulation of anti-apoptotic BCL-2 family members with the exception of MCL-1 (Figure 1A). The CDX2 and CDX4 BH3 profiles showed a concentration-dependent response to activator BH3 peptide BIM suggesting functional BAX and/or BAK. CDX2 and CDX4 cells also responded to activator BID peptide. Sensitizer BH3 peptides caused a low percentage of cytochrome *c* release in CDX2 cells (< 16% in all sensitizer peptides; Figure 2D) and CDX4 cells (< 24% in all sensitizer peptides; Figure 2E) compared to CDX3 (< 70% in all sensitizer peptides; Figure 2C). These sensitizer response data suggests that CDX2 and 4 are not ‘primed’ and likely use downregulation of BH3-only activator proteins to evade apoptosis (Figure 1A). Consistent with *in vivo* chemosensitivity date, the CDX3 BH3 profile was statistically distinct from both CDX2 and CDX4 profiles ($P < 0.05$; Figure 2F)

The data described from the retrospective analyses of BH3 profiles of CDX2, CDX3 and CDX4 (Figure 2) and their *in vivo* responses to cisplatin/etoposide [46] suggests that BH3 profiling can predict chemotherapy response. To test this hypothesis, we took advantage of the newly derived CDX3P (derived at disease progression and matched to CDX3) and the baseline-progression pair of CDX derived from patient 8 (CDX8 and CDX8P) to determine whether prospective BH3 profiling using sensitizer peptides could predict *in vivo* response to cisplatin/etoposide.

BH3 Profiling vs SCLC CDX Response to Chemotherapy

The derivation of CDX matched pairs from SCLC patients before chemotherapy and again after initial treatment response had relapsed with progressive disease overcomes a major obstacle and represents a new avenue for research into the mechanisms of acquired chemotherapy resistance. Based on the validation data above, we hypothesised that BH3 profiling would predict SCLC responses to chemotherapy and that CDX3P and CDX8P would reveal altered BH3 profiles compared to their baseline counterparts. The CDX3P BH3 profile was broadly similar to that of CDX3 although CDX3P was more 'primed' as evidenced by a 1.6 fold increase in cytochrome *c* release in response to all of the added BH3 peptides (Figure 3A and 3B). BIM and BID caused a concentration dependent cytochrome c release in CDX3P (Figure 3B) and the BH3 sensitizer peptides PUMA, BMF, BAD and HRK caused 54-81% (75 μM) increases in cytochrome *c* release. In contrast, NOXA peptide had no effect, implying no dependency on MCL-1 for evading apoptosis. These data would suggest evasion of apoptosis in CDX3P remains via upregulation of another anti-apoptotic Bcl-2 family member (Figure 1A). Closer examination of the profile shows that the response to the HRK sensitizer peptide in CDX3P is significantly different to CDX3 ($P = 0.015$) suggesting CDX3P has increased its dependency on BCL-x_L for evading apoptosis which could explain the more 'primed' profile overall. Western blotting analysis of CDX3 and CDX3P showed significantly higher levels of MCL-1, BCL-2, BIM and BAX in the relapse model, suggesting that CDX3P is more 'primed' than CDX3 (Figure 5A and B). Although CDX3P did not display elevated BCL-x_L levels, the dependency towards BCL-x_L could be due to a change in BCL-x_L phosphorylation (S62) that has been

shown to antagonize the interaction between BCL-x_L and BAX. A decrease in phospho-BCL-x_L results in more BCL-x_L bound to BAX, thus increasing BCL-x_L anti-apoptotic function [60]. These data predict that in *in vivo* efficacy experiments, the CDX derived at patient relapse with disease progression would remain chemosensitive.

Cells from disaggregated CDX8 and CDX8P were also subjected to BH3 profiling before *in vivo* cisplatin/etoposide responses were known. In contrast to CDX3 and CDX3P, this matched pair of CDX displayed strikingly different BH3 profiles from one another. CDX8 exhibited a high response (> 53% cytochrome *c* released) to all 75 μM peptides, except the sensitizer NOXA peptide, consistent with a highly 'primed' MCL-1 independent model more likely to rely on BCL-x_L (based on sensitizer HRK peptide response; Figure 4A). Activator BH3 peptides had less of an effect on CDX8P compared to CDX8 and the sensitizer BH3 peptides response were minimal (< 17% in all sensitizer peptides; Figure 4B) in this model. Eight of the BH3 peptide conditions selected, were significantly different ($P < 0.05$) between CDX8 and CDX8P. Whilst, the BH3 profile of CDX8 suggests evasion of apoptosis via upregulation of anti-apoptotic Bcl-2 family members (Figure 1A), the BH3 profile of CDX8P implies an apoptotic block via downregulation of BH3-only activator Bcl-2 family proteins (Figure 4A and B).

These data imply that during disease progression following chemotherapy in patient 8, alterations in how the Bcl-2 family regulates apoptosis have occurred. As a result we predicted that CDX8 would respond better to cisplatin/etoposide compared to CDX8P. There was no difference in the expression of Bcl-2 family members between CDX8 and CDX8P by Western blotting analysis (Figure 5A and C) suggesting that the BH3 profile-implied change in apoptotic block mechanism is more likely due to changes in post-translational modifications to the Bcl-2 family members to alter their interactions.

Comparative analysis of cisplatin/etoposide treatment of baseline and relapse CDX derived from patient 3 and 8.

Neither patient 3 nor patient 8 were re-challenged with chemotherapy after their relapses with progressive disease due to inability to tolerate further chemotherapy.

Based on their respective disease free intervals, patient 3 but not patient 8 might have been expected to respond to chemotherapy rechallenge. Adopting the same cisplatin/etoposide preclinical drug study design as previously reported [46] we interrogated CDX3P and CDX8/8P chemosensitivity *in vivo*. When mice bearing CDX3P were treated with cisplatin/etoposide, there was a greater than 70% median tumor regression and the median time to four times initial tumor volume (4xITV) increased from 20 days for vehicle control to 63 in treated mice (log-rank P < 0.0001; Figure 4D and F). In agreement with our previous study of CDX3 [46], the median time to 4xITV in CDX3 went from 24 for vehicle control to 62 days in treated mice (log-rank P < 0.0001) compared to the vehicle treated group (Figure 3E). There was no significant difference between time to 4xITV for vehicle treated CDX3 vs. CDX3P or cisplatin/etoposide treated CDX3 vs. CDX3P indicating that both models are similar in chemotherapy response.

In contrast, when CDX8 was treated with cisplatin/etoposide the tumors regressed by ~50% before tumor regrowth and the median time to 4xITV was 40 days in vehicle treated tumors compared to 72 days in cisplatin/etoposide treated tumors (log-rank p=0.005; Figure 4C). As observed with the other patient baseline CDX models [46], the *in vivo* chemotherapy response in CDX8 mirrored that of the donor patient (Table 1, Figure 4C and E). CDX8P, however, did not regress when challenged with cisplatin/etoposide (Figure 4D) and the median time to 4xITV was 17 days and 24 days for vehicle and cisplatin/etoposide treated animals respectively which, whilst still significant (log-rank P = 0.007) was considerably less than in CDX8 (Figure 4E and F). CDX8P grew significantly faster than CDX8 (log-rank P < 0.0001) and therefore the reduced efficacy of cisplatin/etoposide is not a simple manifestation of reduced proliferation rate known to decrease responses to both cisplatin and etoposide.

BH3 Profiling as a Predictive Biomarker for Chemotherapy Responses in SCLC

The data in Figures 3 and 4 testify that BH3 profiling successfully predicted the responses of CDX models to cisplatin/etoposide treatment. A significant difference in response to sensitizer BH3 peptides between clinical partial response and

progressive disease was observed ($P = 9x10^{-6}$; Figure 5D). We also tested the strength of these predictions based on BH3 profiling to segregate clinical chemotherapy partial response and progressive disease with no response to chemotherapy in a binary fashion with ROC analysis. The area under the resultant ROC curve was 1 ($P = 0.049$; Figure 5E), supporting the ability of BH3 profiling to discriminate clinical response and progressive disease patients and we propose that BH3 profiling can be used as a binary predictor to of chemotherapy response in SCLC.

CDX	Patient Initial Response to Chemotherapy	Overall Survival (Days)	Progression Free Survival (Days)
3	Partial response, chemotherapy sensitive	295	241
8	Partial response, chemotherapy refractory	182	153

Table 1: Clinical response, overall survival and progression free survival of CDX donor patient 3 and 8. Overall survival was calculated from day of consent until death and progression free survival was calculated from day of consent to date of progression.

CDX	CTC # baseline	CTC # progression	Site of progression	Progressive CDX sample taken on day
3	507	463	Nodes	241
8	388	1796	Bone and Liver	161

Table 2: Circulating tumor cell (CTC) count using the CellSearch platform for baseline and progression blood sample for patient 3 and 8. Site of patient progression and day progression sample was taken (calculated from day of consent) are indicated.

Figure 1:

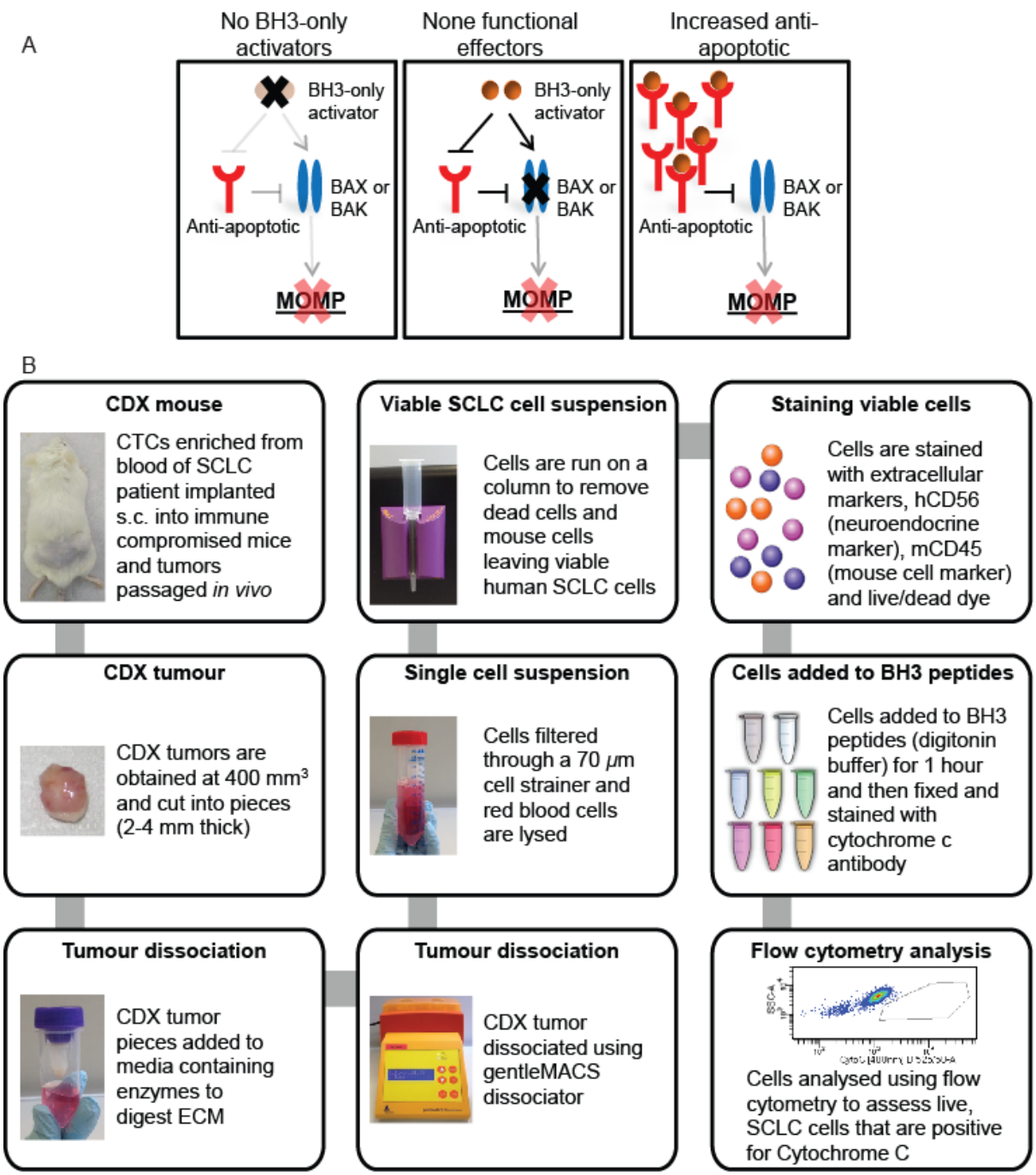
A
No BH3-only activators
None functional effectors
Increased anti-apoptotic
BH3-only activator
BAX or BAK
Anti-apoptotic
MOMP
B
CDX mouse
CTCs enriched from blood of SCLC patient implanted s.c. into immune compromised mice and tumors passaged *in vivo*
Viable SCLC cell suspension
Cells are run on a column to remove dead cells and mouse cells leaving viable human SCLC cells
Staining viable cells
Cells are stained with extracellular markers, hCD56 (neuroendocrine marker), mCD45 (mouse cell marker) and live/dead dye
CDX tumour
CDX tumors are obtained at 400 mm³ and cut into pieces (2-4 mm thick)
Single cell suspension
Cells filtered through a 70 μm cell strainer and red blood cells are lysed
Cells added to BH3 peptides
Cells added to BH3 peptides (digitonin buffer) for 1 hour and then fixed and stained with cytochrome c antibody
Tumour dissociation
CDX tumor pieces added to media containing enzymes to digest ECM
Tumour dissociation
CDX tumor dissociated using gentleMACS dissociator
Flow cytometry analysis
Cells analysed using flow cytometry to assess live, SCLC cells that are positive for Cytochrome C

Figure 1: Apoptotic blocks and BH3 profiling in CDX Schematic. (A) Cancer cells can evade intrinsic apoptosis by three main mechanisms involving the Bcl-2 family members; down regulation of BH3-only activators, Loss or inactivation of pro-apoptotic effectors BAX and BAK or upregulation of anti-apoptotic Bcl-2 family members. All prevent mitochondrial outer membrane permeabilization (MOMP). (B) CDX tumors were resected at 400 mm^3 and disaggregated using tumor dissociation enzyme kit and dissociator to break up the extracellular matrix (ECM). Cells were run on a column to remove dead cells and mouse cells. Viable cells were then labelled with humanCD56 a neuroendocrine marker that identifies human SCLC cells, mouseCD45 marker to identify mouse cells and live/dead dye to identify viable cells. Permeabilized cells were then added to specific pro-apoptotic BH3 peptides for one hour and then fixed and stained with cytochrome *c* antibody. The next day cells were analysed by flow cytometry for cytochrome *c* positive cells.

Figure 2:

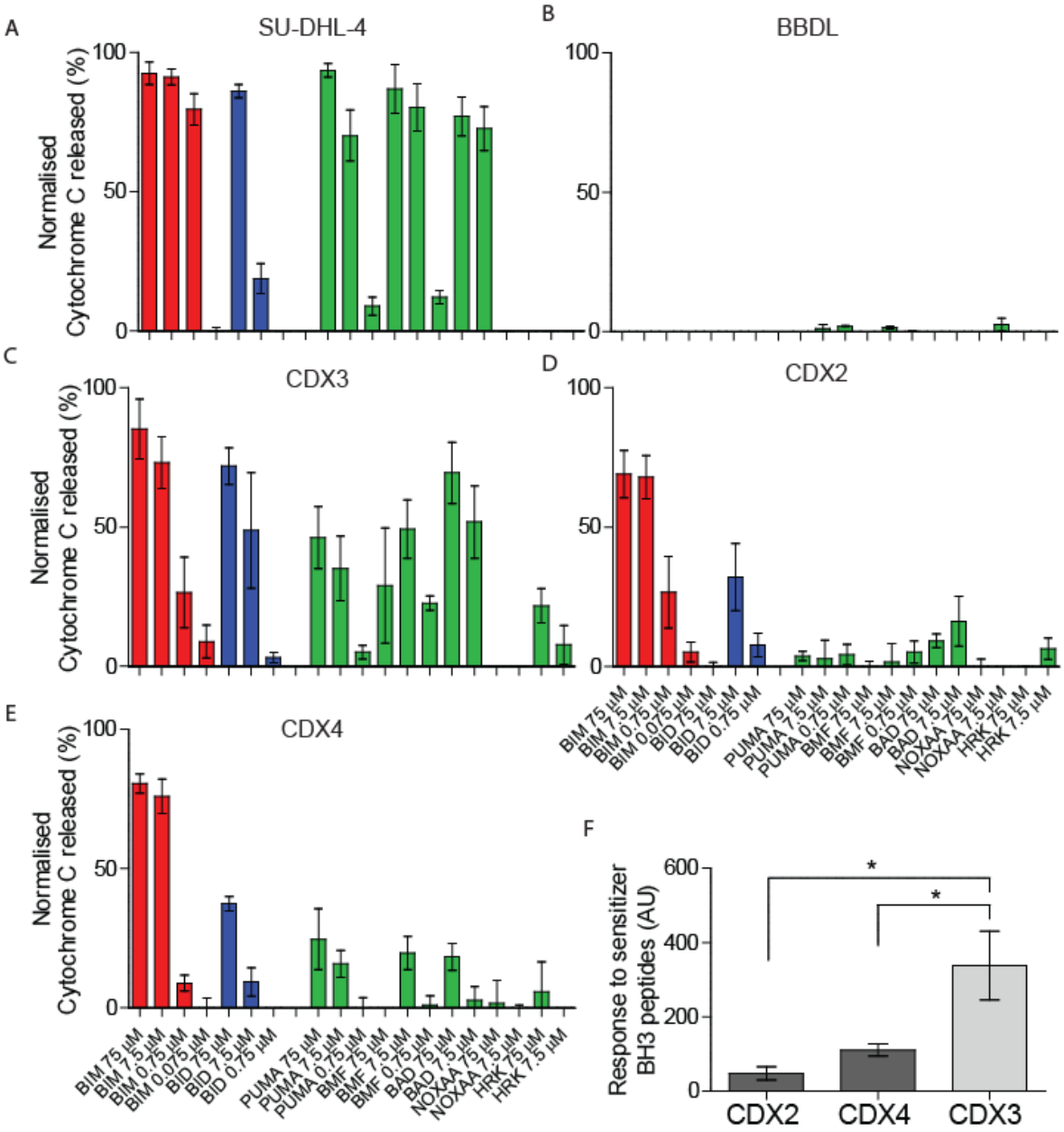
A
SU-DHL-4
B
BBDL
Normalised Cytochrome C released (%)
100
50
0
C
CDX3
D
CDX2
E
CDX4
BIM 75 µM
BIM 7.5 µM
BIM 0.75 µM
BIM 0.075 µM
BID 75 µM
BID 7.5 µM
BID 0.75 µM
PUMA 75 µM
PUMA 7.5 µM
PUMA 0.75 µM
BMF 75 µM
BMF 7.5 µM
BMF 0.75 µM
BAD 75 µM
BAD 7.5 µM
NOXAA 75 µM
NOXAA 7.5 µM
HRK 75 µM
HRK 7.5 µM
F
Response to sensitizer BH3 peptides (AU)
600
400
200
0
*
*
CDX2
CDX4
CDX3

Figure 2: BH3 profiling in Lymphoma Cell Lines and SCLC CDX. (A-B) SU-DHL-4 and BBDL cell lines were lightly permeabilized and treated with indicated concentration of BH3 peptide for 1 hour and then fixed and stained with cytochrome *c* antibody overnight. Cell were analysed by flow cytometry the next day to determine the percentage of cytochrome *c* positive cells within the parent population. (C-E) CDX3, CDX2 and CDX4 tumors were disaggregated and stained with human neuroendocrine marker (hCD56) to identify human SCLC cells, mouse cell marker (mCD45) to gate away from mouse cells and a live/dead dye to identify viable cells and BH3 profiled as in Figure 2A-B. The next day CDX tumor cells were analysed by flow cytometry to determine the percentage of cytochrome *c* positive cells within the parent population of viable, hCD56+ and mCD45- cells. Percentage cytochrome *c* positive cells were converted to percentage cytochrome *c* released (% positive minus 100). All BH3 peptides were normalised to FMO (fluorescence minus one; no cytochrome *c* antibody) and PUMA2A controls. PUMA2A is a mutated PUMA peptide that cannot induce mitochondrial outer membrane permeabilization. (F) CDX3, CDX2 and CDX4 were separated depending on donor patient clinical response to chemotherapy; progressive disease (CDX2 and CDX4, dark grey bars) or partial response (CDX3, light grey bar). The total response to sensitizer BH3 peptides (total cytochrome *c* released) was calculated for each biological replicate for each model. All graphs represent the means of ≥ 3 independent experiments ± SEM. *P < 0.05 according two tailed unpaired t-test.

Figure 3:

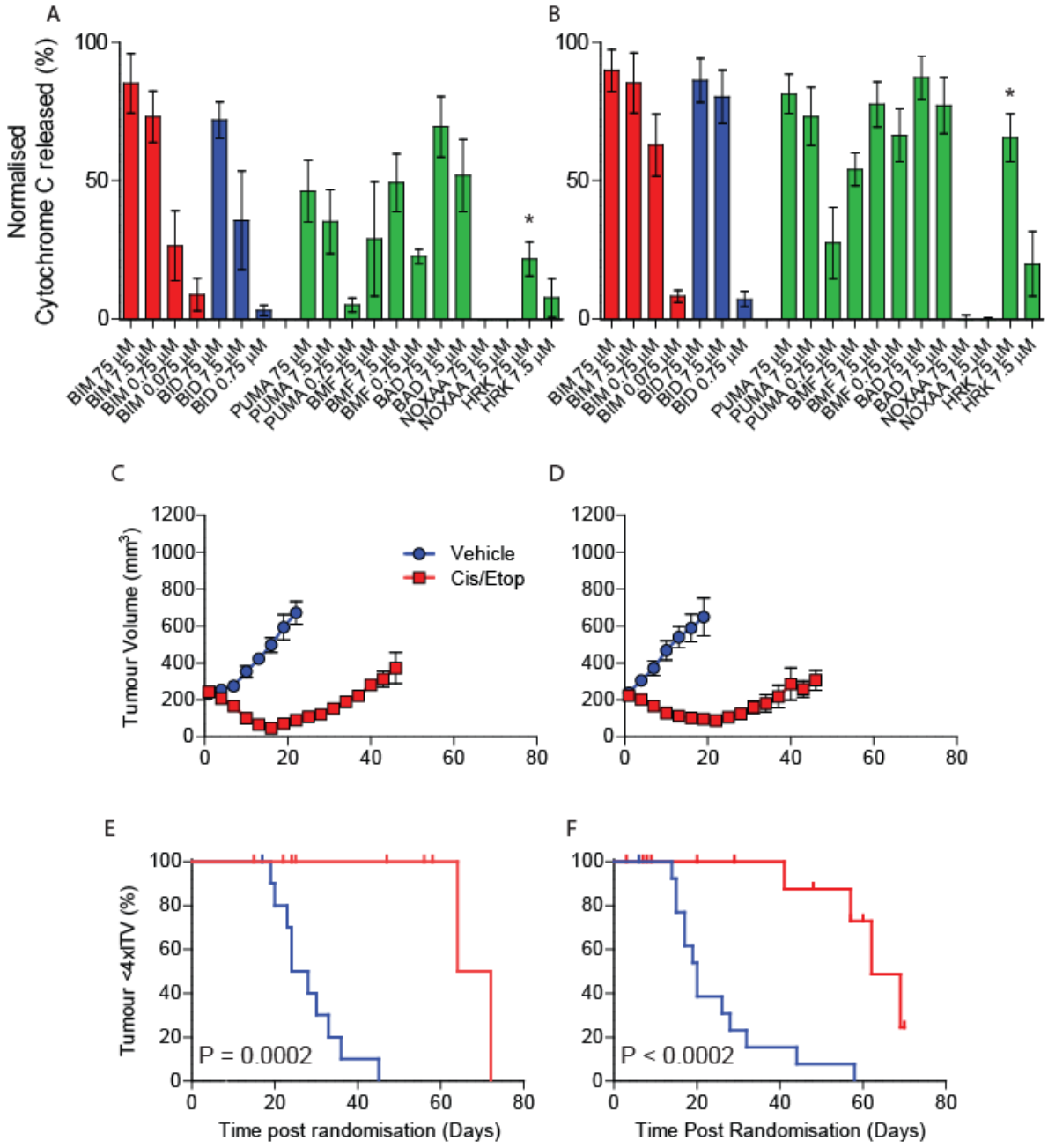
A
B
Normalised Cytochrome C released (%)
100
50
0
*
BIM 75 µM
BIM 7.5 µM
BIM 0.75 µM
BIM 0.075 µM
BID 75 µM
BID 7.5 µM
BID 0.75 µM
PUMA 75 µM
PUMA 7.5 µM
PUMA 0.75 µM
BMF 75 µM
BMF 7.5 µM
BMF 0.75 µM
BAD 75 µM
BAD 7.5 µM
NOXAA 75 µM
NOXAA 7.5 µM
HRK 75 µM
HRK 7.5 µM
C
D
Tumour Volume (mm3)
1200
1000
800
600
400
200
0
Vehicle
Cis/Etop
0
20
40
60
80
E
F
Tumour <4xITV (%)
P = 0.0002
P < 0.0002
Time post randomisation (Days)
Time Post Randomisation (Days)

Figure 3: BH3 profiling in paired presentation and relapse SCLC CDX3 vs *in vivo* cisplatin/etoposide efficacy. CDX3 (A) and CDX3P (B) tumors were BH3 profiled and processed as in Figure 2. All graphs represent the means of ≥ 3 independent experiments ± SEM. Each BH3 peptide at indicated concentration was compared between CDX3 and CDX3P, * $P < 0.05$ according two tailed unpaired t-test. Tumor volume of vehicle and cisplatin/etoposide treated groups in CDX3 (C) and CDX3P (D) over time after randomisation, represent mean ± SEM. Kaplan-Meier survival curve comparing vehicle and cisplatin/etoposide treated groups in CDX3 (E) and CDX3P (F) from randomisation until the tumor reaches four times initial tumor volume (4xITV). P calculated by log-rank test. Figure 3A is the same BH3 profile from Figure 2C and Figures 3C was taken from Hodgkinson *et al*., to allow side by side comparison of BH3 profiles and tumor volume of baseline (CDX3) and progression (CDX3P) models [46].

Figure 4:

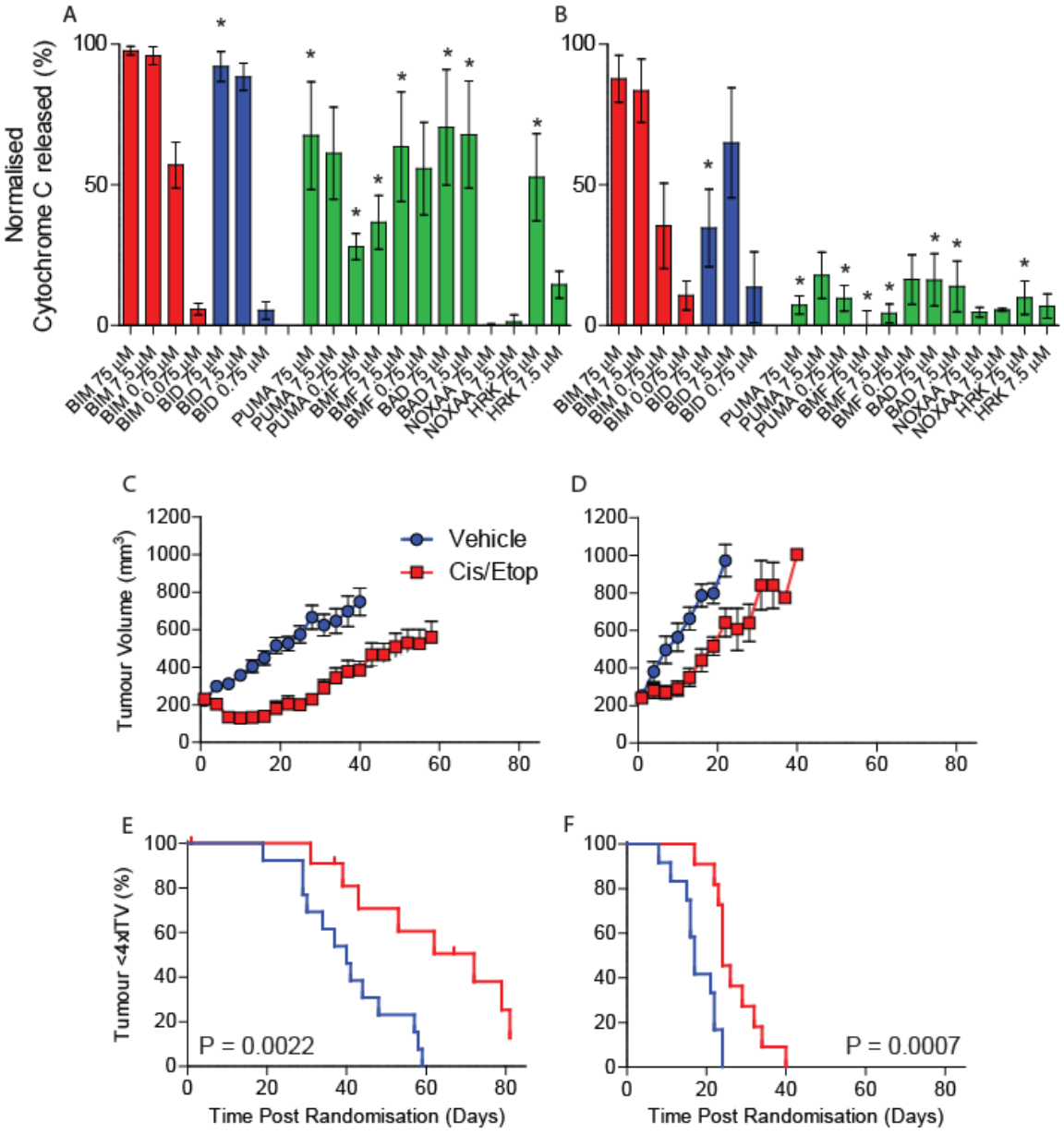
A
B
Normalised Cytochrome C released (%)
100
50
0
BIM 75 µM
BIM 7.5 µM
BIM 0.75 µM
BIM 0.075 µM
BID 75 µM
BID 7.5 µM
BID 0.75 µM
PUMA 75 µM
PUMA 7.5 µM
PUMA 0.75 µM
BMF 75 µM
BMF 7.5 µM
BMF 0.75 µM
BAD 75 µM
BAD 7.5 µM
NOXAA 75 µM
NOXAA 7.5 µM
HRK 75 µM
HRK 7.5 µM
C
D
Tumour Volume (mm3)
1200
1000
800
600
400
200
0
Vehicle
Cis/Etop
0
20
40
60
80
E
F
Tumour <4xTV (%)
100
80
60
40
20
P = 0.0022
P = 0.0007
Time Post Randomisation (Days)

Figure 4: BH3 profiling in paired presentation and relapse SCLC CDX8 vs *in vivo* cisplatin/etoposide efficacy. CDX8 (A) and CDX8P (B) tumors were BH3 profiled and processed as in figure 2. All graphs represent the means of ≥ 3 independent experiments ± SEM. Each BH3 peptide at indicated concentration was compared between CDX8 and CDX8P, *P < 0.05 according two tailed unpaired t-test. Tumor volume of vehicle and cisplatin/etoposide treated groups in CDX8 (C) and CDX8P (D) over time after randomisation, represent mean ± SEM. Kaplan-Meier survival curve comparing vehicle and cisplatin/etoposide treated groups in CDX8 (E) and CDX8P (F) from randomisation until the tumor reaches four times initial tumor volume (4xITV). P calculated by log-rank test.

Figure 5:

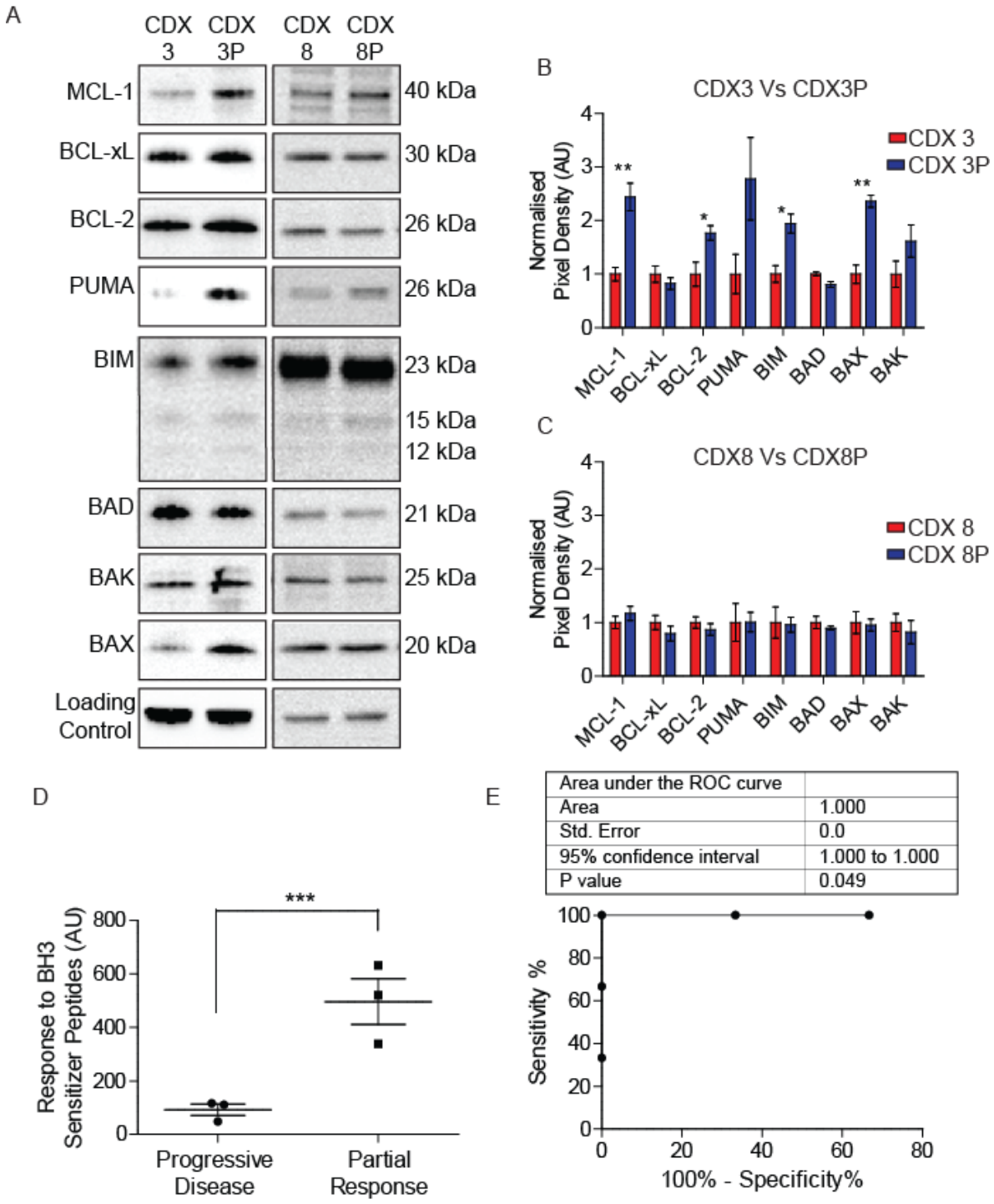
A
CDX 3
CDX 3P
CDX 8
CDX 8P
MCL-1
BCL-xL
BCL-2
PUMA
BIM
BAD
BAK
BAX
Loading Control
40 kDa
30 kDa
26 kDa
26 kDa
23 kDa
15 kDa
12 kDa
21 kDa
25 kDa
20 kDa
B
CDX3 Vs CDX3P
Normalised Pixel Density (AU)
CDX 3
CDX 3P
MCL-1
BCL-xL
BCL-2
PUMA
BIM
BAD
BAX
BAK
C
CDX8 Vs CDX8P
Normalised Pixel Density (AU)
CDX 8
CDX 8P
D
Response to BH3 Sensitizer Peptides (AU)
***
Progressive Disease
Partial Response
E
Area under the ROC curve
Area 1.000
Std. Error 0.0
95% confidence interval 1.000 to 1.000
P value 0.049
Sensitivity %
100% - Specificity%

Figure 5: BH3 profiling as a predictive biomarker for chemotherapy response. (A) Protein levels of MCL-1, BCL-x_L, BCL-2, PUMA, BIM, BAD, BAK, and BAX was determined by Western blotting analysis in CDX3, CDX3P, CDX8, and CDX8P tumors. Loading control for CDX3 and CDX3P was α-tubulin and for CDX8 and CDX8P was Actin. Western blots are representative of three independent experiments. (B-C) 2D densitometry was carried out on n=3 Western blot from figure 5A for CDX3, CDX3P, CDX8, and CDX8P. All CDX replicates were normalised to loading control and then relative expression compared to the average baseline model (CDX3 or CDX8) was determined for baseline and progression (CDX3P or CDX8P) replicates. The graphs compare CDX3 to CDX3P (B) and CDX8 to CDX8P (C). (D) CDX3, CDX2, CDX4, CDX8 were separated depending on donor patients clinical response to chemotherapy; progressive disease (CDX2 and CDX4) or partial response (CDX3 and CDX8) (Table 1 [46]). CDX3P and CDX8P were placed into either progressive disease (CDX8P) or partial response (CDX3P) depending on chemotherapy *in vivo* efficacy. Each CDX mean total response to sensitizer BH3 peptides was plotted in the corresponding groups; progressive disease or partial response. The mean for progressive disease (CDX2, CDX4 and CDX8P) or partial response (CDX3, CDX3P and CDX8) was determined ± SEM. (E) ROC curve analysis on data from Figure 5D. *P < 0.05, **P < 0.01 and ***P < 0.001 according two tailed unpaired t-test.

Supplementary Figure 1

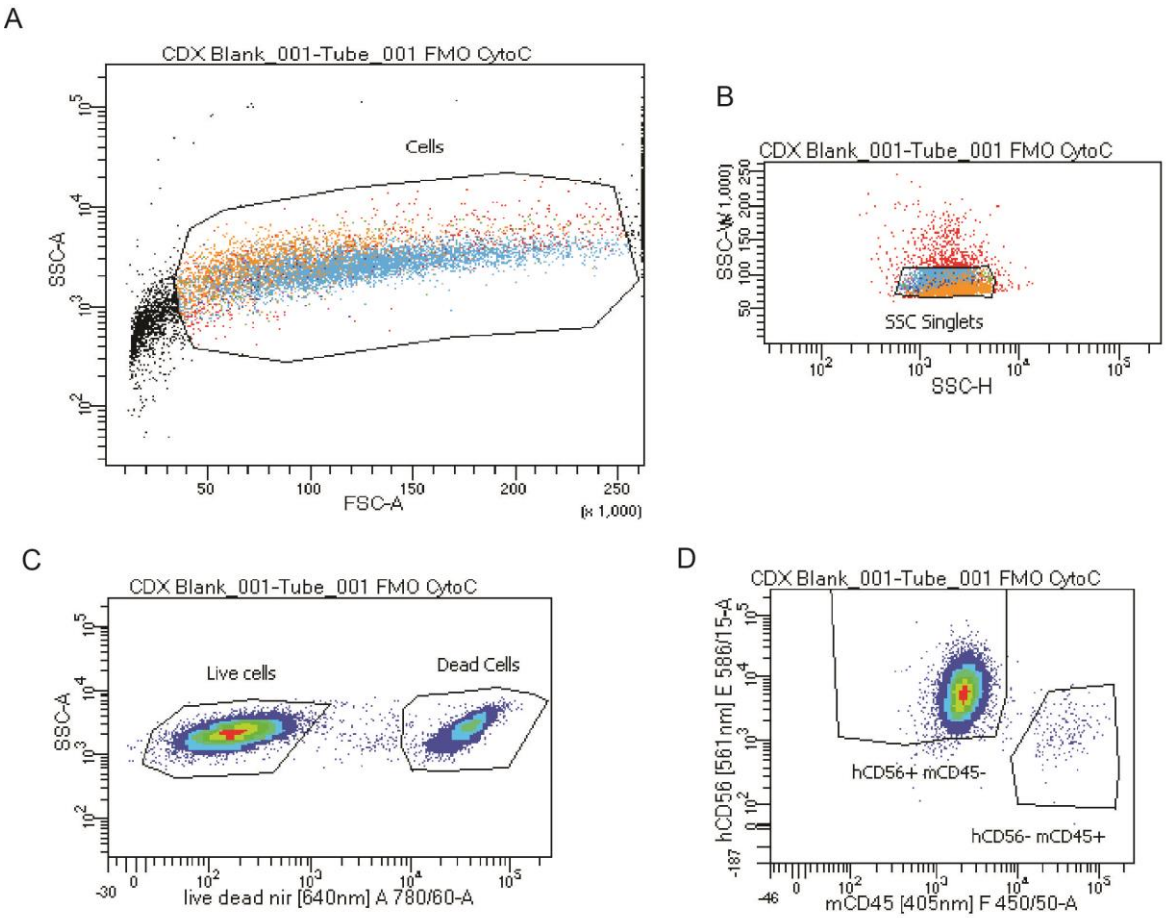

E

Experiment N...	CDX 3 n2 19-6...	Record Date:	Jan 30, 2015 5...
Specimen Na...	CDX Blank_001	$OP:	Cytometry
Tube Name:	Tube_001 FM...	GUID:	12552069-704...

Population	#Events	%Parent	CytoC [4... Median	CytoC [4... rSD
All Events	9,806	####	1,283	571
Cells	7,987	81.5	1,331	441
SSC Singlets	7,265	91.0	1,299	400
Live cells	5,625	77.4	1,341	361
hCD56+ mCD45-	5,372	95.5	1,354	349
hCD56+ Cytochrome C+	5	0.1	2,045	126
hCD56- mCD45+	162	2.9	895	386
Dead Cells	1,449	19.9	1,042	452

Supplementary Figure 1: BH3 profiling gating strategy for SCLC CDX. Flow cytometry was used to analyse cells (LSRFortessa™ analyzer) and then batch analysis was carried out on all BH3 peptides and controls. (A) Cells were gated based on side scatter area vs forward scatter area. (B) Cell singlets were gated from doublets by side scatter width vs side scatter height. (C) Live cells were gated away from dead cells by side scatter area vs live/dead NIR [640 nm]. (D) Human SCLC cells (hCD56+) were gated away from mouse cells (mCD45+) by hCD56 [561 nm] vs mCD45 [405 nm]. This is the final parent population of live, human SCLC cells. (E) Statistics table of events in each group, percentage parent population and median events.

Supplementary Figure 2:

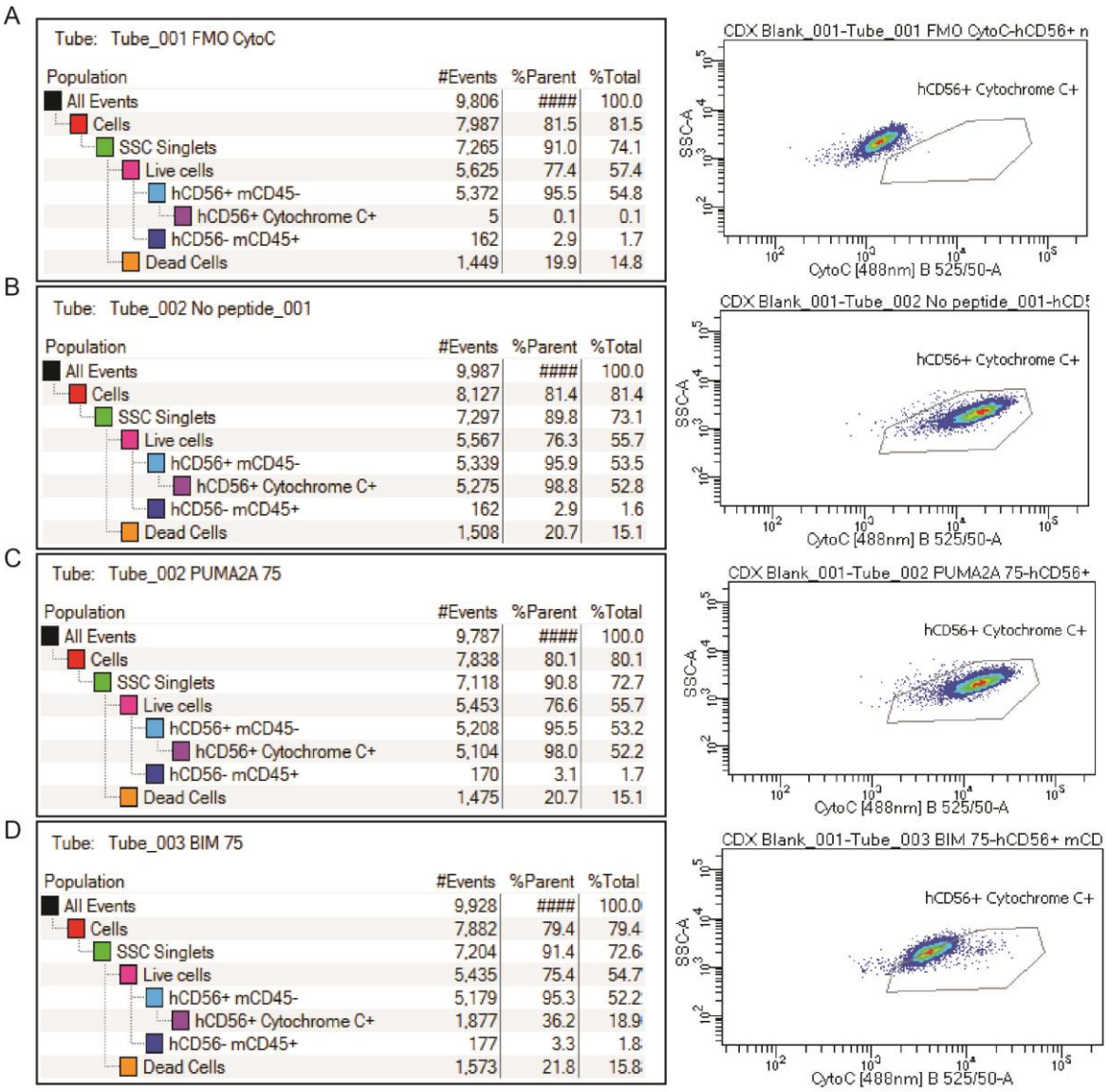

Supplementary Figure 2: BH3 profiling gating strategy for cytochrome *c* positive SCLC CDX cells. Cytochrome *c* positive cells are identified within the parent population of viable human SCLC cells from Supplementary Figure 1D. Within this parent population the percentage of cells that stain positive for cytochrome *c* can be determined using side scatter area vs human cytochrome *c* [488]. (A) The percentage parent population within each gate was set using the gating strategy shown in Supplementary Figure 1. This is shown here for the (A) FMO control (no cytochrome *c* antibody), No peptide control (B), 75 µM PUMA2A peptide negative control (C) and 75 µM BIM (D). The percentage cytochrome *c* positive cells within the final parent population can be converted to percentage cytochrome *c* released (cytochrome *c* positive percentage minus 100). This was then put into a bar chart for each peptide to make the BH3 profile shown in Figure 2, 3 and 4.

BH3 Peptide	Concentrations studied (µM)
BIM	75, 7.5, 0.75 and 0.075
BID	75, 7.5 and 0.75
PUMA	75, 7.5 and 0.75
BMF	75, 7.5 and 0.75
BAD	75 and 7.5
NOXA	75 and 7.5
HRK	75 and 7.5
PUMA2A	75

Supplementary Table 1: BH3 peptides used to run a full BH3 profile

Discussion

Improved treatment outcomes for SCLC patients are long overdue. Resurgence in SCLC research is ongoing and the NCI recently classed SCLC as a priority disease of unmet need [61]. Recent developments have included expansion of SCLC GEMMs [43], more comprehensive genomic profiling of SCLC biopsies [22-24] and broader use of SCLC PDX [38, 39] and our exploitation of CTCs to develop CDX models [46]. As novel therapeutics enter the clinic, predictive biomarkers are required for patient stratification. It is highly likely that these targeted drugs and therapies will be combined with the standard of care (SOC), platinum based chemotherapy and topoisomerase inhibitors, and we reason that prediction of chemotherapy response, both at patient presentation and upon relapse would assist trial design and treatment selection.

BH3 profiling uses synthetic BH3 peptides derived from the BH3 domain of the pro-apoptotic BH3-only activator and sensitizer proteins to interrogate the propensity of cytochrome *c* release from mitochondria. When carefully selected panel of BH3 peptides are used, BH3 profiling can reveal what apoptotic block tumor cells are likely using to avoid apoptosis and thus how 'primed' for apoptosis the model is to predict response to cytotoxic therapies. It is also possible to infer which anti-apoptotic proteins a cell has become most reliant through the response to specific sensitizers and the specificity in binding amongst Bcl-2 family of proteins [50, 52, 62].

The two step (retrospective then prospective) data sets presented here demonstrate that sensitivity to BH3 peptides predicts for response to chemotherapy in SCLC CDX models, which mirror initial donor patient response to chemotherapy and their likelihood of response to chemotherapy rechallenge at disease progression. A biomarker to stratify upfront the SCLC patients that are chemorefractory (10-30%) should be of benefit as it may give them the option to enter clinical trials at an earlier stage of their disease, resulting in a greater OS.

BH3 profiling is a tool to understand mechanisms of response/resistance to chemotherapy and how this may change with disease progression using the CDX matched pair baseline and progression models (Figure 3A-B and Figure 4A-B).

BH3 profiling on a larger dataset of CDX with a range of response to chemotherapy may be used to identify common patterns of sensitivity to specific BH3 peptides and mechanisms to evade apoptosis (Figure 1A). This information could aid therapeutic decisions of rational drug combinations with SOC, which could then be tested *in vivo* in CDX. For example CDX3, CDX3P and CDX8 had a large response to the BAD peptide (Figure 3A-B and 4A respectively) suggesting that the BH3 mimetic Navitoclax (modelled on BAD [33, 63, 64]), may be efficacious in these models in combination with SOC.

Patient 3 had a partial response to SOC, lasting more than three months and were determined chemosensitive (Table1). CDX3 response to SOC mirrored the donor patient response [46]. CDX3P BH3 profile and response to SOC mirrored CDX3 and the CTC count between this matched pair were comparable (Table 2). This suggests the relapse of patient 3, was likely due to outgrowth of sensitive clones that were not eradicated by first line SOC. Unfortunately this patient did not tolerate SOC, completing 2 out of 4 cycles so was not able to have chemotherapy rechallenge. The second line response rate to SOC of a group of SCLC patients with sensitive cell clones is much higher (50-60% [9]) compared to the average second line response rate (20% [9]).

CDX8 BH3 profile revealed a 'primed' model but CDX8P had a significantly different BH3 profile (Figure 4A-B), identifying a resistant model. This matched pair BH3 profiles (Figure 4A-B) suggests that initially the model would respond to SOC indicated by CDX8 tumor cells high response to sensitizer BH3 peptides. However, this would result in relapse, indicated by CDX8P tumor cells poor response to sensitizer BH3 peptides. Patient 8 had a partial response to SOC but relapsed in under three months (Table 1). CDX8 response to SOC mirrored donor patient response (Figure 4C and E). The rapid growth of CDX8P tumors and poor response to SOC *in vivo,* suggests the outgrowth was likely due to resistant cell clones. SOC in CDX8P did not cause any tumor regression whereas SOC caused 51% mean tumor regression in CDX8 (Figure 4C-D), suggesting CDX8P was a more aggressive and resistant tumor. The progressive disease blood sample from patient 8 had 4.6 fold higher CTC count (Table2), suggesting a more aggressive

disease. CTC count has prognostic value in SCLC. Patients with a higher CTC count had a poorer OS [45].

BH3 profiling of CDX cannot offer direct benefit to donor patients because of the lag time to generate these models and the aggressive course of the disease but it does show proof of principle. In ongoing efforts, the next objective is to migrate the CDX BH3 profiling approach for application to single freshly enriched CTCs in real time, allowing BH3 profiling to be used as a predictive biomarker for response to chemotherapy in patients.

Finally, we report here for the first time, using minimally invasive clinical sampling, patient derived models of progressive SCLC that can be directly compared to the patient's tumor biology at disease presentation and prior to treatment. This matched pair CDX approach provides a unique platform to study progression of the disease and acquired chemotherapy resistance. The first two such CDX pairs contrast relapse with little change in chemotherapy response (CDX3/3P) with the more anticipated scenario of acquired drug resistance (CDX8/8P). We anticipate that as the panels of available matched CDX models expand, studies to examine therapy resistance mechanisms and the SCLC stem cell hypothesis will progress.

Acknowledgements

CRUK Core funding to CRUK MI code C5759/A20971. The authors thank Kristopher Frese and Alice Lallo for editorial advice.

References

1. Arriola, E., et al., *Genetic changes in small cell lung carcinoma.* Clin Transl Oncol, 2008. **10**(4): p. 189-97.
2. Devesa, S.S., et al., *International lung cancer trends by histologic type: male:female differences diminishing and adenocarcinoma rates rising.* Int J Cancer, 2005. **117**(2): p. 294-9.
3. Thatcher, N., C. Faivre-Finn, and P. Lorigan, *Management of small-cell lung cancer.* Ann Oncol, 2005. **16 Suppl 2**: p. ii235-9.
4. Hansen, H.H., P. Dombernowsky, and F.R. Hirsch, *Staging procedures and prognostic features in small cell anaplastic bronchogenic carcinoma.* Semin Oncol, 1978. **5**(3): p. 280-7.
5. Kato, Y., et al., *Oat cell carcinoma of the lung. A review of 138 cases.* Cancer, 1969. **23**(3): p. 517-24.
6. Lally, B.E., et al., *Small cell lung cancer: have we made any progress over the last 25 years?* Oncologist, 2007. **12**(9): p. 1096-104.
7. Chan, B.A. and J.I. Coward, *Chemotherapy advances in small-cell lung cancer.* J Thorac Dis, 2013. **5 Suppl 5**: p. S565-78.
8. Fujii, M., et al., *Influence of the timing of tumor regression after the initiation of chemoradiotherapy on prognosis in patients with limited-disease small-cell lung cancer achieving objective response.* Lung Cancer, 2012. **78**(1): p. 107-11.
9. Huisman, C., et al., *Second-line chemotherapy and its evaluation in small cell lung cancer.* Cancer Treat Rev, 1999. **25**(4): p. 199-206.
10. Burrell, R.A., et al., *The causes and consequences of genetic heterogeneity in cancer evolution.* Nature, 2013. **501**(7467): p. 338-45.
11. Stewart, C.A. and L.A. Byers, *Altering the Course of Small Cell Lung Cancer: Targeting Cancer Stem Cells via LSD1 Inhibition.* Cancer Cell, 2015. **28**(1): p. 4-6.
12. Sarvi, S., et al., *CD133+ cancer stem-like cells in small cell lung cancer are highly tumorigenic and chemoresistant but sensitive to a novel neuropeptide antagonist.* Cancer Res, 2014. **74**(5): p. 1554-65.
13. Byers, L.A., et al., *Proteomic profiling identifies dysregulated pathways in small cell lung cancer and novel therapeutic targets including PARP1.* Cancer Discov, 2012. **2**(9): p. 798-811.
14. Cardnell, R.J., et al., *Proteomic markers of DNA repair and PI3K pathway activation predict response to the PARP inhibitor BMN 673 in small cell lung cancer.* Clin Cancer Res, 2013. **19**(22): p. 6322-8.
15. de Marinis, F., et al., *A phase II study of the histone deacetylase inhibitor panobinostat (LBH589) in pretreated patients with small-cell lung cancer.* J Thorac Oncol, 2013. **8**(8): p. 1091-4.
16. Gray, J., et al., *Combination of HDAC and topoisomerase inhibitors in small cell lung cancer.* Cancer Biol Ther, 2012. **13**(8): p. 614-22.
17. Tsurutani, J., et al., *Antiproliferative effects of the histone deacetylase inhibitor FR901228 on small-cell lung cancer lines and drug-resistant sublines.* Int J Cancer, 2003. **104**(2): p. 238-42.
18. Mohammad, H.P., et al., *A DNA Hypomethylation Signature Predicts Antitumor Activity of LSD1 Inhibitors in SCLC.* Cancer Cell, 2015. **28**(1): p. 57-69.
19. Reck, M., et al., *Ipilimumab in combination with paclitaxel and carboplatin as first-line therapy in extensive-disease-small-cell lung cancer: results from a randomized, double-blind, multicenter phase 2 trial.* Ann Oncol, 2013. **24**(1): p. 75-83.
20. Spigel, D.R. and M.A. Socinski, *Rationale for chemotherapy, immunotherapy, and checkpoint blockade in SCLC: beyond traditional treatment approaches.* J Thorac Oncol, 2013. **8**(5): p. 587-98.

21. Watson, I.R., et al., *Emerging patterns of somatic mutations in cancer.* Nat Rev Genet, 2013. **14**(10): p. 703-18.
22. Rudin, C.M., et al., *Comprehensive genomic analysis identifies SOX2 as a frequently amplified gene in small-cell lung cancer.* Nat Genet, 2012. **44**(10): p. 1111-6.
23. authors, A.l.o. and p. affiliations appears at the end of the, *Comprehensive genomic profiles of small cell lung cancer.* Nature, 2015.
24. Peifer, M., et al., *Integrative genome analyses identify key somatic driver mutations of small-cell lung cancer.* Nat Genet, 2012. **44**(10): p. 1104-10.
25. Marte, B., *Tumour heterogeneity.* Nature, 2013. **501**(7467): p. 327.
26. Stewart, D.J., *Tumor and host factors that may limit efficacy of chemotherapy in non-small cell and small cell lung cancer.* Crit Rev Oncol Hematol, 2010. **75**(3): p. 173-234.
27. Griffiths, G.J., et al., *Cellular damage signals promote sequential changes at the N-terminus and BH-1 domain of the pro-apoptotic protein Bak.* Oncogene, 2001. **20**(52): p. 7668-76.
28. Makin, G.W., et al., *Damage-induced Bax N-terminal change, translocation to mitochondria and formation of Bax dimers/complexes occur regardless of cell fate.* EMBO J, 2001. **20**(22): p. 6306-15.
29. Brunelle, J.K. and A. Letai, *Control of mitochondrial apoptosis by the Bcl-2 family.* J Cell Sci, 2009. **122**(Pt 4): p. 437-41.
30. Sartorius, U.A. and P.H. Krammer, *Upregulation of Bcl-2 is involved in the mediation of chemotherapy resistance in human small cell lung cancer cell lines.* Int J Cancer, 2002. **97**(5): p. 584-92.
31. Kaiser, U., et al., *Expression of bcl-2--protein in small cell lung cancer.* Lung Cancer, 1996. **15**(1): p. 31-40.
32. Ikegaki, N., et al., *Expression of bcl-2 in small cell lung carcinoma cells.* Cancer Res, 1994. **54**(1): p. 6-8.
33. Oltersdorf, T., et al., *An inhibitor of Bcl-2 family proteins induces regression of solid tumours.* Nature, 2005. **435**(7042): p. 677-81.
34. Tahir, S.K., et al. *Influence of Bcl-2 family members on the cellular response of small-cell lung cancer cell lines to ABT-737*. in *Cancer Res*. 2007.
35. Shoemaker, A.R., et al., *Activity of the Bcl-2 family inhibitor ABT-263 in a panel of small cell lung cancer xenograft models.* Clin Cancer Res, 2008. **14**(11): p. 3268-77.
36. Gandhi, L., et al., *Phase I study of Navitoclax (ABT-263), a novel Bcl-2 family inhibitor, in patients with small-cell lung cancer and other solid tumors.* J Clin Oncol, 2011. **29**(7): p. 909-16.
37. Rudin, C.M., et al., *Phase II study of single-agent navitoclax (ABT-263) and biomarker correlates in patients with relapsed small cell lung cancer.* Clin Cancer Res, 2012. **18**(11): p. 3163-9.
38. Gardner, E.E., et al., *Rapamycin rescues ABT-737 efficacy in small cell lung cancer.* Cancer Res, 2014. **74**(10): p. 2846-56.
39. Faber, A.C., et al., *Assessment of ABT-263 activity across a cancer cell line collection leads to a potent combination therapy for small-cell lung cancer.* Proc Natl Acad Sci U S A, 2015. **112**(11): p. E1288-96.
40. Meuwissen, R., et al., *Induction of small cell lung cancer by somatic inactivation of both Trp53 and Rb1 in a conditional mouse model.* Cancer Cell, 2003. **4**(3): p. 181-9.
41. Schaffer, B.E., et al., *Loss of p130 accelerates tumor development in a mouse model for human small-cell lung carcinoma.* Cancer Res, 2010. **70**(10): p. 3877-83.
42. Cui, M., et al., *PTEN is a potent suppressor of small cell lung cancer.* Mol Cancer Res, 2014. **12**(5): p. 654-9.
43. Gazdar, A.F., et al., *The comparative pathology of genetically engineered mouse models for neuroendocrine carcinomas of the lung.* J Thorac Oncol, 2015. **10**(4): p. 553-64.

44. Richmond, A. and Y. Su, *Mouse xenograft models vs GEM models for human cancer therapeutics.* Dis Model Mech, 2008. **1**(2-3): p. 78-82.
45. Hou, J.M., et al., *Clinical significance and molecular characteristics of circulating tumor cells and circulating tumor microemboli in patients with small-cell lung cancer.* J Clin Oncol, 2012. **30**(5): p. 525-32.
46. Hodgkinson, C.L., et al., *Tumorigenicity and genetic profiling of circulating tumor cells in small-cell lung cancer.* Nat Med, 2014.
47. Kumar Biswas, S., et al., *Down-regulation of Bcl-2 is associated with cisplatin resistance in human small cell lung cancer H69 cells.* Mol Cancer Ther, 2004. **3**(3): p. 327-34.
48. Chipuk, J.E., et al., *The BCL-2 family reunion.* Mol Cell, 2010. **37**(3): p. 299-310.
49. Chen, L., et al., *Differential targeting of prosurvival Bcl-2 proteins by their BH3-only ligands allows complementary apoptotic function.* Mol Cell, 2005. **17**(3): p. 393-403.
50. Chonghaile, T.N. and A. Letai, *Mimicking the BH3 domain to kill cancer cells.* Oncogene, 2008. **27 Suppl 1**: p. S149-57.
51. Kuwana, T., et al., *BH3 domains of BH3-only proteins differentially regulate Bax-mediated mitochondrial membrane permeabilization both directly and indirectly.* Mol Cell, 2005. **17**(4): p. 525-35.
52. Letai, A.G., *Diagnosing and exploiting cancer's addiction to blocks in apoptosis.* Nat Rev Cancer, 2008. **8**(2): p. 121-32.
53. Deng, J., et al., *BH3 profiling identifies three distinct classes of apoptotic blocks to predict response to ABT-737 and conventional chemotherapeutic agents.* Cancer Cell, 2007. **12**(2): p. 171-85.
54. Ni Chonghaile, T., et al., *Pretreatment mitochondrial priming correlates with clinical response to cytotoxic chemotherapy.* Science, 2011. **334**(6059): p. 1129-33.
55. Vo, T.T., et al., *Relative mitochondrial priming of myeloblasts and normal HSCs determines chemotherapeutic success in AML.* Cell, 2012. **151**(2): p. 344-55.
56. Evans, W.K., et al., *VP-16 alone and in combination with cisplatin in previously treated patients with small cell lung cancer.* Cancer, 1984. **53**(7): p. 1461-6.
57. Ryan, J. and A. Letai, *BH3 profiling in whole cells by fluorimeter or FACS.* Methods, 2013. **61**(2): p. 156-64.
58. Martin-Fernandez, C., et al., *Blocking phosphoinositide 3-kinase activity in colorectal cancer cells reduces proliferation but does not increase apoptosis alone or in combination with cytotoxic drugs.* Mol Cancer Res, 2009. **7**(6): p. 955-65.
59. Ni Chonghaile, T. and A. Letai, *Mimicking the BH3 domain to kill cancer cells.* Oncogene, 2008. **27 Suppl 1**: p. S149-57.
60. Upreti, M., et al., *Identification of the major phosphorylation site in Bcl-xL induced by microtubule inhibitors and analysis of its functional significance.* J Biol Chem, 2008. **283**(51): p. 35517-25.
61. http://deainfo.nci.nih.gov/advisory/ctac/workgroup/SCLC/SCLC%20Congressional%20Response.pdf
62. Letai, A., et al., *Distinct BH3 domains either sensitize or activate mitochondrial apoptosis, serving as prototype cancer therapeutics.* Cancer Cell, 2002. **2**(3): p. 183-92.
63. Ackler, S., et al., *ABT-263 and rapamycin act cooperatively to kill lymphoma cells in vitro and in vivo.* Mol Cancer Ther, 2008. **7**(10): p. 3265-74.
64. Tse, C., et al., *ABT-263: a potent and orally bioavailable Bcl-2 family inhibitor.* Cancer Res, 2008. **68**(9): p. 3421-8.

Chapter 6

Discussion

6. Discussion

6.1 Overview

Prognosis is poor for both mCRC and SCLC patients and curative surgery is rarely an option. Treatment options are limited, thus representing an area of unmet clinical need in both diseases.

CRC patient prognosis worsens with increased stage, and the five year survival rate of mCRC is 5% (Chapter 1.1.1.1; Table 2; (6, 12)). First line therapy for mCRC revolves around chemotherapy and targeted therapies such as Bevacizumab and Cetuximab (previously described in Chapter 1.1.1.2, Table 3; (6, 17, 20)). The addition of targeted therapies on a chemotherapy backbone has only improved the OS of mCRC patients by 1.5-2.6 months (386). This is largely due to the heterogeneity of advanced disease and innate/acquired resistance to therapy due to multiple mutations in non-redundant pathways (33, 34). In England, the NHS offers routine CRC screening via faecal occult blood test to all adults over 60 years of age (387). This CRC screening method has proved successful with a 15-33% reduction in CRC specific mortality in the screened groups whereby CRC was detected earlier in the screened groups than those not screened and therefore, curative surgery was possible (388).

Unfortunately and in contrast to CRC, early screening methods to detect SCLC have been unsuccessful (389) and currently no SCLC screening programmes are available on the NHS (390). Lung Health UK (391) are a private company that provide SCLC screening to people that are over 40 years of age and are current or former smokers. This service involves a blood test (EarlyCDT® - Lung) which measures a panel of 7 autoantibodies associated specifically with lung cancer. Currently this screening method has not proved successful in increasing OS but may be used as a complimentary tool with CT scans for early detection (392, 393). Ability to detect SCLC early has contributed to a major obstacle in SCLC treatment where most patients present with ES (41) or LS (stage III) disease with unresectable tumours (37). SCLC has a poor prognosis, the five year survival rate for patients with LS SCLC is 31%, 19% and 8% for stage I, II and III respectively and for ES (IV) is 2% (394). Surgery is only performed on approximately 5% of

SCLC patients therefore first line therapy consists of chemotherapy +/- radiation (previously described Chapter 1.1.2.2, Figure 7; (42)). Initially, the majority of SCLC patients respond to first line therapy (80-90% of LS and 70-85% of ES patients) however, virtually all patients will relapse with progressive disease within 3-18 months (48, 62), highlighting another obstacle in SCLC treatment: the rapid development of chemotherapy resistant disease.

As such, treatment for mCRC and SCLC has made little progress in 30 years. There is a clear unmet need to improve current therapies and develop new ones, with the goal to increase PFS and OS in both diseases. In order for this approach to be successful predictive biomarkers must be developed to stratify patients that will respond to these therapies. Currently, CRC patients are screened for *KRAS* mutations prior to Cetuximab treatment, an example of precision medicine and the first use of genetic screening as a predictive biomarker in CRC patients (20, 395). There is also evidence that CRC patients with other alterations, such as *BRAF* or *PIK3CA* mutations, will respond poorly to Cetuximab (20). New predictive biomarkers are needed to stratify all the different CRC subtypes (previously discussed Chapter 1.1.1.3, Figure 5), to ensure the most suitable treatment. There is a lack of predictive biomarkers and genetic screening in SCLC and no available targeted therapies in the clinic (Chapter 1.4.1, Table 4; (396)). This is largely due to the heterogeneity of the disease and innate/acquired chemotherapy resistance (previously discussed Chapter 1.1.2.2 and 1.1.2.3, Figure 8). The aim of this PhD project was to develop a rational drug combination to improve current treatment of mCRC and SCLC and to develop a predictive biomarker to identify chemo-refractory SCLC patients (10-20% of LS and 15-30% of ES patients; (48, 61)).

The rational drug combination of a PI3Ki (PI3K inhibitor; PI-103 or GDC-0941) and BH3 mimetic (ABT-737 or Navitoclax) was investigated in preclinical CRC and SCLC models. The research in my thesis confirmed that combining ABT-737 with PI-103 was more effective than either drug alone *in vitro* in CRC and SCLC (Chapter 3, Figure 1; Chapter 4, Figure 1 and 2), and GDC-0941/Navitoclax combination improved OS *in vivo,* compared to either drug as a single agent and SOC in SCLC CDX (Chapter 4, Figure 5 and 6; (83)). ABT-737/Navitoclax directly interacts with the anti-apoptotic proteins, BCL-2, BCL-xL and BCL-w (317),

antagonising their interactions with pro-apoptotic BH3-only proteins and effector proteins. The exact mechanism of PI3Ki sensitisation to ABT-737 or Navitoclax has not yet been determined in the preclinical models used in this study. However, PI3K inhibition is likely causing sensitivity to ABT-737 through a mechanism altering the availability of Bcl-2 family members binding sites (84, 85, 258). This could be via a decrease in available binding sites (through PTM or protein expression) for anti-apoptotic Bcl-2 family members or conversely via an increase in binding sites (also through PTM or protein expression) for pro-apoptotic Bcl-2 family members causing a shift in cell survival equilibrium, thus 'priming' (lowering the apoptotic threshold), which subsequently increases cellular sensitivity to ABT-737 or Navitoclax. Preclinical data (Chapter 3 and 4) provides support for any future clinical trials in CRC and SCLC with the PI3Ki and BH3 mimetic combination.

BH3 profiling was carried out on SCLC CDX in order to identify any differences between chemo-sensitive (CDX3) and chemo-refractory models (CDX2 and CDX4), therefore potentially enabling BH3 profiling to predict for CDX response to SOC *in vivo*. The method employs BH3 peptides derived from the BH3 domain of the pro-apoptotic BH3-only proteins, to interrogate MOMP (discussed in Chapter 1.3.4, Figure 19). A common mechanism for cancer cells to evade apoptosis is via dysregulation of the Bcl-2 family proteins, which regulate the intrinsic apoptotic pathway (250). BH3 profiling can distinguish between the three main so-called apoptotic blocks involving Bcl-2 family proteins via measurement of the cellular response to specific pro-apoptotic activator or sensitizer BH3 peptides (previously discussed Chapter 1.3.4, Figure 19). Responses of CDX2, CDX3 and CDX4 to SOC (cisplatin/etoposide) mirrors the patient response in the original tumour from which CTCs and subsequent CDX were presumably derived (83). BH3 profiling revealed that the chemo-sensitive model, CDX3, was highly sensitive to sensitizer BH3 peptides compared to the chemo-refractory models (CDX2 and CDX4) (Chapter 5, Figure 2). This suggests that CDX3 is a 'primed' model that would likely respond to cytotoxic treatment, which was indeed the case (83). Furthermore in three recently established CDX models; CDX3P (paired progression model of CDX3), CDX8 and CDX8P (paired progression model of CDX8), BH3 profiling carried out prospectively to chemotherapy response, indicated that CDX3P and

CDX8 would likely respond well to cytotoxic treatment and CDX8P would exhibit a poorer response (Chapter 5, Figure 3 and 4 green bars). Indeed, this was shown to be an accurate prediction following completion of *in vivo* SOC chemotherapy efficacy studies (Chapter 5, Figure 3 and 4), thus BH3 profiling can be used as a predictive biomarker for CDX response to cytotoxic therapy (Chapter 5). Unfortunately due to the lag time from patient blood being taken to palpable CDX, BH3 profiling of CDX tumours could not currently be used in real time to help aid treatment decisions, but the aim is to develop this method in order to apply BH3 profiling to freshly enriched CTCs from patients in order to augment clinical decision-making. In this case chemo-refractory patients could be identified prior to administration of toxic and potentially ineffective chemotherapy and instead be prioritised for clinical trials, or once proven in the clinic, offered alternative therapeutic options, such as the combination with PI3Ki (GDC-0941) and Navitoclax (Chapter 4, Figure 5 and 6).

6.2 PI3K pathway inhibitors in combination with BH3 mimetics

The rational drug combination of a PI3K pathway inhibitor and BH3 mimetic was first investigated in haematological malignancies (332, 333, 397). Lymphoma cell lines and cell line xenografts were sensitised to Navitoclax when combined with rapamycin, which inhibits the mTORC1 pathway. Data suggested that cell cycle arrest caused by rapamycin potentiates Navitoclax, although a mechanism was not proposed and there were no changes described in protein levels of the Bcl-2 family proteins, including MCL-1 (397). This is consistent with our findings *in vitro* in SCLC cell lines (Chapter 4, Figure 2D and supplementary Figure 4A). Furthermore, a study in NSCLC showed that cells that expressed high levels of BCL-xL were resistant to PI3K inhibitor LY294002-induced apoptosis (398). Subsequently, the combination of ABT-737 (to target BCL-xL) with LY294002 (to target PI3K) led to enhanced apoptosis. This sensitisation was associated with an increase in BIM levels after PI3K inhibition (398), which we did not observe *in vitro* in CRC or SCLC cell lines (Chapter 3, Figure 2A; Chapter 4, supplementary Figure 4A). Two recent studies have described mTOR inhibition sensitising to ABT-737/Navitoclax in various SCLC preclinical models (84, 85). Gardner *et al*., demonstrated that rapamycin rescues ABT-737 efficacy in SCLC cell lines

(including H146, used in results described in Chapter 4) and PDX models (84). Furthermore ABT-737 treatment reduced BAX levels, which is self-limiting in nature due to the BAX-dependent induction of apoptosis by ABT-737. The combination of rapamycin with ABT-737 prevented this ABT-737-induced reduction of BAX, therefore restoring ABT-737-induced apoptosis (84). Faber *et al*., demonstrated that in preclinical studies the mTORC1/2 inhibitor AZD8055 sensitised to Navitoclax in SCLC cell lines (including H1048, also used in results described in Chapter 4), GEMMS and PDX models, an effect that was consistent with MCL-1 downregulation by AZD8055 (85). However, this finding was not recapitulated in experiments using H1048 cells described in Chapter 4 (Figure 2D) where MCL-1 levels were unaffected by treatment with PI3K pathway inhibitors. Data presented in this thesis, in addition to current literature, demonstrates that PI3K pathway inhibitors and BH3 mimetics prove efficacious in preclinical models. However, it suggests that the PI3K downstream mechanism is likely to be cell-context dependent and warrants further investigation.

6.3 PI3K-dependent MCL-1-independent sensitisation to ABT-737

ABT-737/Navitoclax is a BCL-2, BCL-xL and BCL-w antagonist with poor affinity for MCL-1 (315, 316, 336, 399) which is an established resistance factor for this combination, whereby high MCL-1 can compensate for ABT-737/Navitoclax antagonism of BCL-2, BCL-xL and BCL-w (previously discussed in Chapter 1.3.7). Furthermore, in the presence of ABT-737/Navitoclax, resistant cells can become dependent on MCL-1 for survival (315, 316, 336, 399).

As previously described, the active PI3K/AKT pathway positively regulates MCL-1 via inactivation of GSK3β, which negatively regulates MCL-1 stability (Chapter 1.2.4, Figure 10; (134)). In the CRC cell lines HCT-116 and SW620, levels of nine Bcl-2 family proteins were assessed after treatment with the dual PI3K/mTOR inhibitor PI-103. Of those, only MCL-1 levels were reduced after treatment (Chapter 3, Figure 2A). This was consistent with data shown by Faber *et al*., where treatment with AZD8055 led to downregulation of MCL-1 in SCLC preclinical models (85). In contrast to findings in CRC, in the SCLC cell lines H1048, H526 and DMS114 MCL-1 levels were unaffected by treatment with any of

the PI3K pathway inhibitors (Chapter 4, supplementary Figure 4A). This is consistent with data from Gardner *et al*., Ackler *et al.,* and Qian *et al*., who all observed no change in MCL-1 levels after treatment with rapamycin or LY294002 (84, 397, 398). Taken together this suggests that MCL-1 regulation by PI3K/AKT is cell context dependent and/or PI3K pathway inhibitor dependent.

The work presented in this thesis confirms that an MCL-1-independent pathway sensitises cells to ABT-737 in MEFs (mouse embryonic fibroblasts), CRC and SCLC cell lines (Chapter 3, Figure 2B-D and W3A-C; Chapter 4, Figure 2D-F and supplementary Figure 4). MCL-1 knockdown sensitised both CRC and SCLC cells to ABT-737 (Chapter 3, Figure 2B-C; Chapter 4, Figure 2D-F) suggesting that MCL-1 is downstream of PI3K. However, PI-103 treatment further and significantly sensitised MCL-1 knock-down cells to ABT-737 which suggests that an MCL-1-independent mechanism is also partly responsible for sensitisation to ABT-737 when PI3K is inhibited in both CRC and SCLC (Chapter 3, Figure 2B-D; Chapter 4, Figure 2D-F). A similar study was carried out in MEFs in order to confirm an MCL-1-independent mechanism for sensitising cells to ABT-737 following PI3K inhibition. The combination of PI-103 and ABT-737 caused significant cell death in both the parental and MCL-$1^{-/-}$ MEFs (Chapter 3 Figure W3A-C) which indicates MCL-1 is not essential for PI-103 sensitisation to ABT-737. The mechanism for PI-103 sensitisation to ABT-737 may be different in CRC, SCLC and MEFs. Although data in this thesis confirms that MCL-1 is a resistance factor for ABT-737 efficacy, and targeting MCL-1 downregulation to increase the potency of ABT-737 is a rational approach, we highlight that additional MCL-1-independent pathways influence response to ABT-737 when PI3K pathway is inhibited.

6.4 PI3K-dependent AKT/mTOR-independent sensitisation to ABT-737

AKT and mTOR are the main known downstream effectors of the PI3K pathway. However, none of the CRC cell lines used in this study (SW620, HCT-116 or DLD-1), were sensitised to ABT-737 in combination with the AKT inhibitors MK-2206/AKTi1/2, or the mTOR inhibitors KU-0063794/rapamycin. It is possible that the PI3K signalling mechanism, which causes sensitivity to ABT-737 when PI3K is inhibited, is PI3K-dependent, but AKT- and mTOR-independent in CRC (Chapter

3, Figure 3C-E and Table 2). In support of these findings Vasudevan *et al*., demonstrated that some *PIK3CA* mutant cell lines were dependent on PI3K signalling for proliferation and/or survival but not dependent on AKT. This included the CRC cell lines HCT-116 and DLD-1, used in this study (155). Whilst AKT is the main known effector of PI3K signalling pathway in the majority of cell types, AKT-independent PI3K-dependent signalling pathways have been suggested (155, 157, 158, 291).

To investigate potential downstream effectors of the PI3K pathway, a siRNA library screen was designed to identify siRNA sensitizers to ABT-737. Many PH domain containing proteins can interact with PtdIns(3,4,5)P_3, the product of Class I PI3K (151, 152). Because PH domain containing proteins have the potential to interact with PtdIns(3,4,5)P_3, these therefore formed the foundation of the siRNA library screen. SW620 cells were chosen because they showed the greatest sensitisation to ABT-737 when PI3K was inhibited (Chapter 3, Figure 1A). None of the candidate siRNAs demonstrated a sensitisation towards ABT-737 on the same scale as MCL-1 siRNA and whilst some hits were deemed to be significant based on a t-test, none of the mean robust Z-scores reached a score of <-2 or >2 (Chapter 3, Figure 4A). However, siRNA library screens have inherent problems that could account for these observations. Firstly, it is not known whether the siRNA in the library actually caused knock-down of their target proteins at the time of ABT-737 treatment. Secondly, it is not known to what degree knock-down occurred for each of these target proteins, something that is not practical to determine for each of the siRNAs in the library. The transfection protocol was optimised to ensure maximal effect of MCL-1 siRNA, and it is therefore likely that other proteins would not have been depleted to the same extent as MCL-1 following the addition of ABT-737. Based on this, it was pertinent to further pursue the hits which had the greatest effect on ABT-737 sensitivity in order to confirm or discount them.

Three of the top four sensitizer candidate siRNAs (SOS1, BMX and SGK1) were further validated. PLEKHB2 was discounted due to the recent findings that its PH domain binds preferentially to phosphatidylserine, rather than PtdIns(3,4,5)P3 (400), and is therefore an unlikely downstream target of PI3K signalling. SW620

cells were transfected with SMARTpool siRNA or individual oligos that make up the SMARTpool targeting SOS1, BMX or SGK1 mRNA, and a concentration response to ABT-737 was carried out (Chapter 3, Figure 4B and Figure W6A). SOS1, BMX or SGK1 mRNA was measured by qPCR (Chapter 3, Figure 4C and Figure W6B). BMX knock-down positively correlated with ABT-737 efficacy suggesting that cells that expressed less BMX mRNA were more sensitive to ABT-737(Chapter 3, Figure 4B-C and Figure W6A-B). PI-103 treatment did not further sensitise BMX RNAi cells to ABT-737 indicating that BMX acts downstream of PI3K in SW620 cells (Chapter 3, Figure 4F). SOS1 and SGK1 knock-down did not positively correlate with ABT-737 efficacy suggesting that sensitisation was due to off-target effects of some of the oligos, rather than knockdown of the intended target (Chapter 3, Figure 4B-C and Figure W6A-B). BMX knock-down was further investigated in an additional CRC cell line (HCT116) whereby siRNA-mediated knock-down of BMX caused sensitisation to ABT-737 (Chapter 3, Figure 4D). As previously mentioned BMX is a member of the Tec family of NRTK (Chapter 1.2.6) and the Tec kinase inhibitor Ibrutinib sensitised DLD-1, HCT-116 and SW620 cells to ABT-737 (Chapter 3, Figure 4E and Figure W8) confirming that BMX inhibition by RNAi and pharmacological inhibitors sensitise to ABT-737 via on-target effects.

Relatively little is known about BMX and its downstream effectors despite it being implicated in regulating many signal transduction pathways including apoptosis, proliferation and angiogenesis (As discussed previously in Chapter 1.2.6; (163, 166, 168, 170-173, 258, 401)). A main known downstream target of BMX is STAT3. Activation of STAT3 via BMX has been shown to be required for mutant *PIK3CA* induced transformation, independent of AKT and mTOR activation (157). STAT3 may regulate apoptosis by controlling levels of BCL-xL (402) or p53 (403), thus PI3K inhibition could sensitise to ABT-737 via inhibition of BMX and STAT3. Interestingly a phospho-kinase array in H1048 cells revealed decreased phospho-STAT3 in both BMX knock down cells and Ibrutinib treated cells compared to the untreated cells (Chapter 4, Figure 3E-F), indicating a link between the two pathways. However, further validation of the role of STAT3 as a BMX effector in CRC and SCLC and its ability to regulate ABT-737-induced apoptosis is required.

The siRNA screen revealed two interesting siRNAs that caused resistance to ABT-737 (Chapter 3, Figure 4A). These were siRNAs targeting PIK3CB or PIK3R1 mRNA. *PIK3CB* encodes the p110β catalytic subunit (Chapter 1.2.2, Figure 9) and the different p110 isoforms have been demonstrated to have different effects in several studies (e.g. (404)), Knock-down of PIK3CB could therefore lead to a compensatory up-regulation of a different p110 isoform which may be responsible for activating the signalling pathway responsible for ABT-737 sensitivity. In this scenario, PIK3CB knockdown would cause ABT-737 resistance. *PIK3R1* encodes the three PI3K regulatory isoforms p85α, p55α and p50α (Chapter 1.2.2, Figure 9) therefore, knock down of PIK3R1 should reduce levels of all three proteins. Abell *et al.,* showed that p55α and p50α are negative regulators of PI3K activity and STAT3-dependent upregulation of p55α and p50α during breast involution causes the switch from survival to apoptosis (405). Hence one hypothesis is that PIK3R1 RNAi could cause a decrease in p55α and p50α, preventing their negative regulation of p110 and therefore upregulating PI3K activity.

6.5 BMX is a PI3K downstream effector

Findings described in Chapter 3 in CRC led to the hypothesis that cells which express high levels of BMX would likely use the PI3K/BMX pathway for survival. Data obtained from CCLE revealed relatively high levels of BMX mRNA in SCLC cell lines compared to other cancer types (406) and BMX has also been shown to be expressed in 75% of SCLC patient samples (173). Whilst preclinical studies in SCLC demonstrated good single agent ABT-737 efficacy (87, 88, 317), disappointingly this did not translate to the clinic (89). Therefore, SCLC was a good candidate to further study the rational drug combination of PI3Ki with ABT-737. We hypothesised that inhibition of the PI3K/BMX pathway in SCLC would increase the potency of ABT-737. Interestingly, inhibition with PI-103 or Ibrutinib significantly increased ABT-737-induced apoptosis in H1048 and H526 cells (Chapter 4, Figure 2A-B), confirming my results in CRC, although BMX was shown to regulate the AKT/mTOR pathway in those SCLC cell lines (Chapter 4, Figure 1A and 3E-F). Further studies confirmed that AKT or mTOR inhibitors, MK-2206 and KU-0063794 respectively, also sensitised to ABT-737 in H1048 and H526 cells (Chapter 4, Figure 4) suggesting that in SCLC AKT/mTOR is important in

mediating ABT-737 sensitivity. The results of this thesis (Chapter 4) show for the first time that BMX can regulate AKT/mTOR pathway activity in SCLC. Furthermore, these data again highlight cell-context dependent mechanism(s) acting downstream of PI3K, where ABT-737 sensitivity can be regulated via both AKT/mTOR-dependent and –independent pathways.

The mechanism by which BMX regulates AKT/mTOR signalling in SCLC is not yet understood although mechanisms that link BMX to AKT/mTOR signalling have been reported in other cell types (171, 401). Active BMX mediates TNF-induced recruitment of the p85 subunit of PI3K resulting in AKT activation in human umbilical vein endothelial cells (HUVEC), whilst knock-out of BMX in mouse lung endothelial cells blocks TNF-induced activation of AKT compared to wild type (401). BMX has also been implicated in a positive feed-forward mechanism in endothelial and epithelial cells, where active BMX upregulates VEGF, which is secreted and binds to its receptors, further activating BMX and resulting in AKT activation (171).

We observed a significant increase in ABT-737-induced apoptosis when combined with PI-103 or Ibrutinib after only 4 hours (Chapter 4. Figure 2A-B) suggesting that sensitisation to ABT-737 involves post-translational modification(s) (PTM) which commonly occur more rapidly than changes in gene expression. Recently BMX was identified as the tyrosine kinase that phosphorylates and inactivates the pro-apoptotic effector protein BAK (258). Inactivation of BMX through PI3K/BMX pathway inhibition could therefore lead to BAK dephosphorylation in SCLC. In this model, ABT-737-induced BCL-2, BCL-xL or BCL-w antagonism would release BIM to activate available dephosphorylated BAK resulting in BAK homo-oligomerization and MOMP, cytochrome c release and activation of apoptosis.

6.6 BMX mutation in H1048 cells

H1048 cells have a heterozygous mutation in the BMX tyrosine kinase domain (R656C (180)). Using the informatics tool mutationassessor.org (203), R656C *BMX* scores a high functional impact score (FIS, 4.705), however, the actual impact of this mutation on BMXs function is unknown. The functional mutation could affect BMX in various ways and would need to be further investigated but,

for example, it could change BMX specificity for its effector protein. This could either be via reduced specificity (loss of function), increased specificity for an effector (gain of function) or gain of new effector(s) (switch of function) resulting in a new biological function (203). Since knock-down of BMX by RNAi (Chapter 4, Figure 3A-D) has a functional effect in sensitising H1048 cells to ABT-737, it is likely that the functional impact of R656C mutation has retained wild-type PI3K/BMX pathway properties. H1048 also has an oncogenic activating mutation in *PIK3CA* (180) and as BMX is downstream of PI3K this suggests that coexistence of *BMX* and *PIK3CA* mutations would engender differing oncogenic mechanisms to provide a selective advantage to cells that harbour both mutations.

6.7 Hypothetical mechanism of ABT-737-induced apoptosis by PI3K pathway inhibition

As previously described, cancer cells have evolved mechanisms to evade apoptosis via dysregulation of the Bcl-2 family of proteins (Chapter 1.3.4, Figure 19). Figure 25 is a schematic of the Bcl-2 family which describes how their interactions may alter after treatment with a PI3Ki and/or ABT-737. The schematic refers to four different cell-context dependent scenarios (Figure 25A-D) which represent an untreated cancer cell (A), a PI3Ki treated cancer cell (B), an ABT-737 treated cancer cell (C) and a cancer cell treated with PI3Ki and ABT-737 in combination (D). In this schematic the untreated cancer cell (Figure 25A) has activated PI3K signalling and evades apoptosis via upregulation of the anti-apoptotic proteins, BCL-2, BCL-xL and MCL-1. As described previously (Chapter 1.2.4), active PI3K signalling stabilises MCL-1 (134) and phosphorylates the pro-apoptotic BH3-only protein BAD. Phospho-BAD, is sequestered thus preventing antagonism of BCL-2 and BCL-xL (133). Following treatment with a PI3Ki alone (Figure 25B) the PI3K pathway is blocked causing cell cycle arrest in this model (382). MCL-1 is no longer stable resulting in MCL-1 downregulation and BAD is no longer sequestered leaving it free to antagonise BCL-2 and BCL-xL. The overall effect of PI3Ki is a decrease in available anti-apoptotic protein binding sites and an increase in pro-apoptotic protein binding sites, thus ‘priming’ the cell by lowering the apoptotic threshold. In this model when cancer cells are treated with ABT-737 alone (Figure 25C), ABT-737 antagonises BCL-2 and BCL-xL. The PI3K pathway

is active in this scenario and therefore MCL-1 is stable and phospho-BAD, is sequestered. The overall effect of ABT-737 is a low level of apoptosis as ABT-737 binds BCL-2 and BCL-xL, lowering the number of anti-apoptotic binding sites available, and releasing the pro-apoptotic BH3-only protein BIM that can activate BAX/BAK. Therefore when the cells are treated with a PI3Ki and ABT-737 in combination (Figure 25D), the PI3Ki 'primes' the cell for apoptosis, as described in Figure 25B, and this lowering of the apoptotic threshold potentiates ABT-737 resulting in increased apoptosis compared to ABT-737 treatment alone.

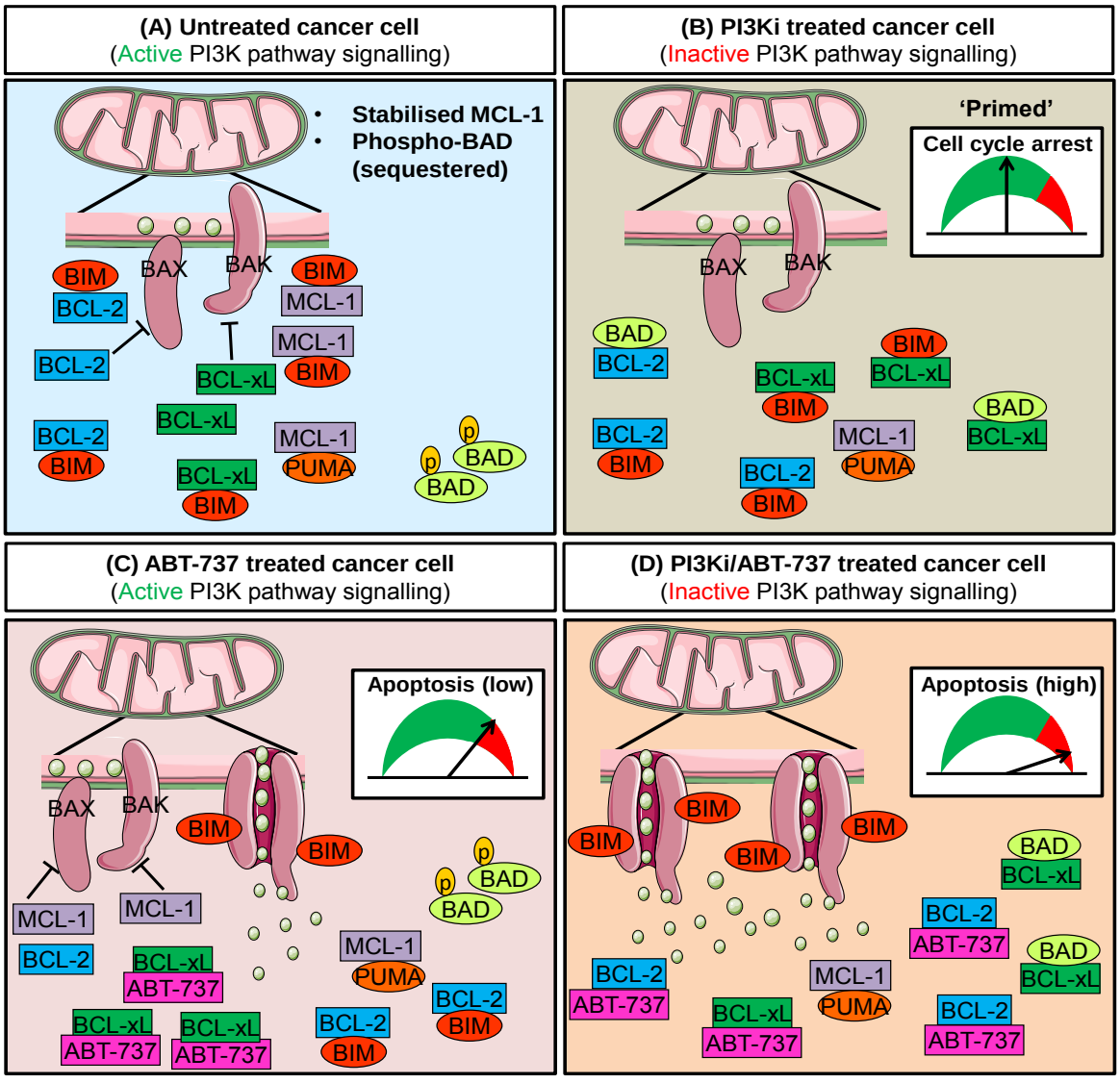

Figure 25: A model for Bcl-2 family interactions in cancer cells after PI3K inhibition and/or ABT-737 treatment. (A) Untreated cancer cell evades apoptosis via upregulation of anti-apoptotic Bcl-2 family proteins (BCL-2, BCL-xL and MCL-1). Active PI3K pathway signalling stabilises MCL-1 and sequesters pro-apoptotic phospho-BAD. (B) PI3K pathway is blocked with a PI3K inhibitor (PI3Ki) which destabilises MCL-1 and releases BAD. The cell cycle is blocked but cells are 'primed' as the apoptotic threshold has been reduced. (C) ABT-737 treatment antagonises BCL-2 and BCL-xL, which releases BIM to activate apoptosis (low levels). (D) PI3Ki and ABT-737 in combination 'primes' the cell, which potentiates ABT-737-induced apoptosis. Illustration made using Servier Medical Art.

6.8 GDC-0941 and Navitoclax combination increases overall survival *in vivo* compared to standard of care

In SCLC *in vivo* preclinical models (H1048 xenograft and CDX2) the rational drug combination, GDC-0941 and Navitoclax, showed greater efficacy than either drug as a single agent (Chapter 4, Figure 5 and 6). The rationale for this combination *in vivo* is that PI3K pathway inhibition by GDC-0941 'primes' the tumour for apoptosis, which potentiates the effect of Navitoclax. The H1048 xenograft was chosen to investigate the GDC-0941/Navitoclax combination *in vivo* due to the high level of sensitisation shown *in vitro* (Chapter 4, Figure 1B and Supplementary Figure 3) and therefore, it was hypothesised that the combination would improve the modest single agent efficacy of Navitoclax shown by Shoemaker *et al.,* (88). In agreement with Shoemaker *et al*., H1048 xenograft tumours grow rapidly and reached tumour endpoint (four times the initial tumour volume (4xITV)) within 9 days. However, the GDC-0941/Navitoclax combination significantly increased tumour end point to 32 days and proved more efficacious than either drug as a single agent (Chapter 4, Figure 5C). The H1048 tumour doubling time was significantly increased (2 fold) in the GDC-0941/Navitoclax combination group compared to single agent GDC-0941 or Navitoclax, suggesting that only the combination impedes tumour growth (Chapter 4, Figure 5D).

CDX2 is a chemo-refractory model with a poor response to cisplatin/etoposide, mirroring the response to SOC of donor patient (83). It was therefore a 'high hurdle' to test the GDC-0941/Navitoclax combination in CDX2. The combination proved efficacious in CDX2 with none of the animals reaching the experimental endpoint (4xITV) on day 93, which was significant compared to either drug as a single agent (Chapter 4, Figure 6D). Furthermore the GDC-0941/Navitoclax combination caused prolonged tumour regression (~30 days, 94% mean tumour regression) compared to either drug as a single agent (Chapter 4, Figure 6B-C) and remarkably one animal had no palpable tumour at the end of the experimental time course (Chapter 4, Figure 6C). This combination was also more efficacious than cisplatin/etoposide (83) treatment, which caused 51% tumour regression and all animals reached their endpoint by day 50, suggesting that GDC-

0941/Navitoclax combination could offer an alternative therapy for chemo-refractory patients.

6.9 CDX2 BH3 profiling versus *in vivo* Navitoclax efficacy

BH3 profiling of treatment-naïve CDX2 tumours demonstrated a poor response to the pro-apoptotic BH3-only sensitizer peptides (Chapter 5, Figure 2D). This suggests CDX2 tumour cells evade apoptosis via downregulation of pro-apoptotic activator BH3-only proteins such as BIM (previously discussed Chapter 1.3.4, Figure 19) thus confirming the chemo-refractory nature of this model (83). From the poor response of CDX2 tumours to sensitizer BH3 peptides I hypothesised that Navitoclax would have poor single agent efficacy because Navitoclax is modelled on pro-apoptotic BH3-only BAD protein (317, 336). However, Navitoclax showed good single agent efficacy in CDX2 causing 80% mean tumour regression although tumours regrew as soon as Navitoclax was removed at the end of the dosing period (Chapter 4 Figure 6B). The BH3 profiling of CDX2 tumour cells showed the greatest amount of cytochrome c release of all the sensitizer peptides with the BAD peptide (9-16%; Chapter 5, Figure 2D). This coupled with the slow growth of CDX2 tumours (Vehicle group 37 day 4xITV compared to H1048 xenograft, 9 day 4xITV; Chapter 4 Figure 5 and 6) could explain the apparent discrepancy between the BH3 profiling data and *in vivo* Navitoclax efficacy whereby albeit low levels of apoptosis (if continually present) would result in tumour regression where the opposing tumour growth rate was low.

6.10 Overall conclusions of this thesis

The rational drug combination of a PI3Ki with BH3 mimetic has proved to be an efficacious combination in multiple cancers using various preclinical models. Data described in this thesis demonstrates that this is also the case in CRC and SCLC and supports additional recently published data in SCLC (84, 85) and is also consistent with parallel studies in NSCLC (398) and haematological malignancies (332, 333, 397).

BMX has been shown to be an important PI3K downstream effector (Chapter 3, Figure 4; Chapter 4, Figure 3A-D and Supplementary Figure 5A-C) and the

PI3K/BMX pathway has been shown to have anti-apoptotic functions in some cancer contexts, suggesting it has potential as an attractive drug target. Evidence presented here demonstrates that a rational drug combination of GDC-0941 or Ibrutinib with Navitoclax could provide an alternative treatment in mCRC and SCLC and should be considered in clinical trials in these cancers.

BH3 profiling on disaggregated CDX tumours presented in this thesis also demonstrates the ability to identify chemo-refractory and chemo-sensitive CDX models. There is potential to build on these findings in order to develop this technology for use on patients in real time through tumour biopsies or CTCs in order to identify chemo-refractory patients and enable alternative therapy such as the PI3Ki/BH3 mimetic combination.

6.11 Possible directions for future work

This thesis has highlighted a number of findings which warrant further study.

1. Development of BH3 profiling on a single cell platform which could be used on CTCs enriched from patient blood. This would be useful in cancers such as SCLC where patient biopsy samples are challenging. BH3 profiling could be used to predict in real time how patients will respond to chemotherapy and may be used to aid therapeutic decision making.
2. Development of BH3 profiling on patient tumour specimens such as CRC (where surgery is more routinely carried out) to investigate if this BH3 profiling can predict for response to chemotherapy.
3. Investigation of dynamic BH3 profiling *ex vivo* on CDX, PDX or patient samples to identify potential therapies that would be beneficial to that specific model/patient. In dynamic BH3 profiling cells are treated with a drug prior to BH3 profiling and BH3 profiling can reveal whether the drug increases ‘priming’. Multiple drugs can be used to target various pathways to reveal which therapy would be most beneficial to treat that specific cancer (precision medicine).
4. Further exploration of the mechanisms downstream of PI3K in CRC and SCLC in order to determine which downstream effectors sensitise cells to ABT-737/Navitoclax when PI3K is inhibited. Given the evidence presented

in this thesis, focus would initially be on BMX and the importance of STAT3 and BAK as potential downstream effectors of PI3K signalling. Initial studies would include the design of a phospho-kinase array containing all Bcl-2 family members in order to identify any PTMs which occur after PI3K pathway inhibition with the goal of defining the precise mechanisms that underpin the drug combination effects.

5. Investigation of the potential correlation between BMX expression and prognosis in SCLC using a SCLC Tissue Microarray (TMA) to determine BMX expression and prognostic significance.
6. Investigation of the rational drug combination of GDC-0941/Navitoclax in other CDX models (the laboratory now has 15 CDX) to determine whether OS can be improved compared to SOC therefore providing much-needed alternative therapies in chemo-sensitive, chemo-refractory patients and relapsed SCLC patients.

Chapter 7

References

7. References

1. Hanahan D, Weinberg RA. The hallmarks of cancer. Cell. 2000;100:57-70.
2. Hanahan D, Weinberg RA. Hallmarks of cancer: the next generation. Cell. 2011;144:646-74.
3. Cancer Research UK, http://www.cancerresearchuk.org/health-professional/cancer-statistics/worldwide-cancer, Accessed [July] [2015].
4. Arriola E, Canadas I, Arumi M, Rojo F, Rovira A, Albanell J. Genetic changes in small cell lung carcinoma. Clin Transl Oncol. 2008;10:189-97.
5. Cancer Research UK, http://www.cancerresearchuk.org/health-professional/cancer-statistics/worldwide-cancer, Accessed [July] [2015].
6. Cunningham D, Atkin W, Lenz HJ, Lynch HT, Minsky B, Nordlinger B, et al. Colorectal cancer. Lancet. 2010;375:1030-47.
7. Ferlay J, Soerjomataram I, Ervik M, Dikshit R, Eser S, Mathers C, Rebelo M, Parkin DM, Forman D, Bray, F. GLOBOCAN 2012 v1.1, Cancer Incidence and Mortality Worldwide: IARC CancerBase No. 11 [Internet]. Lyon, France: International Agency for Research on Cancer; 2014. Available from:http://globocan.iarc.fr, accessed on 16/01/2015
8. Ferlay J, Soerjomataram I, Ervik M, Dikshit R, Eser S, Mathers C, Rebelo M, Parkin DM, Forman D, Bray, F. GLOBOCAN 2012 v1.1, Cancer Incidence and Mortality Worldwide: IARC CancerBase No. 11 [Internet]. Lyon, France: International Agency for Research on Cancer; 2014. Available from:http://globocan.iarc.fr, accessed on 16/01/2015.
9. Ferlay J, Soerjomataram I, Ervik M, Dikshit R, Eser S, Mathers C, Rebelo M, Parkin DM, Forman D, Bray, F. GLOBOCAN 2012 v1.1, Cancer Incidence and Mortality Worldwide: IARC CancerBase No. 11 [Internet]. Lyon, France: International Agency for Research on Cancer; 2014. Available from:http://globocan.iarc.fr, accessed on 16/01/2015.
10. Brenner H, Stock C, Hoffmeister M. Effect of screening sigmoidoscopy and screening colonoscopy on colorectal cancer incidence and mortality: systematic review and meta-analysis of randomised controlled trials and observational studies. BMJ. 2014;348:g2467.
11. Sobin LH, Compton CC. TNM seventh edition: what's new, what's changed: communication from the International Union Against Cancer and the American Joint Committee on Cancer. Cancer. 2010;116:5336-9.
12. Gunderson LL, Jessup JM, Sargent DJ, Greene FL, Stewart AK. Revised TN categorization for colon cancer based on national survival outcomes data. J Clin Oncol. 2010;28:264-71.
13. Koopman M, Venderbosch S, Nagtegaal ID, van Krieken JH, Punt CJ. A review on the use of molecular markers of cytotoxic therapy for colorectal cancer, what have we learned? Eur J Cancer. 2009;45:1935-49.
14. Ross JS, Torres-Mora J, Wagle N, Jennings TA, Jones DM. Biomarker-based prediction of response to therapy for colorectal cancer: current perspective. Am J Clin Pathol. 2010;134:478-90.
15. Yang SY, Sales KM, Fuller B, Seifalian AM, Winslet MC. Apoptosis and colorectal cancer: implications for therapy. Trends Mol Med. 2009;15:225-33.

16. Morgan RG. Leucovorin enhancement of the effects of the fluoropyrimidines on thymidylate synthase. Cancer. 1989;63:1008-12.
17. Souglakos J, Androulakis N, Syrigos K, Polyzos A, Ziras N, Athanasiadis A, et al. FOLFOXIRI (folinic acid, 5-fluorouracil, oxaliplatin and irinotecan) vs FOLFIRI (folinic acid, 5-fluorouracil and irinotecan) as first-line treatment in metastatic colorectal cancer (MCC): a multicentre randomised phase III trial from the Hellenic Oncology Research Group (HORG). Br J Cancer. 2006;94:798-805.
18. Hoffe SE, Shridhar R, Biagioli MC. Radiation therapy for rectal cancer: current status and future directions. Cancer Control. 2010;17:25-34.
19. Fakih MG. Metastatic colorectal cancer: current state and future directions. J Clin Oncol. 2015;33:1809-24.
20. Ortega J, Vigil CE, Chodkiewicz C. Current progress in targeted therapy for colorectal cancer. Cancer Control. 2010;17:7-15.
21. Varey AH, Rennel ES, Qiu Y, Bevan HS, Perrin RM, Raffy S, et al. VEGF 165 b, an antiangiogenic VEGF-A isoform, binds and inhibits bevacizumab treatment in experimental colorectal carcinoma: balance of pro- and antiangiogenic VEGF-A isoforms has implications for therapy. Br J Cancer. 2008;98:1366-79.
22. http://www.cancer.gov/about-cancer/treatment/drugs/fda-bevacizumab
23. http://www.cancer.gov/about-cancer/treatment/drugs/fda-cetuximab#Anchor-Colorecta-60318
24. http://www.cancer.gov/about-cancer/treatment/drugs/fda-cetuximab#Anchor-Colorecta-60318
25. Vogelstein B, Fearon ER, Hamilton SR, Kern SE, Preisinger AC, Leppert M, et al. Genetic alterations during colorectal-tumor development. N Engl J Med. 1988;319:525-32.
26. Fearon ER, Vogelstein B. A genetic model for colorectal tumorigenesis. Cell. 1990;61:759-67.
27. Saif MW, Chu E. Biology of colorectal cancer. Cancer J. 2010;16:196-201.
28. Rowan AJ, Lamlum H, Ilyas M, Wheeler J, Straub J, Papadopoulou A, et al. APC mutations in sporadic colorectal tumors: A mutational "hotspot" and interdependence of the "two hits". Proc Natl Acad Sci U S A. 2000;97:3352-7.
29. Bienz M. beta-Catenin: a pivot between cell adhesion and Wnt signalling. Curr Biol. 2005;15:R64-7.
30. Yuen ST, Davies H, Chan TL, Ho JW, Bignell GR, Cox C, et al. Similarity of the phenotypic patterns associated with BRAF and KRAS mutations in colorectal neoplasia. Cancer Res. 2002;62:6451-5.
31. Liu P, Cheng H, Roberts TM, Zhao JJ. Targeting the phosphoinositide 3-kinase pathway in cancer. Nat Rev Drug Discov. 2009;8:627-44.
32. Vanhaesebroeck B, Guillermet-Guibert J, Graupera M, Bilanges B. The emerging mechanisms of isoform-specific PI3K signalling. Nat Rev Mol Cell Biol. 2010;11:329-41.
33. Budinska E, Popovici V, Tejpar S, D'Ario G, Lapique N, Sikora KO, et al. Gene expression patterns unveil a new level of molecular heterogeneity in colorectal cancer. J Pathol. 2013;231:63-76.
34. Linnekamp JF, Wang X, Medema JP, Vermeulen L. Colorectal cancer heterogeneity and targeted therapy: a case for molecular disease subtypes. Cancer Res. 2015;75:245-9.
35. Ferlay J, Soerjomataram I, Ervik M, Dikshit R, Eser S, Mathers C, Rebelo M, Parkin DM, Forman D, Bray, F. GLOBOCAN 2012 v1.1, Cancer Incidence and Mortality

Worldwide: IARC CancerBase No. 11 [Internet]. Lyon, France: International Agency for Research on Cancer; 2014. Available from: http://globocan.iarc.fr, accessed on 16/01/2015.
36. Travis WD. Lung tumours with neuroendocrine differentiation. Eur J Cancer. 2009;45 Suppl 1:251-66.
37. van Meerbeeck JP, Fennell DA, De Ruysscher DK. Small-cell lung cancer. Lancet. 2011;378:1741-55.
38. Devesa SS, Bray F, Vizcaino AP, Parkin DM. International lung cancer trends by histologic type: male:female differences diminishing and adenocarcinoma rates rising. Int J Cancer. 2005;117:294-9.
39. Antony GK, Bertino E, Franklin M, Otterson GA, Dudek AZ. Small cell lung cancer in never smokers: report of two cases. J Thorac Oncol. 2010;5:747-8.
40. Cancer Treatment Centers of America. Small cell lung cancer risk factors 2014 [cited 2014 June 25]; Available from: http://www.cancercenter.com/lung-cancer/risk-factors/tab/small-cell-lung-cancer-risk-factors/.
41. Thatcher N, Faivre-Finn C, Lorigan P. Management of small-cell lung cancer. Ann Oncol. 2005;16 Suppl 2:ii235-9.
42. Hansen HH, Dombernowsky P, Hirsch FR. Staging procedures and prognostic features in small cell anaplastic bronchogenic carcinoma. Seminars in oncology. 1978;5:280-7.
43. http://www.cancer.org/cancer/lungcancer-smallcell/detailedguide/small-cell-lung-cancer-treating-surgery
44. Kato Y, Ferguson TB, Bennett DE, Burford TH. Oat cell carcinoma of the lung. A review of 138 cases. Cancer. 1969;23:517-24.
45. http://www.cancerresearchuk.org/about-cancer/type/lung-cancer/treatment/radiotherapy/radiotherapy-for-small-cell-lung-cancer
46. Knox RJ, Friedlos F, Lydall DA, Roberts JJ. Mechanism of cytotoxicity of anticancer platinum drugs: evidence that cis-diamminedichloroplatinum(II) and cis-diammine-(1,1-cyclobutanedicarboxylato)platinum(II) differ only in the kinetics of their interaction with DNA. Cancer Res. 1986;46:1972-9.
47. Hande KR. Etoposide: four decades of development of a topoisomerase II inhibitor. Eur J Cancer. 1998;34:1514-21.
48. Lally BE, Urbanic JJ, Blackstock AW, Miller AA, Perry MC. Small cell lung cancer: have we made any progress over the last 25 years? Oncologist. 2007;12:1096-104.
49. http://www.cancer.org/cancer/lungcancer-smallcell/detailedguide/small-cell-lung-cancer-survival-rates
50. Eisenhauer EA, Therasse P, Bogaerts J, Schwartz LH, Sargent D, Ford R, et al. New response evaluation criteria in solid tumours: revised RECIST guideline (version 1.1). Eur J Cancer. 2009;45:228-47.
51. De Ruysscher D, Pijls-Johannesma M, Bentzen SM, Minken A, Wanders R, Lutgens L, et al. Time between the first day of chemotherapy and the last day of chest radiation is the most important predictor of survival in limited-disease small-cell lung cancer. J Clin Oncol. 2006;24:1057-63.
52. Stewart DJ. Mechanisms of resistance to cisplatin and carboplatin. Critical reviews in oncology/hematology. 2007;63:12-31.

53. Karran P, Bignami M. DNA damage tolerance, mismatch repair and genome instability. BioEssays : news and reviews in molecular, cellular and developmental biology. 1994;16:833-9.
54. Achanzar WE, Webber MM, Waalkes MP. Altered apoptotic gene expression and acquired apoptotic resistance in cadmium-transformed human prostate epithelial cells. The Prostate. 2002;52:236-44.
55. Salvesen GS, Riedl SJ. Caspase mechanisms. Advances in experimental medicine and biology. 2008;615:13-23.
56. Wang S. Design of small-molecule Smac mimetics as IAP antagonists. Current topics in microbiology and immunology. 2011;348:89-113.
57. Nomura T, Yamasaki M, Nomura Y, Mimata H. Expression of the inhibitors of apoptosis proteins in cisplatin-resistant prostate cancer cells. Oncology reports. 2005;14:993-7.
58. Yang X, Xing H, Gao Q, Chen G, Lu Y, Wang S, et al. Regulation of HtrA2/Omi by X-linked inhibitor of apoptosis protein in chemoresistance in human ovarian cancer cells. Gynecologic oncology. 2005;97:413-21.
59. Thomas H, Coley HM. Overcoming multidrug resistance in cancer: an update on the clinical strategy of inhibiting p-glycoprotein. Cancer Control. 2003;10:159-65.
60. Clinicaltrials.gov
61. Fujii M, Hotta K, Takigawa N, Hisamoto A, Ichihara E, Tabata M, et al. Influence of the timing of tumor regression after the initiation of chemoradiotherapy on prognosis in patients with limited-disease small-cell lung cancer achieving objective response. Lung Cancer. 2012;78:107-11.
62. Huisman C, Postmus PE, Giaccone G, Smit EF. Second-line chemotherapy and its evaluation in small cell lung cancer. Cancer Treat Rev. 1999;25:199-206.
63. Seifter EJ, Ihde DC. Therapy of small cell lung cancer: a perspective on two decades of clinical research. Seminars in oncology. 1988;15:278-99.
64. Greaves M, Maley CC. Clonal evolution in cancer. Nature. 2012;481:306-13.
65. Stewart DJ. Tumor and host factors that may limit efficacy of chemotherapy in non-small cell and small cell lung cancer. Critical reviews in oncology/hematology. 2010;75:173-234.
66. Peifer M, Fernandez-Cuesta L, Sos ML, George J, Seidel D, Kasper LH, et al. Integrative genome analyses identify key somatic driver mutations of small-cell lung cancer. Nat Genet. 2012;44:1104-10.
67. Rudin CM, Durinck S, Stawiski EW, Poirier JT, Modrusan Z, Shames DS, et al. Comprehensive genomic analysis identifies SOX2 as a frequently amplified gene in small-cell lung cancer. Nat Genet. 2012;44:1111-6.
68. authors Alo, affiliations appears at the end of the p. Comprehensive genomic profiles of small cell lung cancer. Nature. 2015.
69. Umemura S, Mimaki S, Makinoshima H, Tada S, Ishii G, Ohmatsu H, et al. Therapeutic priority of the PI3K/AKT/mTOR pathway in small cell lung cancers as revealed by a comprehensive genomic analysis. J Thorac Oncol. 2014;9:1324-31.
70. Watson IR, Takahashi K, Futreal PA, Chin L. Emerging patterns of somatic mutations in cancer. Nat Rev Genet. 2013;14:703-18.
71. Pleasance ED, Stephens PJ, O'Meara S, McBride DJ, Meynert A, Jones D, et al. A small-cell lung cancer genome with complex signatures of tobacco exposure. Nature. 2010;463:184-90.

72. Wistuba, II, Gazdar AF, Minna JD. Molecular genetics of small cell lung carcinoma. Semin Oncol. 2001;28:3-13.
73. Mori N, Yokota J, Akiyama T, Sameshima Y, Okamoto A, Mizoguchi H, et al. Variable mutations of the RB gene in small-cell lung carcinoma. Oncogene. 1990;5:1713-7.
74. Yokomizo A, Tindall DJ, Drabkin H, Gemmill R, Franklin W, Yang P, et al. PTEN/MMAC1 mutations identified in small cell, but not in non-small cell lung cancers. Oncogene. 1998;17:475-9.
75. Gao J, Aksoy BA, Dogrusoz U, Dresdner G, Gross B, Sumer SO, et al. Integrative analysis of complex cancer genomics and clinical profiles using the cBioPortal. Sci Signal. 2013;6:pl1.
76. Cerami E, Gao J, Dogrusoz U, Gross BE, Sumer SO, Aksoy BA, et al. The cBio cancer genomics portal: an open platform for exploring multidimensional cancer genomics data. Cancer discovery. 2012;2:401-4.
77. Marte B. Tumour heterogeneity. Nature. 2013;501:327.
78. Burrell RA, McGranahan N, Bartek J, Swanton C. The causes and consequences of genetic heterogeneity in cancer evolution. Nature. 2013;501:338-45.
79. Chan BA, Coward JI. Chemotherapy advances in small-cell lung cancer. Journal of thoracic disease. 2013;5 Suppl 5:S565-78.
80. http://www.cancer.org/cancer/lungcancer-smallcell/detailedguide/small-cell-lung-cancer-treating-surgery
81. Meuwissen R, Linn SC, Linnoila RI, Zevenhoven J, Mooi WJ, Berns A. Induction of small cell lung cancer by somatic inactivation of both Trp53 and Rb1 in a conditional mouse model. Cancer Cell. 2003;4:181-9.
82. Cui M, Augert A, Rongione M, Conkrite K, Parazzoli S, Nikitin AY, et al. PTEN is a potent suppressor of small cell lung cancer. Mol Cancer Res. 2014;12:654-9.
83. Hodgkinson CL, Morrow CJ, Li Y, Metcalf RL, Rothwell DG, Trapani F, et al. Tumorigenicity and genetic profiling of circulating tumor cells in small-cell lung cancer. Nat Med. 2014.
84. Gardner EE, Connis N, Poirier JT, Cope L, Dobromilskaya I, Gallia GL, et al. Rapamycin rescues ABT-737 efficacy in small cell lung cancer. Cancer Res. 2014;74:2846-56.
85. Faber AC, Farago AF, Costa C, Dastur A, Gomez-Caraballo M, Robbins R, et al. Assessment of ABT-263 activity across a cancer cell line collection leads to a potent combination therapy for small-cell lung cancer. Proc Natl Acad Sci U S A. 2015;112:E1288-96.
86. Daniel VC, Marchionni L, Hierman JS, Rhodes JT, Devereux WL, Rudin CM, et al. A primary xenograft model of small-cell lung cancer reveals irreversible changes in gene expression imposed by culture in vitro. Cancer Res. 2009;69:3364-73.
87. Tahir SK, Yang X, Anderson MG, Morgan-Lappe SE, Sarthy AV, Chen J, et al. Influence of Bcl-2 family members on the cellular response of small-cell lung cancer cell lines to ABT-737. Cancer Res; 2007 Feb 1. p. 1176-83.
88. Shoemaker AR, Mitten MJ, Adickes J, Ackler S, Refici M, Ferguson D, et al. Activity of the Bcl-2 family inhibitor ABT-263 in a panel of small cell lung cancer xenograft models. Clin Cancer Res. 2008;14:3268-77.
89. Rudin CM, Hann CL, Garon EB, Ribeiro de Oliveira M, Bonomi PD, Camidge DR, et al. Phase II study of single-agent navitoclax (ABT-263) and biomarker correlates in patients with relapsed small cell lung cancer. Clin Cancer Res. 2012;18:3163-9.

90. Schaffer BE, Park KS, Yiu G, Conklin JF, Lin C, Burkhart DL, et al. Loss of p130 accelerates tumor development in a mouse model for human small-cell lung carcinoma. Cancer Res. 2010;70:3877-83.
91. McFadden DG, Papagiannakopoulos T, Taylor-Weiner A, Stewart C, Carter SL, Cibulskis K, et al. Genetic and clonal dissection of murine small cell lung carcinoma progression by genome sequencing. Cell. 2014;156:1298-311.
92. Christensen CL, Kwiatkowski N, Abraham BJ, Carretero J, Al-Shahrour F, Zhang T, et al. Targeting transcriptional addictions in small cell lung cancer with a covalent CDK7 inhibitor. Cancer Cell. 2014;26:909-22.
93. Gazdar AF, Savage TK, Johnson JE, Berns A, Sage J, Linnoila RI, et al. The comparative pathology of genetically engineered mouse models for neuroendocrine carcinomas of the lung. J Thorac Oncol. 2015;10:553-64.
94. Richmond A, Su Y. Mouse xenograft models vs GEM models for human cancer therapeutics. Dis Model Mech. 2008;1:78-82.
95. Pandita A, Aldape KD, Zadeh G, Guha A, James CD. Contrasting in vivo and in vitro fates of glioblastoma cell subpopulations with amplified EGFR. Genes Chromosomes Cancer. 2004;39:29-36.
96. Rubio-Viqueira B, Jimeno A, Cusatis G, Zhang X, Iacobuzio-Donahue C, Karikari C, et al. An in vivo platform for translational drug development in pancreatic cancer. Clin Cancer Res. 2006;12:4652-61.
97. Dalerba P, Dylla SJ, Park IK, Liu R, Wang X, Cho RW, et al. Phenotypic characterization of human colorectal cancer stem cells. Proc Natl Acad Sci U S A. 2007;104:10158-63.
98. Li C, Heidt DG, Dalerba P, Burant CF, Zhang L, Adsay V, et al. Identification of pancreatic cancer stem cells. Cancer Res. 2007;67:1030-7.
99. Beniers AJ, Peelen WP, Schaafsma HE, Beck JL, Ramaekers FC, Debruyne FM, et al. Establishment and characterization of five new human renal tumor xenografts. Am J Pathol. 1992;140:483-95.
100. Beniers AJ, van Moorselaar RJ, Peelen WP, Debruyne FM, Schalken JA. Differential sensitivity of renal cell carcinoma xenografts towards therapy with interferon-alpha, interferon-gamma, tumor necrosis factor and their combinations. Urological research. 1991;19:91-8.
101. Engelman JA. Targeting PI3K signalling in cancer: opportunities, challenges and limitations. Nat Rev Cancer. 2009;9:550-62.
102. Dominguez V, Raimondi C, Somanath S, Bugliani M, Loder MK, Edling CE, et al. Class II phosphoinositide 3-kinase regulates exocytosis of insulin granules in pancreatic beta cells. J Biol Chem. 2011;286:4216-25.
103. Engelman JA, Luo J, Cantley LC. The evolution of phosphatidylinositol 3-kinases as regulators of growth and metabolism. Nat Rev Genet. 2006;7:606-19.
104. Vogt PK. PI 3-kinase, mTOR, protein synthesis and cancer. Trends Mol Med. 2001;7:482-4.
105. Huang CH, Mandelker D, Gabelli SB, Amzel LM. Insights into the oncogenic effects of PIK3CA mutations from the structure of p110alpha/p85alpha. Cell Cycle. 2008;7:1151-6.
106. Murillo MM, Zelenay S, Nye E, Castellano E, Lassailly F, Stamp G, et al. RAS interaction with PI3K p110alpha is required for tumor-induced angiogenesis. J Clin Invest. 2014;124:3601-11.

107. Fruman DA, Meyers RE, Cantley LC. Phosphoinositide kinases. Annu Rev Biochem. 1998;67:481-507.
108. Koyama S, Yu H, Dalgarno DC, Shin TB, Zydowsky LD, Schreiber SL. Structure of the PI3K SH3 domain and analysis of the SH3 family. Cell. 1993;72:945-52.
109. Katso R, Okkenhaug K, Ahmadi K, White S, Timms J, Waterfield MD. Cellular function of phosphoinositide 3-kinases: implications for development, homeostasis, and cancer. Annu Rev Cell Dev Biol. 2001;17:615-75.
110. Vivanco I, Sawyers CL. The phosphatidylinositol 3-Kinase AKT pathway in human cancer. Nat Rev Cancer. 2002;2:489-501.
111. Ong SH, Hadari YR, Gotoh N, Guy GR, Schlessinger J, Lax I. Stimulation of phosphatidylinositol 3-kinase by fibroblast growth factor receptors is mediated by coordinated recruitment of multiple docking proteins. Proc Natl Acad Sci U S A. 2001;98:6074-9.
112. Pawson T. Specificity in signal transduction: from phosphotyrosine-SH2 domain interactions to complex cellular systems. Cell. 2004;116:191-203.
113. Buday L, Downward J. Epidermal growth factor regulates p21ras through the formation of a complex of receptor, Grb2 adapter protein, and Sos nucleotide exchange factor. Cell. 1993;73:611-20.
114. Castellano E, Downward J. RAS Interaction with PI3K: More Than Just Another Effector Pathway. Genes & cancer. 2011;2:261-74.
115. Milella M, Falcone I, Conciatori F, Cesta Incani U, Del Curatolo A, Inzerilli N, et al. PTEN: Multiple Functions in Human Malignant Tumors. Frontiers in oncology. 2015;5:24.
116. Helgason CD, Kalberer CP, Damen JE, Chappel SM, Pineault N, Krystal G, et al. A dual role for Src homology 2 domain-containing inositol-5-phosphatase (SHIP) in immunity: aberrant development and enhanced function of b lymphocytes in ship -/- mice. J Exp Med. 2000;191:781-94.
117. Scheid MP, Huber M, Damen JE, Hughes M, Kang V, Neilsen P, et al. Phosphatidylinositol (3,4,5)P3 is essential but not sufficient for protein kinase B (PKB) activation; phosphatidylinositol (3,4)P2 is required for PKB phosphorylation at Ser-473: studies using cells from SH2-containing inositol-5-phosphatase knockout mice. J Biol Chem. 2002;277:9027-35.
118. Ericson K, Gan C, Cheong I, Rago C, Samuels Y, Velculescu VE, et al. Genetic inactivation of AKT1, AKT2, and PDPK1 in human colorectal cancer cells clarifies their roles in tumor growth regulation. Proc Natl Acad Sci U S A. 2010;107:2598-603.
119. Chen WS, Xu PZ, Gottlob K, Chen ML, Sokol K, Shiyanova T, et al. Growth retardation and increased apoptosis in mice with homozygous disruption of the Akt1 gene. Genes Dev. 2001;15:2203-8.
120. Cho H, Thorvaldsen JL, Chu Q, Feng F, Birnbaum MJ. Akt1/PKBalpha is required for normal growth but dispensable for maintenance of glucose homeostasis in mice. J Biol Chem. 2001;276:38349-52.
121. Garofalo RS, Orena SJ, Rafidi K, Torchia AJ, Stock JL, Hildebrandt AL, et al. Severe diabetes, age-dependent loss of adipose tissue, and mild growth deficiency in mice lacking Akt2/PKB beta. J Clin Invest. 2003;112:197-208.
122. Calleja V, Laguerre M, de Las Heras-Martinez G, Parker PJ, Requejo-Isidro J, Larijani B. Acute regulation of PDK1 by a complex interplay of molecular switches. Biochem Soc Trans. 2014;42:1435-40.

123. Alessi DR, Deak M, Casamayor A, Caudwell FB, Morrice N, Norman DG, et al. 3-Phosphoinositide-dependent protein kinase-1 (PDK1): structural and functional homology with the Drosophila DSTPK61 kinase. Curr Biol. 1997;7:776-89.
124. Stephens L, Anderson K, Stokoe D, Erdjument-Bromage H, Painter GF, Holmes AB, et al. Protein kinase B kinases that mediate phosphatidylinositol 3,4,5-trisphosphate-dependent activation of protein kinase B. Science. 1998;279:710-4.
125. Sarbassov DD, Guertin DA, Ali SM, Sabatini DM. Phosphorylation and regulation of Akt/PKB by the rictor-mTOR complex. Science. 2005;307:1098-101.
126. Frias MA, Thoreen CC, Jaffe JD, Schroder W, Sculley T, Carr SA, et al. mSin1 is necessary for Akt/PKB phosphorylation, and its isoforms define three distinct mTORC2s. Curr Biol. 2006;16:1865-70.
127. Jacinto E, Facchinetti V, Liu D, Soto N, Wei S, Jung SY, et al. SIN1/MIP1 maintains rictor-mTOR complex integrity and regulates Akt phosphorylation and substrate specificity. Cell. 2006;127:125-37.
128. Pearce LR, Huang X, Boudeau J, Pawlowski R, Wullschleger S, Deak M, et al. Identification of Protor as a novel Rictor-binding component of mTOR complex-2. Biochem J. 2007;405:513-22.
129. Thedieck K, Polak P, Kim ML, Molle KD, Cohen A, Jeno P, et al. PRAS40 and PRR5-like protein are new mTOR interactors that regulate apoptosis. PLoS One. 2007;2:e1217.
130. Woo SY, Kim DH, Jun CB, Kim YM, Haar EV, Lee SI, et al. PRR5, a novel component of mTOR complex 2, regulates platelet-derived growth factor receptor beta expression and signaling. J Biol Chem. 2007;282:25604-12.
131. Zinzalla V, Stracka D, Oppliger W, Hall MN. Activation of mTORC2 by association with the ribosome. Cell. 2011;144:757-68.
132. Yang WL, Wang J, Chan CH, Lee SW, Campos AD, Lamothe B, et al. The E3 ligase TRAF6 regulates Akt ubiquitination and activation. Science. 2009;325:1134-8.
133. Datta SR, Dudek H, Tao X, Masters S, Fu H, Gotoh Y, et al. Akt phosphorylation of BAD couples survival signals to the cell-intrinsic death machinery. Cell. 1997;91:231-41.
134. Maurer U, Charvet C, Wagman AS, Dejardin E, Green DR. Glycogen synthase kinase-3 regulates mitochondrial outer membrane permeabilization and apoptosis by destabilization of MCL-1. Mol Cell. 2006;21:749-60.
135. Diehl JA, Cheng M, Roussel MF, Sherr CJ. Glycogen synthase kinase-3beta regulates cyclin D1 proteolysis and subcellular localization. Genes Dev. 1998;12:3499-511.
136. Cardone MH, Roy N, Stennicke HR, Salvesen GS, Franke TF, Stanbridge E, et al. Regulation of cell death protease caspase-9 by phosphorylation. Science. 1998;282:1318-21.
137. Brunet A, Bonni A, Zigmond MJ, Lin MZ, Juo P, Hu LS, et al. Akt promotes cell survival by phosphorylating and inhibiting a Forkhead transcription factor. Cell. 1999;96:857-68.
138. Mayo LD, Donner DB. A phosphatidylinositol 3-kinase/Akt pathway promotes translocation of Mdm2 from the cytoplasm to the nucleus. Proc Natl Acad Sci U S A. 2001;98:11598-603.
139. Zhou BP, Liao Y, Xia W, Zou Y, Spohn B, Hung MC. HER-2/neu induces p53 ubiquitination via Akt-mediated MDM2 phosphorylation. Nat Cell Biol. 2001;3:973-82.
140. Liu C, Li Y, Semenov M, Han C, Baeg GH, Tan Y, et al. Control of beta-catenin phosphorylation/degradation by a dual-kinase mechanism. Cell. 2002;108:837-47.

141. Graff JR, Konicek BW, McNulty AM, Wang Z, Houck K, Allen S, et al. Increased AKT activity contributes to prostate cancer progression by dramatically accelerating prostate tumor growth and diminishing p27Kip1 expression. J Biol Chem. 2000;275:24500-5.
142. Guertin DA, Sabatini DM. Defining the role of mTOR in cancer. Cancer Cell. 2007;12:9-22.
143. Peterson TR, Laplante M, Thoreen CC, Sancak Y, Kang SA, Kuehl WM, et al. DEPTOR is an mTOR inhibitor frequently overexpressed in multiple myeloma cells and required for their survival. Cell. 2009;137:873-86.
144. Avruch J, Long X, Lin Y, Ortiz-Vega S, Rapley J, Papageorgiou A, et al. Activation of mTORC1 in two steps: Rheb-GTP activation of catalytic function and increased binding of substrates to raptor. Biochem Soc Trans. 2009;37:223-6.
145. Saucedo LJ, Gao X, Chiarelli DA, Li L, Pan D, Edgar BA. Rheb promotes cell growth as a component of the insulin/TOR signalling network. Nat Cell Biol. 2003;5:566-71.
146. Stocker H, Radimerski T, Schindelholz B, Wittwer F, Belawat P, Daram P, et al. Rheb is an essential regulator of S6K in controlling cell growth in Drosophila. Nat Cell Biol. 2003;5:559-65.
147. Inoki K, Corradetti MN, Guan KL. Dysregulation of the TSC-mTOR pathway in human disease. Nat Genet. 2005;37:19-24.
148. Nascimento EB, Ouwens DM. PRAS40: target or modulator of mTORC1 signalling and insulin action? Arch Physiol Biochem. 2009;115:163-75.
149. Gingras AC, Gygi SP, Raught B, Polakiewicz RD, Abraham RT, Hoekstra MF, et al. Regulation of 4E-BP1 phosphorylation: a novel two-step mechanism. Genes Dev. 1999;13:1422-37.
150. Gingras AC, Raught B, Gygi SP, Niedzwiecka A, Miron M, Burley SK, et al. Hierarchical phosphorylation of the translation inhibitor 4E-BP1. Genes Dev. 2001;15:2852-64.
151. Letunic I, Doerks T, Bork P. SMART: recent updates, new developments and status in 2015. Nucleic acids research. 2015;43:D257-60.
152. Schultz J, Milpetz F, Bork P, Ponting CP. SMART, a simple modular architecture research tool: identification of signaling domains. Proc Natl Acad Sci U S A. 1998;95:5857-64.
153. Lemmon MA. Pleckstrin homology (PH) domains and phosphoinositides. Cell Biology of Inositol Lipids and Phosphates. 2007;74:81-93.
154. Samuels Y, Diaz LA, Jr., Schmidt-Kittler O, Cummins JM, Delong L, Cheong I, et al. Mutant PIK3CA promotes cell growth and invasion of human cancer cells. Cancer Cell. 2005;7:561-73.
155. Vasudevan KM, Barbie DA, Davies MA, Rabinovsky R, McNear CJ, Kim JJ, et al. AKT-independent signaling downstream of oncogenic PIK3CA mutations in human cancer. Cancer Cell. 2009;16:21-32.
156. Pearce LR, Komander D, Alessi DR. The nuts and bolts of AGC protein kinases. Nat Rev Mol Cell Biol. 2010;11:9-22.
157. Hart JR, Liao L, Yates JR, 3rd, Vogt PK. Essential role of Stat3 in PI3K-induced oncogenic transformation. Proc Natl Acad Sci U S A. 2011;108:13247-52.
158. Hart JR, Liao L, Ueno L, Yates JR, 3rd, Vogt PK. Protein expression profiles of C3H 10T1/2 murine fibroblasts and of isogenic cells transformed by the H1047R mutant of phosphoinositide 3-kinase (PI3K). Cell Cycle. 2011;10:971-6.

159. Qiu Y, Kung HJ. Signaling network of the Btk family kinases. Oncogene. 2000;19:5651-61.
160. Chott A, Sun Z, Morganstern D, Pan J, Li T, Susani M, et al. Tyrosine kinases expressed in vivo by human prostate cancer bone marrow metastases and loss of the type 1 insulin-like growth factor receptor. Am J Pathol. 1999;155:1271-9.
161. Rajantie I, Ekman N, Iljin K, Arighi E, Gunji Y, Kaukonen J, et al. Bmx tyrosine kinase has a redundant function downstream of angiopoietin and vascular endothelial growth factor receptors in arterial endothelium. Mol Cell Biol. 2001;21:4647-55.
162. Jarboe JS, Dutta S, Velu SE, Willey CD. Mini-review: bmx kinase inhibitors for cancer therapy. Recent patents on anti-cancer drug discovery. 2013;8:228-38.
163. Ekman N, Arighi E, Rajantie I, Saharinen P, Ristimaki A, Silvennoinen O, et al. The Bmx tyrosine kinase is activated by IL-3 and G-CSF in a PI-3K dependent manner. Oncogene. 2000;19:4151-8.
164. Qiu Y, Robinson D, Pretlow TG, Kung HJ. Etk/Bmx, a tyrosine kinase with a pleckstrin-homology domain, is an effector of phosphatidylinositol 3'-kinase and is involved in interleukin 6-induced neuroendocrine differentiation of prostate cancer cells. Proc Natl Acad Sci U S A. 1998;95:3644-9.
165. Chen R, Kim O, Li M, Xiong X, Guan JL, Kung HJ, et al. Regulation of the PH-domain-containing tyrosine kinase Etk by focal adhesion kinase through the FERM domain. Nat Cell Biol. 2001;3:439-44.
166. Chen S, Jiang X, Gewinner CA, Asara JM, Simon NI, Cai C, et al. Tyrosine Kinase BMX Phosphorylates Phosphotyrosine-Primed Motif Mediating the Activation of Multiple Receptor Tyrosine Kinases. Sci Signal. 2013;6:ra40.
167. Takesono A, Finkelstein LD, Schwartzberg PL. Beyond calcium: new signaling pathways for Tec family kinases. J Cell Sci. 2002;115:3039-48.
168. Jiang T, Guo Z, Dai B, Kang M, Ann DK, Kung HJ, et al. Bi-directional regulation between tyrosine kinase Etk/BMX and tumor suppressor p53 in response to DNA damage. J Biol Chem. 2004;279:50181-9.
169. Kim O, Yang J, Qiu Y. Selective activation of small GTPase RhoA by tyrosine kinase Etk through its pleckstrin homology domain. J Biol Chem. 2002;277:30066-71.
170. Bagheri-Yarmand R, Mandal M, Taludker AH, Wang RA, Vadlamudi RK, Kung HJ, et al. Etk/Bmx tyrosine kinase activates Pak1 and regulates tumorigenicity of breast cancer cells. J Biol Chem. 2001;276:29403-9.
171. Chau CH, Chen KY, Deng HT, Kim KJ, Hosoya K, Terasaki T, et al. Coordinating Etk/Bmx activation and VEGF upregulation to promote cell survival and proliferation. Oncogene. 2002;21:8817-29.
172. Xue LY, Qiu Y, He J, Kung HJ, Oleinick NL. Etk/Bmx, a PH-domain containing tyrosine kinase, protects prostate cancer cells from apoptosis induced by photodynamic therapy or thapsigargin. Oncogene. 1999;18:3391-8.
173. Guo L, Chen P, Zhou Y, Sun Y. Non-receptor tyrosine kinase Etk is involved in the apoptosis of small cell lung cancer cells. Exp Mol Pathol. 2010;88:401-6.
174. Guo L, Zhou Y, Sun Y, Zhang F. Non-receptor tyrosine kinase Etk regulation of drug resistance in small-cell lung cancer. Eur J Cancer. 2010;46:636-41.
175. Guo S, Sun F, Guo Z, Li W, Alfano A, Chen H, et al. Tyrosine kinase ETK/BMX is up-regulated in bladder cancer and predicts poor prognosis in patients with cystectomy. PLoS One. 2011;6:e17778.

176. Samuels Y, Wang Z, Bardelli A, Silliman N, Ptak J, Szabo S, et al. High frequency of mutations of the PIK3CA gene in human cancers. Science. 2004;304:554.
177. Thomas RK, Baker AC, Debiasi RM, Winckler W, Laframboise T, Lin WM, et al. High-throughput oncogene mutation profiling in human cancer. Nat Genet. 2007;39:347-51.
178. Walls M, Baxi SM, Mehta PP, Liu KK, Zhu J, Estrella H, et al. Targeting small cell lung cancer harboring PIK3CA mutation with a selective oral PI3K inhibitor PF-4989216. Clin Cancer Res. 2014;20:631-43.
179. Bader AG, Kang S, Zhao L, Vogt PK. Oncogenic PI3K deregulates transcription and translation. Nat Rev Cancer. 2005;5:921-9.
180. Forbes SA, Beare D, Gunasekaran P, Leung K, Bindal N, Boutselakis H, et al. COSMIC: exploring the world's knowledge of somatic mutations in human cancer. Nucleic acids research. 2015;43:D805-11.
181. Lee JY, Engelman JA, Cantley LC. Biochemistry. PI3K charges ahead. Science. 2007;317:206-7.
182. Miled N, Yan Y, Hon WC, Perisic O, Zvelebil M, Inbar Y, et al. Mechanism of two classes of cancer mutations in the phosphoinositide 3-kinase catalytic subunit. Science. 2007;317:239-42.
183. Zhao L, Vogt PK. Helical domain and kinase domain mutations in p110alpha of phosphatidylinositol 3-kinase induce gain of function by different mechanisms. Proc Natl Acad Sci U S A. 2008;105:2652-7.
184. Berenjeno IM, Vanhaesebroeck B. PI3K regulatory subunits lose control in cancer. Cancer Cell. 2009;16:449-50.
185. Jaiswal BS, Janakiraman V, Kljavin NM, Chaudhuri S, Stern HM, Wang W, et al. Somatic mutations in p85alpha promote tumorigenesis through class IA PI3K activation. Cancer Cell. 2009;16:463-74.
186. Huang CH, Mandelker D, Schmidt-Kittler O, Samuels Y, Velculescu VE, Kinzler KW, et al. The structure of a human p110alpha/p85alpha complex elucidates the effects of oncogenic PI3Kalpha mutations. Science. 2007;318:1744-8.
187. Philp AJ, Campbell IG, Leet C, Vincan E, Rockman SP, Whitehead RH, et al. The phosphatidylinositol 3'-kinase p85alpha gene is an oncogene in human ovarian and colon tumors. Cancer Res. 2001;61:7426-9.
188. Yuan TL, Cantley LC. PI3K pathway alterations in cancer: variations on a theme. Oncogene. 2008;27:5497-510.
189. Abubaker J, Bavi P, Al-Harbi S, Ibrahim M, Siraj AK, Al-Sanea N, et al. Clinicopathological analysis of colorectal cancers with PIK3CA mutations in Middle Eastern population. Oncogene. 2008;27:3539-45.
190. Jhawer M, Goel S, Wilson AJ, Montagna C, Ling YH, Byun DS, et al. PIK3CA mutation/PTEN expression status predicts response of colon cancer cells to the epidermal growth factor receptor inhibitor cetuximab. Cancer Res. 2008;68:1953-61.
191. Ollikainen M, Gylling A, Puputti M, Nupponen NN, Abdel-Rahman WM, Butzow R, et al. Patterns of PIK3CA alterations in familial colorectal and endometrial carcinoma. Int J Cancer. 2007;121:915-20.
192. Planchon SM, Waite KA, Eng C. The nuclear affairs of PTEN. J Cell Sci. 2008;121:249-53.
193. Jensen RB, Carreira A, Kowalczykowski SC. Purified human BRCA2 stimulates RAD51-mediated recombination. Nature. 2010;467:678-83.

194. Chen ZH, Zhu M, Yang J, Liang H, He J, He S, et al. PTEN interacts with histone H1 and controls chromatin condensation. Cell reports. 2014;8:2003-14.
195. Trotman LC, Pandolfi PP. PTEN and p53: who will get the upper hand? Cancer Cell. 2003;3:97-9.
196. Ferlay J, Shin HR, Bray F, Forman D, Mathers C, Parkin DM. Estimates of worldwide burden of cancer in 2008: GLOBOCAN 2008. Int J Cancer. 2010;127:2893-917.
197. Parsons DW, Wang TL, Samuels Y, Bardelli A, Cummins JM, DeLong L, et al. Colorectal cancer: mutations in a signalling pathway. Nature. 2005;436:792.
198. Rychahou PG, Kang J, Gulhati P, Doan HQ, Chen LA, Xiao SY, et al. Akt2 overexpression plays a critical role in the establishment of colorectal cancer metastasis. Proc Natl Acad Sci U S A. 2008;105:20315-20.
199. Carpten JD, Faber AL, Horn C, Donoho GP, Briggs SL, Robbins CM, et al. A transforming mutation in the pleckstrin homology domain of AKT1 in cancer. Nature. 2007;448:439-44.
200. Seshagiri S, Stawiski EW, Durinck S, Modrusan Z, Storm EE, Conboy CB, et al. Recurrent R-spondin fusions in colon cancer. Nature. 2012;488:660-4.
201. Cancer Genome Atlas N. Comprehensive molecular characterization of human colon and rectal cancer. Nature. 2012;487:330-7.
202. Brannon AR, Vakiani E, Sylvester BE, Scott SN, McDermott G, Shah RH, et al. Comparative sequencing analysis reveals high genomic concordance between matched primary and metastatic colorectal cancer lesions. Genome biology. 2014;15:454.
203. Reva B, Antipin Y, Sander C. Predicting the functional impact of protein mutations: application to cancer genomics. Nucleic acids research. 2011;39:e118.
204. Adzhubei IA, Schmidt S, Peshkin L, Ramensky VE, Gerasimova A, Bork P, et al. A method and server for predicting damaging missense mutations. Nature methods. 2010;7:248-9.
205. Grasso CS, Wu YM, Robinson DR, Cao X, Dhanasekaran SM, Khan AP, et al. The mutational landscape of lethal castration-resistant prostate cancer. Nature. 2012;487:239-43.
206. The results <published or shown> here are in whole or part based upon data generated by the TCGA Research Network: http://cancergenome.nih.gov/
207. Arcaro A, Wymann MP. Wortmannin is a potent phosphatidylinositol 3-kinase inhibitor: the role of phosphatidylinositol 3,4,5-trisphosphate in neutrophil responses. Biochem J. 1993;296 (Pt 2):297-301.
208. Vlahos CJ, Matter WF, Hui KY, Brown RF. A specific inhibitor of phosphatidylinositol 3-kinase, 2-(4-morpholinyl)-8-phenyl-4H-1-benzopyran-4-one (LY294002). J Biol Chem. 1994;269:5241-8.
209. Knight ZA, Shokat KM. Chemically targeting the PI3K family. Biochem Soc Trans. 2007;35:245-9.
210. Marone R, Cmiljanovic V, Giese B, Wymann MP. Targeting phosphoinositide 3-kinase: moving towards therapy. Biochim Biophys Acta. 2008;1784:159-85.
211. Hayakawa M, Kaizawa H, Kawaguchi K, Ishikawa N, Koizumi T, Ohishi T, et al. Synthesis and biological evaluation of imidazo[1,2-a]pyridine derivatives as novel PI3 kinase p110alpha inhibitors. Bioorg Med Chem. 2007;15:403-12.
212. clinicaltrials.gov
213. Maira SM, Stauffer F, Brueggen J, Furet P, Schnell C, Fritsch C, et al. Identification and characterization of NVP-BEZ235, a new orally available dual phosphatidylinositol 3-

kinase/mammalian target of rapamycin inhibitor with potent in vivo antitumor activity. Mol Cancer Ther. 2008;7:1851-63.
214. Serra V, Markman B, Scaltriti M, Eichhorn PJ, Valero V, Guzman M, et al. NVP-BEZ235, a dual PI3K/mTOR inhibitor, prevents PI3K signaling and inhibits the growth of cancer cells with activating PI3K mutations. Cancer Res. 2008;68:8022-30.
215. http://www.cancer.gov/about-cancer/treatment/drugs/fda-ibrutinib
216. Young RM, Staudt LM. Targeting pathological B cell receptor signalling in lymphoid malignancies. Nat Rev Drug Discov. 2013;12:229-43.
217. Pan Z, Scheerens H, Li SJ, Schultz BE, Sprengeler PA, Burrill LC, et al. Discovery of selective irreversible inhibitors for Bruton's tyrosine kinase. ChemMedChem. 2007;2:58-61.
218. Honigberg LA, Smith AM, Sirisawad M, Verner E, Loury D, Chang B, et al. The Bruton tyrosine kinase inhibitor PCI-32765 blocks B-cell activation and is efficacious in models of autoimmune disease and B-cell malignancy. Proc Natl Acad Sci U S A. 2010;107:13075-80.
219. Sadhu C, Dick K, Tino WT, Staunton DE. Selective role of PI3K delta in neutrophil inflammatory responses. Biochem Biophys Res Commun. 2003;308:764-9.
220. Doukas J, Wrasidlo W, Noronha G, Dneprovskaia E, Fine R, Weis S, et al. Phosphoinositide 3-kinase gamma/delta inhibition limits infarct size after myocardial ischemia/reperfusion injury. Proc Natl Acad Sci U S A. 2006;103:19866-71.
221. Kong D, Yamori T. ZSTK474 is an ATP-competitive inhibitor of class I phosphatidylinositol 3 kinase isoforms. Cancer Sci. 2007;98:1638-42.
222. Shapiro GI, Edelman G, Calvo E, Aggarwal SK, Laird AD. Targeting aberrant PI3K pathway signaling with XL147, a potent, selective and orally bioavailable PI3K inhibitor. Molecular Cancer Therapeutics. 2007;6:3594s-s.
223. Raynaud FI, Eccles S, Clarke PA, Hayes A, Nutley B, Alix S, et al. Pharmacologic characterization of a potent inhibitor of class I phosphatidylinositide 3-kinases. Cancer Res. 2007;67:5840-50.
224. Raynaud FI, Eccles SA, Patel S, Alix S, Box G, Chuckowree I, et al. Biological properties of potent inhibitors of class I phosphatidylinositide 3-kinases: from PI-103 through PI-540, PI-620 to the oral agent GDC-0941. Mol Cancer Ther. 2009;8:1725-38.
225. clinicaltrials.gov
226. Wyllie AH. Apoptosis: an overview. Br Med Bull. 1997;53:451-65.
227. Kerr JF, Wyllie AH, Currie AR. Apoptosis: a basic biological phenomenon with wide-ranging implications in tissue kinetics. Br J Cancer. 1972;26:239-57.
228. Fadok VA, Bratton DL, Rose DM, Pearson A, Ezekewitz RA, Henson PM. A receptor for phosphatidylserine-specific clearance of apoptotic cells. Nature. 2000;405:85-90.
229. Li P, Nijhawan D, Budihardjo I, Srinivasula SM, Ahmad M, Alnemri ES, et al. Cytochrome c and dATP-dependent formation of Apaf-1/caspase-9 complex initiates an apoptotic protease cascade. Cell. 1997;91:479-89.
230. Savill J, Fadok V. Corpse clearance defines the meaning of cell death. Nature. 2000;407:784-8.
231. Wang X. The expanding role of mitochondria in apoptosis. Genes Dev. 2001;15:2922-33.
232. Youle RJ, Strasser A. The BCL-2 protein family: opposing activities that mediate cell death. Nat Rev Mol Cell Biol. 2008;9:47-59.

233. Fu NY, Sukumaran SK, Kerk SY, Yu VC. Baxbeta: a constitutively active human Bax isoform that is under tight regulatory control by the proteasomal degradation mechanism. Mol Cell. 2009;33:15-29.
234. Lovell JF, Billen LP, Bindner S, Shamas-Din A, Fradin C, Leber B, et al. Membrane binding by tBid initiates an ordered series of events culminating in membrane permeabilization by Bax. Cell. 2008;135:1074-84.
235. Spencer SL, Gaudet S, Albeck JG, Burke JM, Sorger PK. Non-genetic origins of cell-to-cell variability in TRAIL-induced apoptosis. Nature. 2009;459:428-32.
236. Kvansakul M, Yang H, Fairlie WD, Czabotar PE, Fischer SF, Perugini MA, et al. Vaccinia virus anti-apoptotic F1L is a novel Bcl-2-like domain-swapped dimer that binds a highly selective subset of BH3-containing death ligands. Cell Death Differ. 2008;15:1564-71.
237. Moldoveanu T, Liu Q, Tocilj A, Watson M, Shore G, Gehring K. The X-ray structure of a BAK homodimer reveals an inhibitory zinc binding site. Mol Cell. 2006;24:677-88.
238. Suzuki M, Youle RJ, Tjandra N. Structure of Bax: coregulation of dimer formation and intracellular localization. Cell. 2000;103:645-54.
239. Hsu SY, Kaipia A, McGee E, Lomeli M, Hsueh AJ. Bok is a pro-apoptotic Bcl-2 protein with restricted expression in reproductive tissues and heterodimerizes with selective anti-apoptotic Bcl-2 family members. Proc Natl Acad Sci U S A. 1997;94:12401-6.
240. Griffiths GJ, Dubrez L, Morgan CP, Jones NA, Whitehouse J, Corfe BM, et al. Cell damage-induced conformational changes of the pro-apoptotic protein Bak in vivo precede the onset of apoptosis. J Cell Biol. 1999;144:903-14.
241. Griffiths GJ, Corfe BM, Savory P, Leech S, Esposti MD, Hickman JA, et al. Cellular damage signals promote sequential changes at the N-terminus and BH-1 domain of the pro-apoptotic protein Bak. Oncogene. 2001;20:7668-76.
242. Makin GW, Corfe BM, Griffiths GJ, Thistlethwaite A, Hickman JA, Dive C. Damage-induced Bax N-terminal change, translocation to mitochondria and formation of Bax dimers/complexes occur regardless of cell fate. EMBO J. 2001;20:6306-15.
243. Letai AG. Diagnosing and exploiting cancer's addiction to blocks in apoptosis. Nat Rev Cancer. 2008;8:121-32.
244. Green DR. Apoptotic pathways: ten minutes to dead. Cell. 2005;121:671-4.
245. Newmeyer DD, Ferguson-Miller S. Mitochondria: releasing power for life and unleashing the machineries of death. Cell. 2003;112:481-90.
246. Wei MC, Zong WX, Cheng EH, Lindsten T, Panoutsakopoulou V, Ross AJ, et al. Proapoptotic BAX and BAK: a requisite gateway to mitochondrial dysfunction and death. Science. 2001;292:727-30.
247. Lithgow T, van Driel R, Bertram JF, Strasser A. The protein product of the oncogene bcl-2 is a component of the nuclear envelope, the endoplasmic reticulum, and the outer mitochondrial membrane. Cell growth & differentiation : the molecular biology journal of the American Association for Cancer Research. 1994;5:411-7.
248. Pinton P, Rizzuto R. Bcl-2 and Ca2+ homeostasis in the endoplasmic reticulum. Cell Death Differ. 2006;13:1409-18.
249. Chipuk JE, Moldoveanu T, Llambi F, Parsons MJ, Green DR. The BCL-2 family reunion. Mol Cell. 2010;37:299-310.
250. Chonghaile TN, Letai A. Mimicking the BH3 domain to kill cancer cells. Oncogene. 2008;27 Suppl 1:S149-57.

251. Liu X, Dai S, Zhu Y, Marrack P, Kappler JW. The structure of a Bcl-xL/Bim fragment complex: implications for Bim function. Immunity. 2003;19:341-52.
252. Sattler M, Liang H, Nettesheim D, Meadows RP, Harlan JE, Eberstadt M, et al. Structure of Bcl-xL-Bak peptide complex: recognition between regulators of apoptosis. Science. 1997;275:983-6.
253. Aouacheria A, Brunet F, Gouy M. Phylogenomics of life-or-death switches in multicellular animals: Bcl-2, BH3-Only, and BNip families of apoptotic regulators. Molecular biology and evolution. 2005;22:2395-416.
254. Chen L, Willis SN, Wei A, Smith BJ, Fletcher JI, Hinds MG, et al. Differential targeting of prosurvival Bcl-2 proteins by their BH3-only ligands allows complementary apoptotic function. Mol Cell. 2005;17:393-403.
255. Kuwana T, Bouchier-Hayes L, Chipuk JE, Bonzon C, Sullivan BA, Green DR, et al. BH3 domains of BH3-only proteins differentially regulate Bax-mediated mitochondrial membrane permeabilization both directly and indirectly. Mol Cell. 2005;17:525-35.
256. Upreti M, Galitovskaya EN, Chu R, Tackett AJ, Terrano DT, Granell S, et al. Identification of the major phosphorylation site in Bcl-xL induced by microtubule inhibitors and analysis of its functional significance. J Biol Chem. 2008;283:35517-25.
257. Yamamoto K, Ichijo H, Korsmeyer SJ. BCL-2 is phosphorylated and inactivated by an ASK1/Jun N-terminal protein kinase pathway normally activated at G(2)/M. Mol Cell Biol. 1999;19:8469-78.
258. Fox JL, Storey A. BMX Negatively Regulates BAK Function, Thereby Increasing Apoptotic Resistance to Chemotherapeutic Drugs. Cancer Res. 2015;75:1345-55.
259. Akiyama T, Tanaka S. Bim: guardian of tissue homeostasis and critical regulator of the immune system, tumorigenesis and bone biology. Arch Immunol Ther Exp (Warsz). 2011;59:277-87.
260. Li QL, Ito K, Sakakura C, Fukamachi H, Inoue K, Chi XZ, et al. Causal relationship between the loss of RUNX3 expression and gastric cancer. Cell. 2002;109:113-24.
261. Yamamura Y, Lee WL, Inoue K, Ida H, Ito Y. RUNX3 cooperates with FoxO3a to induce apoptosis in gastric cancer cells. J Biol Chem. 2006;281:5267-76.
262. O'Connor L, Strasser A, O'Reilly LA, Hausmann G, Adams JM, Cory S, et al. Bim: a novel member of the Bcl-2 family that promotes apoptosis. EMBO J. 1998;17:384-95.
263. Xiao C, Srinivasan L, Calado DP, Patterson HC, Zhang B, Wang J, et al. Lymphoproliferative disease and autoimmunity in mice with increased miR-17-92 expression in lymphocytes. Nat Immunol. 2008;9:405-14.
264. Luciano F, Jacquel A, Colosetti P, Herrant M, Cagnol S, Pages G, et al. Phosphorylation of Bim-EL by Erk1/2 on serine 69 promotes its degradation via the proteasome pathway and regulates its proapoptotic function. Oncogene. 2003;22:6785-93.
265. Hubner A, Barrett T, Flavell RA, Davis RJ. Multisite phosphorylation regulates Bim stability and apoptotic activity. Mol Cell. 2008;30:415-25.
266. Strasser A. The role of BH3-only proteins in the immune system. Nat Rev Immunol. 2005;5:189-200.
267. Ramesh S, Qi XJ, Wildey GM, Robinson J, Molkentin J, Letterio J, et al. TGF beta-mediated BIM expression and apoptosis are regulated through SMAD3-dependent expression of the MAPK phosphatase MKP2. EMBO Rep. 2008;9:990-7.

268. Degli Esposti M, Ferry G, Masdehors P, Boutin JA, Hickman JA, Dive C. Post-translational modification of Bid has differential effects on its susceptibility to cleavage by caspase 8 or caspase 3. J Biol Chem. 2003;278:15749-57.
269. Zha J, Weiler S, Oh KJ, Wei MC, Korsmeyer SJ. Posttranslational N-myristoylation of BID as a molecular switch for targeting mitochondria and apoptosis. Science. 2000;290:1761-5.
270. Terrano DT, Upreti M, Chambers TC. Cyclin-dependent kinase 1-mediated Bcl-xL/Bcl-2 phosphorylation acts as a functional link coupling mitotic arrest and apoptosis. Mol Cell Biol. 2010;30:640-56.
271. Fox JL, Ismail F, Azad A, Ternette N, Leverrier S, Edelmann MJ, et al. Tyrosine dephosphorylation is required for Bak activation in apoptosis. EMBO J. 2010;29:3853-68.
272. Ren D, Tu HC, Kim H, Wang GX, Bean GR, Takeuchi O, et al. BID, BIM, and PUMA are essential for activation of the BAX- and BAK-dependent cell death program. Science. 2010;330:1390-3.
273. Chipuk JE, Green DR. How do BCL-2 proteins induce mitochondrial outer membrane permeabilization? Trends Cell Biol. 2008;18:157-64.
274. Kim H, Rafiuddin-Shah M, Tu HC, Jeffers JR, Zambetti GP, Hsieh JJ, et al. Hierarchical regulation of mitochondrion-dependent apoptosis by BCL-2 subfamilies. Nat Cell Biol. 2006;8:1348-58.
275. Certo M, Del Gaizo Moore V, Nishino M, Wei G, Korsmeyer S, Armstrong SA, et al. Mitochondria primed by death signals determine cellular addiction to antiapoptotic BCL-2 family members. Cancer Cell. 2006;9:351-65.
276. Letai A, Bassik MC, Walensky LD, Sorcinelli MD, Weiler S, Korsmeyer SJ. Distinct BH3 domains either sensitize or activate mitochondrial apoptosis, serving as prototype cancer therapeutics. Cancer Cell. 2002;2:183-92.
277. Oh KJ, Barbuto S, Pitter K, Morash J, Walensky LD, Korsmeyer SJ. A membrane-targeted BID BCL-2 homology 3 peptide is sufficient for high potency activation of BAX in vitro. J Biol Chem. 2006;281:36999-7008.
278. Walensky LD, Pitter K, Morash J, Oh KJ, Barbuto S, Fisher J, et al. A stapled BID BH3 helix directly binds and activates BAX. Mol Cell. 2006;24:199-210.
279. Gavathiotis E, Suzuki M, Davis ML, Pitter K, Bird GH, Katz SG, et al. BAX activation is initiated at a novel interaction site. Nature. 2008;455:1076-81.
280. Uren RT, Dewson G, Chen L, Coyne SC, Huang DC, Adams JM, et al. Mitochondrial permeabilization relies on BH3 ligands engaging multiple prosurvival Bcl-2 relatives, not Bak. J Cell Biol. 2007;177:277-87.
281. Willis SN, Chen L, Dewson G, Wei A, Naik E, Fletcher JI, et al. Proapoptotic Bak is sequestered by Mcl-1 and Bcl-xL, but not Bcl-2, until displaced by BH3-only proteins. Genes Dev. 2005;19:1294-305.
282. Willis SN, Fletcher JI, Kaufmann T, van Delft MF, Chen L, Czabotar PE, et al. Apoptosis initiated when BH3 ligands engage multiple Bcl-2 homologs, not Bax or Bak. Science. 2007;315:856-9.
283. Yin XM, Wang K, Gross A, Zhao Y, Zinkel S, Klocke B, et al. Bid-deficient mice are resistant to Fas-induced hepatocellular apoptosis. Nature. 1999;400:886-91.
284. Kaufmann T, Tai L, Ekert PG, Huang DC, Norris F, Lindemann RK, et al. The BH3-only protein bid is dispensable for DNA damage- and replicative stress-induced apoptosis or cell-cycle arrest. Cell. 2007;129:423-33.

285. McDonnell TJ, Deane N, Platt FM, Nunez G, Jaeger U, McKearn JP, et al. bcl-2-immunoglobulin transgenic mice demonstrate extended B cell survival and follicular lymphoproliferation. Cell. 1989;57:79-88.
286. Seto M, Jaeger U, Hockett RD, Graninger W, Bennett S, Goldman P, et al. Alternative promoters and exons, somatic mutation and deregulation of the Bcl-2-Ig fusion gene in lymphoma. EMBO J. 1988;7:123-31.
287. Tsujimoto Y, Gorham J, Cossman J, Jaffe E, Croce CM. The t(14;18) chromosome translocations involved in B-cell neoplasms result from mistakes in VDJ joining. Science. 1985;229:1390-3.
288. Ikegaki N, Katsumata M, Minna J, Tsujimoto Y. Expression of bcl-2 in small cell lung carcinoma cells. Cancer Res. 1994;54:6-8.
289. Monni O, Joensuu H, Franssila K, Klefstrom J, Alitalo K, Knuutila S. BCL2 overexpression associated with chromosomal amplification in diffuse large B-cell lymphoma. Blood. 1997;90:1168-74.
290. Cimmino A, Calin GA, Fabbri M, Iorio MV, Ferracin M, Shimizu M, et al. miR-15 and miR-16 induce apoptosis by targeting BCL2. Proc Natl Acad Sci U S A. 2005;102:13944-9.
291. Hanada M, Delia D, Aiello A, Stadtmauer E, Reed JC. bcl-2 gene hypomethylation and high-level expression in B-cell chronic lymphocytic leukemia. Blood. 1993;82:1820-8.
292. Cummins JM, He Y, Leary RJ, Pagliarini R, Diaz LA, Jr., Sjoblom T, et al. The colorectal microRNAome. Proc Natl Acad Sci U S A. 2006;103:3687-92.
293. Mott JL, Kobayashi S, Bronk SF, Gores GJ. mir-29 regulates Mcl-1 protein expression and apoptosis. Oncogene. 2007;26:6133-40.
294. Rampino N, Yamamoto H, Ionov Y, Li Y, Sawai H, Reed JC, et al. Somatic frameshift mutations in the BAX gene in colon cancers of the microsatellite mutator phenotype. Science. 1997;275:967-9.
295. Sinicrope FA, Rego RL, Okumura K, Foster NR, O'Connell MJ, Sargent DJ, et al. Prognostic impact of bim, puma, and noxa expression in human colon carcinomas. Clin Cancer Res. 2008;14:5810-8.
296. Boisvert-Adamo K, Aplin AE. Mutant B-RAF mediates resistance to anoikis via Bad and Bim. Oncogene. 2008;27:3301-12.
297. Goldstein NB, Johannes WU, Gadeliya AV, Green MR, Fujita M, Norris DA, et al. Active N-Ras and B-Raf inhibit anoikis by downregulating Bim expression in melanocytic cells. J Invest Dermatol. 2009;129:432-7.
298. Zuckerman V, Wolyniec K, Sionov RV, Haupt S, Haupt Y. Tumour suppression by p53: the importance of apoptosis and cellular senescence. J Pathol. 2009;219:3-15.
299. Marion RM, Strati K, Li H, Murga M, Blanco R, Ortega S, et al. A p53-mediated DNA damage response limits reprogramming to ensure iPS cell genomic integrity. Nature. 2009;460:1149-53.
300. Vogelstein B, Lane D, Levine AJ. Surfing the p53 network. Nature. 2000;408:307-10.
301. Markowitz SD, Bertagnolli MM. Molecular origins of cancer: Molecular basis of colorectal cancer. N Engl J Med. 2009;361:2449-60.
302. Chong MJ, Murray MR, Gosink EC, Russell HR, Srinivasan A, Kapsetaki M, et al. Atm and Bax cooperate in ionizing radiation-induced apoptosis in the central nervous system. Proc Natl Acad Sci U S A. 2000;97:889-94.
303. Nakano K, Vousden KH. PUMA, a novel proapoptotic gene, is induced by p53. Mol Cell. 2001;7:683-94.

304. Oda E, Ohki R, Murasawa H, Nemoto J, Shibue T, Yamashita T, et al. Noxa, a BH3-only member of the Bcl-2 family and candidate mediator of p53-induced apoptosis. Science. 2000;288:1053-8.
305. Kannan K, Kaminski N, Rechavi G, Jakob-Hirsch J, Amariglio N, Givol D. DNA microarray analysis of genes involved in p53 mediated apoptosis: activation of Apaf-1. Oncogene. 2001;20:3449-55.
306. Moroni MC, Hickman ES, Lazzerini Denchi E, Caprara G, Colli E, Cecconi F, et al. Apaf-1 is a transcriptional target for E2F and p53. Nat Cell Biol. 2001;3:552-8.
307. Robles AI, Bemmels NA, Foraker AB, Harris CC. APAF-1 is a transcriptional target of p53 in DNA damage-induced apoptosis. Cancer Res. 2001;61:6660-4.
308. Rozenfeld-Granot G, Krishnamurthy J, Kannan K, Toren A, Amariglio N, Givol D, et al. A positive feedback mechanism in the transcriptional activation of Apaf-1 by p53 and the coactivator Zac-1. Oncogene. 2002;21:1469-76.
309. Ding HF, McGill G, Rowan S, Schmaltz C, Shimamura A, Fisher DE. Oncogene-dependent regulation of caspase activation by p53 protein in a cell-free system. J Biol Chem. 1998;273:28378-83.
310. MacLachlan TK, El-Deiry WS. Apoptotic threshold is lowered by p53 transactivation of caspase-6. Proc Natl Acad Sci U S A. 2002;99:9492-7.
311. Mihara M, Erster S, Zaika A, Petrenko O, Chittenden T, Pancoska P, et al. p53 has a direct apoptogenic role at the mitochondria. Mol Cell. 2003;11:577-90.
312. Russo A, Bazan V, Iacopetta B, Kerr D, Soussi T, Gebbia N. The TP53 colorectal cancer international collaborative study on the prognostic and predictive significance of p53 mutation: influence of tumor site, type of mutation, and adjuvant treatment. J Clin Oncol. 2005;23:7518-28.
313. Waters JS, Webb A, Cunningham D, Clarke PA, Raynaud F, di Stefano F, et al. Phase I clinical and pharmacokinetic study of bcl-2 antisense oligonucleotide therapy in patients with non-Hodgkin's lymphoma. J Clin Oncol. 2000;18:1812-23.
314. O'Brien S, Moore JO, Boyd TE, Larratt LM, Skotnicki AB, Koziner B, et al. 5-year survival in patients with relapsed or refractory chronic lymphocytic leukemia in a randomized, phase III trial of fludarabine plus cyclophosphamide with or without oblimersen. J Clin Oncol. 2009;27:5208-12.
315. Konopleva M, Contractor R, Tsao T, Samudio I, Ruvolo PP, Kitada S, et al. Mechanisms of apoptosis sensitivity and resistance to the BH3 mimetic ABT-737 in acute myeloid leukemia. Cancer Cell. 2006;10:375-88.
316. van Delft MF, Wei AH, Mason KD, Vandenberg CJ, Chen L, Czabotar PE, et al. The BH3 mimetic ABT-737 targets selective Bcl-2 proteins and efficiently induces apoptosis via Bak/Bax if Mcl-1 is neutralized. Cancer Cell. 2006;10:389-99.
317. Oltersdorf T, Elmore SW, Shoemaker AR, Armstrong RC, Augeri DJ, Belli BA, et al. An inhibitor of Bcl-2 family proteins induces regression of solid tumours. Nature. 2005;435:677-81.
318. Del Gaizo Moore V, Schlis KD, Sallan SE, Armstrong SA, Letai A. BCL-2 dependence and ABT-737 sensitivity in acute lymphoblastic leukemia. Blood. 2008;111:2300-9.
319. Mason KD, Vandenberg CJ, Scott CL, Wei AH, Cory S, Huang DC, et al. In vivo efficacy of the Bcl-2 antagonist ABT-737 against aggressive Myc-driven lymphomas. Proc Natl Acad Sci U S A. 2008;105:17961-6.
320. clinicaltrials.com

321. Premkumar DR, Jane EP, DiDomenico JD, Vukmer NA, Agostino NR, Pollack IF. ABT-737 synergizes with bortezomib to induce apoptosis, mediated by Bid cleavage, Bax activation, and mitochondrial dysfunction in an Akt-dependent context in malignant human glioma cell lines. The Journal of pharmacology and experimental therapeutics. 2012;341:859-72.
322. Harrison LR, Micha D, Brandenburg M, Simpson KL, Morrow CJ, Denneny O, et al. Hypoxic human cancer cells are sensitized to BH-3 mimetic-induced apoptosis via downregulation of the Bcl-2 protein Mcl-1. J Clin Invest. 2011;121:1075-87.
323. Klymenko T, Brandenburg M, Morrow C, Dive C, Makin G. The Novel Bcl-2 Inhibitor ABT-737 Is More Effective in Hypoxia and Is Able to Reverse Hypoxia-Induced Drug Resistance in Neuroblastoma Cells. Mol Cancer Ther. 2011;10:2373-83.
324. Vaupel P, Thews O, Hoeckel M. Treatment resistance of solid tumors: role of hypoxia and anemia. Med Oncol. 2001;18:243-59.
325. Vogler M, Dinsdale D, Dyer MJ, Cohen GM. Bcl-2 inhibitors: small molecules with a big impact on cancer therapy. Cell Death Differ. 2009;16:360-7.
326. Gandhi L, Camidge DR, Ribeiro de Oliveira M, Bonomi P, Gandara D, Khaira D, et al. Phase I study of Navitoclax (ABT-263), a novel Bcl-2 family inhibitor, in patients with small-cell lung cancer and other solid tumors. J Clin Oncol. 2011;29:909-16.
327. (clinicaltrials.gov)
328. Roberts AW, Seymour JF, Brown JR, Wierda WG, Kipps TJ, Khaw SL, et al. Substantial Susceptibility of Chronic Lymphocytic Leukemia to BCL2 Inhibition: Results of a Phase I Study of Navitoclax in Patients With Relapsed or Refractory Disease. J Clin Oncol. 2011.
329. Faber AC, Coffee EM, Costa C, Dastur A, Ebi H, Hata AN, et al. mTOR inhibition specifically sensitizes colorectal cancers with KRAS or BRAF mutations to BCL-2/BCL-XL inhibition by suppressing MCL-1. Cancer discovery. 2014;4:42-52.
330. Tan N, Wong M, Nannini MA, Hong R, Lee LB, Price S, et al. Bcl-2/Bcl-xL inhibition increases the efficacy of MEK inhibition alone and in combination with PI3 kinase inhibition in lung and pancreatic tumor models. Mol Cancer Ther. 2013;12:853-64.
331. Clinicaltrial.gov
332. Cervantes-Gomez F, Lamothe B, Woyach JA, Wierda WG, Keating MJ, Balakrishnan K, et al. Pharmacological and Protein Profiling Suggests Venetoclax (ABT-199) as Optimal Partner with Ibrutinib in Chronic Lymphocytic Leukemia. Clin Cancer Res. 2015;21:3705-15.
333. Choudhary GS, Al-Harbi S, Mazumder S, Hill BT, Smith MR, Bodo J, et al. MCL-1 and BCL-xL-dependent resistance to the BCL-2 inhibitor ABT-199 can be overcome by preventing PI3K/AKT/mTOR activation in lymphoid malignancies. Cell death & disease. 2015;6:e1593.
334. Kang MH, Reynolds CP. Bcl-2 inhibitors: targeting mitochondrial apoptotic pathways in cancer therapy. Clin Cancer Res. 2009;15:1126-32.
335. Konopleva M, Watt J, Contractor R, Tsao T, Harris D, Estrov Z, et al. Mechanisms of antileukemic activity of the novel Bcl-2 homology domain-3 mimetic GX15-070 (obatoclax). Cancer Res. 2008;68:3413-20.
336. Tse C, Shoemaker AR, Adickes J, Anderson MG, Chen J, Jin S, et al. ABT-263: a potent and orally bioavailable Bcl-2 family inhibitor. Cancer Res. 2008;68:3421-8.

337. Langer CJ, Albert I, Ross HJ, Kovacs P, Blakely LJ, Pajkos G, et al. Randomized phase II study of carboplatin and etoposide with or without obatoclax mesylate in extensive-stage small cell lung cancer. Lung Cancer. 2014;85:420-8.
338. Paik PK, Rudin CM, Pietanza MC, Brown A, Rizvi NA, Takebe N, et al. A phase II study of obatoclax mesylate, a Bcl-2 antagonist, plus topotecan in relapsed small cell lung cancer. Lung Cancer. 2011;74:481-5.
339. Doi K, Li R, Sung SS, Wu H, Liu Y, Manieri W, et al. Discovery of marinopyrrole A (maritoclax) as a selective Mcl-1 antagonist that overcomes ABT-737 resistance by binding to and targeting Mcl-1 for proteasomal degradation. J Biol Chem. 2012;287:10224-35.
340. Vela L, Marzo I. Bcl-2 family of proteins as drug targets for cancer chemotherapy: the long way of BH3 mimetics from bench to bedside. Curr Opin Pharmacol. 2015;23:74-81.
341. Sun H, Nikolovska-Coleska Z, Yang CY, Xu L, Liu M, Tomita Y, et al. Structure-based design of potent, conformationally constrained Smac mimetics. Journal of the American Chemical Society. 2004;126:16686-7.
342. Park CM, Sun C, Olejniczak ET, Wilson AE, Meadows RP, Betz SF, et al. Non-peptidic small molecule inhibitors of XIAP. Bioorganic & medicinal chemistry letters. 2005;15:771-5.
343. Silke J, Vucic D. IAP family of cell death and signaling regulators. Methods in enzymology. 2014;545:35-65.
344. Petersen SL, Wang L, Yalcin-Chin A, Li L, Peyton M, Minna J, et al. Autocrine TNFalpha signaling renders human cancer cells susceptible to Smac-mimetic-induced apoptosis. Cancer Cell. 2007;12:445-56.
345. Wu H, Tschopp J, Lin SC. Smac mimetics and TNFalpha: a dangerous liaison? Cell. 2007;131:655-8.
346. clinicaltrials.com
347. Pukac L, Kanakaraj P, Humphreys R, Alderson R, Bloom M, Sung C, et al. HGS-ETR1, a fully human TRAIL-receptor 1 monoclonal antibody, induces cell death in multiple tumour types in vitro and in vivo. Br J Cancer. 2005;92:1430-41.
348. Trarbach T, Moehler M, Heinemann V, Kohne CH, Przyborek M, Schulz C, et al. Phase II trial of mapatumumab, a fully human agonistic monoclonal antibody that targets and activates the tumour necrosis factor apoptosis-inducing ligand receptor-1 (TRAIL-R1), in patients with refractory colorectal cancer. Br J Cancer. 2010;102:506-12.
349. clinicaltrials.com
350. clinicaltrials.gov
351. Weinstein IB. Cancer. Addiction to oncogenes--the Achilles heal of cancer. Science. 2002;297:63-4.
352. Shortt J, Johnstone RW. Oncogenes in cell survival and cell death. Cold Spring Harbor perspectives in biology. 2012;4.
353. Samuels Y, Ericson K. Oncogenic PI3K and its role in cancer. Curr Opin Oncol. 2006;18:77-82.
354. Workman P, Clarke PA, Raynaud FI, van Montfort RL. Drugging the PI3 kinome: from chemical tools to drugs in the clinic. Cancer Res. 2010;70:2146-57.
355. Wujcik D. Science and mechanism of action of targeted therapies in cancer treatment. Seminars in oncology nursing. 2014;30:139-46.
356. Workman P. Scoring a bull's-eye against cancer genome targets. Curr Opin Pharmacol. 2001;1:342-52.

357. Workman P. The opportunities and challenges of personalized genome-based molecular therapies for cancer: targets, technologies, and molecular chaperones. Cancer Chemother Pharmacol. 2003;52 Suppl 1:S45-56.
358. Workman P, Kaye SB. Translating basic cancer research into new cancer therapeutics. Trends Mol Med. 2002;8:S1-9.
359. Kantarjian HM, Cortes JE, O'Brien S, Luthra R, Giles F, Verstovsek S, et al. Long-term survival benefit and improved complete cytogenetic and molecular response rates with imatinib mesylate in Philadelphia chromosome-positive chronic-phase chronic myeloid leukemia after failure of interferon-alpha. Blood. 2004;104:1979-88.
360. Druker BJ. Current treatment approaches for chronic myelogenous leukemia. Cancer J. 2001;7 Suppl 1:S14-8.
361. Bartram CR, Grosveld G. [Philadelphia translocation and the human c-abl oncogene--relations in the light of molecular genetics]. Klinische Padiatrie. 1985;197:196-202.
362. Groffen J, Stephenson JR, Heisterkamp N, Bartram C, de Klein A, Grosveld G. The human c-abl oncogene in the Philadelphia translocation. Journal of cellular physiology Supplement. 1984;3:179-91.
363. Rosti G, Martinelli G, Bassi S, Amabile M, Trabacchi E, Giannini B, et al. Molecular response to imatinib in late chronic-phase chronic myeloid leukemia. Blood. 2004;103:2284-90.
364. Weisberg E, Griffin JD. Mechanisms of resistance imatinib (STI571) in preclinical models and in leukemia patients. Drug resistance updates : reviews and commentaries in antimicrobial and anticancer chemotherapy. 2001;4:22-8.
365. Kobayashi S, Boggon TJ, Dayaram T, Janne PA, Kocher O, Meyerson M, et al. EGFR mutation and resistance of non-small-cell lung cancer to gefitinib. N Engl J Med. 2005;352:786-92.
366. Killock D. Lung cancer: a new generation of EGFR inhibition. Nature reviews Clinical oncology. 2015;12:373.
367. Flaherty KT, Puzanov I, Kim KB, Ribas A, McArthur GA, Sosman JA, et al. Inhibition of mutated, activated BRAF in metastatic melanoma. N Engl J Med. 2010;363:809-19.
368. Nazarian R, Shi H, Wang Q, Kong X, Koya RC, Lee H, et al. Melanomas acquire resistance to B-RAF(V600E) inhibition by RTK or N-RAS upregulation. Nature. 2010;468:973-7.
369. Cai J, Ma H, Huang F, Zhu D, Bi J, Ke Y, et al. Correlation of bevacizumab-induced hypertension and outcomes of metastatic colorectal cancer patients treated with bevacizumab: a systematic review and meta-analysis. World journal of surgical oncology. 2013;11:306.
370. Petrelli F, Borgonovo K, Cabiddu M, Lonati V, Barni S. Relationship between skin rash and outcome in non-small-cell lung cancer patients treated with anti-EGFR tyrosine kinase inhibitors: a literature-based meta-analysis of 24 trials. Lung Cancer. 2012;78:8-15.
371. Bedard PL, Hansen AR, Ratain MJ, Siu LL. Tumour heterogeneity in the clinic. Nature. 2013;501:355-64.
372. http://www.cancer.gov/about-cancer/treatment/types/targeted-therapies/targeted-therapies-fact-sheet
373. http://www.cancer.gov/about-cancer/treatment/types/targeted-therapies/targeted-therapies-fact-sheet#q8

374. Li Z, Jin K, Lan H, Teng L. Heterogeneity in primary colorectal cancer and its corresponding metastases: a potential reason of EGFR-targeted therapy failure? Hepato-gastroenterology. 2011;58:411-6.
375. Clark A, Ellis M, Erlichman C, Lutzker S, Zwiebel J. Development of rational drug combinations with investigational targeted agents. Oncologist. 2010;15:496-9.
376. O'Reilly KE, Rojo F, She QB, Solit D, Mills GB, Smith D, et al. mTOR inhibition induces upstream receptor tyrosine kinase signaling and activates Akt. Cancer Res. 2006;66:1500-8.
377. Prahallad A, Sun C, Huang S, Di Nicolantonio F, Salazar R, Zecchin D, et al. Unresponsiveness of colon cancer to BRAF(V600E) inhibition through feedback activation of EGFR. Nature. 2012;483:100-3.
378. Clinicaltrial.gov
379. (clinicaltrials.gov)
380. Regulatory watch: FDA guidance on co-developing investigational drugs. Nature reviews Drug discovery. 2011;10:86.
381. Datta SR, Brunet A, Greenberg ME. Cellular survival: a play in three Akts. Genes Dev. 1999;13:2905-27.
382. Martin-Fernandez C, Bales J, Hodgkinson C, Welman A, Welham MJ, Dive C, et al. Blocking phosphoinositide 3-kinase activity in colorectal cancer cells reduces proliferation but does not increase apoptosis alone or in combination with cytotoxic drugs. Mol Cancer Res. 2009;7:955-65.
383. https://pubchem.ncbi.nlm.nih.gov/
384. Hou JM, Krebs MG, Lancashire L, Sloane R, Backen A, Swain RK, et al. Clinical significance and molecular characteristics of circulating tumor cells and circulating tumor microemboli in patients with small-cell lung cancer. J Clin Oncol. 2012;30:525-32.
385. Evans WK, Feld R, Osoba D, Shepherd FA, Dill J, Deboer G. VP-16 alone and in combination with cisplatin in previously treated patients with small cell lung cancer. Cancer. 1984;53:1461-6.
386. http://www.cancer.gov/about-cancer/treatment/drugs/fda-cetuximab#Anchor-Colorecta-60318
387. http://www.cancerscreening.nhs.uk/bowel/eligible-bowel-cancer-screening.html
388. http://www.cancer.gov/types/colorectal/hp/colorectal-screening-pdq
389. http://deainfo.nci.nih.gov/advisory/ctac/workgroup/SCLC/SCLC%20Congressional%20Response.pdf
390. http://www.cancerscreening.nhs.uk/
391. https://www.lunghealthuk.com/
392. Jett JR, Peek LJ, Fredericks L, Jewell W, Pingleton WW, Robertson JF. Audit of the autoantibody test, EarlyCDT(R)-lung, in 1600 patients: an evaluation of its performance in routine clinical practice. Lung Cancer. 2014;83:51-5.
393. Macdonald IK, Murray A, Healey GF, Parsy-Kowalska CB, Allen J, McElveen J, et al. Application of a high throughput method of biomarker discovery to improvement of the EarlyCDT((R))-Lung Test. PLoS One. 2012;7:e51002.
394. http://www.cancer.org/cancer/lungcancer-smallcell/detailedguide/small-cell-lung-cancer-survival-rates

395. Van Cutsem E, Kohne CH, Hitre E, Zaluski J, Chang Chien CR, Makhson A, et al. Cetuximab and chemotherapy as initial treatment for metastatic colorectal cancer. N Engl J Med. 2009;360:1408-17.
396. http://deainfo.nci.nih.gov/advisory/ctac/workgroup/SCLC/SCLC%20Congressional%20Response.pdf
397. Ackler S, Xiao Y, Mitten MJ, Foster K, Oleksijew A, Refici M, et al. ABT-263 and rapamycin act cooperatively to kill lymphoma cells in vitro and in vivo. Mol Cancer Ther. 2008;7:3265-74.
398. Qian J, Zou Y, Rahman JS, Lu B, Massion PP. Synergy between phosphatidylinositol 3-kinase/Akt pathway and Bcl-xL in the control of apoptosis in adenocarcinoma cells of the lung. Mol Cancer Ther. 2009;8:101-9.
399. Chen S, Dai Y, Harada H, Dent P, Grant S. Mcl-1 down-regulation potentiates ABT-737 lethality by cooperatively inducing Bak activation and Bax translocation. Cancer Res. 2007;67:782-91.
400. Uchida Y, Hasegawa J, Chinnapen D, Inoue T, Okazaki S, Kato R, et al. Intracellular phosphatidylserine is essential for retrograde membrane traffic through endosomes. Proc Natl Acad Sci U S A. 2011;108:15846-51.
401. Zhang R, Xu Y, Ekman N, Wu Z, Wu J, Alitalo K, et al. Etk/Bmx transactivates vascular endothelial growth factor 2 and recruits phosphatidylinositol 3-kinase to mediate the tumor necrosis factor-induced angiogenic pathway. J Biol Chem. 2003;278:51267-76.
402. Bromberg JF, Wrzeszczynska MH, Devgan G, Zhao Y, Pestell RG, Albanese C, et al. Stat3 as an oncogene. Cell. 1999;98:295-303.
403. Niu G, Wright KL, Ma Y, Wright GM, Huang M, Irby R, et al. Role of Stat3 in regulating p53 expression and function. Mol Cell Biol. 2005;25:7432-40.
404. Kumar A, Redondo-Munoz J, Perez-Garcia V, Cortes I, Chagoyen M, Carrera AC. Nuclear but not cytosolic phosphoinositide 3-kinase beta has an essential function in cell survival. Mol Cell Biol. 2011;31:2122-33.
405. Abell K, Bilancio A, Clarkson RW, Tiffen PG, Altaparmakov AI, Burdon TG, et al. Stat3-induced apoptosis requires a molecular switch in PI(3)K subunit composition. Nat Cell Biol. 2005;7:392-8.
406. Barretina J, Caponigro G, Stransky N, Venkatesan K, Margolin AA, Kim S, et al. The Cancer Cell Line Encyclopedia enables predictive modelling of anticancer drug sensitivity. Nature. 2012;483:603-7.

Chapter 8

Appendices

8. Appendices

8.1 Appendix I

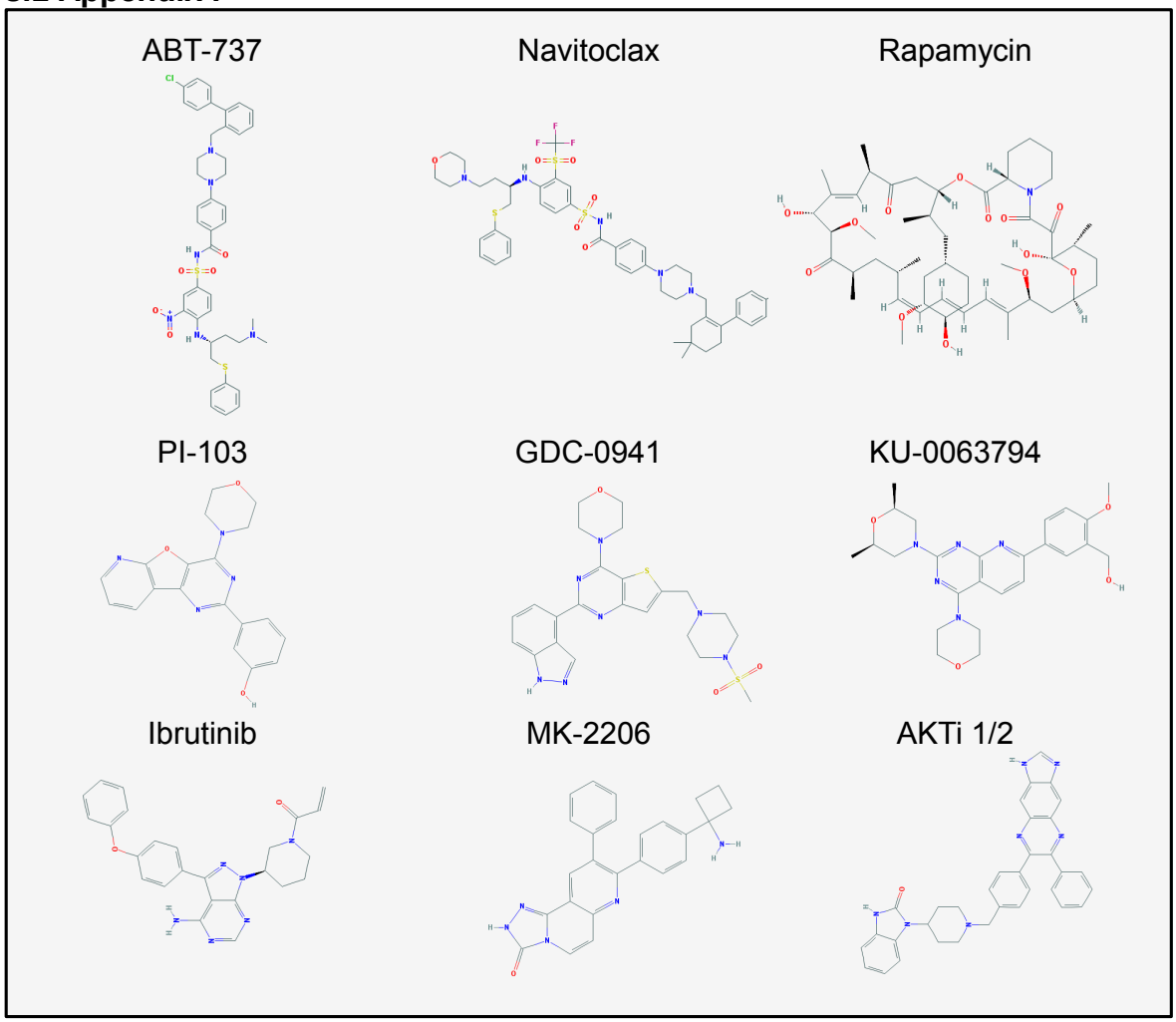

Figure 26: Chemical structure of drugs used in this thesis. ABT-737 (PubChem CID: 11228183) and Navitoclax (PubChem CID: 249785338) are BH3 mimetics that target the anti-apoptotic Bcl-2 members. P1-103 (PubChem CID: 9884685) is a dual PI3K/mTOR inhibitor and GDC-0941 (PubChem CID: 17755052) is a specific class I PI3K inhibitor. Rapamycin (PubChem CID: 5284616) and KU-0063794 (PubChem CID: 16736978) are mTORC1 and mTORC1/2 inhibitors respectively. MK-2206 (PubChem CID: 24964624) and AKTi 1/2 (PubChem CID: 10196499) are allosteric AKT inhibitors. Ibrutinib (PubChem CID: 24821094) is a TEC kinase inhibitor. All drug structures were taken from PubChem.

8.2 Appendix II

BMX	GUACCAGUCUAGCGCAAUA
	GAAGAUACCUCGGGCAGUU
	GAAGAGAGCCGAAGUCAGU
	GAGCAUUUAUGGUUAGAAA
MCL-1	GGUUUGGCAUAUCUAAUAA
	GAAGGUGGCAUCAGGAAUG
	GAUUAUCUCUCGGUACCUU
	CGAAGGAAGUAUCGAAUUU
Non-targeting	UGGUUUACAUGUCGACUAA

Table 13: BMX, MCL-1 and non-targeting siRNAs target sequence.

8.3 Appendix III

Plate	Well	Gene Symbol	Sequence
Plate 1	B04	SOS1	AACAGAAGCUGAUCGCAUA
Plate 1	B04		GGCAGAAAUUCGACAAUAU
Plate 1	B04		GGAUAUGUUUCAUCAAGAU
Plate 1	B04		UAGUAGCAGUCUUAGAAUA
Plate 1	B05	CYTH2	UGGCAGUGCUCCAUGCUUU
Plate 1	B05		AAACCGAACUGCUUUGAAC
Plate 1	B05		GUAAGACCUUGCAACGGAA
Plate 1	B05		GAACACACCCGAGGAGAUC
Plate 1	B06	SWAP70	CAGGAGAGCUUUACGCUAA
Plate 1	B06		GCAUAGUGUUACCGAUUUA
Plate 1	B06		AGGAUUAAUUCGACUGAUA
Plate 1	B06		CCGAGUAUGUGCUGUUAAA
Plate 1	B09	AKAP13	UGGAUGAGCUGAUCAGUAU
Plate 1	B09		ACACAUAGCCCUAGAGUUC
Plate 1	B09		GGUCAAACGGCAAGAAGUA
Plate 1	B09		GAUGAGCAGUUCAGUUGUU
Plate 1	C04	PLCXD2	GGGAUGGGCUGAUGGAAAU
Plate 1	C04		GAACCUGACAUUUCGAGAA
Plate 1	C04		ACAAGUGUGCGCAAACUAA
Plate 1	C04		GGACAAAGACAUCAUCGGA
Plate 1	C05	DOCK2	GGUCUUUGAUGCGAAGUUA
Plate 1	C05		CUACAUUACUCUCUUACAA
Plate 1	C05		GGUACAAGCUUGGUCAGAA
Plate 1	C05		CAAGGUGGCUGUCCCUAUU
Plate 1	C06	PIK3CA	GCGAAAUUCUCACACUAUU
Plate 1	C06		GUGGUAAAGUUCCCAGAUA
Plate 1	C06		GCUUAGAGUUGGAGUUUGA
Plate 1	C06		GACCCUAGCCUUAGAUAAA
Plate 1	C07	GAB2	GAUGCAGGCCUGACCUUUA
Plate 1	C07		UCAAGUCCAUGGCUUCUAU
Plate 1	C07		CAACUCUGUUCACGUUUGA
Plate 1	C07		GCACCGGCAGCGUUGAUUA
Plate 1	C08	CYTH1	GAGAUGAGUUUAAUAUCCA
Plate 1	C08		AAGAGACGCUGGUUCAUUC
Plate 1	C08		ACAGCUACGUUCCCAGUGA
Plate 1	C08		UCACUGAUCUUAAUCUCGU
Plate 1	C09	RASA1	GAACAUACUUUCAGAGCUU
Plate 1	C09		GCAAGGAAAUCUAUAAUAC
Plate 1	C09		CCACCGACAUUGAGAUAUA
Plate 1	C09		GAACAAGUACUCAAUGACA
Plate 1	D04	CYTH4	UUGCACGGUUCCUGUAUAA
Plate 1	D04		GAGAAGGAGCUGUGUAUUG
Plate 1	D04		GAAUUAUACCUCUUGAGAA
Plate 1	D04		UGAGAUUGCAGAUGUGUUU
Plate 1	D05	TEC	GAAAUUGUCUAGUAAGUGA
Plate 1	D05		GUACAAAGUCGCAAUCAAA
Plate 1	D05		GUAAUUACGUAACGGGAAA

Plate 1	D05		GAAGGUGGUUUUAUGGUAA
Plate 1	D06	RASA3	AAAGAAGGGUUCAUGAUCA
Plate 1	D06		CCGGAGGGAUUCCAUCAUA
Plate 1	D06		GAUCGACAUUCUCACCAAA
Plate 1	D06		UGAAAUUCCUCGGAGCUUU
Plate 1	D07	VAV1	CGACAAAGCUCUACUCAUC
Plate 1	D07		GCAGCGAGUUCUCAAAUAU
Plate 1	D07		GCCAUCAGCAUUAAAUAUA
Plate 1	D07		UCAAAUACAAGGAGAGGUU
Plate 1	D09	BTK	GCGGAAGGGUGAUGAAUAU
Plate 1	D09		GGUGAUACGUCAUUAUGUU
Plate 1	D09		CAACUCUGCAGGACUCAUA
Plate 1	D09		UGAGCAAUAUUCUAGAUGU
Plate 1	E04	VAV3	GAAACAUUAUCACGACUUU
Plate 1	E04		GCAAUUAGCAUUAAGUACA
Plate 1	E04		AGUACAAGAUAGCCAAUAA
Plate 1	E04		AGACCGAACUUAUUAAUAG
Plate 1	E05	ARAP3	GUAAUGAGAUAGUACAGUU
Plate 1	E05		GCAGAAAUGUGCGGCUCUA
Plate 1	E05		ACACGGGAGUGGACAGUGA
Plate 1	E05		GAACGGGAGUGGCCUUUGG
Plate 1	E06	RASA2	GCAAAUAACUGUGUAGAAG
Plate 1	E06		AAACGAUGGUUCUGCUUAA
Plate 1	E06		AUUCAGAGGUUCAGGGUAA
Plate 1	E06		ACUAAAGAGUCCAGUGGUA
Plate 1	E07	PHLDB1	CUGCAGAGGCCAUGCGUAU
Plate 1	E07		CUGAAAGUGCAAACGGACA
Plate 1	E07		GCCCUCACCUUCUGCGUAA
Plate 1	E07		UGGAGAGGCUGGAACGCCA
Plate 1	E08	ARAP1	GGAGUGGCCUAUUAAGAGU
Plate 1	E08		UAACAAGGACGCUUACUCU
Plate 1	E08		CCGCAGGGAUCUUACAUCU
Plate 1	E08		GAUCACCUGCGAUACUUUG
Plate 1	E09	GAB3	GGACUUCAAUUCAGCAUCA
Plate 1	E09		GAGAUGACCCAAACACUAA
Plate 1	E09		CCAAUGAACUCAGGAAGCA
Plate 1	E09		UGUGAUAGCUGGUCAAACU
Plate 1	F04	TIAM1	GCAGGCUACUGUCGGAAUU
Plate 1	F04		GUAUAAAGAUGGUUCCAAA
Plate 1	F04		GAACCGAAGCUGUAAAGAA
Plate 1	F04		CAAAUUAGCCAUAGCAACA
Plate 1	F05	PREX1	AAGAUGGGACAGCGGAUUA
Plate 1	F05		CCACGGACAUCAUGCGGAA
Plate 1	F05		ACGUCAUGAUUGCGGAGAA
Plate 1	F05		CCUUUAAGCAGCUGGACGA
Plate 1	F06	DOCK1	GUACCGAGGUUACACGUUA
Plate 1	F06		GAAAGUCGAUGGUGGUGAA
Plate 1	F06		UAAAUGAGCAGCUGUACAA
Plate 1	F06		GGCCCAAGCCUGACUAUUU
Plate 1	F07	GAB1	CAUCAAAGCUAGACACUAU
Plate 1	F07		GAUGCUGGAUUGACAUUUA
Plate 1	F07		GAGGAGAUGGUUCGUGUUA

Plate 1	F07		UGACCGAUCUCCUGUGGAA
Plate 1	F08	AKT2	ACACAAGGUACUUCGAUGA
Plate 1	F08		GCAAGGCACGGGCUAAAGU
Plate 1	F08		GUGAAUACAUCAAGACCUG
Plate 1	F08		CAUGAAUGACUUCGACUAU
Plate 1	F09	AKT1	CAUCACACCACCUGACCAA
Plate 1	F09		ACAAGGACGGGCACAUUAA
Plate 1	F09		CAAGGGCACUUUCGGCAAG
Plate 1	F09		UCACAGCCCUGAAGUACUC
Plate 1	G04	SGK1	UCAUGGAGAUUAAGAGUCA
Plate 1	G04		GUCCAAUCCUCAUGCUAAA
Plate 1	G04		GGAUGGGUCUGAACGACUU
Plate 1	G04		GGAGCUGUCUUGUAUGAGA
Plate 1	G05	ARAP2	GGACGAUAAACUUCGAAAU
Plate 1	G05		CUAAGGAGCUCUACCCAUA
Plate 1	G05		GUAAGAAGACAUUGGGUUA
Plate 1	G05		GCAAAUUUGUCUAUGCUUA
Plate 1	G06	PIK3CD	ACGAUGAGCUGUUCCAGUA
Plate 1	G06		CCAAAGACAACAGGCAGUA
Plate 1	G06		GCGUGGGCAUCAUCUUUAA
Plate 1	G06		CGAGUGAAGUUUAACGAAG
Plate 1	G07	MTOR	GGCCAUAGCUAGCCUCAUA
Plate 1	G07		CAAAGGACUUCGCCCAUAA
Plate 1	G07		GCAGAAUUGUCAAGGGAUA
Plate 1	G07		CCAAAGCACUACACUACAA
Plate 1	G08	PREX2	GAAGCGGACUCCACGGAAA
Plate 1	G08		GAACACCUAUGUCAGAGAA
Plate 1	G08		CAAGAUACCUGGGUCAUGA
Plate 1	G08		GAAGCGAAUUUGUGUCAUG
Plate 1	G09	PHLDB3	GAACUGUGGCCGUGGGAAU
Plate 1	G09		GCAUUUGGAUGGACGUCAU
Plate 1	G09		UGGCCUACUAUGCGGACAA
Plate 1	G09		CUCCUGUGAUACCGAAUUA

Plate 2	B04	PIK3R1	AGUAAAGCAUUGUGUCAUA
Plate 2	B04		CCAACAACGGUAUGAAUAA
Plate 2	B04		GACGAGAGACCAAUACUUG
Plate 2	B04		UAUUGAAGCUGUAGGGAAA
Plate 2	B05	PLCL2	GGUUUAGGCAGAACGGAAA
Plate 2	B05		AGGAGAUGUUACUGACGAA
Plate 2	B05		GAAGAUACAUGCCGAGUCA
Plate 2	B05		CGAGCAAAAUUGAGCUUAA
Plate 2	B06	PIK3CB	GGAUUCAGUUGGAGUGAUU
Plate 2	B06		GGCGGUGGAUUCACAGAUA
Plate 2	B06		GAUUAUGUGUUGCAAGUCA
Plate 2	B06		CCAUAGAGGCUGCCAUAAA
Plate 2	B07	AKT3	GCACACACUCUAACUGAAA
Plate 2	B07		GAAGAGGGGAGAAUAUAUA
Plate 2	B07		GUACCGUGAUCUCAAGUUG
Plate 2	B07		GACAGAUGGCUCAUUCAUA
Plate 2	B08	MYO10	GGACAUAAAUCUCAACUUG
Plate 2	B08		CGUCGUAGCUGAUGUCUUA

Plate 2	B08		GCGGGAGAAUUGUAGAUUA
Plate 2	B08		GGAGGAAAUUUCAGGGAAU
Plate 2	B09	RPTOR	UGGCUAGUCUGUUUCGAAA
Plate 2	B09		CACGGAAGAUGUUCGACAA
Plate 2	B09		AGAAGGGCAUUACGAGAUU
Plate 2	B09		UGGAGAAGCGUGUCAGAUA
Plate 2	C04	ITK	AGACAUCAGUACCGGAUUU
Plate 2	C04		ACAGUUUGGUGCCUAAAUA
Plate 2	C04		UCAACUAUCACCAACAUAA
Plate 2	C04		CCACACACGUCUACCAGAU
Plate 2	C05	SBF1	GCGCCGAGCUCUUCCGUAA
Plate 2	C05		CUACGGACCUGUUCGAUGA
Plate 2	C05		GCGGAGCCUUCACAGGAAA
Plate 2	C05		GAUACAGCUUCACCUAUGU
Plate 2	C06	PDPK1	UAUAUUAUGUGGAUCCUGU
Plate 2	C06		GACCAGAGGCCAAGAAUUU
Plate 2	C06		GCAGCAACAUAGAGCAGUA
Plate 2	C06		GAAGCAGGCUGGCGGAAAC
Plate 2	C07	CYTH3	GGGAAUUCAGUUUCUAAUA
Plate 2	C07		GAACGAGCCAUUUAAGAUC
Plate 2	C07		GAGAAGGCCUAAAUAAGAC
Plate 2	C07		AGAGAUCCCUUCUAUGACA
Plate 2	C08	RICTOR	GACACAAGCACUUCGAUUA
Plate 2	C08		GAAGAUUUAUUGAGUCCUA
Plate 2	C08		GCGAGCUGAUGUAGAAUUA
Plate 2	C08		GGGAAUACAACUCCAAAUA
Plate 2	C09	DAPP1	GCACUCUGAUGGUUCUAAA
Plate 2	C09		GAUCCUAGACCUAACAGAA
Plate 2	C09		GCUGGAAAUUGGUCAAGGA
Plate 2	C09		GGAAUGAACUGAAAUACUU
Plate 2	D04	ARHGEF4	UGUCUGCGCUGACGAAGUG
Plate 2	D04		GCUCAGAACUCAUCUACUC
Plate 2	D04		CAACGGGACUGAACCACAU
Plate 2	D04		CAGCGAAUGUUCUUUCUCU
Plate 2	D05	GSK3B	GAUCAUUUGGUGUGGUAUA
Plate 2	D05		GCUAGAUCACUGUAACAUA
Plate 2	D05		GUUCCGAAGUUUAGCCUAU
Plate 2	D05		GCACCAGAGUUGAUCUUUG
Plate 2	D06	SGK2	GAAAGAGCCUUAUGAUCGA
Plate 2	D06		GGGAUGACCUGUACCACAA
Plate 2	D06		GAGAUUAAGAACCAUGUAU
Plate 2	D06		GUUCUACGCUGCUGAGGUG
Plate 2	D07	PLEKHA1	GGAAUGGGUAAAUGUGUUA
Plate 2	D07		GUAACAACGUCUCGAACUU
Plate 2	D07		CCUAAACCACCUCAAGAUA
Plate 2	D07		GCAAAGCGACAUAAUGAUG
Plate 2	D08	ARHGEF6	GAGGAUGUCUUAUAUCUUA
Plate 2	D08		GGACGUUCCUCUUCUCUUA
Plate 2	D08		GAGGAGGAAUAUGUGAUUA
Plate 2	D08		GGACAUCAUUUACGUCACA
Plate 2	D09	SH3BP2	GUGAGGAACUAUCGCAUUU
Plate 2	D09		GGACGAAACCUCUAACAAA

Plate 2	D09		GCAGGGAGAUUGGCCACUU
Plate 2	D09		GGAGGGCGAGGUCCUGUUU
Plate 2	E04	VAV2	CUGAAAGUCUGCCACGAUA
Plate 2	E04		UGGCAGCUGUCUUCAUUAA
Plate 2	E04		GUGGGAGGGUCGUCUGGUA
Plate 2	E04		GCCGCUGGCUCAUCGAUUG
Plate 2	E05	SGK3	GAAAGCUGCCCAAGUGUAA
Plate 2	E05		GGAGAUAUGCAGAGUUUGA
Plate 2	E05		GUGUGUAUCUUCUGACUAU
Plate 2	E05		GCAUUGGGUUACUUACAUU
Plate 2	E06	ADAP1	AGCAUAAACCUUAGCGAGU
Plate 2	E06		GGGCCAAGUACGAGCGACA
Plate 2	E06		UCGGGAAUCCACCGGAAUA
Plate 2	E06		CGUGUCGCAUCCUGGAAUA
Plate 2	E07	ARHGAP1	GCCAAGUGCUCAAAUAUGA
Plate 2	E07		GGCGGAAGAUCAUUGUGUU
Plate 2	E07		UAACCUGGCUGUUGUUUUC
Plate 2	E07		GGGAAGUGCAGCAGAAGUA
Plate 2	E08	PLEK2	GAGCAGGGAAGCACCUAUA
Plate 2	E08		CCGAGUGGAUUGAAGCUAU
Plate 2	E08		GAAGGUGCGUCGCUUUGUU
Plate 2	E08		GACACACACUAUUACAUUC
Plate 2	E09	ADAP2	GAGUUAAAUCUGUGCGACU
Plate 2	E09		AAGUAUGAGAGACGGGAAU
Plate 2	E09		CUUCAAGCACCACGCAGAA
Plate 2	E09		GAUAUGAAGCCUACGAAGA
Plate 2	F04	FGD6	GAAGGGACCGGUUUUAUAA
Plate 2	F04		GAAUUCCGAGUCUAAAGUA
Plate 2	F04		CUAAGCAGCUCAAAUUAAC
Plate 2	F04		GCUCGUCUGUUACGCCAAA
Plate 2	F05	BMX	GUACCAGUCUAGCGCAAUA
Plate 2	F05		GAAGAUACCUCGGGCAGUU
Plate 2	F05		GAAGAGAGCCGAAGUCAGU
Plate 2	F05		GAGCAUUUAUGGUUAGAAA
Plate 2	F06	PTPN9	GAAAACAACGCUAGAAAUU
Plate 2	F06		GGACAGUUCAGUACAAUGU
Plate 2	F06		GUCAGUAACUCUCCUACGA
Plate 2	F06		AAAUUGAUCUCGCCACUUG
Plate 2	F07	GSK3A	UCACAAGCUUUAACUGAGA
Plate 2	F07		GAAGGUGACCACAGUCGUA
Plate 2	F07		GAGUUCAAGUUCCCUCAGA
Plate 2	F07		CUGGACCACUGCAAUAUUG
Plate 2	F08	PLEKHA2	AGCAAGGGAAUGUGCGGAA
Plate 2	F08		GCAAGUUUCUGCGGAGGUA
Plate 2	F08		UUCGAAGGUCUCAGAGUUA
Plate 2	F08		ACAUCGAGGAGCAUGAGAA
Plate 2	F09	PLEKHB2	CGAGAGCGCUAUCGAGACA
Plate 2	F09		GGACAAACACAGCGUAUGU
Plate 2	F09		GCAGUUUAGCACAGCGAAU
Plate 2	F09		CCAGAUUGUUUGUCGAGAU
Plate 2	G04	PIK3R2	GCGCCCAGCUUAAGGUCUA
Plate 2	G04		GGAACGCACUUGGUACGUG

Plate 2	G04		GGACAAGAGCCGCGAGUAU
Plate 2	G04		GGAAAGGCGGGAACAAUAA
Plate 2	G05	MCF2	GAACUGGGCAAGAUGAUAA
Plate 2	G05		UAACAGAACGGGAUAAGUU
Plate 2	G05		GAAGAAGGCACUCGAUGCA
Plate 2	G05		GAGCUCAGUUAGUGAUUUG
Positive		MCL-1	GGUUUGGCAUAUCUAAUAA
			GAAGGUGGCAUCAGGAAUG
			GAUUAUCUCUCGGUACCUU
			CGAAGGAAGUAUCGAAUUU
Negative		Non-targeting	GAACUGGGCAAGAUGAUAA

Table 14: Candidates for siRNA library screen and controls (MCL-1 and non-targeting) siRNAs target sequence.

8.4 Appendix IV

PLATE 1	Mother plate											
	1	2	3	4	5	6	7	8	9	10	11	12
A												
B				SOS1	CYTH2	SWAP70	MCL-1	NT	AKAP13			
C				PLCXD2	DOCK2	PIK3CA	GAB2	CYTH1	RASA1			
D				CYTH4	TEC	RASA3	VAV1		BTK			
E				VAV3	ARAP3	RASA2	PHLDB1	ARAP1	GAB3			
F				TIAM1	PREX1	DOCK1	GAB1	AKT2	AKT1			
G				SGK1	ARAP2	PIK3CD	MTOR	PREX2	PHLDB3			
H												

PLATE 2	Mother plate											
	1	2	3	4	5	6	7	8	9	10	11	12
A												
B				PIK3R1	PLCL2	PIK3CB	AKT3	MYO10	RPTOR			
C				ITK	SBF1	PDPK1	CYTH3	RICTOR	DAPP1			
D				ARHGEF4	GSK3B	SGK2	PLEKHA1	ARHGEF6	SH3BP2			
E				VAV2	SGK3	ADAP1	ARHGAP1	PLEK2	ADAP2			
F				FGD6	BMX	PTPN9	GSK3A	PLEKHA2	PLEKHB2			
G				PIK3R2	MCF2	MCL-1	NT					
H												

Figure 27: Mother plate layout for siRNA library screen. The siRNA library screen consisted of 65 candidate SMARTpool siRNAs targeting the mRNA of potential downstream effectors of PI3K. The candidates were randomly split into two pates and the SMARTpool siRNA for each candidate was reconstituted in one well of the mother plate (mother plate 1 or 2). From the mother plate the daughter plates were produced. Daughter plates were drug treated with either 4 μM ABT-737 or DMSO equivalent for 72 hours and then analysed by SRB assay.